1-1-2010

Shear Stress Analysis Of Levees Subjected To Combined Surge And Wave Overtopping

Justin Michael Shaw

SHEAR STRESS ANALYSIS OF LEVEES SUBJECTED TO COMBINED SURGE AND WAVE OVERTOPPING

By

Justin Michael Shaw

A Thesis
Submitted to the Faculty of
Mississippi State University
in Partial Fulfillment of the Requirements
for the Degree of Master of Science
in Civil and Environmental Engineering
in the Department of Civil and Environmental Engineering

Mississippi State, Mississippi

December 2010

SHEAR STRESS ANALYSIS OF LEVEES SUBJECTED TO COMBINED SURGE AND WAVE OVERTOPPING

By

Justin Michael Shaw

Approved:

Isaac L Howard Assistant Professor of Civil and Environmental Engineering (Major Professor)	Steven A Hughes Adjunct Professor of Civil and Environmental Engineering (Committee Member)
James L Martin Professor of Civil and Environmental Engineering (Committee Member)	William H McAnally Research Professor of Civil and Environmental Engineering (Committee Member)
James L Martin Professor and Graduate Coordinator of Civil and Environmental Engineering	Sarah A Rajala Dean of the Bagley College of Engineering

Name: Justin Michael Shaw

Date of Degree: December 10, 2010

Institution: Mississippi State University

Major Field: Civil and Environmental Engineering

Major Professor: Isaac L Howard

Title of Study: SHEAR STRESS ANALYSIS OF LEVEES SUBJECTED TO COMBINED SURGE AND WAVE OVERTOPPING

Pages in Study: 176

Candidate for Degree of Master of Science

Storm surge above the levee crest elevation combined with levee wave overtopping can place large shear stresses on the levee landward slope face. Previous research has examined overtopping flow conditions, but the resulting shear stress has not been thoroughly analyzed. The purpose of this thesis is to examine multiple combinations of overtopping flow conditions and the resultant shear stress along the levee's landward slope. This thesis presents measurements of depth, velocity, discharge, and wave height, and it estimates shear stress using data collected from a scaled physical model. Shear stress is estimated using three equations including a version of Saint-Venant equations that accounts for unsteady, non-uniform flow. The objective of this thesis is to develop shear stress estimates on the landward slope of a levee during combined wave and surge overtopping for conditions and dimensions typical to levees along the Gulf coast of the United States.

DEDICATION

First and foremost, I would like to thank the good people at Mississippi State University for giving me the opportunity to further my education. Dr. Howard, thank you for assisting me throughout this process and having my best interests at heart. You stepped up in a big way and I appreciate it. Dr. Hughes, thank you for giving me the opportunity to learn. I broke a laser, gave your computer a virus, and was late on several occasions, but you never lost your patience and answered every one of my questions. I am eternally grateful. Dr. Martin, thank you for opening my eyes to grad school. Your Open Channel class, though very early in the morning, sparked my desire for an advanced degree. Dr. McAnally, argh matey, you advised me through every major decision I came across while in school. Thank you for your kindness, your sense of humor, and Sedimentation Engineering (it was my favorite course).

My family, Mom, Dad, Taylor, Hayden, Grandma, and Richard, thank you for always supporting me and being there for a good laugh. Anna S, thank you for everything that you do. You mean the world to me. I need to thank Trey D, Chris H, Richie M, Kim P, John R, and Jeremy S for making everyday an exciting one. Finally to my friends: Kylie A, Sam B, The Bells, Tucker B, Phillip B, William D, The Destins, Steve E, Tyler G, Martin H, the Hunnicutts, Brandon J, all the Lowery's, the Nascas, Ryan P, Chris R, Blake S, David T, Joe T, The Tums, Ben W, Brooks W, Blake W, and to all the others I failed to mention…Thank you.

ACKNOWLEDGEMENTS

Hugh Acuff, Julie Cohen, and Tim Nisley were invaluable with their experimentation assistance. Thank you for all the hard work. Trey Davis, Chris Hall, and Jeremy Sharp added much appreciated insight.

TABLE OF CONTENTS

LIST OF TABLES

LIST OF FIGURES

LIST OF SYMBOLS

A = Cross-sectional Area of Flow
B = Dike Crest Width
C = Chezy Coefficient
C_s = 1; Surge Overtopping Shear Stress Coefficient
E = Modulus of Elasticity
F_1 = Force in Direction 1
F_2 = Force in Direction 2
F_{cv} = Resultant Force Acting on Fluid in Control Volume
F_b = Body Force
F_e = Elastic Compression Force
F_g = Gravitational Force
F_i = Inertial Force
F_n = Normal Force
F_{pr} = Pressure Force
F_{sx} = Surface Force Acting on x Plane
F_μ = Viscous Force
F_σ = Surface Tension Force
F_r = Froude Number
H_{m0} = Significant Wave Height
H_{rms} = Root-mean-square Wave Height
H_s = Significant Wave Height
L = Length
L_0 = Deep Water Wave Length
$L_{m-1,0}$ = Mean Energy Wave Length
N_x = Prototype to Model Scale Ratio of Parameter X
R = Hydraulic Radius
R_c = Freeboard
S_f = Friction Slope
S_0 = Channel Slope
T_m = Mean Wave Period
$T_{m-1,0}$ = Mean Energy Wave Period
T_p = Peak Wave Period
$\forall$ = Volume
X_m = Model Dimension of Parameter X
X_p = Prototype Dimension of Parameter X

c_1 = Coefficient; 1.5 for Wave Spectra and 1.0 for Regular Waves
c_2 = Dike Slope Coefficient
c_3 = 0.75
cv = Control Volume
cs = Control Surface
d_m = Average Flow Thickness on Landward Slope
f = Bottom Friction Coefficient
f_D = Darcy Friction Factor
f_F = Fanning Friction Factor
g = Gravity
h = Flow Depth
h_0 = Initial Flow Thickness
h_{12} = Average Flow Thickness between Two Points
h_1 = Flow thickness at Pressure First Gauge
h_2 = Flow thickness at Pressure Second Gauge
h_4 = Depth at Gauge 4
h_7 = Depth at Gauge 7
h_a = Flow Thickness at the Seaward Crest Edge
h_b = Flow Thickness Along Landward Slope
h_c = Critical Depth
h_{CR} = Dike Crest Flow Thickness
k_1 = Factor
m = Mass
n = Manning's Roughness Coefficient
$\check{n}$ = Normal Direction
p = Pressure
q = Discharge per Unit Width
q_c = Critical Discharge per Unit Width
q_{rms} = Root-mean-square Unit Discharge
q_{ws} = Combined Overtopping Unit Discharge
s_1 = Down Slope Distance from Crest to First Gauge
s_2 = Down Slope Distance from Crest to Second Gauge
$s_{2,1}$ = Distance between First and Second Gauges
s_b = Landward Slope Parallel Coordinate
s_D = Downslope Coordinate
t = Time
v = Velocity
v_0 = Initial Velocity
$v_1(i)$ = Velocity at First Gauge
$v_2(i)$ = Velocity at Second Gauge
$v_1(i+1)$ = Velocity at First Gauge, One Time Increment Longer
$v_2(i+1)$ = Velocity at Second Gauge, One Time Increment Longer
v_4 = Velocity at Gauge 4
v_7 = Velocity at Gauge 7
v_c = Critical Velocity
v_m = Mean Velocity on Landward Slope

x_A = Horizontal Coordinate Beginning at Slack Water Line
x_{CR} = Dike Crest Coordinate
x_Z = Horizontal Projection of Wave Run-up
$x_{Z,P}$ = Horizontal Wave Run-up Length for Plunging Breakers
$x_{Z,S}$ = Horizontal Wave Run-up Length for Surging Breakers
α = Seaward Slope Angle
β = Landward Slope Angle
β_f = Momentum Flux Correction Factor
γ = Shear Strain
γ_w = Fluid Specific Weigh
γ_b = Berm Influence Factor
γ_f = Roughness Influence Factor
γ_β = Wave Angle Influence Factor
γ_v = Vertical Wall on Slope Influence Factor
θ = Slope Angle Measured from Horizontal
μ = Dynamic Viscosity
ξ = Surf Similarity Parameter
ξ_{gr} = Transition Point Between Plunging and Surging Breakers
ρ = Fluid Density
σ = Surface Tension
σ_{xx} = Normal Force Acting on x Plane
τ = Shear Stress
τ_0 = Average Shear Stress
$\tau_{0,1/3}$ = Average of Highest 1/3 Shear Stress
$\tau_{0,1/10}$ = Average of Highest 1/10 Shear Stress
$\tau_{0,1/100}$ = Average of Highest 1/100 Shear Stress
τ_1 = Shear Stress along Direction 1
τ_2 = Shear Stress along Direction 2
τ_{yx} = Shear Stress Acting on x Plane in y Direction
τ_{zx} = Shear Stress Acting on x Plane in z Direction

CHAPTER I

INTRODUCTION

Levees are used throughout the world to protect communities and resources from elevated water levels in coastal and inland areas. These flood protection systems are at risk of failure due to several mechanisms; erosion is the primary mechanism investigated herein. Terms related to levee geometry and flow conditions used in this thesis are located in Figure 1.1. Storm surge elevations of 7.6 m during Hurricane Katrina caused erosion on the levees landward slope in several locations contributing to the failure of 272 km of levees in Louisiana (ASCE 2007, Irish et al. 2003). Storm surge inundated coastal regions and raised water levels above the levee crest producing negative freeboard conditions which resulted in levee failures in some instances and flooding in all instances.

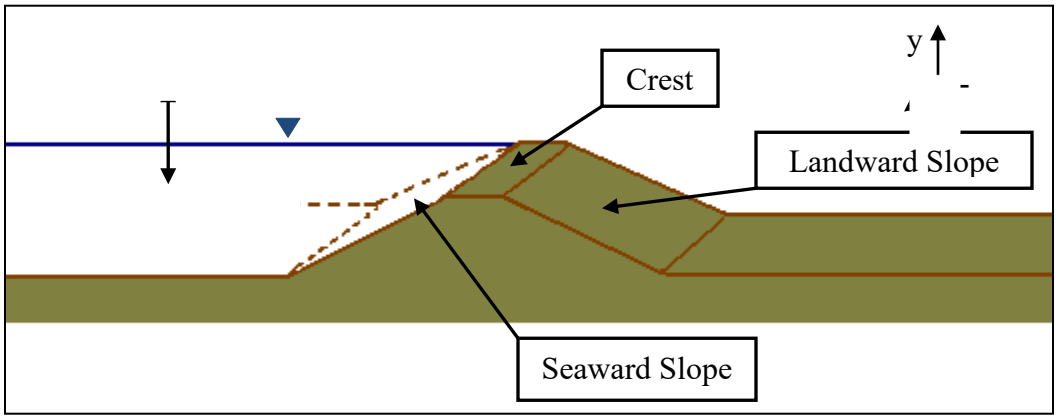

Figure 1.1 Levee Terminology

Levee overtopping is typically categorized as: 1) surge, 2) wave, and 3) combined surge and wave. Surge overflow is a relatively steady flow of water over a levee's crest and down its landward slope. Wave-only overtopping is typically defined as the water level being below the levee crest and waves spilling over periodically, but the crest and landward slope are not constantly under a sheet of water. Combined wave and surge overtopping is a combination of surge overflow and waves which is thought to be the most destructive overtopping condition due to large peaks in depth and velocity (ASCE 2007, Hughes 2008, Hughes and Nadal, 2009, Nadal and Hughes 2009). Figure 1.2 shows common erosion progression on a levee's landward slope during surge overflow; note erosion appearing on the landward slope.

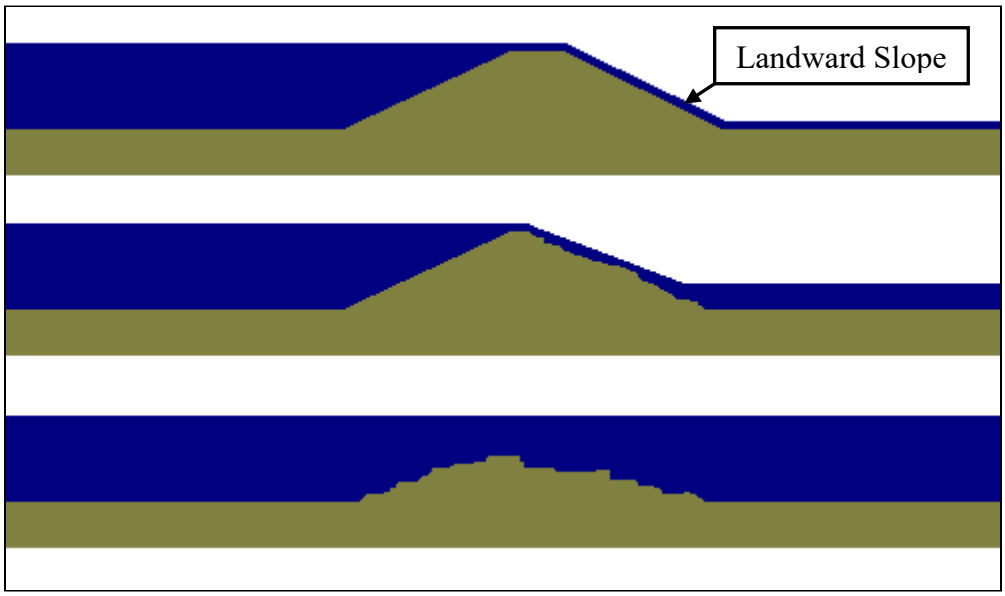

Figure 1.2 Erosion of a Levee due to Surge Overflow Causing Failure

1.1 Purpose of Research

The purpose of this thesis was to develop a capability for estimating shear stress on the landward slope of an earthen levee due to combined wave and surge overtopping. Shear stress estimation was needed for the design of levee armoring systems in other research areas. This study expanded on previous research at the Coastal and Hydraulics Laboratory (CHL) of the US Army Engineer Research and Development Center (ERDC) in Vicksburg, Mississippi, and it refined the relationship between overtopping conditions and shear stress on the landward slope of a levee. This improved overtopping characterization was used in calculation of shear stress along the levee face. This research was funded by the Department of Homeland Security (DHS) through its Southeast Region Research Initiative (SERRI). DHS is a governmental agency whose objective is to protect the population and economy of the United States through a five goal process (DHS 2008):

- Protect the Nation from Dangerous People
- Protect the Nation from Dangerous Goods
- Protect Civil Infrastructure
- Strengthen the Nation's Preparedness and Emergency Response Capabilities
- Strengthen and Unify DHS Operations and Management.

The research in this thesis will assist in protecting infrastructure and will enhance response and recovery effectiveness in natural disaster prone areas.

1.2 Objectives and Scope

The *Increasing Community Disaster Resilience through Targeted Strengthening of Critical Infrastructure* project (referred to hereafter as the *Resilience* project) was developed by faculty at Mississippi State University (MSU) and key partners (e.g. ERDC) in response to the damage from Hurricane Katrina. One of the *Resilience* project's purposes was to develop readily available infrastructure protection methods that can be deployed before a natural disaster. This thesis is related entirely to Task 1: Erosion Protection for Earthen Levees.

The objective of Task 1 was to develop a rapidly deployable erosion protection system (aka armoring systems) for earthen levees. This thesis addresses overtopping conditions and the resultant shear stresses generated on the levee face. Freeboard, wave height, and wave period were varied in a scaled physical model to simulate a range of overtopping conditions from which shear stresses were estimated over a model levee. Data and calculations presented in this thesis are fully valid only for the levee configuration and overtopping conditions considered.

Flow velocity and flow thickness measurements were recorded on a typical levee section. These measurements were used to calculate shear stress along the levee face. This thesis does not examine soil erosion rates, nor does it explore the effect of levee armoring. The objective of this thesis is to develop shear stress estimates on the landward slope of an earthen levee during combined wave and surge overtopping for conditions and dimensions typical to levees along the Gulf coast.

A key element of the scope of this thesis was the interaction with ERDC. ERDC is composed of five technical areas to assist the United States Army: Warfighter Support, Installations, Environment, Water Resources, and Information Technology. Research centers are located in Illinois, Mississippi, New Hampshire, and Virginia.

CHAPTER II

REVIEW OF LITERATURE

Overtopping flow exerts a unique set of loadings on the landward levee face that is a function of several variables. Surge, wave, and combined overtopping are displayed in Figure 2.1. Surge overtopping produces steady discharge with relatively constant flow thickness and velocity. Wave overtopping generates intermittent discharge with large flow thickness and velocity peaks as waves crash over and spill down the levee's landward slope. Wave and surge overtopping combines flow thickness and velocity peaks associated with wave overtopping and the additional discharge of surge overtopping. The purpose of this literature review is to examine methods of estimating discharge, flow thickness, and velocity on a levee's crest and landward slope as well as examining the relationship between shear stress, flow thickness, and velocity. Depth and flow thickness are used to describe the difference between water surface and channel bottom elevations. Flow thickness typically describes this difference along the levee slopes and other locations with larger slopes while depth is used to describe other areas.

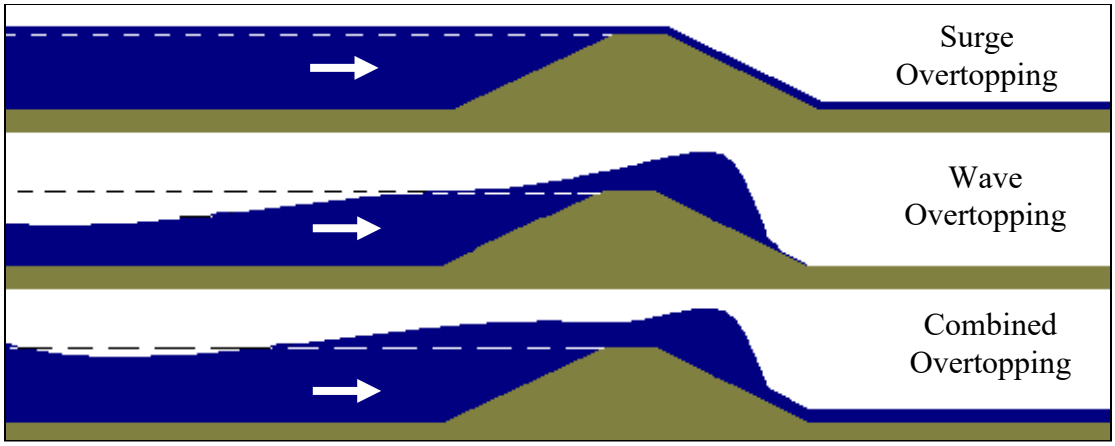

Figure 2.1 Overtopping Scenarios

2.1 Surge Overtopping

Surge overtopping of a levee is considered to be well represented by steady flow in this thesis, and this is a common approximation because the time variation is much smaller than that of wave overtopping. Overtopping discharge reaches critical depth somewhere on the crest and becomes supercritical on the landward slope, similar to flow over a broad-crested weir until the landward side water level approaches the seaward side water level. Steady discharge over a sufficiently long broad-crested weir can be estimated with Equation 2-1 (Henderson 1966, Chaudhry 1993).

$$q = {}^{2}/_{3}\, R_c \sqrt{{}^{2}/_{3}\, g R_c} \tag{2-1}$$

where:

q = Discharge per Unit Width (*Volume*/*Time* per *Length*)
g = Gravity (*Length*/*Time*/*Time*)
R_c = Negative Freeboard Upstream of the Weir (*Length*)

Equation 2-1 was developed assuming flow along the weir crest reaches critical flow (Chaudhry 1993). Discharge can be estimated by measuring negative freeboard

over a weir common during controlled reservoir letdowns using Equation 2-1 (Strum 2001). Discharge per unit width may be used alongside the Froude number (F_r) to determine critical velocity. F_r is the dimensionless ratio of stream velocity to wave velocity and indicates if the flow regime has reached critical or supercritical conditions (Henderson 1966); see Table 2.1. Flow is critical if a small amplitude shallow water gravity wave has the same velocity as the flow. Subcritical flow occurs when a small amplitude gravity wave is greater than flow velocity and is typically shown as a water surface disturbance moving upstream. Supercritical flow is characterized by small depths and large velocities when flow velocity is greater than a small amplitude gravity wave and disturbances do not move upstream.

Table 2.1 Froude Flow Regime Classification

Froude Number	**Flow Classification**
$F_r < 1$	Subcritical
$F_r = 1$	Critical
$F_r > 1$	Supercritical

Hughes (2008) used Equations 2-2 through 2-4 to determine critical depth and velocity on a levee crest during surge overtopping. Critical flow may be calculated by setting the Froude number to one and solving Equation 2-2. Equations 2-3 and 2-4 use the flow rate estimated by Equation 2-1 with the Froude number equal to one to calculate critical depth and velocity on a levee crest during surge overtopping.

$$q = F_r\sqrt{gh^3} \tag{2-2}$$

$$h_c = {}^2/_3\, R_c = \left(\frac{q^2}{g}\right)^{1/3} \tag{2-3}$$

$$v_c = \sqrt{gh_c} = \sqrt{{}^2/_3\, gR_c} \tag{2-4}$$

where:

h = Flow Depth (*Length)*
h_c = Critical Depth (*Length)*
v_c = Critical Velocity (*Length/Time)*

Critical flow is reached along the levee crest frequently near the landward slope edge. Surge overtopping flow then transitions into supercritical flow and spills down the landward slope. Chezy's equation may be used to calculate velocity assuming steady flow and small slopes (Chaudhry 1993). The typical landward levee slope, including the model levee examined in this thesis, is not considered small and the Chezy equations may not be applicable (Hughes 2009). Supercritical flow on the landward slope will accelerate until terminal velocity, which is typically restricted by the turbulent boundary layer. The Chezy equation for steady, non-uniform flow is shown in Equation 2-5.

$$v = C\sqrt{RS_f} \tag{2-5}$$

where:

v = Velocity (*Length/Time)*
C = Chezy Coefficient ($L^{1/2}/T$)
R = Hydraulic Radius (*Length*)
S_f = Friction Slope (*Length*/*Length*)

Chezy's coefficient can be estimated through empirical relationships, field observations, or by Equation 2-6 (Hughes 2008, Chaudhry 1993, Henderson 1966).

$$C = \frac{R^{1/6}}{n} = \sqrt{\frac{8g}{f_D}} = \sqrt{\frac{2g}{f_F}} \tag{2-6}$$

where:

n = Manning's Roughness Coefficient (*Dimensionless*)
f_D = Darcy Friction Factor (*Dimensionless*)
f_F = Fanning Friction Factor (*Dimensionless*)

Chezy's equation may be manipulated assuming a very wide channel (hydraulic radius equals flow thickness) and friction slope equal to the levee slope (terminal velocity) producing Equation 2-7. The levee slope may be written as $sin(\theta)$ where θ is the slope angle measured from the horizontal.

$$v_c = \sqrt{\frac{8g}{f_D}}\sqrt{h_c sin(\theta)} \tag{2-7}$$

Manning's equation is the most common estimation of velocity on a sloped bed, i.e. landward slope of a levee, and is derived from Chezy's equation (Equation 2-5) by converting C into a Manning's roughness coefficient; Equations 2-8 and 2-9.

$$v = \frac{1.49}{n} R^{2/3}\sqrt{S_f} \quad \text{English} \tag{2-8}$$

$$v = \frac{1}{n} R^{2/3}\sqrt{S_f} \quad \text{Metric} \tag{2-9}$$

By applying steady, uniform flow assumptions the Manning's equation can be simplified into Equations 2-10 and 2-11 by setting the hydraulic radius equal to depth, converting the friction slope into the levee slope implying terminal velocity has been reached, and setting the flow rate equal to depth times velocity (Hughes 2008).

$$v_c = \left[\frac{1.49\sqrt{sin(\theta)}}{n}\right]^{3/5} q_c^{2/5} \quad \text{English} \quad (2\text{-}10)$$

$$v_c = \left[\frac{\sqrt{sin(\theta)}}{n}\right]^{3/5} q_c^{2/5} \quad \text{Metric} \quad (2\text{-}11)$$

where:

q_c = Critical Discharge per Unit Width (*Volume/Time* per *Length)*

2.2 Wave Overtopping

Wave overtopping may be more catastrophic than surge overtopping due to depth and velocity peaks as waves spill over the levee crest. Multiple studies have been performed examining overtopping discharge of flood protections structures. Van der Meer (2002) developed a set of empirical equations to estimate average wave overtopping discharge. These equations were developed by examining several shoreline protection systems including those with smooth, rough, steep, and/or mild slopes, long or short crests widths, and with or without a vertical wall. Discharges from 0.1 to 100 liter/second per meter were examined and Equations 2-12 and 2-13 are the results of the Van der Meer (2002) study as given in Pullen et al. (2007).

$$\frac{q}{\sqrt{gH_{m0}^3}} = \frac{0.067}{\sqrt{tan(\alpha)}}\gamma_b(\xi)exp\left(-4.75\frac{R_c}{H_{m0}}\frac{1}{\xi\gamma_b\gamma_f\gamma_\beta\gamma_v}\right) \quad \text{where } \xi < 5 \tag{2-12}$$

with a maximum of

$$\frac{q}{\sqrt{gH_{m0}^3}} = 0.2\gamma_b(\xi)exp\left(-2.6\frac{R_c}{H_{m0}}\frac{1}{\gamma_f\gamma_\beta}\right) \tag{2-13}$$

$$\xi = \frac{tan(\alpha)}{\sqrt{\frac{H_{m0}}{L_{m-1,0}}}} \tag{2-14}$$

$$L_{m-1,0} = \frac{g}{2\pi}T_{m-1,0}^2 \tag{2-15}$$

where:

q	=	Unit Discharge (m^3/s per m)
H_{m0}	=	Significant Wave Height (m)
α	=	Seaward Slope Angle
ξ	=	Surf Similarity Parameter (*Dimensionless*)
R_c	=	Freeboard (m)
γ_b	=	Berm Influence Factor (*Dimensionless*)
γ_f	=	Roughness Influence Factor (*Dimensionless*)
γ_β	=	Wave Angle Influence Factor (*Dimensionless*)
γ_v	=	Vertical Wall on Slope Influence Factor (*Dimensionless*)
$L_{m-1,0}$	=	Mean Energy Wave Length (m)
$T_{m-1,0}$	=	Mean Energy Wave Period (s)

Equations developed by Van der Meer (2002) are empirically based on numerous model studies. Pullen et al. (2007) suggested using Equations 2-12 and 2-13 in design with a factor one standard deviation higher than average discharge for increased protection as seen in Equations 2-16 and 2-17.

$$\frac{q}{\sqrt{gH_{m0}^3}} = \frac{0.067}{\sqrt{tan(\alpha)}}\gamma_b(\xi)exp\left(-4.3\frac{R_c}{H_{m0}}\frac{1}{\xi\gamma_b\gamma_f\gamma_\beta\gamma_v}\right) \quad \text{where } \xi < 5 \qquad (2\text{-}16)$$

with a maximum of

$$\frac{q}{\sqrt{gH_{m0}^3}} = 0.2exp\left[-2.3\frac{R_c}{H_{m0}\gamma_f\gamma_\beta}\right] \qquad (2\text{-}17)$$

Okayasu et al. (2005) measured wave overtopping depth and velocity using smooth and stepped seawalls. Laser Doppler Velocimeters (LDVs) measured overtopping velocity and a catch basin was used to determine overtopping volume. Significant wave heights ($H_{1/3}$) and wave periods ($T_{1/3}$) were generated by an absorption-type wave generator (Okayasu et al. 2005). Table 2.2 provides wave conditions of Okayasu et al. (2005).

Table 2.2 Okayasu et al. (2005) Wave Conditions

Case		$H_{1/3}$ (cm)	$T_{1/3}$ (s)	**Case**		$H_{1/3}$ (cm)	$T_{1/3}$ (s)	**Case**		$H_{1/3}$ (cm)	$T_{1/3}$ (s)
A	1	9.6	1.40	B	1	6.7	1.37	C	1	8.4	1.40
	2	9.8	1.59		2	8.4	1.40		2	8.4	1.61
	3	10.9	1.42		3	8.4	1.61		3	10.1	1.42
	4	11.4	1.59		4	10.1	1.42		4	10.1	1.61

Overtopping volume captured in the basin was comparable to equations used to estimate wave overtopping discharge using depth and velocity; these equations were not included in the literature. A three-dimension *Large Eddy Simulation* (3D *LES*) numerical model was developed and compared to physically modeled data. The numerical and

physical wave overtopping depths and velocities were not in agreement, and wave overtopping volume in the numerical model was half the volume measured in the physical model. According to Okayasu et al. (2005) the discrepancy was possibly due to a bottom non-slip condition with velocity and wave reflection altered depth readings.

Typically wave overtopping flow thickness decreases along the crest and down the landward slope similar to surge flow. Schüttrumpf et al. (2005) studied wave parameters at a seadike toe, wave transformation on the seaward slope, wave run-up and run-down on the seaward slope, wave overtopping on a dike crest, and wave overtopping on the landward slope of smooth seadikes. Tests were performed in a 100 m long, 2 m wide, and 1.25 m deep flume with a flap-type wave generator that produced irregular waves with heights up to 0.25 m, periods of 1.5 to 6 seconds, and freeboard up to 0.2 m. Roughly 50 waves were tested during each experimental run before wave reflection interfered because a damper was not installed. The seaward and landward slopes varied. Overtopping discharge was measured by load cells located in a basin landward of the dike. Flow thickness was measured by resistance wave gauges inlaid on the dike surface. Data were sampled at 40-Hz, and flow thickness was confirmed with video recording. Flow thickness less than eight millimeters was discarded. Velocity measurements were recorded at 20-Hz using micro propellers mounted on the dike surface.

Wave overtopping depth along the crest decreased from the seaward to the landward edge due to acceleration of flow down the landward slope. Depth at the seaward edge of a dike crest may be estimated with Equations 2-18 through 2-20 which are a derivation of Hunt's (1959) wave run-up formula. Plunging breakers occur when a

wave has crested and is crashing on itself. Surging breakers do not crash and are typically found on steep slopes

$$h_A(x_*) = c_2(x_z - x_A) = c_2 x_* \tag{2-18}$$

$$x_{Z,P} = c_1\sqrt{H_s L_0} \quad \text{Plunging Breakers where } \xi \leq \xi_{gr} \tag{2-19}$$

$$x_{Z,S} = c_1 \frac{\xi H_s}{tan(\alpha)} \quad \text{Surging Breakers where } \xi > \xi_{gr} \tag{2-20}$$

where:

h_A = Flow Thickness at the Seaward Crest Edge (m)
c_2 = Dike Slope Coefficient
x_Z = Horizontal Projection of Wave Run-up (m)
x_A = Horizontal Coordinate Beginning at Slack Water Level (m)
$x_{Z,P}$ = Horizontal Wave Run-up Length for Plunging Breakers (m)
c_1 = Coefficient, 1.5 for Wave Spectra and 1.0 for Regular Waves
H_s = Significant Wave Height (m)
L_0 = Deep Water Wave Length (m)
$x_{Z,S}$ = Horizontal Wave Run-up Length for Surging Breakers (m)
ξ_{gr} = Transition Point between Plunging and Surging Breakers

A portion of wave runup spills over the crest as overtopping while the rest flows down the seaward slope as run-down. Schüttrumpf and Oumeraci (2005) ignored wave run-down in forming flow thickness and velocity relationships along a dike. Equation 2-21 estimates depth during wave overtopping along the dike crest.

$$\frac{h_{cr}(x_{cr})}{h_{cr}(x_{cr}=0)} = \frac{c_2(x_{cr})}{c_2(x_{cr}=0)} = exp\left(-c_3\frac{x_{cr}}{B}\right) \tag{2-21}$$

where:

h_{cr} = Dike Crest Depth (m)
$h_{cr}(x_{cr}=0)$ = Flow Thickness on Dike Crest at the Seaward Edge (m)
x_{cr} = Dike Crest Coordinate (m)
c_3 = 0.75
B = Dike Crest Width (m)

Equation 2-21 is appropriate for all waves (regular and irregular, plunging and surging, etc.), and it describes crest depth as a function of initial crest depth and relative

location showing depth decreases along the crest width similar to surge overtopping as seen in Figure 2.2.

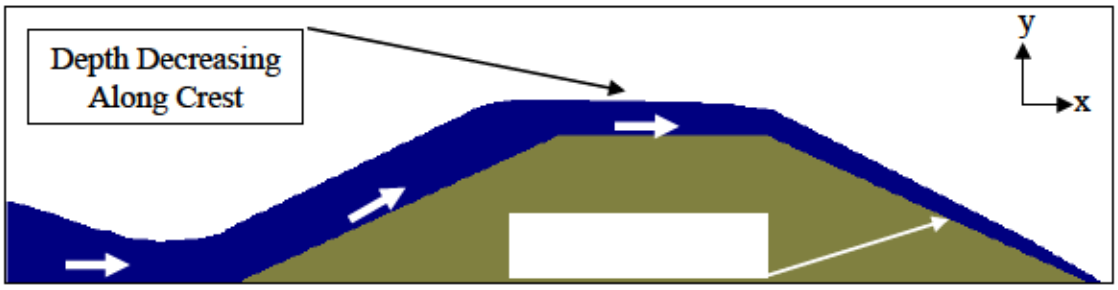

Figure 2.2 Wave Overtopping Discharge

Schüttrumpf and Oumeraci (2005) used two-dimensional Navier-Stokes equations to predict flow thickness on the landward slope. Equation 2-22 was derived from the continuity equation.

$$h = \frac{v_0 h_0}{v} \tag{2-22}$$

where:

v = Velocity (*Length*/*Time*)
v_0 = Initial Velocity at Landward Edge of Crest (*Length*/*Time*)
h_0 = Initial Depth at Landward Edge of Crest (*Length*)

Crest velocities increase to critical and often supercritical values. Flow thickness decreases down the landward slope while velocity increases to terminal velocity (assuming the landward slope is sufficiently long) similar to surge overtopping. Navier-Stokes principals were used to determine crest velocities; see Equation 2-23 where f is the dimensionless bottom friction coefficient.

$$v = v_0 exp\left(-\frac{xf}{2h}\right) \tag{2-23}$$

Equations 2-22 and 2-23 predict a decrease in depth and velocity over the crest width due to wave energy dissipation and bottom friction if the discharge has been pushed onto the crest by wave run-up since gravity and not momentum becomes the driving force. Bottom friction effects decrease as flow thickness increases but Schüttrumpf and Oumeraci (2005) noted that bottom friction had a "significant influence…on overtopping velocity," and crest velocity during wave overtopping was practically the same at the seaward and landward crest edges which could be affected by the bottom friction coefficient studied (f = 0.0058). Equations 2-24 through 2-28 estimate depth and velocity along the landward slope during wave overtopping. Similar to surge overtopping, depth decreased and velocity increased along the landward slope during wave overtopping.

$$v = \frac{v_0 + \frac{k_1 h}{f} tanh\left(\frac{k_1 t}{2}\right)}{1 + \frac{f v_0}{h k_1} tanh\left(\frac{k_1 t}{2}\right)} \tag{2-24}$$

$$t \approx -\frac{v_0}{g sin(\beta)} + \sqrt{\frac{v^2}{g^2 sin^2(\beta)} + \frac{2s}{g sin(\beta)}} \tag{2-25}$$

$$k_1 = \sqrt{\frac{2fgsin(\beta)}{h}} \tag{2-26}$$

$$v_B = \sqrt{\frac{2h_B g sin(\beta)}{f}} \tag{2-27}$$

$$h_B(s_B) = \frac{v_B(s_B = 0) h_B(s_B = 0)}{v_B(s_B)} \tag{2-28}$$

where:

k_1 = Factor (*Dimensionless*)
t = Time
β = Landward Slope Angle
h_B = Flow Thickness Along Landward Slope (*Length*)
s_B = Landward Slope Parallel Coordinate (*Length*)
$s_B=0$ = Landward Slope Parallel Coordinate at Crest Edge (*Length*)

Reeve, et al. (2008) developed a numerical model using Reynolds Averaged Navier-Stokes (RANS) equations to simulate irregular wave overtopping of a seawall with conditions listed in Table 2.3 where R is dimensionless freeboard defined as freeboard divided by significant wave height (R_c/H_{m0}). About 200 waves were run through the simulation.

Table 2.3 Reeve et al. (2008) Wave Overtopping Conditions

Run	$\boldsymbol{R_c}$ (m)	$\boldsymbol{R}$	**Slope**
1	0.900	0.39	1V:3H
2	1.125	0.49	1V:3H
3	1.350	0.59	1V:3H
4	1.575	0.68	1V:3H
5	1.800	0.78	1V:3H
6	2.250	0.98	1V:3H
7	0.5625	0.33	1V:4H
8	0.675	0.39	1V:4H
9	0.900	0.52	1V:4H
10	1.125	0.65	1V:4H
11	1.350	0.78	1V:4H
12	1.575	0.91	1V:4H
13	1.800	1.04	1V:4H

The significant wave height (H_s) was 1.22 m with a mean wave period (T_m) of 3.8 s and a peak wave period (T_p) of 5.0 s. A numerical analysis of irregular wave overtopping on 1V:3H and 1V:4H sloped seawalls with positive freeboard between 0.1 and 0.3 meters produced Equation 2-29.

$$\frac{q}{\sqrt{gH_s^3}}\frac{\sqrt{tan(\alpha)}}{\xi} = 0.09exp(-4.12R_c) \tag{2-29}$$

The model results were larger than previous studies performed by Van der Meer (2002). Reeve et al. (2008) used the RANS model with wave overtopping, zero freeboard, a surf similarity parameter (ξ) of 1.715, and conditions in Table 2.4 to compare to a study performed by Schüttrumpf et al. (2001).

Table 2.4 Reeve et al. (2008) Zero Freeboard Irregular Wave Characteristics

Run	H_s	T_m	T_p
	(m)	(s)	(s)
1	0.56	3.5	5.06
2	0.81	4.1	5.73
3	0.82	3.6	5.00
4	0.83	3.6	5.00
5	0.83	3.7	5.00
6	1.22	3.8	5.00
7	1.23	3.9	5.00
8	1.24	3.9	5.00
9	1.39	4.0	5.00
10	1.48	4.6	6.02

The results of the numerical model agreed with Schüttrumpf et al. (2001) relationships which validated the Reeve et al. (2008) numerical model for zero freeboard shown in Equations 2-30 and 2-31.

$$\frac{q}{\sqrt{2gH_s^3}} = 0.038(\xi) \qquad \xi < 2 \qquad (2\text{-}30)$$

$$\frac{q}{\sqrt{2gH_s^3}} = \left(0.096 - \frac{0.160}{\xi^3}\right) \qquad \xi \geq 2 \qquad (2\text{-}31)$$

Wave overtopping has similar physical characteristics to surge overtopping in that the landward slope velocity increases while flow thickness decreases over space, and both are limited by terminal velocity. Although average overtopping flow rates may be similar, the intermittent nature of wave overtopping produces depth and velocity peaks which can be more destructive than surge overtopping.

2.3 Combined Wave and Surge Overtopping

Combined wave and surge overtopping produces a nearly continual discharge over the levee with depth and velocity peaks associated caused by waves. Pullen et al. (2007) proposed calculating combined overtopping discharge by adding surge and wave discharge using Equations 2-32 through 2-35 where R_c is negative freeboard. Reeve et al. (2008) performed a numerical analysis of combined overtopping on 1V:3H, 1V:4H, and 1V:6H sloped seawalls using conditions shown in Table 2.5.

$$q_{overflow} = 0.6\sqrt{g|R_c^3|} \tag{2-32}$$

$$q_{overtop} = 0.0537\xi\sqrt{gH_{m0}^3} \qquad \xi < 2 \tag{2-33}$$

$$q_{overtop} = \left(0.136 - \frac{0.226}{\xi^3}\right)\sqrt{gH_{m0}^3} \qquad \xi \geq 2 \tag{2-34}$$

$$q = q_{overflow} + q_{overtop} \tag{2-35}$$

The wave characteristics in Table 2.5 provided a surf similarity parameter less than two. Equations 2-36 and 2-37, proposed by Reeve et al. (2008), estimate average wave/surge discharge as a function of wave height, surf similarity, freeboard, levee slope, and gravity.

$$\frac{q}{\sqrt{gH_s^3}}\frac{\sqrt{tan(\alpha)}}{\xi} = 0.051exp\left(-1.98\frac{R_c}{H_s\xi}\right) \qquad \text{Breaking Waves} \tag{2-36}$$

$$\frac{q}{\sqrt{gH_s^3}} = 0.233exp\left(-1.29\frac{R_c}{H_s}\right) \qquad \text{Non-Breaking Waves} \tag{2-37}$$

Table 2.5 Reeve et al. (2008) Combined Overtopping Wave Characteristics

Run	H_s	T_m	T_p	R_c	R	Slope
	(m)	(s)	(s)	(m)		
1	1.22	3.8	5.00	−0.061	−0.027	1H:3V
2	1.22	3.8	5.00	−0.122	−0.053	1H:3V
3	1.22	3.8	5.00	−0.244	−0.106	1H:3V
4	1.39	4.0	5.00	−0.278	−0.113	1H:3V
5	1.22	3.8	5.00	−0.366	−0.159	1H:3V
6	1.22	3.8	5.00	−0.488	−0.212	1H:3V
7	1.39	4.0	5.00	−0.556	−0.226	1H:3V
8	1.22	3.8	5.00	−0.610	−0.265	1H:3V
9	1.24	3.9	5.00	−0.620	−0.267	1H:3V
10	1.22	3.8	5.00	−0.732	−0.318	1H:3V
11	1.22	3.8	5.00	−0.854	−0.371	1H:3V
12	1.24	3.9	5.00	−0.868	−0.374	1H:3V
13	1.22	3.8	5.00	−0.976	−0.424	1H:3V
14	1.22	3.8	5.00	−1.098	−0.477	1H:3V
15	1.22	3.8	5.00	−1.220	−0.530	1H:3V
16	1.22	3.8	5.00	−0.061	−0.035	1H:4V
17	1.22	3.8	5.00	−0.122	−0.071	1H:4V
18	1.48	4.6	6.02	−0.296	−0.129	1H:4V
19	1.22	3.8	5.00	−0.244	−0.141	1H:4V
20	0.83	3.7	5.00	−0.249	−0.175	1H:4V
21	1.22	3.8	5.00	−0.366	−0.212	1H:4V
22	1.22	3.8	5.00	−0.488	−0.283	1H:4V
23	1.22	3.8	5.00	−0.610	−0.353	1H:4V
24	1.48	4.6	6.02	−0.888	−0.388	1H:4V
25	1.22	3.8	5.00	−0.732	−0.424	1H:4V
26	1.22	3.8	5.00	−0.854	−0.495	1H:4V
27	0.83	3.7	5.00	−0.747	−0.525	1H:4V
28	1.22	3.8	5.00	−0.976	−0.566	1H:4V
29	1.22	3.8	5.00	−1.098	−0.636	1H:4V
30	0.56	3.5	5.06	−0.056	−0.071	1H:6V
31	1.22	3.8	5.00	−0.061	−0.053	1H:6V
32	1.22	3.8	5.00	−0.122	−0.106	1H:6V
33	1.22	3.8	5.00	−0.244	−0.212	1H:6V
34	0.80	4.7	7.20	−0.320	−0.239	1H:6V
35	1.22	3.8	5.00	−0.366	−0.318	1H:6V
36	1.22	3.8	5.00	−0.488	−0.424	1H:6V
37	0.56	3.5	5.06	−0.560	−0.710	1H:6V
38	1.22	3.8	5.00	−0.610	−0.530	1H:6V
39	0.80	4.7	7.20	−0.640	−0.477	1H:6V
40	1.22	3.8	5.00	−0.732	−0.636	1H:6V
41	1.22	3.8	5.00	−0.854	−0.742	1H:6V

Hughes and Nadal (2009) developed a discharge relationship for wave and surge overtopping under a variety of flow conditions using a small-scale physical levee model. Testing took place in a 45 m flume with the levee crest roughly 32 m from the wave board. The levee is shown in Figure 2.3. Overtopping water was recirculated to an input manifold seaward of the levee allowing for long duration testing. Flow thickness was recorded by pressure cells inlaid on the crest and landward slope as shown in Figure 2.4.

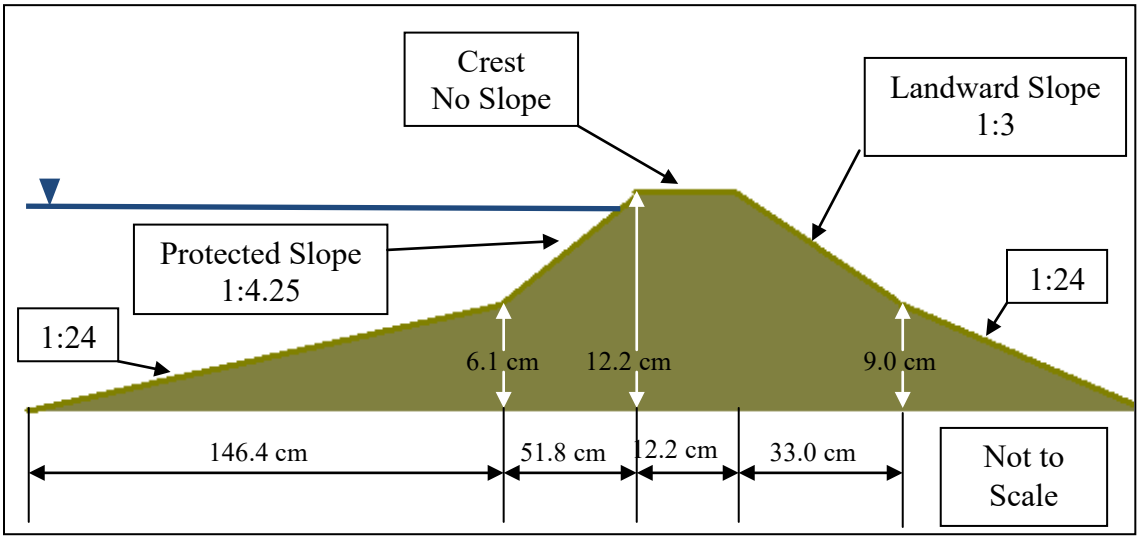

Figure 2.3 Hughes and Nadal (2009) Levee Profile

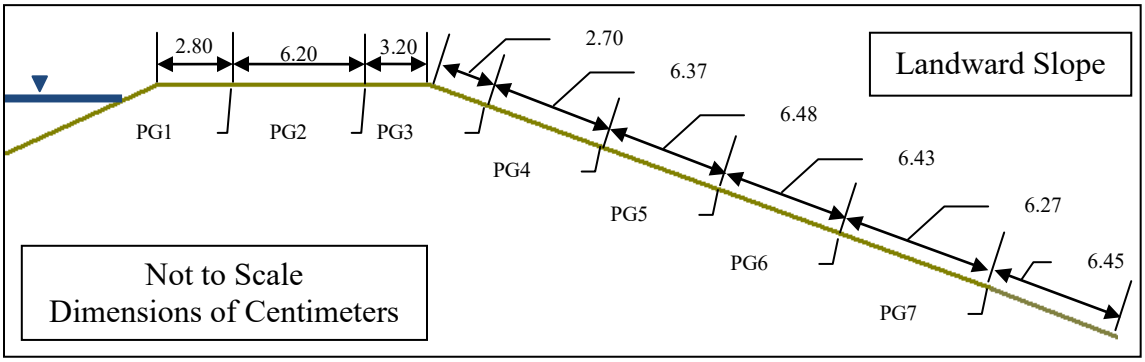

Figure 2.4 Hughes and Nadal (2009) Pressure Cell Locations

A Laser Doppler Velocimeter (LDV) system recorded velocity above the pressure gauge mounted at PG2. Data were collected at 50-Hz during 27 runs lasting five minutes. Each run was a variation of the following prototype conditions which can be scaled to model size using a 25:1 length scale.

- Freeboard: -0.3, -0.9, and -1.5 m
- Significant Wave Height: 0.9, 1.8, and 2.7 m
- Peak Wave Period: 6, 10, and 14 s

Hughes and Nadal (2009) measured depth and velocity at PG2 of Figure 2.4, calculated discharge, and used flow thickness recorded at PG4 and PG7 to estimate velocity. This method of velocity estimation assumes instantaneous discharge does not significantly change over short distances along the landward slope, which is a valid assumption (Hughes and Shaw, In Press). Hughes and Nadal (2009) developed Equation 2-38 for combined overtopping discharge. Figure 2.5 plots Equation 2-38 against Equation 2-37 showing Reeve et al. (2008) over predicts combined discharge for a given freeboard and significant wave height.

$$\frac{q_{ws}}{\sqrt{gH_{m0}}} = 0.034 + \left(-\frac{R_c}{H_{m0}}\right)^{1.58} \tag{2-38}$$

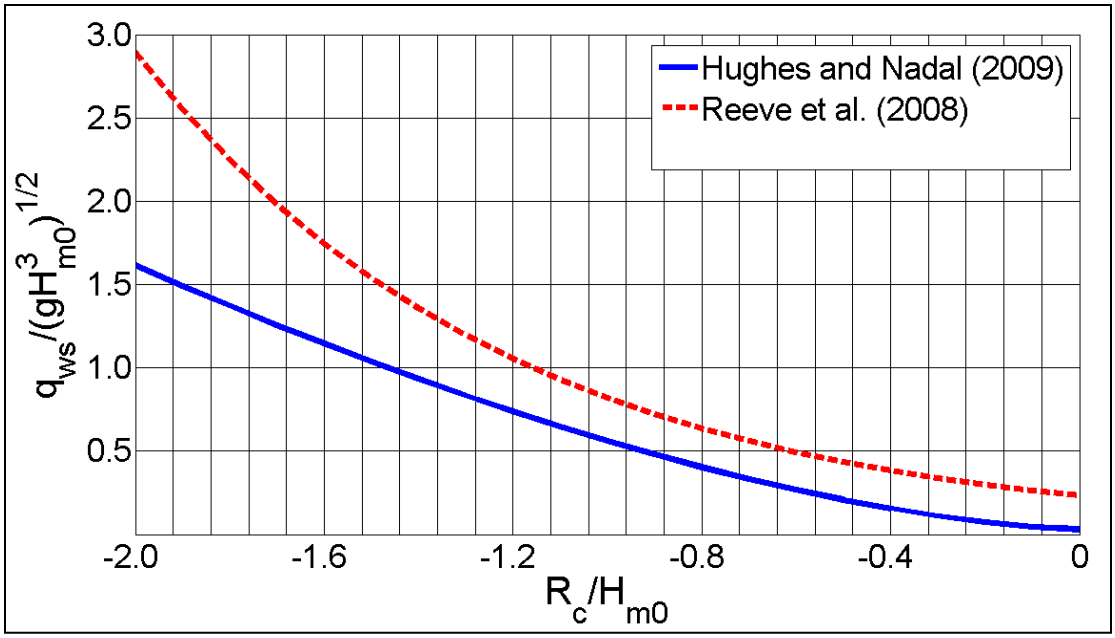

Figure 2.5 Hughes and Nadal (2009) Combined Overtopping Discharge Comparison

Hughes and Nadal (2009) developed Equations 2-39 and 2-40 to estimate average flow thickness and velocity on the landward slope using a line of best fit and the Chezy equations on data recorded during testing. These equations are only applicable to landward slopes of 1V:3H with a small friction factor.

$$d_m = 0.4\left[\frac{1}{gsin(\theta)}\right]^{1/3} q_{ws}^{2/3} \quad (2\text{-}39)$$

$$v_m = 2.5\left(q_{ws}gsin(\theta)\right)^{1/3} \quad (2\text{-}40)$$

where:

d_m = Average Flow Thickness on Landward Slope (*Length*)
q_{ws} = Combined Overtopping Unit Discharge (*Volume/Time per Length*)
v_m = Mean Velocity on Landward Slope (*Length*/*Time*)

Hughes and Shaw (In Press) examined instantaneous discharge of surge and combined overtopping on the levee presented in Figures 2.3 and 2.4. Data were collected

at 100-Hz during 9 runs lasting ten minutes. Each run was a variation of prototype conditions listed on page 24 of this thesis. Flow thickness and velocity were measured at PG2 and PG6 of Figure 2.4 to test the hypothesis that "instantaneous discharge for combined wave and surge overtopping is conserved between the levee crest and landward slope" (Hughes and Shaw, In Press). The difference in unit root-mean-squared instantaneous discharge (Δq_{rms}) is typically less than a quarter percent of the total combined overtopping discharge as shown in Table 2.6.

Table 2.6 Hughes and Shaw (2011) Combined Overtopping Root-Mean-Squared Discharge Difference between Gauges 2 and 6

Run	Δq_{rms} (m^3/s per m)	**% of Combined Overtopping Discharge**
13	0.0009	0.21
14	0.0019	0.24
15	0.0031	0.25
16	0.0017	0.08
17	0.0027	0.12
18	0.0038	0.15
19	0.0009	0.03
20	0.0015	0.04
21	0.0033	0.10

2.4 Shear Stress Due to Overtopping

Shear stress is typically defined as a function of depth and slope in open channel flow (Wurbs and James 2002). Equation 2-41 describes shear stress on a channel bed in steady, uniform flow.

$$\tau = \gamma_w h S_f \quad (2\text{-}41)$$

where:

τ = Shear Stress (*Force*/*Area*)
γ_w = Fluid Specific Weight (*Force*/*Volume*)
S_f = Slope of Energy Grade Line (*Length*/*Length*)

Equation 2-41 is valid for steady flow on small channel slopes where terminal velocity has been reached. However, a levee's landward slope is typically considered steep because *sin(θ)* is greater than 0.01 (Henderson 1966, Hughes 2009, Hughes and Nadal 2009). Combined overtopping flow is unsteady and non-uniform and Equation 2-41 may not account for spatial and temporal changes in depth and velocity.

Conservation of mass and conservation of momentum equations can be used to describe fluid flow. Conservation of mass is commonly referred to as the continuity equation, and states the change of mass within a control volume is equal to the difference between inflow and outflow of mass. Conservation of momentum (i.e., the equations of motion) describes the forces acting on a body (fluid or solid) and the resultant accelerations. Navier-Stokes equations are a set of differential equations describing viscous, incompressible flow and can be used to solve for shear stress. When used in combination with the continuity equation, Navier-Stokes equations "provide a complete mathematical description of the flow of incompressible Newtonian fluids" (Munson et al. 2006). The continuity and momentum equations can be used to solve for shear stress.

As previously mentioned, the continuity equation is defined as fluid into a control volume equal to fluid leaving plus fluid stored. Munson et al. (2006) expresses the continuity equation by accounting for control volume as per Equation 2-42. This

equation accounts for a change in mass within the control volume in addition to mass flowing through the control volume.

$$\frac{\partial}{\partial t}\int_{cv}\rho d\forall + \int_{cs}\rho V \cdot \hat{n} dA = 0 \tag{2-42}$$

where:

$\forall$ = Volume
$\check{n}$ = Normal Direction
cv = Control Volume
cs = Control Surface
A = Cross-sectional Area of Flow

The net mass flow rate (Equation 2-42) can be described using Cartesian coordinates using Equation 2-43. The full continuity equation relates density and velocity to describe conservation of mass, Equation 2-44. Equation 2-44 is a reconfiguration of Equation 2-43. The x, y, and z directions refer to Figure 1.1 unless otherwise specified.

$$Net\ Rate\ of\ Mass\ Outflow = \left[\frac{\partial(\rho u)}{\partial x} + \frac{\partial(\rho v)}{\partial y} + \frac{\partial(\rho w)}{\partial z}\right]\Delta x \Delta y \Delta z \tag{2-43}$$

$$\frac{\partial \rho}{\partial t} + \frac{\partial(\rho u)}{\partial x} + \frac{\partial(\rho v)}{\partial y} + \frac{\partial(\rho w)}{\partial z} = 0 \tag{2-44}$$

where:

u = Velocity in the Horizontal x Direction
v = Velocity in the Horizontal y Direction
w = Velocity in the Vertical z Direction

In most applications water is considered incompressible which means density is a constant and can be largely ignored (Panton 2005). The continuity equation can be written as Equation 2-45 for incompressible flows.

$$\frac{\partial u}{\partial x} + \frac{\partial v}{\partial y} + \frac{\partial w}{\partial z} = 0 \tag{2-45}$$

The shallow water (Saint-Venant) equations are a variation of Navier-Stokes that can be applied under the following conditions (Strum 2001):

1) Vertical accelerations are negligible
2) Hydrostatic pressure distribution
3) Small channel bottom slope
4) Stable channel bed
5) One dimensional flow
6) Bed friction does not change during steady and unsteady flow.

The shallow water conservation of mass equation relates changes in depth to changes in discharge using Equation 2-46 where the x-direction is parallel and y-direction is perpendicular to the channel bed. Equation 2-46 can be used with the momentum equation to estimate shear stress.

$$\frac{\partial y}{\partial t} + \frac{\partial q}{\partial x} = 0 \tag{2-46}$$

The momentum equation examines body and surface force effects on momentum. Body forces act within a control volume, such as gravity, and surface forces act on the control volume boundary, such as shear stress (Panton 2005). Munson et al. (2006) expresses the momentum equations in terms of volume, Equation 2-47.

$$\sum F_{cv} = \frac{\partial}{\partial t}\int_{cv} V\rho d\forall + \int_{cs} V\rho V \cdot \hat{n} dA \tag{2-47}$$

where:

F_{cv} = Resultant Force Acting on Fluid in Control Volume

Equation 2-47 can be rewritten as force or mass multiplied by acceleration with a finite control volume and setting mass equal to the differential mass, Δm. Gravity and other body forces can be described using Equation 2-48. The acceleration used is gravity for this example but can be any body force acceleration.

$$\Delta F_b = (\Delta m)g \tag{2-48}$$

where:

ΔF_b = Change in Body Force

Surface forces act in the normal, perpendicular, direction and shear stress is applied tangentially, parallel, to the control surface. Normal stresses are estimated by Equation 2-49 and act orthogonal to the control surface. Shear stresses are estimated by Equations 2-50 and 2-51 which are perpendicular to each other and act along the control surface.

$$\sigma_n = \lim_{\delta A \to 0} \frac{\Delta F_n}{\Delta A} \tag{2-49}$$

$$\tau_1 = \lim_{\delta A \to 0} \frac{\Delta F_1}{\Delta A} \tag{2-50}$$

$$\tau_2 = \lim_{\delta A \to 0} \frac{\Delta F_2}{\Delta A} \tag{2-51}$$

where:

σ_n = Normal Stress
τ_1 = Shear Stress along Direction 1
τ_2 = Shear Stress along Direction 2
F_n = Normal Force
F_1 = Force in Direction 1
F_2 = Force in Direction 2

Equation 2-52 reduces Equation 2-49 through 2-51 to a single equation describing surface forces in the x direction. An example of force directions is shown in Figure 2.6.

$$\delta F_{sx} = \left(\frac{\partial \sigma_{xx}}{\partial x} + \frac{\partial \tau_{yx}}{\partial y} + \frac{\partial \tau_{zx}}{\partial z}\right) \Delta x \Delta y \Delta z \tag{2-52}$$

where:

F_{sx} = Surface Force Acting on x Plane
σ_{xx} = Normal Force Acting on x Plane
τ_{yx} = Shear Stress Acting on x Plane in y Direction
τ_{zx} = Shear Stress Acting on x Plane in z Direction

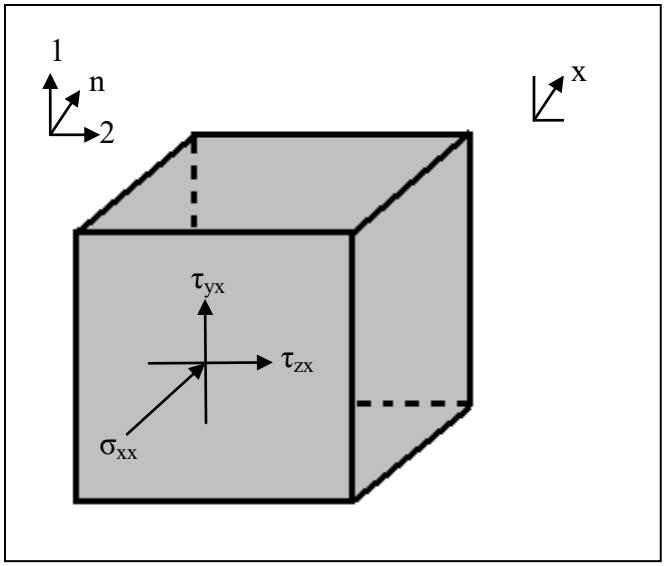

Figure 2.6 Example of Shear and Normal Force Directions

Body and surface forces can be used to represent the equation of motion in the x direction, Equation 2-53. Equation 2-53 can also be solved in y and z directions by adjusting the direction of forces and motion.

$$\rho g_x + \frac{\partial \sigma_{xx}}{\partial x} + \frac{\partial \tau_{yx}}{\partial y} + \frac{\partial \tau_{zx}}{\partial z} = \rho\left(\frac{\partial u}{\partial t} + u\frac{\partial u}{\partial x} + v\frac{\partial u}{\partial y} + w\frac{\partial u}{\partial z}\right) \quad (2\text{-}53)$$

The Saint-Venant equation of motion describes the friction slope as equal to bed slope minus the change in depth over space and the change in velocity over space and time, Equation 2-54, and is a revision of Equation 2-53. Equation 2-55 describes the relation of friction slope to shear stress.

$$S_f = S_0 - \frac{\partial y}{\partial x} - \frac{v}{g}\frac{\partial v}{\partial x} - \frac{1}{g}\frac{\partial v}{\partial t} \tag{2-54}$$

$$S_f = \frac{\tau_0}{\gamma_w R} \tag{2-55}$$

where:

S_f = Friction Slope (*Length*/*Length*)
S_0 = Channel Slope (*Length*/*Length*)
τ_0 = Average Shear Stress (*Force*/*Area*)

Equation 2-54 is not applicable to levees due to steep slopes on the landward and seaward sides. However, as shown in Nadal and Hughes (2009), Equation 2-54 may be applied to a wide channel with steep slopes if the major axis is tilted to the levee slope as shown in Equation 2-56.

$$S_f = \frac{\tau_0}{\gamma h} = \sin\theta - \frac{\partial h}{\partial s_D} - \frac{\partial}{\partial s_D}\left(\frac{v^2}{2g}\right) - \frac{1}{g}\frac{\partial v}{\partial t} \tag{2-56}$$

where:

s_D = Down Slope Coordinate

Equation 2-56 can be rearranged to solve for shear stress in unsteady, non-uniform flow, Equation 2-57. Shear stress solved by Equation 2-57 is the average stress between points 1 and 2.

$$\tau_0 = \gamma_w h_{12}\left[\sin\theta - \frac{\partial h}{\partial s} - \frac{\partial}{\partial s}\left(\frac{v^2}{2g}\right) - \frac{1}{g}\frac{\partial v}{\partial t}\right] \tag{2-57}$$

where:

τ_0 = Average Shear Stress (*Force*/*Area*)
h_{12} = Average Depth between Two Points (*Length*)

Equation 2-57 may be simplified to Equations 2-58 and 2-59. Equation 2-58 assumes steady, uniform flow, averages the depth between two points, and is a variation

of 2-41. Equation 2-59 assumes unsteady, uniform flow by considering depth differences at points 1 and 2.

$$\tau_{0,mean} = \gamma_w d_m \sin\theta \tag{2-58}$$

$$\tau_0 = \gamma_w h_{12}\left[\sin\theta - \frac{\partial h}{\partial s}\right] \tag{2-59}$$

where:

d_m = Mean Depth Perpendicular to Channel Slope

Equation 2-57 is a derivation of Saint-Venant equations used to calculate shear stress as a function of depth and velocity. Equations 2-58 and 2-59 account only for depth and slope while Equation 2-57 is a function of slope, change in depth over space, and change in velocity over space and time. The third term on the right hand side in Equation 2-57 is the convective acceleration (acceleration over distance) and the fourth term is temporal acceleration (acceleration over time).

Nadal and Hughes (2009) estimated shear stress using data from Hughes and Nadal (2009). The convective acceleration term was estimated by determining the difference in velocity between PG4 and PG7; see Figure 2.4. The temporal acceleration term was estimated by determining the difference in velocity divided by the time shift required to align flow thickness and velocity peaks at PG4 and PG7. Empirical relationships between peak shear stress parameters and root-mean-square wave height are shown by Equations 2-60 through 2-64.

$$\tau_{0,1/3} = 0.53\gamma_w H_{rms} \quad (2\text{-}60)$$

$$\tau_{0,1/10} = 0.69\gamma_w H_{rms} \quad (2\text{-}61)$$

$$\tau_{0,1/100} = 0.93\gamma_w H_{rms} \quad (2\text{-}62)$$

$$d_m = 0.4\left[\frac{1}{g\sin\theta}\right]^{1/3}(q_{ws})^{2/3} \quad (2\text{-}63)$$

$$\frac{H_{rms}}{d_m} = 3.43 * exp\left(\frac{R_c}{H_{m0}}\right) \quad (2\text{-}64)$$

where:

$\tau_{0,1/3}$ = Average 1/3 Highest Shear Stresses (*Force*/*Area*)
$\tau_{0,1/10}$ = Average 1/10 Highest Shear Stresses (*Force*/*Area*)
$\tau_{0,1/100}$ = Average 1/100 Highest Shear Stresses (*Force*/*Area*)
H_{rms} = Root-mean-square Wave Height (*Length*)

Average 1/100 highest shear stress can be considered the design shear stress for levees subjected to combined overtopping. Prototype-scale Design shear stresses of nearly 15,000 N/m^2 were estimated during testing. Figure 2.7 displays Equations 2-60 through 2-62 which are dimensionless.

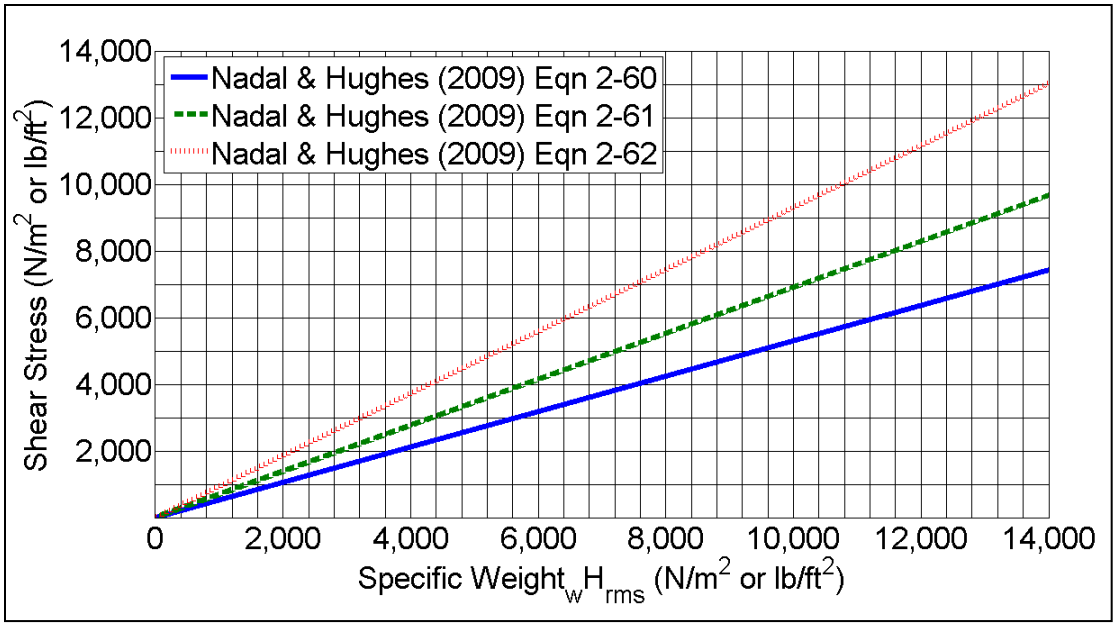

Figure 2.7 Nadal and Hughes (2009) Shear Stress Estimation

Briaud et al. (2008) examined soil erodibility caused by overtopping during Hurricane Katrina. This study focused on soil type and construction methods and their relationship to erosion. A Reynolds-averaged Navier-Stokes (CHEN3D) numerical model was used to estimate three-dimensional free surface flow over a levee with a 5 m crest and 1V:5H landward and seaward slopes. The water surface was placed 1 m above the levee crest before the simulation started, and gravity along with a 3 m/s constant current pushed flow over the levee. Shear stress values from CHEN3D were compared to soil samples to determine erosion rates. The numerical model estimated velocities of nearly 12 m/s near the levee toe, and shear stresses between 50 and 60 N/m^2. These values are much lower than Nadal and Hughes (2009) and shear stresses predicted by this thesis; see Section 4.3. This difference in shear stress can likely be attributed to the difference in landward slope (1V:3H for Nadal and Hughes (2009) and in this thesis) and

to the equations used to estimate shear stress. Briaud et al. (2008) used Equations 2-65 and 2-66 to while Nadal and Hughes (2009) and this thesis use Equations 2-57, 2-58, and 2-59. The values provided by Briaud et al. (2008) were considered too low to be useful for the needs of this thesis.

$$\tau = \eta \frac{\partial \gamma}{\partial t} = \eta \frac{\partial v_x}{\partial z} \tag{2-65}$$

$$\gamma = \frac{\partial u}{\partial z} \tag{2-66}$$

where:

γ = Shear Strain

The Federal Highway Administration (2005) developed Table 2.7 as a reference for designing flexible drainage channel linings. Values listed in Table 2.7 are shown to gain a perspective on the permissive shear stress for typical erosion protection materials used in open channel flow. The plasticity index (*PI*) is a range of water content in percent over which a soil will exhibit plastic behaviors (Budhu 2008). D_{75} and D_{50} represent average grain size of sand, gravel, and riprap. D_{75} is the 75% largest grain size and D_{50} is the median grain size.

Table 2.7 Permissible Shear Stress for Typical Natural Materials

Material		**Permissible Shear Stress** (N/m^2)
Bare Soil Cohesive ($PI = 10$)	Clayey Sands	1.8 to 4.5
	Inorganic Silts	1.1 to 4.0
	Silty Sands	1.1 to 3.4
Bare Soil Cohesive ($PI \geq 20$)	Clayey Sands	4.5
	Inorganic Silts	4.0
	Silty Sands	3.5
	Inorganic Clays	6.6
Bare Soil Non-Cohesive ($PI < 10$)	Finer than Coarse Sand, $D_{75} < 1.3$ mm	1.0
	Finer Gravel, $D_{75} = 7.5$ mm	5.6
	Gravel, $D_{75} = 15$ mm	11
Gravel Mulch	Coarse Gravel, $D_{50} = 25$ mm	19
	Very Coarse Gravel, $D_{50} = 50$ mm	38
Rock Riprap	$D_{50} = 0.15$ m	113
	$D_{50} = 0.30$ m	227

CHAPTER III

EXPERIMENTAL PROGRAM

Testing took place at the Coastal and Hydraulics Laboratory (CHL) of ERDC, with the author of this thesis assisting in the testing. Previous levee overtopping studies at CHL include Hughes (2008), Hughes and Nadal (2009), Nadal and Hughes (2009), and Hughes and Shaw (In Press). The experimental program presented in this thesis is an extension of previous levee overtopping work performed by Hughes and Nadal (2009). Testing conditions, the model levee presented in Figure 2.3, and gauge placement shown in Figure 2.4 were developed by Hughes and Nadal (2009) and used in this work. As a result, Chapter II figures will be referenced and not shown in Chapters III and IV for brevity.

3.1 Similitude of Testing

Large-scale tests are typically expensive and require large areas to perform experiments. These constraints can be alleviated by using scaled models, which are representations of the prototype or full size system. Base units for typical models are force, length, and time which are scaled to a suitable size as per Equation 3-1.

$$N_x = \frac{X_p}{X_m} \tag{3-1}$$

where:

N_x = Prototype to Model Scale Ratio of Parameter X
X_p = Prototype Value of Parameter X
X_m = Model Value of Parameter X

Similitude between a model and prototype is developed by scaling geometry, kinematic motion, and dynamic forces. A model is geometrically similar to a prototype if its dimensions are scaled using the same factor. Kinematic similarity requires a scale motion factor so that model and prototype particle movements are in the same direction. Dynamic (or kinetic) similarity requires a scale mass and force factor between model and prototype. Dynamic similitude is derived for fluid mechanics from Newton's second law which is represented by Equation 3-2 (Skoglund 1967, Hughes 1993).

$$F_i = F_g + F_\mu + F_\sigma + F_e + F_{pr} \tag{3-2}$$

where:

F_i = Inertial Force
F_g = Gravitational Force
F_μ = Viscous Force
F_σ = Surface Tension Force
F_e = Elastic Compression Force
F_{pr} = Pressure Force

Overall dynamic similitude is represented by Equation 3-3 which shows the ratio of model to prototype forces must match the inertia force ratio.

$$\frac{(F_i)_p}{(F_i)_m} = \frac{\left(F_g + F_\mu + F_\sigma + F_e + F_{pr}\right)_p}{\left(F_g + F_\mu + F_\sigma + F_e + F_{pr}\right)_m} \tag{3-3}$$

Perfect similitude requires the scale factor be the same for each dynamic similitude force ratio; see Equation 3-4.

$$\frac{(F_i)_p}{(F_i)_m} = \frac{(F_g)_p}{(F_g)_m} + \frac{(F_\mu)_p}{(F_\mu)_m} + \frac{(F_\sigma)_p}{(F_\sigma)_m} + \frac{(F_e)_p}{(F_e)_m} + \frac{(F_{pr})_p}{(F_{pr})_m} \quad (3\text{-}4)$$

No existing fluid can be scaled in perfect similitude therefore concessions are made in hydraulic similitude that neglect or minimize certain aspects. Equations 3-5 through 3-10 are used in varying combinations to scale hydraulic models.

$$F_r = \frac{V}{\sqrt{gL}} = Froude\ Number \quad (3\text{-}5)$$

$$\frac{\rho LV}{\mu} = Reynolds\ Number \quad (3\text{-}6)$$

$$\frac{\rho LV^2}{\sigma} = Weber\ Number \quad (3\text{-}7)$$

$$\frac{\rho V^2}{E} = Cauchy\ Number \quad (3\text{-}8)$$

$$\frac{p}{\rho V^2} = Euler\ Number \quad (3\text{-}9)$$

$$\frac{L}{Vt} = Strouhal\ Number \quad (3\text{-}10)$$

where:

ρ = Fluid Density (*Mass*/*Volume*)
L = Dimension (*Length*)
μ = Dynamic Viscosity ((*Mass*/ (*Time***Length*)
σ = Surface Tension Force (*Mass*/*Time*^{2})
E = Elastic Compression Force (*Force*/*Area*)
p = Pressure Force (*Force*/*Area*)

The Froude number is considered the most important hydraulic criterion for all but a few free surface flows because inertial forces in free surface flows are typically balanced by gravity. The Reynolds number compares inertial force to viscous fluid force and is used when viscous forces are dominant. The Weber number relates inertial force

to surface tension force typically seen in very small models. The Cauchy number is a function of inertial force and compressive force but is rarely used because water is considered incompressible. The Euler number takes into account pressure. The Strouhal number represents inertial forces caused by convective and temporal acceleration; flow is considered unsteady if the acceleration terms are not constant (Hughes 1993).

Levee overtopping models can be considered short wave coastal models where "the Froude and Reynolds number are important..because similarity of one of these numbers combined with geometric similarity, provides the necessary conditions for hydrodynamic similitude in an overwhelming majority of coastal models" (Hughes 1993). A short-wave hydrodynamic model must be geometrically undistorted with Euler, Froude, Reynolds, and Strouhal ratios similar between model and prototype scales. "These four conditions are the similitude criteria for modeling free surface flows governed by the equations of motion…the model must be geometrically undistorted, and it is assumed that surface tension and compressibility effects are negligible because these forces were not included in the basic equations of motion" (Hughes 1993). The Euler ratio is met if a model is geometrically similar and Froude, Reynolds, and Strouhal ratios are appropriately scaled.

Several factors were considered to select an appropriate scale ratio for testing within this experimental program that is described in Section 3.2, including flume size and recording capabilities of measurement devices. A model-to-prototype length ratio of 1 to 25 was used during testing. As shown in the following Froude number example this creates a time ratio of 1 to 5 since gravity was not scaled.

$$F_r = \left(\frac{V}{\sqrt{gL}}\right)_p = \left(\frac{V}{\sqrt{gL}}\right)_m = \frac{(L/T)_p}{\sqrt{L_p}} = \frac{(L/T)_m}{\sqrt{L_m}} = \frac{(L/T)_p}{\sqrt{L_p}} = \frac{(L/T)_m}{\sqrt{L_m}}$$

$$F_r = \frac{1/1}{\sqrt{1}} = \frac{25/T_m}{\sqrt{25}} \qquad \text{where:} \quad T_m = \frac{25}{\sqrt{25}} = 5$$

3.2 Experimental Setup

Testing was carried out in a 0.91 m wide by 0.91 m deep, and 45.7 m long flume; see Figure 3.1 for a schematic of the experimental setup. A model levee was placed approximately 32 meters from the wave board. Water would flow over the levee into a reservoir, and was circulated by a pump approximately 8 meters from the wave board.

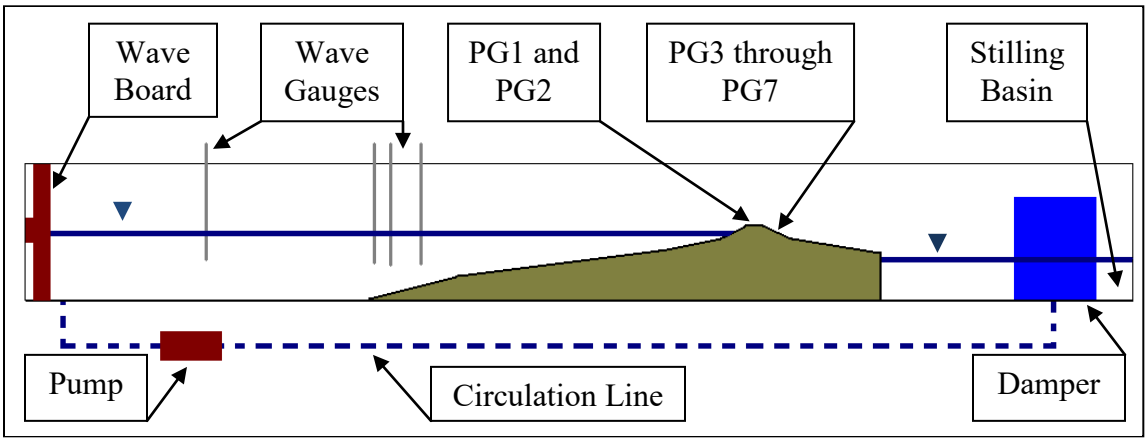

Figure 3.1 Wave Flume Layout

A flow damper was placed above the pump intake to reduce disturbances and allow for easy reading of reservoir water levels; Figure 3.2. The horsehair damper was placed downstream of the levee to avoid pump capitation and to reduce disturbances in the stilling basin allowing for reliable depth readings.

Figure 3.2 Horse Hair Damper

The USACE New Orleans District and ERDC researchers developed dimensions typical to levees along the Gulf coast shown in Figure 2.3 (Hughes and Nadal 2009). Care was taken to design a model that allowed for maximum flow depth for wave development and a large negative freeboard to keep waves from spilling out of the flume (Hughes 2009). The model levee was constructed of high-density foam by ERDC's Model Shop. Pressure gauges were inlaid at points 1 through 7 (PG1 through PG7 in Figure 2.4) on the levee crest and landward slope. Pressure gauges were mounted approximately 8 cm from the flume wall so velocity measurements could be taken with minimal interference; Figure 3.3. Inlaid pressure gauges minimize flow obstructions and allow flow thickness measurements on a continual basis.

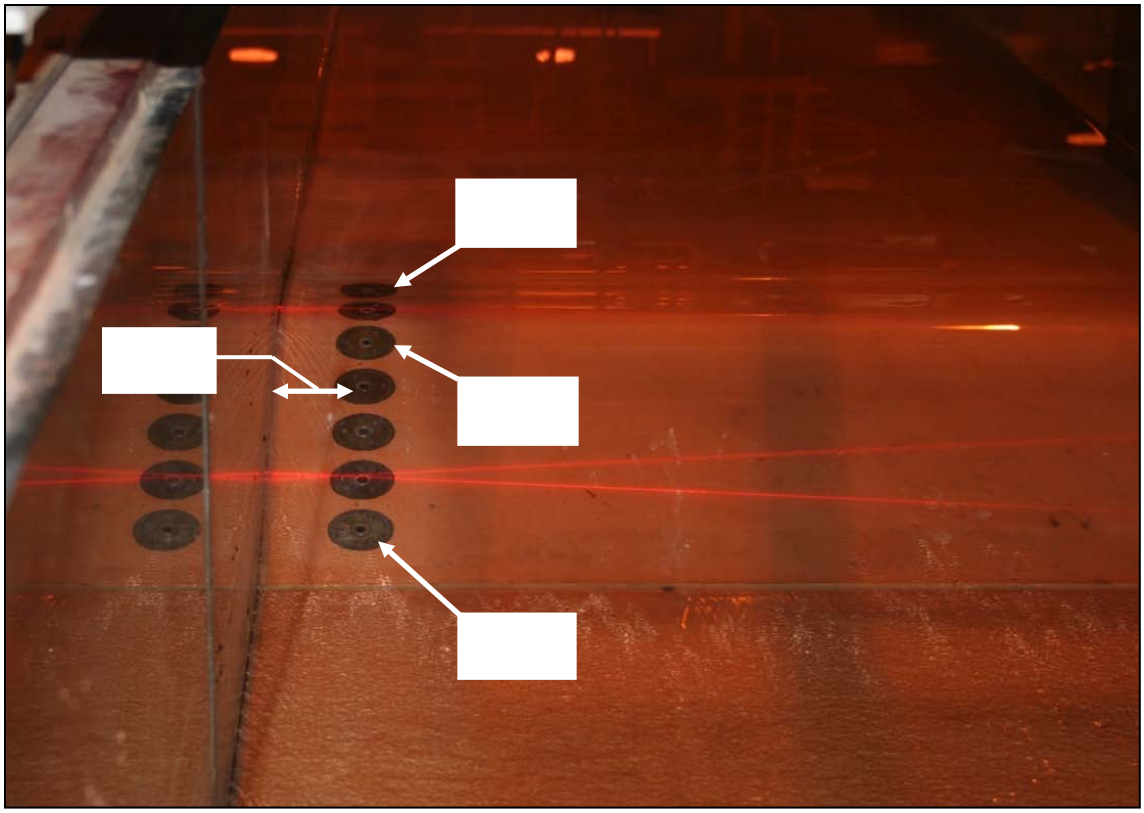

Figure 3.3 Pressure Gauge Placement

Wave gauges were mounted at 4 locations to measure wave heights and periods; Figure 3.1. The wave gauge array was analyzed for irregular wave reflection using the method of Goda and Suzuki (1976). Wave gauge spacing was tuned to cover the entire frequency range of incident and reflected waves. In these experiments waves could be reflected by the levee which would affect wave height measured by the wave gauge array. Incident waves are developed through typical generator processes (i.e. wind or wave board) and have not been affected by structures that cause reflection. Reflected waves are those that have changed direction after bouncing off of a structure.

Velocities were recorded using a Dantec LDV system consisting of two lasers, a processor, and a laptop computer with BSA Flow Software Version 4.50. Dantec

manufactures all the LDV components and provides factory calibration of the lasers. A BSA F30 processor was included in the system which can record velocities to a maximum of 68 m/s. The BSA Flow Software Version 4.50 utilizes a relatively user-friendly interface allowing for measurement configuration. The LDV system is a nonintrusive velocity measurement tool that measures velocity at a point in the water column. The BSA Software specifies the measurement capabilities of the lasers and records velocity measurements taken by the lasers as text files. BSA Software does not allow for user adjustment to laser calibration, but recording intervals and strength can be changed.

The non-coincident system setting records velocity independently at each laser, while the coincident mode records both lasers in unison. The coincident setting requires each laser to actively measure velocity before BSA Software records the data. The LDV system gathers data in dead time mode or burst mode. Burst mode collects data anytime a noticeable change in velocity occurs and dead time collects the first data burst per specified time bin. Other system variables include sample size, sample rate, sample time, velocity range, and laser voltage. Higher voltage increases resolution in poorly seeded water but may damage the lasers if ran for extended periods. Impurities in water enable the Doppler effect, and usually a seeding particle must be mixed with water. Titanium dioxide was used during testing, and it provided nearly perfect system response once properly mixed. The LDV system was calibrated by Dantec with no user adjustments available. Figure 3.4 shows the LDV setup during experimentation.

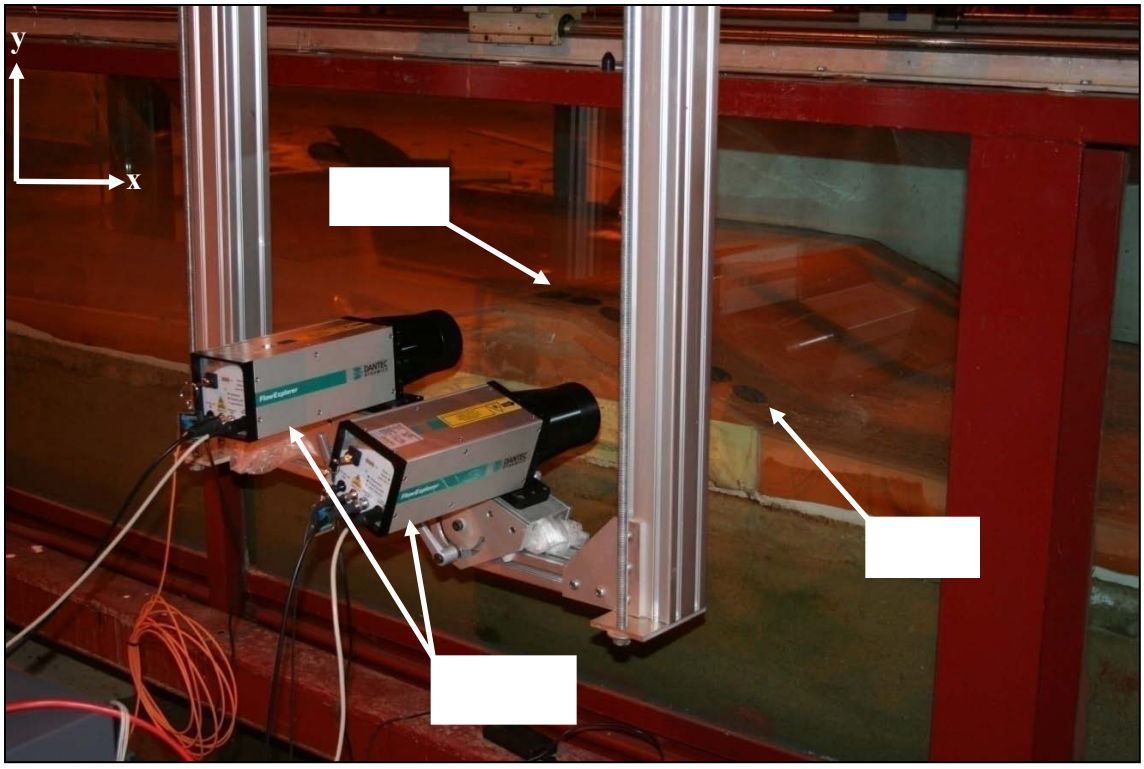

Figure 3.4 Laser Doppler Velocimeter Setup

ERDC researchers designed and built a carriage that allowed the laser to be moved in any direction; see Figure 3.4. Lasers were mounted to the carriage and could be adjusted vertically, horizontally, and rotated nearly 180° in addition to horizontal adjustments in the z direction. The carriage was outfitted with bolts allowing small adjustments using a wrench or drill with a socket bit.

3.3 Test Conditions

ERDC, in collaboration with the USACE New Orleans district and MSU researchers developed wave parameters that span probable combined overtopping conditions due to tropical storms in the Gulf of Mexico; see Table 3.1.

Table 3.1 Prototype-scale Test Parameters

Parameter	English Standard Units	Metric Units
Significant Wave Height	3, 6, and 9 feet	0.91, 1.83, and 2.74 meters
Peak Wave Period	6, 10, 14 seconds	6, 10, 14 seconds
Surge Above Crest	1, 3, and 5 feet	0.30, 0.91, and 1.52 meters

Irregular waves having significant wave height and peak wave period were produced by the wave board. Surge depth above the levee crest was regulated by adjusting the pump discharge. Combinations of the nine parameters gave 27 different runs as shown in Table 3.2. Run numbering began at 25 because runs 1 through 24 were recorded for a separate experiment using the same equipment where the author of this thesis was involved (Hughes and Shaw, In Press).

Prototype Parameters in Table 3.2 represent target wave characteristics for a full size levee overtopping event, and Model Parameters represent those of the scaled model used during testing to simulate the corresponding full size levee overtopping event. Each run lasted ten minutes (100-Hz sampling rate) and produced approximately 60,000 data points. Table 3.3 lists LDV variables for all runs. Tests results were collected in English standard units and converted to metric units during data preconditioning.

Table 3.2 Nominal Test Parameters by Run

Run	Prototype Parameters			Model Parameters		
	Wave Height	Wave Period	Negative Freeboard	Wave Height	Wave Period	Negative Freeboard
	(m)	*(s)*	*(m)*	*(cm)*	*(s)*	*(cm)*
25	0.91	6	0.30	3.7	1.2	1.2
26	0.91	10	0.30	3.7	2.0	1.2
27	0.91	14	0.30	3.7	2.8	1.2
28	1.83	6	0.30	7.3	1.2	1.2
29	1.83	10	0.30	7.3	2.0	1.2
30	1.83	14	0.30	7.3	2.8	1.2
31	2.74	6	0.30	11.0	1.2	1.2
32	2.74	10	0.30	11.0	2.0	1.2
33	2.74	14	0.30	11.0	2.8	1.2
34	0.91	6	0.91	3.7	1.2	3.7
35	0.91	10	0.91	3.7	2.0	3.7
36	0.91	14	0.91	3.7	2.8	3.7
37	1.83	6	0.91	7.3	1.2	3.7
38	1.83	10	0.91	7.3	2.0	3.7
39	1.83	14	0.91	7.3	2.8	3.7
40	2.74	6	0.91	11.0	1.2	3.7
41	2.74	10	0.91	11.0	2.0	3.7
42	2.74	14	0.91	11.0	2.8	3.7
43	0.91	6	1.52	3.7	1.2	6.1
44	0.91	10	1.52	3.7	2.0	6.1
45	0.91	14	1.52	3.7	2.8	6.1
46	1.83	6	1.52	7.3	1.2	6.1
47	1.83	10	1.52	7.3	2.0	6.1
48	1.83	14	1.52	7.3	2.8	6.1
49	2.74	6	1.52	11.0	1.2	6.1
50	2.74	10	1.52	11.0	2.0	6.1
51	2.74	14	1.52	11.0	2.8	6.1

Table 3.3 Laser Doppler Velocimeter Settings Used During Testing

Laser Voltage	1,000 V
Velocity Range	6 m/s
Velocity Center	3 m/s
Dead Time Data Collection	100 reading per second

3.4 Experimental Procedure

Surge overtopping discharge was calculated using Equation 2-1 to determine pump rates. A discharge gauge on the pump was used to determine the flow rate while the pump circulated flow until constant water surface elevations were read at all locations. Surge overtopping elevations were marked on the flume near the pump and in the flume reservoir for each negative freeboard event (0.3 m, 0.91 m, and 1.52 m). During surge overtopping the flume and flume reservoir water levels would remain constant, however during combined overtopping the pump was manually adjusted to compensate for unsteady wave overtopping and to bring reservoir water levels into equilibrium.

Lasers were positioned near the levee toe with laser 1 over gauge 4 (PG4) and laser 2 over gauge 7 (PG7), Figure 2.4, to record maximum velocity along the levee. Velocities were measured above the pressure gauges at the water columns midpoint during 0.91 m and 1.52 m negative freeboard levels. The lasers were placed above the flow during 0.30 m negative freeboard, because flow thickness was very shallow which caused inaccurate readings.

Pressure gauges were calibrated in the morning and afternoon by running a thin layer of water over the levee and setting the gauges to zero. Wave gauges were

calibrated each morning and zeroed before each run by moving the gauge center to water surface. The LDVs recorded velocity separately from the wave and pressure gauges, so a countdown was used to begin each run. This introduced a slight difference in starting times between the velocity and pressure measurements which is addressed in Section 3.5.

3.5 Data Preprocessing

All recorded data were preprocessed in MatLab®. Depth and velocity data were recorded separately requiring start time synchronization. Several other adjustments were made to the recorded depth and velocity data described in Sections 3.5.1 and 3.5.2. The runs were recorded in English standard units and converted to metric units during preprocessing.

3.5.1 Depth Preprocessing

Pressure gauges were zeroed twice each day of testing, but the gauges would deviate off of zero throughout the day. Minimizing the calibration errors was an iterative process where the minimum readings were adjusted to zero for each run and the adjustment factors were averaged for the calibration period. An example would be adjusting runs 25 through 30, which were tested in the afternoon, and using the same adjustment factor for each gauge on the six runs. PG5 recorded erratically and it was not analyzed further.

Pressure gauges recorded a force per unit area which was converted to a flow thickness measurement using Equation 3-11. Flow thickness was considered hydrostatic

at PG1 and PG2 on the levee crest (Equation 3-12), and was adjusted for a 1V:3H slope at PG3 through PG7 on the landward slope (Equation 3-13).

$$p = \frac{F}{A} = \rho g h \tag{3-11}$$

$$h = \frac{p}{\rho g} \tag{3-12}$$

$$h = \frac{1}{\cos(\beta)} \frac{p}{\rho g} \tag{3-13}$$

Depths were adjusted by visual inspection to move minimum depths to zero, Figure 3.5. Depths were adjusted for each run then averaged for morning and afternoon testing times.

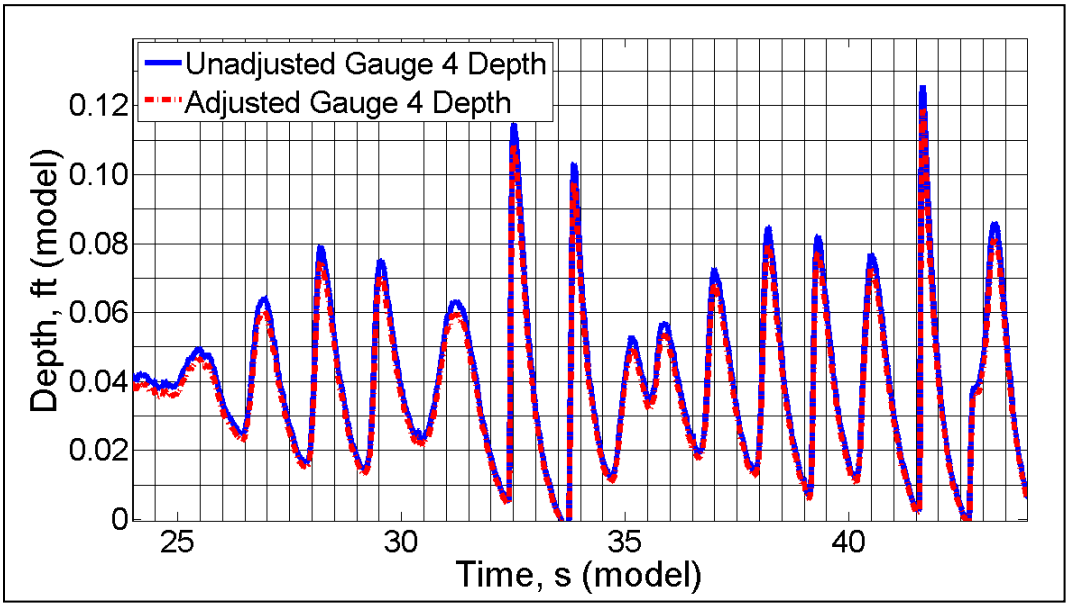

Figure 3.5 Run 28 Adjusted and Unadjusted Depths

A spike removal routine was implemented that removed pressure outliers. The removal routine was developed by the Disaster Prevention Research Institute to remove

signal noise in acoustic Doppler Velocimeters. Flow thickness at PG4 and PG7 was adjusted a final time by comparing unit discharge calculations with Equation 3-14. Since velocity measurements were considered more accurate than flow thickness measurements and since discharge at PG4 and PG7 during each run should be consistent, Flow thickness at PG7 was tweaked to match PG4 discharges.

$$q = v(h) \tag{3-14}$$

3.5.2 Velocity Preprocessing

Velocity was measured by the LDV system in dead time (records one reading per time bin) which produced non-uniformly spaced data, so the velocity data were interpolated to a uniformly spaced time series. Water levels would be below the lasers during surge overtopping with a target negative freeboard of 0.30 m and during wave troughs so no measurements were recorded. The LDV system would linearly connect the last valid point to the next valid point which made the waves appear to have a gradual linear rise. This was corrected by holding the last valid velocity constant over time until the next reading as shown in Figure 3.6.

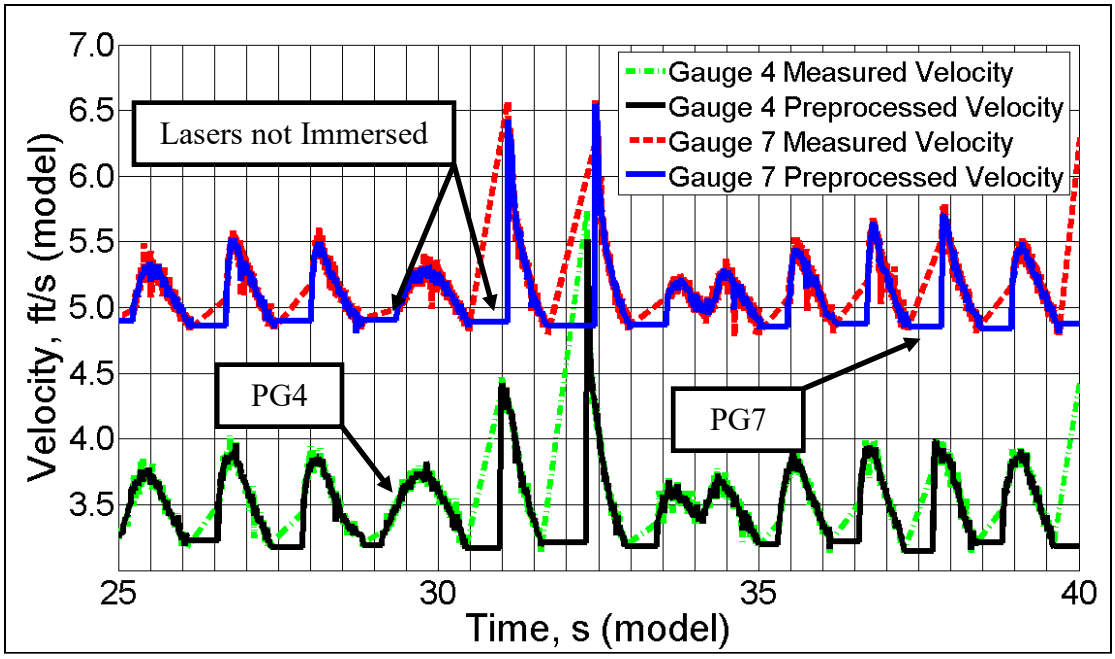

Figure 3.6 Run 37 Velocity Preprocessing

Occasional noise spikes were observed during velocity recordings in some runs. The outliers were typically two or three times larger than any other velocity peak, and were removed by visual inspection; see Figure 3.7. Depth and velocity were recorded using separate systems that did not have a simultaneous starting mechanism, as a result depth and velocity data were synchronized by aligning peaks. This was performed by minimizing the root-mean-square difference between flow thickness and velocity at PG4 and PG7 through a time shift; see Figure 3.8. In this figure the depth time series was temporarily scaled to the same magnitude as velocity to facilitate the overlay.

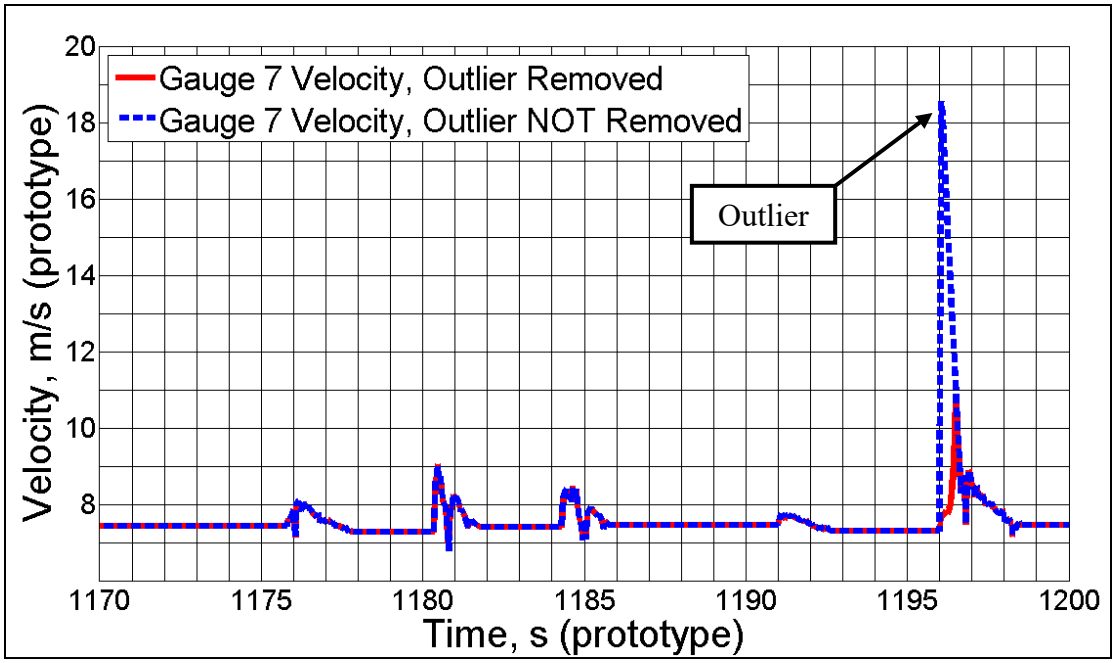

Figure 3.7 Run 28 Velocity Outlier Removal

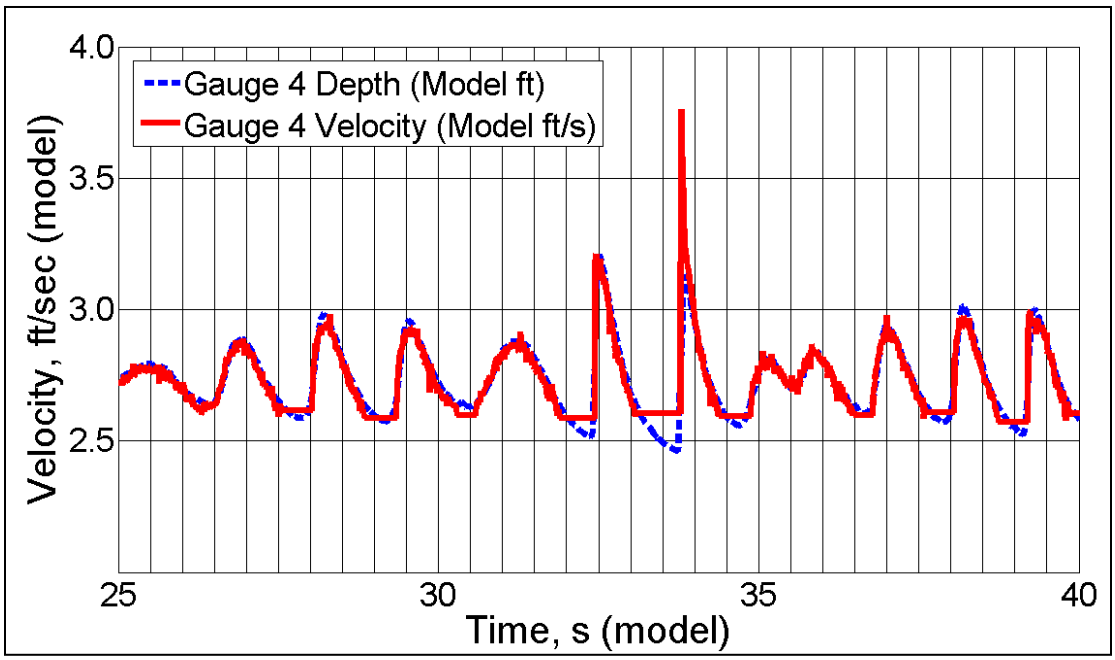

Figure 3.8 Run 37 Aligned Depth and Velocity Data

CHAPTER IV

ANALYSIS

Flow measurements were preprocessed into an acceptable format as discussed in Chapter III, and the data are analyzed in this chapter. These flow conditions (flow thickness, velocity, and discharge) were used to calculate average shear stress between PG4 and PG7 (Figure 2.4). Flow conditions were then used in conjunction with a numerical model to estimate shear stress along the levee crest and landward slope. All analyses were performed in MatLab®.

4.1 Data Adjustments

A time shift was used to synchronize start times of the depth and velocity recording systems as described in Section 3.5.2. Table 4.1 lists time shift alignment corrections for each run. Flow thickness was adjusted for each run and averaged for morning and afternoon testing times; see Table 4.2. Negative values represent a downward flow thickness adjustment and positive values represent an upward flow thickness adjustment in model meters.

Table 4.1 Model Time Shift Alignment Factors

Run	Model Time Shift (*s*)	Run	Model Time Shift (*s*)	Run	Model Time Shift (*s*)
25	0.59	34	0.29	43	0.19
26	-0.46	35	0.78	44	0.26
27	0.48	36	0.91	45	0.23
28	0.52	37	1.47	46	0.40
29	0.36	38	0.56	47	0.37
30	0.44	39	0.47	48	0.46
31	1.01	40	0.34	49	0.50
32	0.12	41	0.92	50	0.37
33	0.45	42	1.23	51	0.34

Table 4.2 Model Average Flow Thickness Adjustment

Runs	Model Flow Thickness Adjustment (*m*)					
	PG1	PG2	PG3	PG4	PG6	PG7
25 - 30	-0.00701	-0.00762	-0.00183	-0.00366	0.00396	0.00396
31 - 35	-0.00762	-0.01097	-0.00030	-0.00671	0.00365	0.00426
36 - 39	-0.00396	-0.00183	-0.03444	0.00152	0.00823	0.00091
40 - 41	-0.00549	-0.00457	0.00396	-0.00030	0.00883	0.00243
42 - 51	-0.00671	-0.00853	0.00548	-0.00305	0.00731	0.00457

Flow thickness at PG4 and PG7 were adjusted a final time by comparing unit discharge as per Equation 3-14. Average discharge for surge and combined overtopping were compared and PG7 flow thickness was adjusted to fit the data around an equilibrium line. Runs 25 and 27 were eliminated from further consideration because their discharge values did not align as shown in Figure 4.1. Runs 25 and 27 were excluded from further analyses because their average combined overtopping was found to be noticeably

different between PG4 and PG7. Including runs 25 and 27 in the analyses could have produced unrealistic flow thickness and velocity relationships especially considering the somewhat unreliable nature of the gauges during smaller magnitude overtopping testing. Surge overtopping average discharge is fairly consistent during each run, while the combined overtopping average discharge is more variable between PG4 and PG7 during each run. Average surge overtopping flow thickness is provided in Table 4.3 with PG5 excluded due to inconsistent recordings.

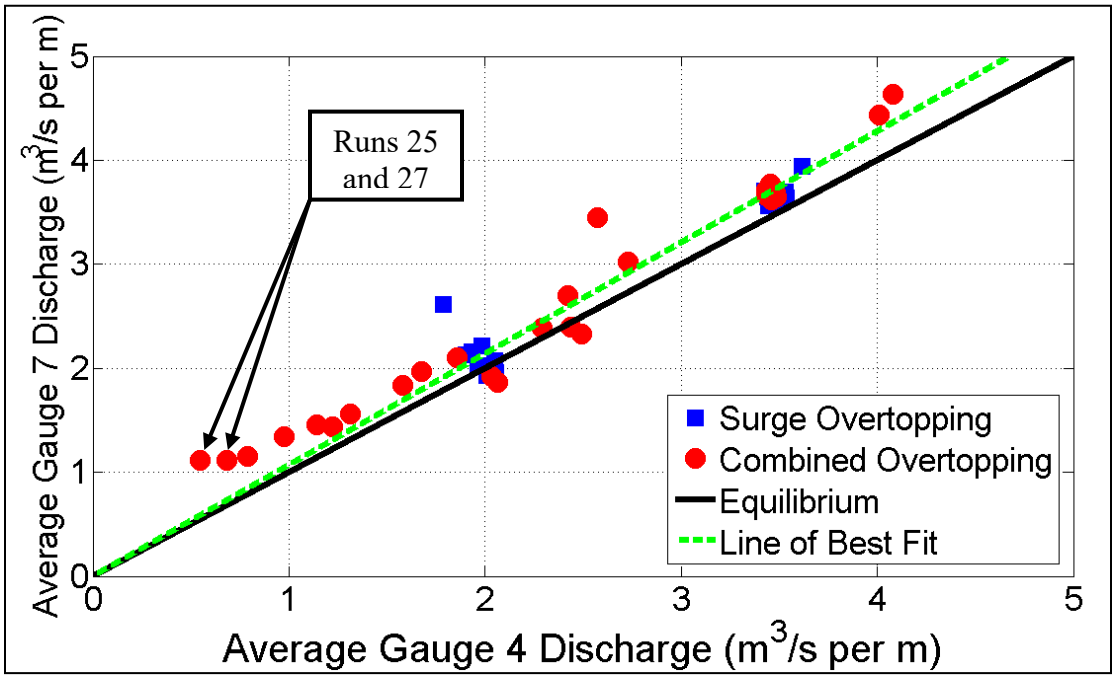

Figure 4.1 Prototype Average Discharge at PG4 and PG7

Table 4.3 Prototype Average Overtopping Flow Thickness

Target Initial Negative Freeboard	Average Surge Overtopping Flow thickness (*m*)					
	PG1	**PG2**	**PG3**	**PG4**	**PG6**	**PG7**
0.30 m Surge Depth	0.23	0.17	0.13	0.08	0.04	0.07
0.91 m Surge Depth	0.68	0.50	0.44	0.37	0.24	0.26
1.52 m Surge Depth	1.02	0.75	0.65	0.61	0.41	0.45

4.2 Flow Conditions

Significant wave height, peak wave period, and initial negative freeboard were used as target flow conditions for testing. Target and tested conditions are listed in Table 4.4. Initial freeboard during the first nine runs was not calculated from Equation 2-1 because velocities were not recorded due to inconsistent readings. The tested negative freeboard is consistently larger than the target freeboard likely due to incorrect placement or reading of water surface indicators.

Table 4.4 Prototype Target and Tested Overtopping Parameters

Run	Target Overtopping Parameters			Tested Overtopping Parameters		
	Significant Wave Height	Peak Wave Period	Initial Negative Freeboard	Significant Wave Height	Peak Wave Period	Initial Negative Freeboard
	(*m*)	(*s*)	(*m*)	(m)	(s)	(m)
26	0.91	10	0.30	0.92	10.04	—
28	1.83	6	0.30	1.78	6.02	—
29	1.83	10	0.30	1.77	10.44	—
30	1.83	14	0.30	1.78	14.62	—
31	2.74	6	0.30	2.56	6.02	—
32	2.74	10	0.30	2.63	10.04	—
33	2.74	14	0.30	2.58	14.62	—
34	0.91	6	0.91	0.85	6.02	1.09
35	0.91	10	0.91	0.85	10.04	1.08
36	0.91	14	0.91	0.84	13.85	1.09
37	1.83	6	0.91	1.60	5.88	1.09
38	1.83	10	0.91	1.73	10.04	1.11
39	1.83	14	0.91	1.71	13.85	1.09
40	2.74	6	0.91	2.47	5.88	1.10
41	2.74	10	0.91	2.60	10.44	1.12
42	2.74	14	0.91	2.53	13.85	1.15
43	0.91	6	1.52	0.70	6.02	1.60
44	0.91	10	1.52	0.78	10.04	1.59
45	0.91	14	1.52	0.80	13.12	1.58
46	1.83	6	1.52	1.27	6.02	1.59
47	1.83	10	1.52	1.62	10.04	1.60
48	1.83	14	1.52	1.64	13.12	1.60
49	2.74	6	1.52	2.37	6.02	1.61
50	2.74	10	1.52	2.53	10.04	1.61
51	2.74	14	1.52	2.54	13.85	1.66

Surge overtopping did not have wave disturbances so a visual inspection of recorded flow thickness at PG4 and PG7 determined surge overtopping duration; see Figure 4.2. Initial recording time was adjusted to begin at 20 seconds (prototype) for each run accounting for each data collection system's varied starting time.

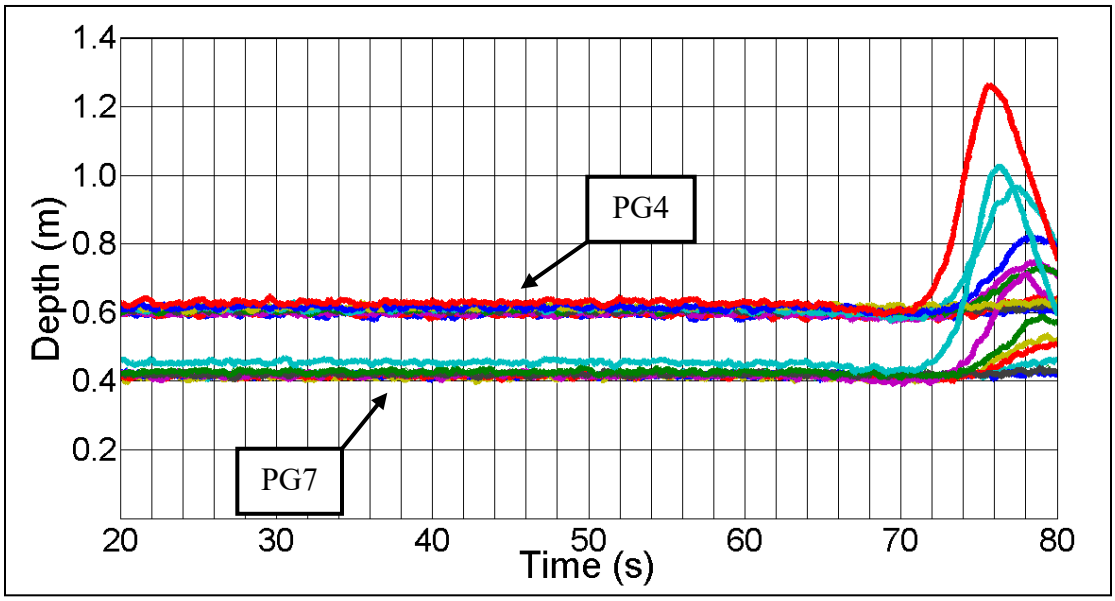

Figure 4.2 Surge Overtopping Flow Thickness at PG4 and PG7 during Runs 43 – 51

A surge overtopping duration of 30 seconds (beginning at 20 and ending at 50 prototype seconds) was considered appropriate as flow thickness and velocity measurements were consistent over that time span at each gauge location. Tables 4.5 and 4.6 list average flow thickness, velocity, discharge, and negative freeboard at PG4 and PG7 during surge overtopping.

Table 4.5 Prototype Surge Overtopping Flow Conditions at PG4

Run	Flow Thickness (m)	Velocity (m/s)	Discharge (m^3/s per m)	Negative Freeboard (m)
26	0.07	—	—	—
28	0.07	—	—	—
29	0.07	—	—	—
30	0.07	—	—	—
31	0.07	—	—	—
32	0.10	—	—	—
33	0.10	—	—	—
34	0.39	5.27	2.03	1.12
35	0.38	5.24	2.01	1.12
36	0.36	5.24	1.90	1.08
37	0.37	5.24	1.96	1.10
38	0.39	5.26	2.05	1.13
39	0.39	5.25	2.06	1.13
40	0.37	5.26	1.93	1.09
41	0.38	5.26	1.98	1.11
42	0.34	5.28	1.79	1.03
43	0.59	5.76	3.43	1.59
44	0.60	5.75	3.44	1.60
45	0.60	5.76	3.45	1.60
46	0.61	5.76	3.49	1.61
47	0.61	5.75	3.50	1.62
48	0.61	5.75	3.52	1.62
49	0.62	5.75	3.53	1.63
50	0.62	5.74	3.53	1.62
51	0.63	5.75	3.62	1.65

Table 4.6 Prototype Surge Overtopping Flow Conditions at PG7

Run	Flow Thickness (m)	Velocity (m/s)	Discharge (m^3/s per m)	Negative Freeboard (m)
26	0.10	—	—	—
28	0.09	—	—	—
29	0.07	—	—	—
30	0.08	—	—	—
31	0.03	—	—	—
32	0.06	—	—	—
33	0.07	—	—	—
34	0.24	7.68	1.83	1.05
35	0.23	7.67	1.80	1.04
36	0.26	7.67	1.99	1.11
37	0.25	7.67	1.89	1.07
38	0.25	7.67	1.93	1.09
39	0.24	7.67	1.83	1.05
40	0.26	7.68	2.02	1.12
41	0.27	7.67	2.07	1.14
42	0.32	7.69	2.45	1.27
43	0.43	8.11	3.46	1.60
44	0.42	8.11	3.41	1.59
45	0.41	8.10	3.33	1.56
46	0.42	8.11	3.38	1.58
47	0.41	8.11	3.36	1.57
48	0.42	8.10	3.38	1.58
49	0.42	8.11	3.40	1.58
50	0.43	8.10	3.46	1.60
51	0.45	8.11	3.69	1.67

Velocities at PG4 are less than PG7 and flow thicknesses at PG4 are greater than PG7, both of which are expected. During small surge overtopping events there are a few runs where the average flow thickness at PG7 is larger than average flow thickness at PG4. This is due to preprocessing methods which averaged depth adjustments twice per day. Negative freeboard was estimated by solving Equation 2-1 for R_c. Average flow thickness, velocity, discharge, and freeboard during surge overtopping are shown in Table 4.7.

Table 4.7 Average Prototype Surge Overtopping Parameters

Target Negative Freeboard	**Flow Thickness**		**Velocity**		**Average Discharge**	**Average Freeboard**
	PG4	**PG7**	**PG4**	**PG7**		
(*m*)	(*m*)	(*m*)	(*m/s*)	(*m/s*)	(m^3/s *per m*)	(*m*)
0.30	0.08	0.07	—	—	—	—
0.91	0.37	0.26	5.26	7.67	1.97	-1.10
1.52	0.61	0.42	5.75	8.11	3.47	-1.60

Combined overtopping flow thickness and velocity analyses began at 170 seconds (prototype); waves were considered fully developed at this point. For smaller negative freeboards waves would typically break as they reached the levee and a pulse of water would flow over the crest and down the landward slope. Figure 4.3 shows a sequence for a high negative freeboard where waves did not break. Frame 1 of Figure 4.3 shows a wave reaching the levee crest 2.70 prototype seconds after the previous wave has passed over the levee. Notice the drawdown near the crest resulting in positive freeboard before

the wave reaches the levee. The wave then crashed over the levee and reached the landward slope toe 3.0 seconds later.

Average combined overtopping discharge can be similar to surge overtopping discharge over an extended time period. The main difference is the variation in flow thickness and velocity peaks experienced during combined overtopping. Table 4.8 lists representative peak flow thickness parameters and Table 4.9 lists representative peak velocity parameters at PG4 and PG7 during combined overtopping. The 1/3, 1/10, and 1/100 denote average of the highest 1/3, 1/10, 1/100 peaks, respectively. If there were 300 peak depth readings, the 1/3, 1/10, 1/100 highest would be an average of the highest 100, 30, and 3 peak values, respectively. Tables 4.10 and 4.11 list combined overtopping discharge for PG4 and PG7.

Average flow thickness, velocity, and discharge, while an accurate and acceptable measure of flow conditions during surge overtopping, are not representative of flow conditions on a levee's landward slope during combined overtopping. Levees that are only subjected to surge overtopping can be designed based on average flow thickness, velocity, and discharge of the largest expected negative freeboard. However, combined overtopping presents a unique design challenge with the addition of waves to surge overtopping where flow thickness, velocity, and discharge are reliant on negative freeboard, wave height, and wave period. Average flow thickness, velocity, and discharge under-predict peak values that may cause erosion; see Tables 4.8, 4.9, 4.10, and 4.11.

Combined overtopping discharges are listed in Tables 4.10 and 4.11. Runs 26 through 33 had some discrepancy between PG4 and PG7 while the remaining runs were

more consistent. This was also seen during low flows in surge overtopping as previously discussed. Wave height and period conditions were analyzed in the frequency domain. Deterministic analysis using the method of Goda and Suzuki (1976) estimated the incident zeroth-moment wave height (H_{m0}), peak spectral wave period (T_p), and the mean spectral energy wave period ($T_{m-1,0}$); Table 4.12.

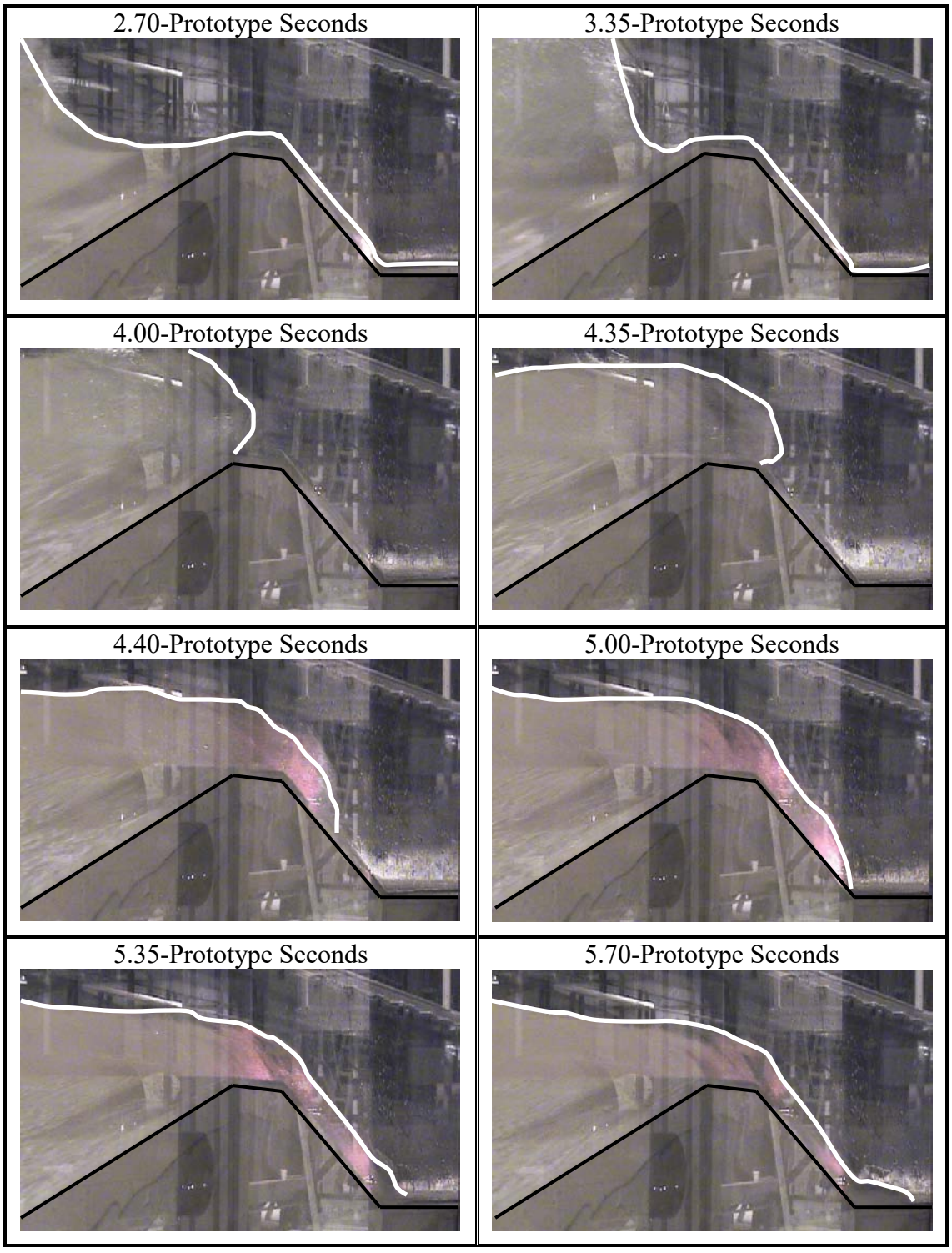

Figure 4.3 Combined Overtopping of Model Levee during Testing

Table 4.8 Prototype Combined Overtopping Flow Thickness

Run	Prototype Flow thickness (*m*)							
	PG4				PG7			
	Average	*1/3*	*1/10*	*1/100*	*Average*	*1/3*	*1/10*	*1/100*
26	0.13	0.48	0.56	0.71	0.14	0.39	0.45	0.52
28	0.18	0.61	0.72	0.93	0.16	0.47	0.54	0.63
29	0.21	0.81	0.98	1.28	0.17	0.61	0.73	0.82
30	0.24	1.02	1.26	1.57	0.18	0.75	0.86	0.94
31	0.23	0.78	0.93	1.15	0.17	0.57	0.66	0.79
32	0.28	1.07	1.32	1.52	0.21	0.84	1.01	1.13
33	0.29	1.33	1.62	1.89	0.22	1.05	1.23	1.35
34	0.38	0.75	0.85	1.02	0.23	0.46	0.53	0.61
35	0.38	0.76	0.87	1.01	0.22	0.49	0.57	0.66
36	0.34	0.74	0.87	1.04	0.25	0.52	0.63	0.76
37	0.41	1.05	1.20	1.37	0.28	0.72	0.83	0.93
38	0.42	1.19	1.40	1.72	0.27	0.84	0.99	1.11
39	0.43	1.28	1.57	1.83	0.27	0.94	1.14	1.25
40	0.42	1.25	1.41	1.64	0.31	0.92	1.04	1.15
41	0.45	1.53	1.84	2.09	0.34	1.20	1.42	1.55
42	0.42	1.65	1.98	2.43	0.38	1.47	1.68	1.82
43	0.59	0.86	0.94	1.01	0.43	0.63	0.70	0.76
44	0.59	0.92	1.01	1.12	0.42	0.87	0.95	1.05
45	0.60	0.95	1.04	1.17	0.42	0.69	0.78	0.89
46	0.59	1.11	1.30	1.45	0.42	0.82	0.96	1.06
47	0.58	1.33	1.52	1.74	0.42	1.06	1.22	1.34
48	0.58	1.39	1.64	1.96	0.41	1.13	1.34	1.49
49	0.58	1.53	1.72	1.86	0.42	1.22	1.37	1.48
50	0.64	1.82	2.10	2.39	0.49	1.57	1.82	1.93
51	0.65	1.95	2.30	2.72	0.51	1.80	2.08	2.27

Table 4.9 Prototype Combined Overtopping Velocity

Run	**Prototype Velocity** (*m/s*)							
	PG4				**PG7**			
	Average	*1/3*	*1/10*	*1/100*	*Average*	*1/3*	*1/10*	*1/100*
26	4.87	7.06	7.71	8.52	7.44	9.21	9.76	10.49
28	5.10	7.91	8.37	8.97	7.61	10.42	11.15	12.17
29	5.04	8.48	9.13	10.11	7.58	11.15	12.04	13.12
30	5.04	8.86	9.74	10.97	7.57	11.59	12.81	14.36
31	5.12	8.30	8.79	9.99	7.64	11.01	11.75	13.06
32	5.18	9.24	10.09	11.35	7.67	11.90	12.91	14.46
33	5.16	9.72	10.76	11.78	7.68	12.64	13.96	16.49
34	5.27	6.36	6.96	8.21	7.68	9.02	9.84	11.10
35	5.27	6.34	6.84	7.71	7.68	8.91	9.64	10.66
36	5.24	6.36	6.85	7.92	7.68	8.78	9.36	10.33
37	5.36	7.78	8.69	9.45	7.78	10.95	12.15	13.21
38	5.40	8.53	9.35	10.82	7.82	11.51	12.75	14.47
39	5.39	8.23	9.09	10.68	7.80	10.93	12.29	14.61
40	5.44	8.78	9.65	11.07	7.85	12.05	13.21	14.66
41	5.52	9.50	10.39	11.68	7.93	12.72	14.14	15.90
42	5.53	9.48	10.41	11.55	7.90	12.70	14.29	16.42
43	5.75	6.38	6.54	6.69	8.10	8.74	8.92	9.11
44	5.73	6.50	6.68	6.88	8.08	8.81	8.98	9.22
45	5.72	6.51	6.69	6.98	8.08	8.80	8.99	9.24
46	5.71	6.88	7.29	7.82	8.06	9.47	10.18	11.89
47	5.68	7.57	8.34	9.46	8.03	10.46	11.89	13.09
48	5.67	7.55	8.32	9.81	8.02	10.07	11.12	13.05
49	5.65	8.32	9.05	10.30	8.01	11.88	13.39	14.98
50	5.77	9.14	10.15	11.70	8.10	12.63	14.05	15.54
51	5.77	8.94	9.92	11.11	8.08	11.85	13.38	15.69

Table 4.10 Prototype Combined Overtopping Discharge

Run	Discharge (m^3/s per m)							
	PG4				PG7			
	Average	*1/3*	*1/10*	*1/100*	*Average*	*1/3*	*1/10*	*1/100*
26	0.68	2.99	3.71	5.13	1.04	3.31	3.97	5.06
28	0.97	3.81	4.52	5.42	1.25	4.27	5.03	6.52
29	1.14	5.57	7.10	9.11	1.36	6.06	7.64	9.25
30	1.31	7.43	9.35	12.76	1.46	7.67	9.31	11.02
31	1.22	5.08	6.11	7.51	1.34	5.45	6.67	8.79
32	1.58	7.75	9.68	12.70	1.72	8.40	10.82	14.46
33	1.67	10.20	13.10	16.10	1.84	11.32	14.02	16.59
34	2.04	4.68	5.67	7.09	1.80	4.10	4.92	6.01
35	2.06	4.72	5.66	6.79	1.74	4.24	5.17	6.41
36	1.86	4.61	5.70	7.22	1.97	4.50	5.57	7.16
37	2.29	7.59	9.12	11.12	2.23	7.31	8.99	10.66
38	2.44	9.16	11.34	14.87	2.24	8.75	10.58	12.41
39	2.49	9.79	12.89	15.94	2.18	9.28	11.68	14.32
40	2.42	9.71	11.60	14.01	2.53	10.11	11.86	13.58
41	2.73	12.52	15.74	20.17	2.82	13.32	16.31	19.14
42	2.57	14.10	17.74	22.90	3.22	16.45	20.08	24.03
43	3.43	5.45	6.08	6.66	3.47	5.46	6.14	6.81
44	3.44	5.96	6.69	7.69	3.42	5.94	6.74	7.74
45	3.46	6.12	6.91	8.12	3.39	6.07	6.96	8.04
46	3.48	7.65	9.38	11.04	3.41	7.41	8.82	10.01
47	3.48	9.91	12.06	14.30	3.45	9.98	11.88	13.40
48	3.48	10.30	12.98	17.76	3.43	10.49	12.71	14.41
49	3.46	12.06	14.30	15.58	3.52	12.06	14.06	16.28
50	4.01	15.37	18.77	23.32	4.14	15.71	18.58	20.85
51	4.08	16.60	21.11	26.41	4.33	17.96	21.36	23.85

Table 4.11 Prototype Combined Overtopping Average Discharge

Run	Discharge (m^3/s per m)			
	Average of PG4 and PG7			
	Average	*1/3*	*1/10*	*1/100*
26	0.86	3.15	3.84	5.10
28	1.11	4.04	4.77	5.97
29	1.25	5.81	7.37	9.18
30	1.39	7.55	9.33	11.89
31	1.28	5.27	6.39	8.15
32	1.65	8.08	10.25	13.58
33	1.76	10.76	13.56	16.34
34	1.92	4.39	5.29	6.55
35	1.90	4.48	5.42	6.60
36	1.91	4.56	5.63	7.19
37	2.26	7.45	9.05	10.89
38	2.34	8.95	10.96	13.64
39	2.33	9.54	12.29	15.13
40	2.47	9.91	11.73	13.80
41	2.78	12.92	16.02	19.65
42	2.90	15.28	18.91	23.46
43	3.45	5.45	6.11	6.74
44	3.43	5.95	6.72	7.71
45	3.42	6.09	6.94	8.08
46	3.45	7.53	9.10	10.52
47	3.46	9.95	11.97	13.85
48	3.46	10.40	12.84	16.09
49	3.49	12.06	14.18	15.93
50	4.08	15.54	18.68	22.09
51	4.21	17.28	21.24	25.13

Table 4.12 Prototype Combined Overtopping Wave Conditions

Run	H_{m0} (m)	T_p (s)	$T_{m-1,0}$ (s)
26	0.92	10.40	8.70
28	1.78	6.02	5.47
29	1.77	10.44	8.72
30	1.78	14.62	10.64
31	2.56	6.02	5.70
32	2.63	10.04	8.81
33	2.58	14.62	9.96
34	0.85	6.02	5.65
35	0.85	10.04	8.63
36	0.84	13.85	11.34
37	1.61	5.88	5.46
38	1.73	10.04	8.50
39	1.71	13.85	11.23
40	2.47	5.88	5.62
41	2.60	10.04	8.61
42	2.53	13.85	10.65
43	0.70	6.02	5.53
44	0.78	10.04	8.55
45	0.80	13.12	11.39
46	1.27	6.02	5.53
47	1.62	10.04	8.46
48	1.64	13.12	11.05
49	2.37	6.02	5.61
50	2.53	10.04	8.35
51	2.54	13.85	10.40

Previous studies developed equations to estimate combined overtopping discharge as a function of wave height and freeboard; see Section 2.4. Hughes and Nadal (2009) collected data using a scaled physical model and developed Equation 2-36. Reeve et al. (2008) developed Equations 2-34 and 2-35 for combined overtopping using a Reynolds Averaged Navier-Stokes (RANS) numerical model. Figure 4.4 displays previous equations along with values from this thesis. Reeve et al. (2008) tends to overestimate discharge while the Hughes and Nadal (2009) equation was very similar to values from the current work. Equation 2-36 is considered an appropriate estimation of average combined overtopping discharge for this thesis. Hughes and Nadal (2009) developed a dimensionless plot relating discharge to freeboard and wave height. Figure 4.5 plots the work of this thesis represented by squares and triangles and shows good agreement with Hughes and Nadal (2009).

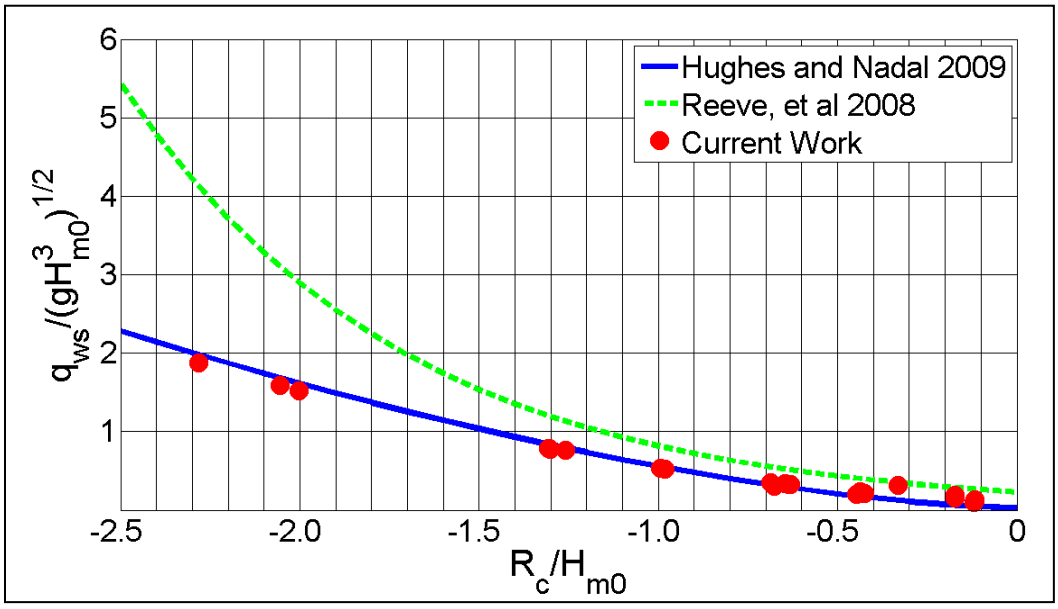

Figure 4.4 Dimensionless Discharge Comparison

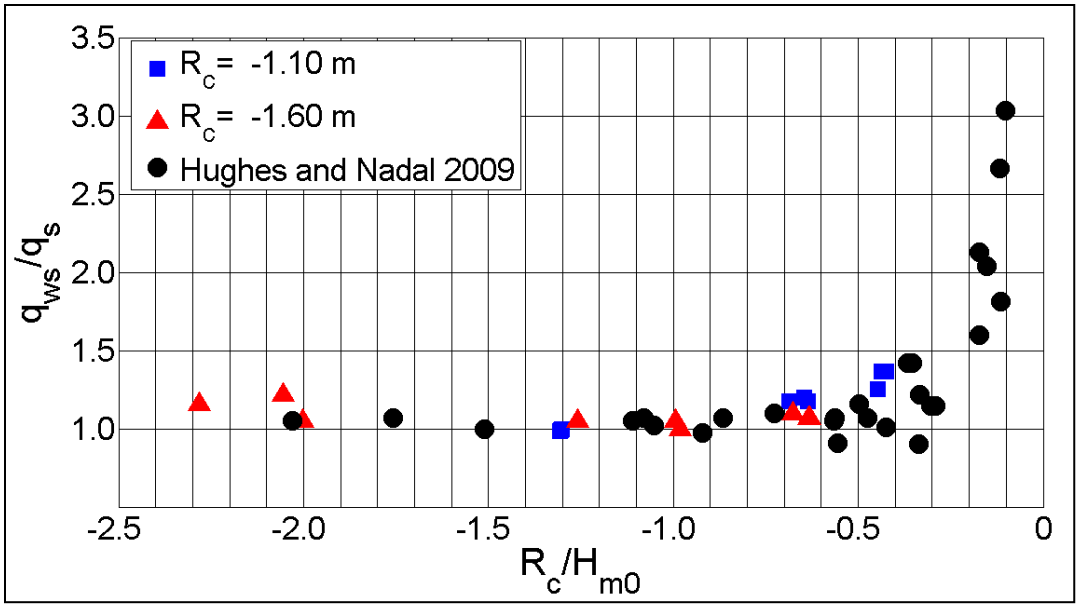

Figure 4.5 Combined Overtopping Dimensionless Comparison

4.3 Shear Stress Analysis

Variations of Equations 2-55 through 2-57 were used to estimate shear stress between PG4 and PG7 on the model levee's landward slope. Equation 4-1 assumes steady, uniform flow and averages the flow thickness between PG4 and PG7. Equation 4-2 assumes steady, non-uniform flow by considering flow thickness differences between PG4 and PG7. Equation 4-3 estimates shear stress in unsteady, non-uniform flow between PG4 and PG7. Equations 4-1 through 4-3 estimate the average landward slope shear stress between PG4 and PG7. A filter was added to remove large shear stress values. This filter removes the temporal acceleration term if velocity at PG4 is larger than PG7 and/or shear stress increased more than 2,000 N/m^2 over a 0.05 second span.

$$\tau_{0,mean} = \gamma_w \left(\frac{h_2+h_1}{2}\right) \sin\theta \quad (4\text{-}1)$$

$$\tau_0 = \gamma_w \left(\frac{h_2+h_1}{2}\right) \left[\sin\theta - \frac{h_2-h_1}{s_{2,1}}\right] \quad (4\text{-}2)$$

$$\tau_0 = \gamma_w \left(\frac{h_2+h_1}{2}\right) \left[\sin\theta - \frac{h_2-h_1}{s_{2,1}} - \frac{v_2^2-v_1^2}{2g(s_{2,1})} - \frac{(v_2(i)-v_2(i+1))+(v_1(i)-v_1(i+1))}{2g(t(i)-t(i+1))}\right] \quad (4\text{-}3)$$

where:

h_1 = Flow thickness at First Pressure Gauge
h_2 = Flow thickness at Second Pressure Gauge
s_1 = Down Slope Distance from Crest to First Gauge
s_2 = Down Slope Distance from Crest to Second Gauge
$s_{2,1}$ = Distance between First and Second Gauges
$v_1(i)$ = Velocity at First Gauge
$v_2(i)$ = Velocity at Second Gauge
$v_1(i+1)$ = Velocity at First Gauge, One Time Increment Later
$v_2(i+1)$ = Velocity at Second Gauge, One Time Increment Later

4.3.1 Surge Overtopping Shear Stress

Surge-only overtopping occurred at the start of the experiment, and analysis was done for the first 30 seconds of each run. Surge overtopping created nearly constant flow thickness and velocity over the levee because the wave board was not activated. Average flow thickness, velocity, and discharge for surge overtopping are presented in Tables 4.5 and 4.6. Average shear stresses estimated by Equations 4-1 through 4-3 are displayed in Table 4.13. Equation 4-2 should predict the largest shear stress during surge only overtopping because the spatial change in flow thickness term would be negative causing Equation 4-2 to be larger than 4-1. Equation 4-3 should estimate the smallest shear stress because the largest velocities are typically downstream which causes the velocity terms to

be negative. Also, if the flow is accelerating the friction slope is less than the channel slope and terminal velocity has not been reached.

A best-fit linear relationship between average shear stress and discharge is plotted in Figure 4.6. As previously noted, Equation 4-2 predicts the largest shear stress followed by Equations 4-1 and 4-3, respectively. Average discharge, freeboard, and shear stresses are located in Table 4.14. Negative freeboard, average discharge, and shear stress using Equation 4-3 were not estimated for runs 26 through 33 in Table 4.13 and for the first row in Table 4.14 because velocity was not recorded due to thin flow thicknesses.

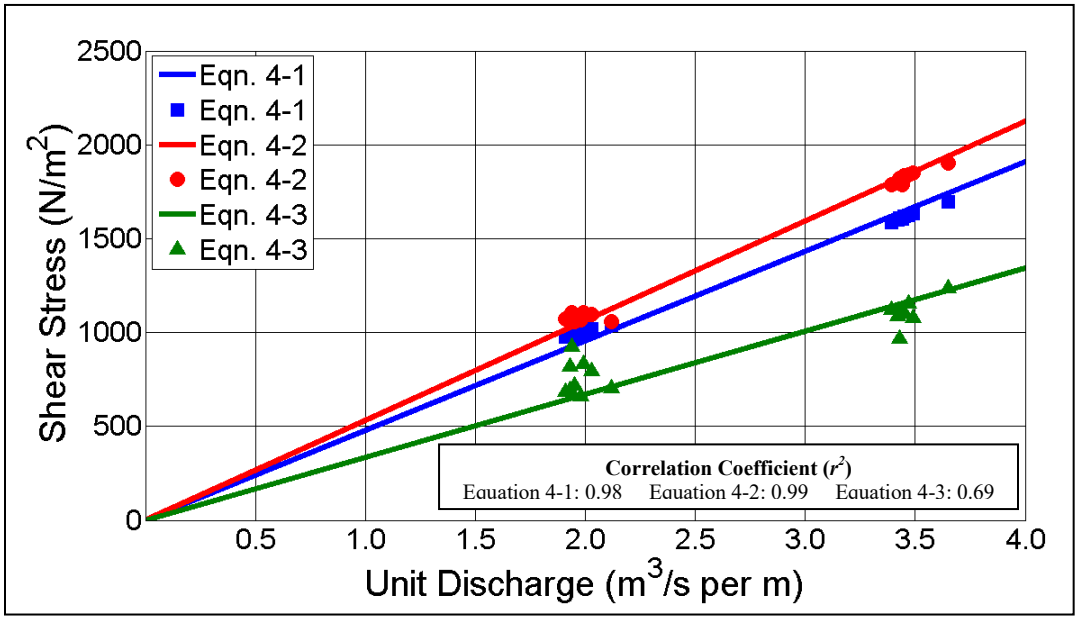

Figure 4.6 Prototype Average Surge Overtopping Shear Stress

Table 4.13 Prototype Surge Overtopping Average Shear Stress

Run	Negative Freeboard	Average Discharge	Average Shear Stress Between PG4 and PG7		
			Equation 4-1	Equation 4-2	Equation 4-3
	(m)	(m^3/s per m)	(N/m^2)	(N/m^2)	(N/m^2)
26	—	—	270	263	—
28	—	—	256	253	—
29	—	—	224	224	—
30	—	—	260	255	—
31	—	—	166	170	—
32	—	—	252	257	—
33	—	—	270	277	—
34	1.09	1.93	986	1,081	817
35	1.08	1.91	977	1,072	685
36	1.09	1.95	988	1,060	718
37	1.09	1.93	982	1,070	694
38	1.11	1.99	1,015	1,107	832
39	1.09	1.94	1,000	1,104	925
40	1.10	1.98	996	1,069	662
41	1.12	2.03	1,021	1,097	796
42	1.15	2.12	1,039	1,059	705
43	1.60	3.44	1,605	1,788	1,121
44	1.59	3.42	1,602	1,796	1,086
45	1.58	3.39	1,588	1,787	1,121
46	1.59	3.44	1,606	1,812	1,120
47	1.60	3.43	1,609	1,821	968
48	1.60	3.45	1,621	1,835	1,103
49	1.61	3.47	1,622	1,840	1,153
50	1.61	3.49	1,636	1,850	1,075
51	1.66	3.65	1,698	1,902	1,236

Table 4.14 Average Surge Overtopping Shear Stress

Negative Freeboard	Average Discharge	Average Shear Stress Between PG4 and PG7		
		Equation 4-1	Equation 4-2	Equation 4-3
(*m*)	(m^3/s *per m*)	(N/m^2)	(N/m^2)	(N/m^2)
—	—	243	243	—
1.10	1.97	1,000	1,080	759
1.60	3.47	1,621	1,826	1,109

Nadal and Hughes (2009) estimated shear stress using Equations 4-1 through 4-3 and found that Equations 4-1 and 4-2 over predicted shear stress when compared to Equation 4-3 because the overtopping flow has not reached terminal velocity. Figure 4.7 displays the surge overtopping shear stress and discharge relationship from Nadal Hughes (2009) and this thesis. The studies predict similar surge overtopping shear stress for discharges less than 4 m^3/s per m.

Hughes and Shaw (2011) recorded flow thickness and velocity at PG2 and PG6 as described in Section 2.3; see Figure 2.4. Data from Hughes and Shaw (2011) were used to estimate shear stress with results shown in Table 4.15. Equations 4-1 through 4-3 follow the same trend previously described with Equation 4-2 estimating the largest shear stress and Equation 4-3 the smallest. Values shown in Table 4.15 are plotted in Figure 4.8.

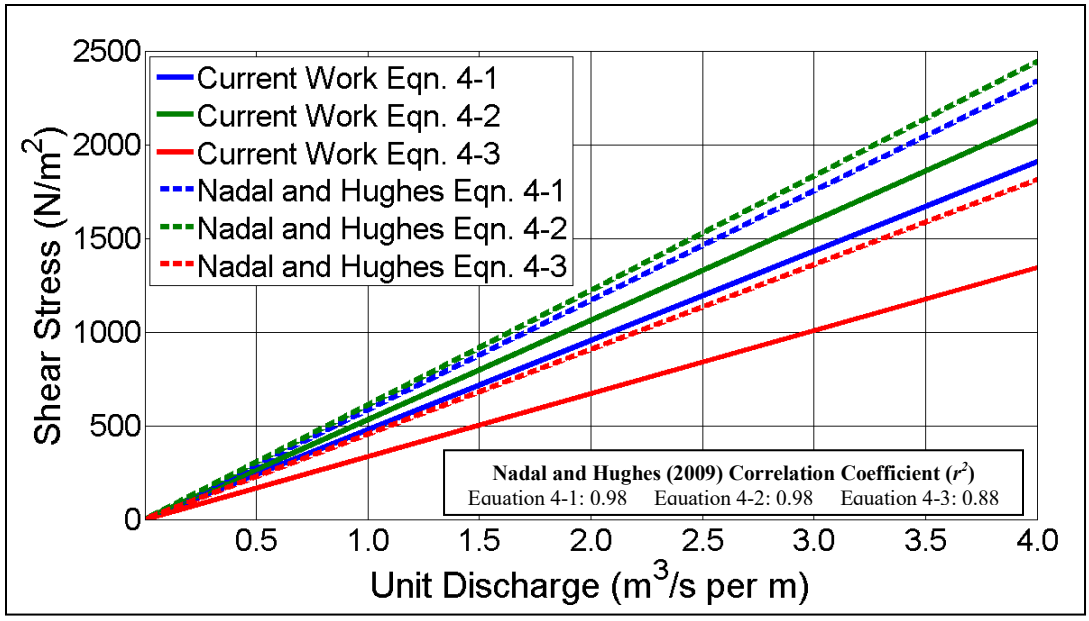

Figure 4.7 Nadal and Hughes (2009) and Prototype Average Surge Overtopping Shear Stress Comparison

Table 4.15 Average Surge Overtopping Shear Stress From Data in Hughes and Shaw (2011)

Run	Negative Freeboard	Average Discharge	Average Shear Stress Between PG2 and PG6		
			Equation 4-1	Equation 4-2	Equation 4-3
	(*m*)	(m^3/s *per m*)	(N/m^2)	(N/m^2)	(N/m^2)
13	0.27	0.25	329	349	1,155
14	0.27	0.26	357	381	263
15	0.38	0.47	529	575	353
16	1.03	1.73	1,352	1,641	923
17	1.09	1.90	1,448	1,771	1,013
18	1.08	1.94	1,477	1,795	939
19	1.57	3.22	2,100	2,716	1,133
20	1.58	3.29	2,146	2,775	1,185
21	1.58	3.42	2,197	2,794	1,119

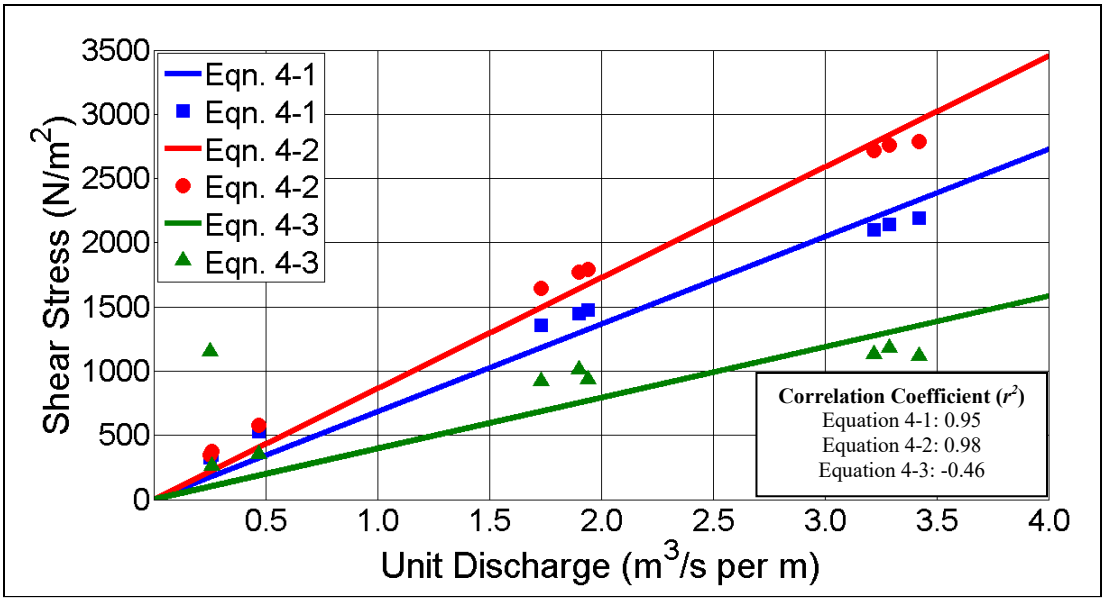

Figure 4.8 Average Surge Overtopping Shear Stress From Data in Hughes and Shaw (2011)

Shear stress estimates using data from Hughes and Shaw (2011) were used to estimate shear stress between the crest-landward slope edge and PG4 based on the assumptions that shear stress does not significantly change between PG2 and the crest-landward edge slope, and the shear stress at PG4 is similar to shear stress at PG6. However, between PG2 and PG6 overtopping flow tends to become supercritical which could make these assumptions invalid. The assumption that shear stress is similar at PG4 and PG6 is more likely to be valid during periods of small overtopping discharge and may be shown not true during large overtopping events.

The thesis work combined with data from Hughes and Shaw (2011) allow for surge overtopping shear stress estimates along the landward slope as shown in Figure 4.9. Zone 1 starts at the crest edge of the landward slope to PG4 and Zone 2 is from PG4 to

PG7. Shear stress beyond PG7 will not be extrapolated due to uncertainty of flow thickness and velocity effects caused by the change in slope near the levee toe.

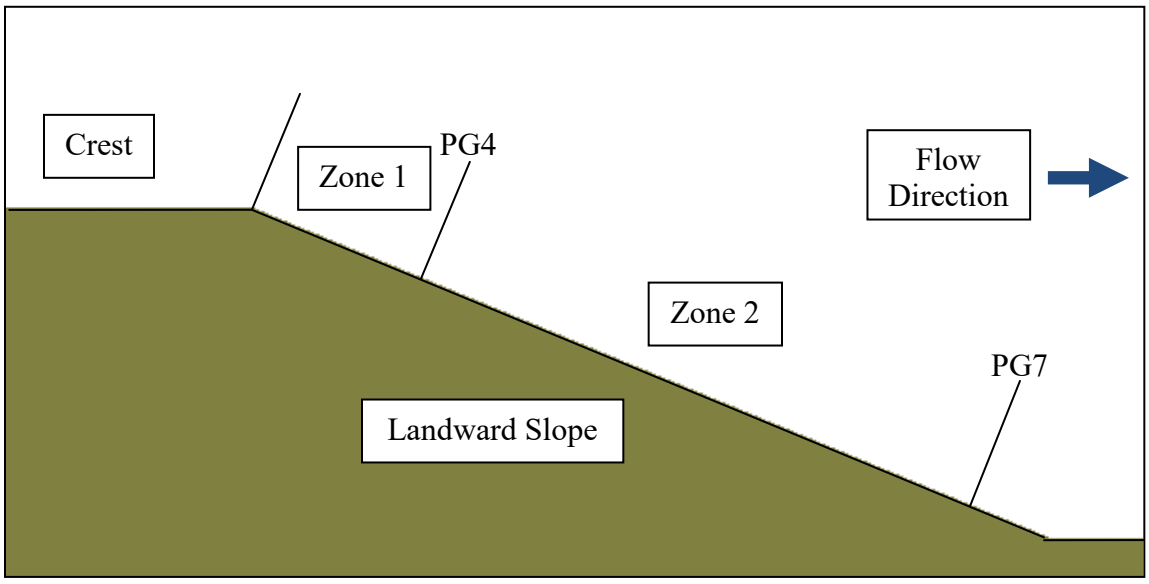

Figure 4.9 Surge Overtopping Shear Stress Estimates

Equations 4-1 and 4-2 overestimate shear stress along the landward slope during previously described overtopping conditions of a levee compared to Equation 4-3, because the overtopping flow is still accelerating. Equation 4-3 is believed to be a more accurate estimation of shear stress along the landward slope during these conditions. Equations 4-4 and 4-5 are used to describe overtopping shear stress for unit discharges less than 4 m^3/s per m and a landward slope of 1V:3H in Zones 1 and 2 with shear stress in N/m^2 and surge overtopping discharge in m^3/s per m. These equations represent the line of best fit forced through zero shown in Figures 4.6 and 4.8. Several assumptions were made to estimate shear stress in Zone 1 that may affect the accuracy of Equation 4-4.

$$\tau_{S,Zone1} = 395 C_s q_s \quad (4\text{-}4)$$

$$\tau_{S,Zone2} = 335 C_s q_s \quad (4\text{-}5)$$

where:

τ_s = Shear Stress (N/m^2)
C_s = 1; Surge Overtopping Shear Stress Constant (Ns/m^4)
q_s = Surge Overtopping Discharge (m^3/s *per* m)

4.3.2 Surge Overtopping Numerical Model Comparison

A surge overtopping numerical model, developed by members of the research team other than the author of this thesis (Sharp and McAnally, In Review), was compared to the physical model results. The numerical model's grid was built in the Surface Water Modeling System (SMS 10.0) designed by Aquaveo and USACE. Aquaveo was originally part of the Engineering Computer Graphics Laboratory at Brigham Young University, and in 2007 became a water resources consulting and training firm that specializes in numerical modeling. SMS 10.0 is compatible with a variety of modeling software packages including AdH, CMS-Wave, FESWMS, and STWAVE (SMS 2010). The numerical model's grid is built and initial flow conditions are assigned in SMS, then numerical modeling software is used to estimate flow conditions.

Adaptive Hydraulics (AdH) numerical modeling software was developed by CHL at ERDC. AdH can examine groundwater flow, sheet flow, 3-D Navier Stokes flow, and 2-D shallow water flow. AdH "dynamically refine(s) the domain mesh in areas where more resolution is needed" (Berger and Tate 2009). After the model grid and flow conditions were built in SMS 10.0, AdH was used to estimate flow thickness and velocity along the entire grid.

The numerical model levee grid was 15 m wide and 610 m long. A large bulb was placed on the landward side of the levee to reduce reflection and upstream flow effects; see Figures 4.10 and 4.11. The levee crest is 4.6 m long in prototype-scale units which is 1.5 m longer than the physical modeled levee. The numerical model's increased crest length likely affected flow thickness and velocity to an unknown extent. The landward slope is the same at 1V:3H yet is longer than the physical modeled levee. The increased landward slope length would not affect flow thickness and velocity because flow along the landward slope is supercritical meaning downstream conditions are not felt upstream. Several surge overtopping conditions were performed with flow thickness and velocity recorded during each test.

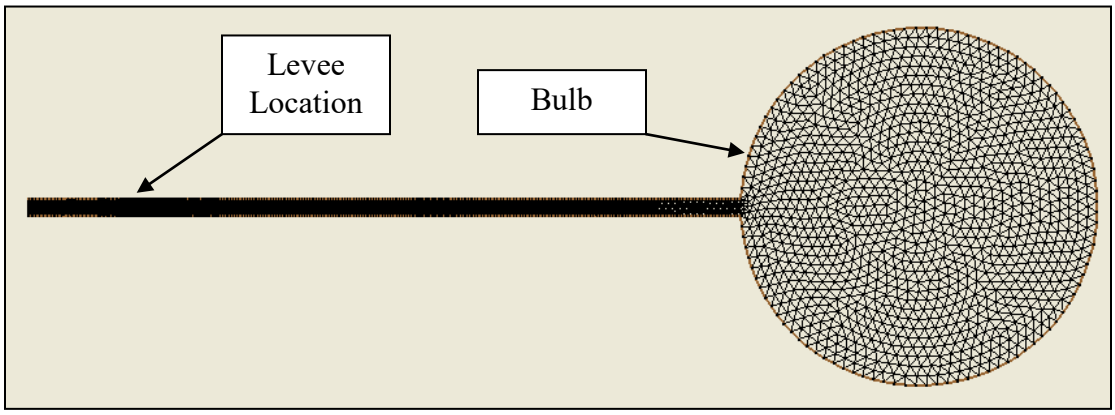

Figure 4.10 Sharp and McAnally (In Review) Numerical Model Levee Grid

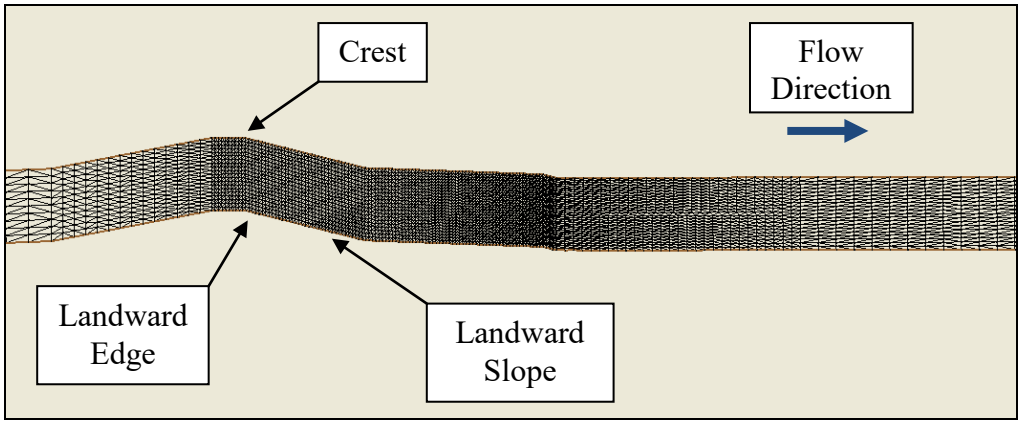

Figure 4.11 Sharp and McAnally (In Review) Numerical Model Levee

Numerically modeled flow thickness, velocity, and discharge are similar to surge overtopping values presented in Section 4.2. The relationship between discharge and freeboard is plotted for the numerical model, this thesis, and Hughes and Shaw (In Press) in Figure 4.12. Flow conditions estimated by the numerical model with a Manning's roughness coefficient of 0.0125 are located in Tables 4.16 and 4.17 with gauge locations shown in Figure 2.4. All pertinent locations were included except the seaward edge and approximate PG1 location. Equation 4-3 was used to estimate shear stress along the landward slope of the numerically modeled levee. Several roughness coefficients (n) were used to estimate shear stress as shown in Table 4.18. Table 4.18 lists average shear stress along the landward slope from crest to levee toe by discharge. Shear stress is the average value from the crest edge to the toe of the slope. The numerical model estimates a similar shear stress when compared to values from this thesis; Figure 4.13.

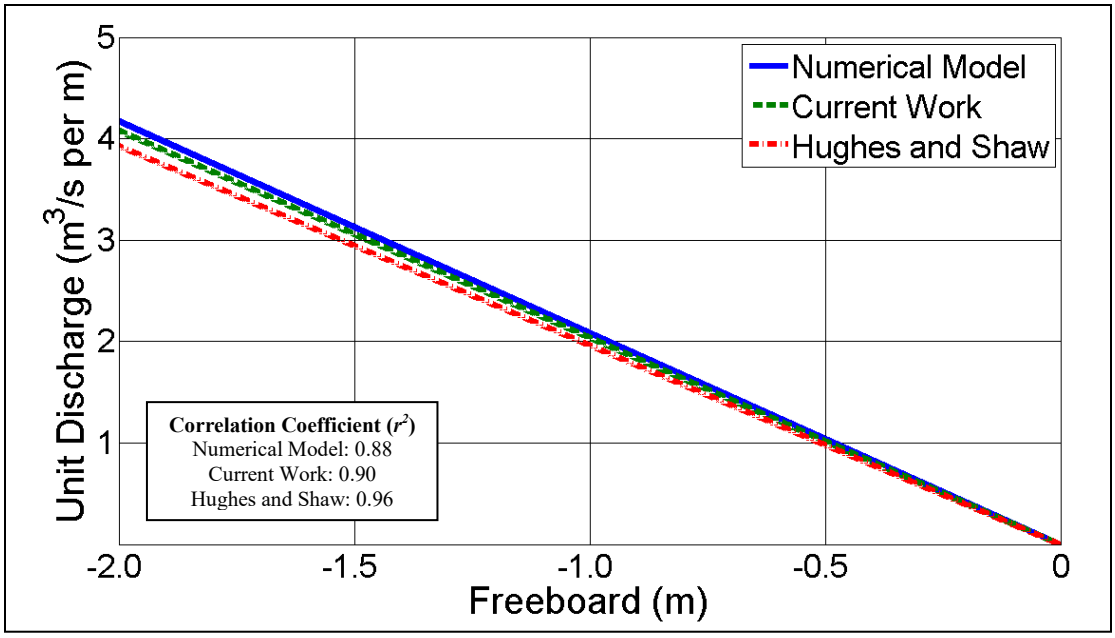

Figure 4.12 Numerical Model Discharge Comparison

Table 4.16 Sharp and McAnally (In Review) Numerical Model Surge Overtopping Depth and Velocity

Numerical Model Recording Location	0.61 m Negative Freeboard		0.91 m Negative Freeboard		1.22 m Negative Freeboard		1.52 m Negative Freeboard	
	Depth	Velocity	Depth	Velocity	Depth	Velocity	Depth	Velocity
	(*m*)	(*m/s*)	(*m*)	(*m/s*)	(*m*)	(*m/s*)	(*m*)	(*m/s*)
Approximate PG2	0.43	1.92	0.65	2.42	0.87	2.86	1.10	3.27
Landward Edge	0.33	2.51	0.49	3.22	0.66	3.80	0.84	4.30
Approximate PG3	0.24	3.52	0.38	4.10	0.54	4.59	0.72	5.02
Approximate PG4	0.18	4.66	0.30	5.15	0.45	5.56	0.61	5.92
Approximate PG5	0.15	5.41	0.26	5.96	0.39	6.35	0.54	6.68
Approximate PG6	0.14	5.93	0.24	6.63	0.35	7.01	0.49	7.33
Approximate PG7	0.13	6.32	0.22	7.18	0.33	7.58	0.45	7.89

Table 4.17 Sharp and McAnally (In Review) Numerical Model Surge Overtopping Discharge

Numerical Model Recording Location	0.61 m Negative Freeboard (m^3/s per m)	0.91 m Negative Freeboard (m^3/s per m)	1.22 m Negative Freeboard (m^3/s per m)	1.52 m Negative Freeboard (m^3/s per m)
Approximate PG2	0.83	1.56	2.48	3.59
Landward Edge	0.83	1.57	2.49	3.60
Approximate PG3	0.83	1.56	2.48	3.59
Approximate PG4	0.83	1.56	2.48	3.59
Approximate PG5	0.82	1.55	2.47	3.58
Approximate PG6	0.83	1.57	2.48	3.60
Approximate PG7	0.82	1.57	2.48	3.59

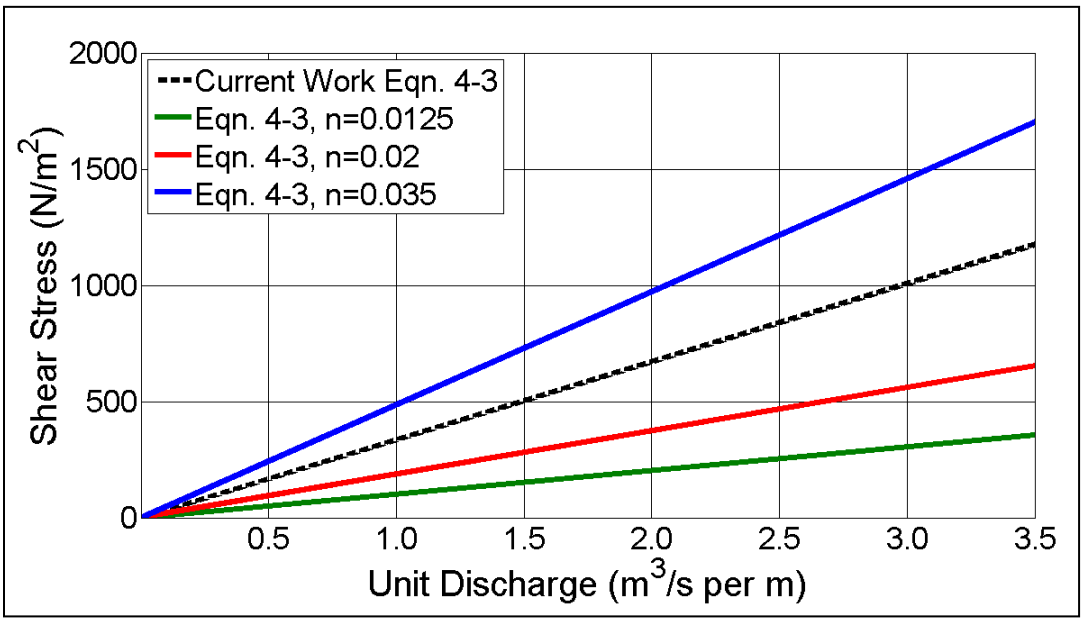

Figure 4.13 Numerical Model Levee Average Surge Overtopping Shear Stress

Table 4.18 Sharp and McAnally (In Review) Numerical Model Surge Overtopping Shear Stress

Average Discharge	**Average Landward Slope Shear Stress Using Equation 4-3 (N/m^2)**		
(m^3/s *per m*)	*n = 0.0125*	*n = 0.02*	*n = 0.035*
0.83	218	328	627
1.56	197	384	911
2.48	234	446	1,189
3.59	300	542	1,481

4.3.3 Combined Overtopping Shear Stress

Combined overtopping produces peak shear stresses due to peaks in velocity and flow thickness associated with waves. Waves were considered fully developed after 300 seconds had passed during each run, and were generated by a wave board that produced irregular waves. Table 4.4 lists target and tested parameters, and Tables 4.8 through 4.12 list overtopping flow thickness, velocity, discharge, and wave conditions.

Combined overtopping shear stress was estimated similar to surge overtopping using Equations 4-1 through 4-3. The largest shear stress from each wave as it passed over PG4 and PG7 was considered the peak shear stress during combined overtopping. Each wave had a combined overtopping peak shear stress and the averages of these peak shear stresses for each run are listed in Table 4.19. Similar to trends noticed during surge overtopping, Equation 4-2 estimated the largest shear stress while Equation 4-3 typically estimated the smallest; see Figure 4.14. Average of the combined overtopping shear stress peaks are nearly double average surge overtopping shear stress as shown in Figure 4.15.

Table 4.19 Combined Overtopping Average Shear Stress

Run	Negative Freeboard	H_{m0}	Average Discharge	Average Combined Overtopping Shear Stress		
				Equation 4-1	Equation 4-2	Equation 4-3
	(*m*)	(*m*)	(m^3/s *per m*)	(N/m^2)	(N/m^2)	(N/m^2)
26	—	0.92	0.86	919	955	838
28	—	1.78	1.11	1,135	1,221	1,238
29	—	1.77	1.25	1,437	1,589	1,333
30	—	1.78	1.39	1,651	1,907	1,394
31	—	2.56	1.28	1,412	1,585	1,523
32	—	2.63	1.65	1,931	2,253	1,765
33	—	2.58	1.76	2,178	2,660	1,588
34	1.09	0.85	1.92	1,414	1,648	1,129
35	1.08	0.85	1.90	1,474	1,704	1,084
36	1.09	0.84	1.91	1,464	1,647	964
37	1.09	1.61	2.26	1,889	2,314	1,764
38	1.11	1.73	2.34	2,177	2,696	1,641
39	1.09	1.71	2.33	2,209	2,736	1,627
40	1.10	2.47	2.47	2,319	2,873	2,033
41	1.12	2.60	2.78	2,816	3,571	2,140
42	1.15	2.53	2.90	2,977	3,678	1,884
43	1.60	0.70	3.45	1,990	2,298	1,130
44	1.59	0.78	3.43	2,088	2,421	1,142
45	1.58	0.80	3.42	2,084	2,418	1,135
46	1.59	1.27	3.45	2,317	2,812	1,452
47	1.60	1.62	3.46	2,715	3,321	1,614
48	1.60	1.64	3.46	2,725	3,303	1,506
49	1.61	2.37	3.49	2,927	3,778	2,040
50	1.61	2.53	4.08	3,637	4,757	1,994
51	1.66	2.54	4.21	3,763	4,801	1,947

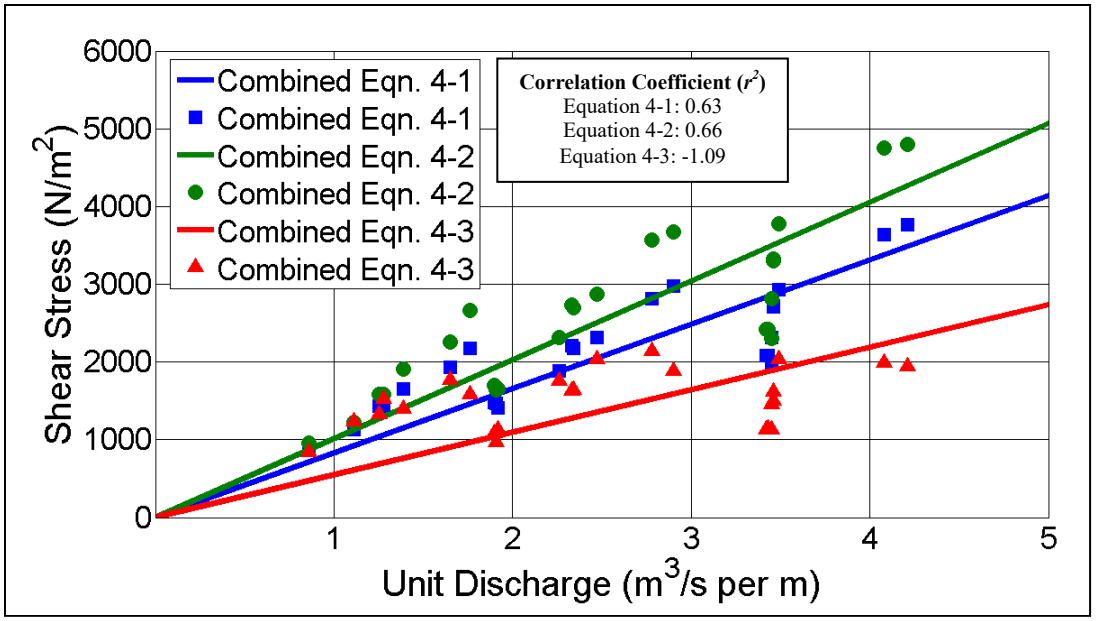

Figure 4.14 Average Combined Overtopping Unit Discharge and Shear Stress

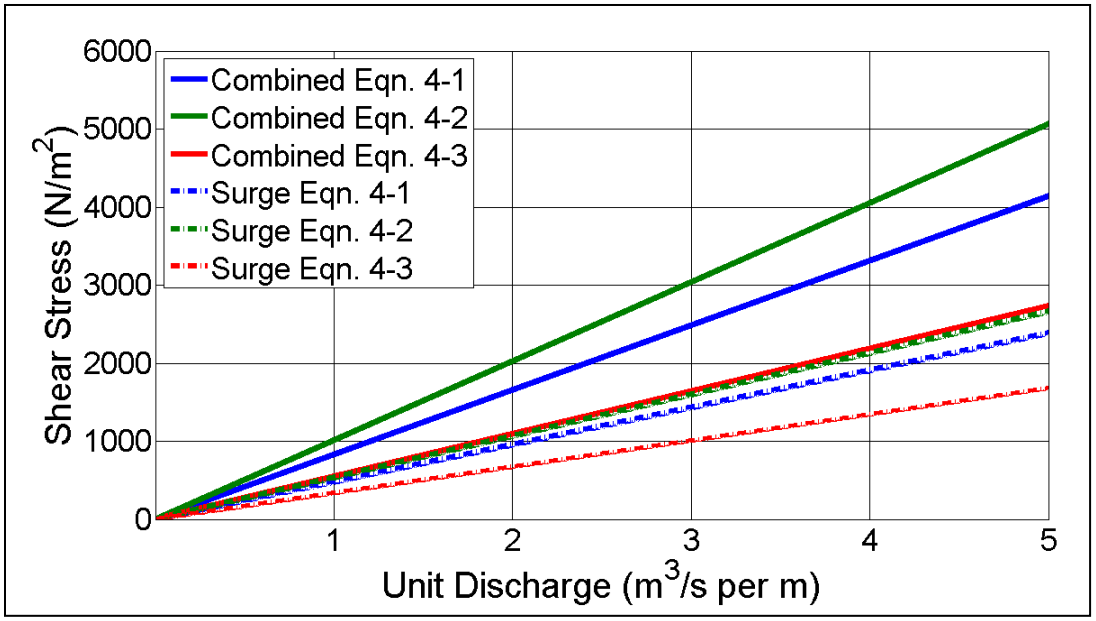

Figure 4.15 Average Surge Overtopping and Combined Overtopping Shear Stress Comparison

Nadal and Hughes (2009) estimated average combined overtopping shear stress using Equations 4-1 through 4-3; Figures 4.16 and 4.19. Figure 4.17 compares average peak combined overtopping shear stress as a function of average combined overtopping discharge for Nadal and Hughes (2009) and this thesis. Discharge is a good predictor for Nadal and Hughes (2009), but does not sufficiently predict combined overtopping shear stress for this thesis. Figure 4.18 plots average combined overtopping shear stress against significant wave height (H_{m0}) for values from the current work producing a better prediction of shear stress estimated by Equation 4-3. Figure 4.20 compares Nadal and Hughes (2009) shear prediction by significant wave height with the current work.

Hughes and Shaw (2011) recorded flow thickness and velocity at PG2 and PG6. Shear stresses estimated from the data were applied from the crest edge of the landward slope to PG4; see Table 4.20 and Figure 4.21.

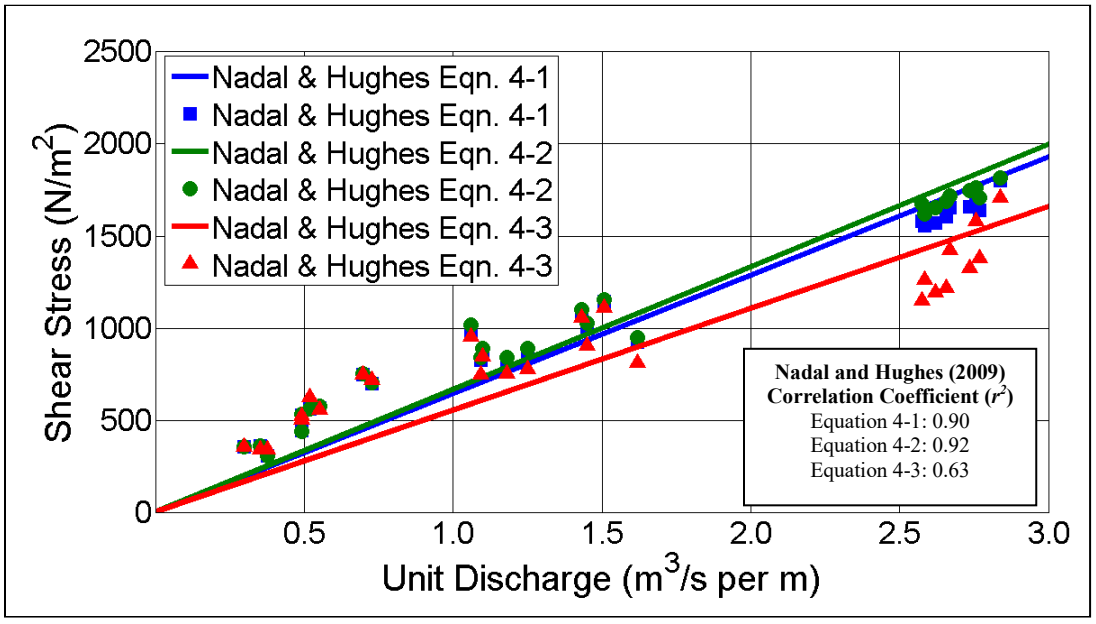

Figure 4.16 Nadal and Hughes (2009) Average Combined Overtopping Discharge and Shear Stress Comparison

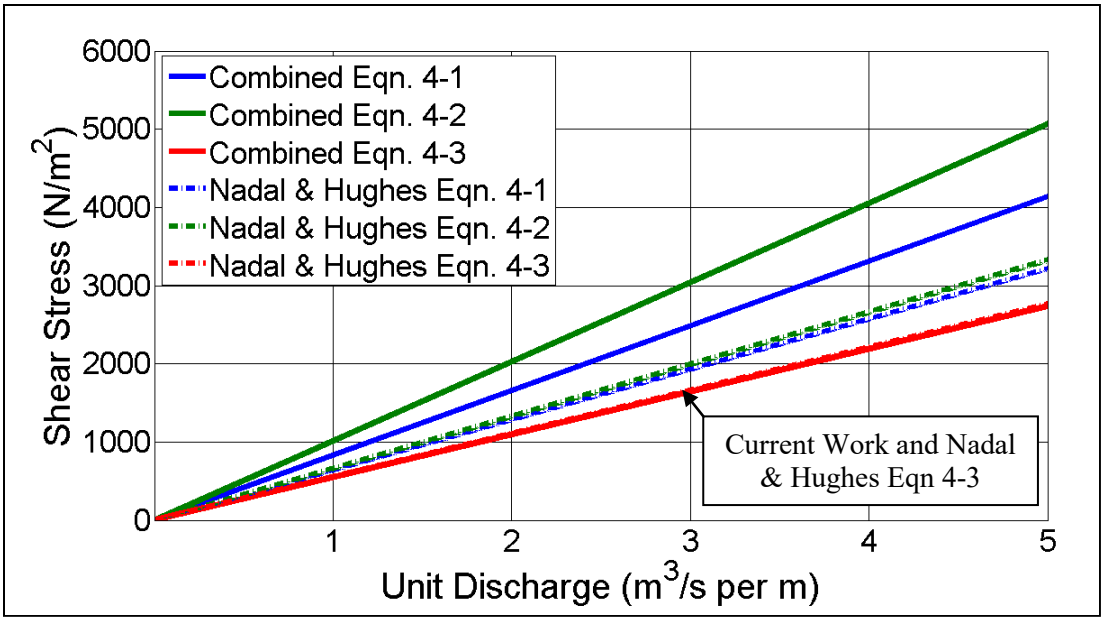

Figure 4.17 Nadal and Hughes (2009) and Current Work Average Combined Overtopping Discharge and Shear Stress Comparison

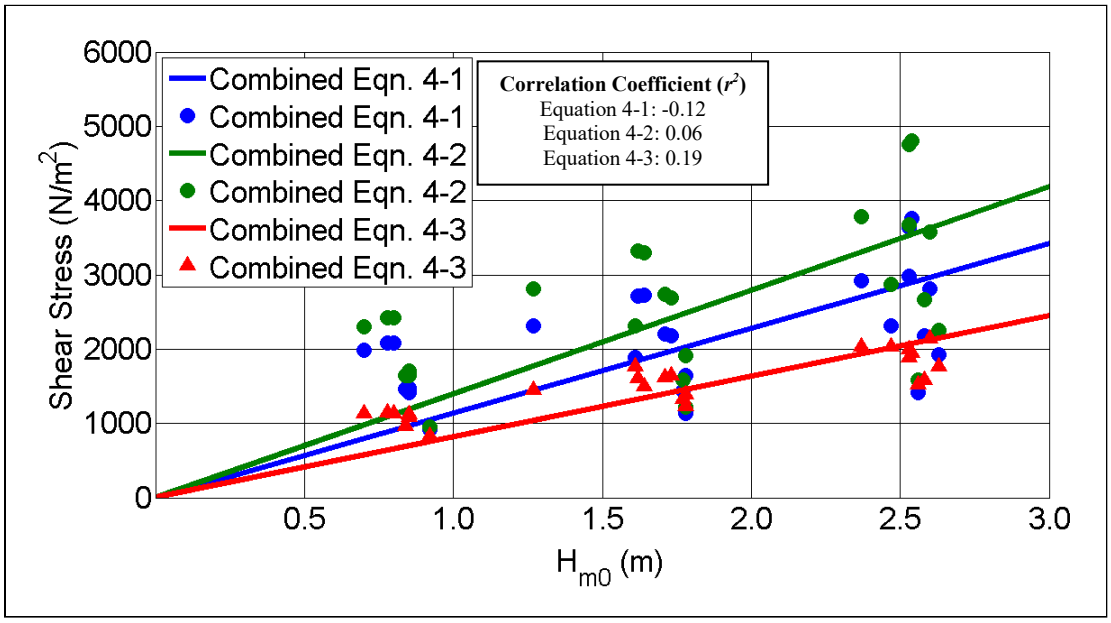

Figure 4.18 Average Combined Overtopping Wave Height and Shear Stress

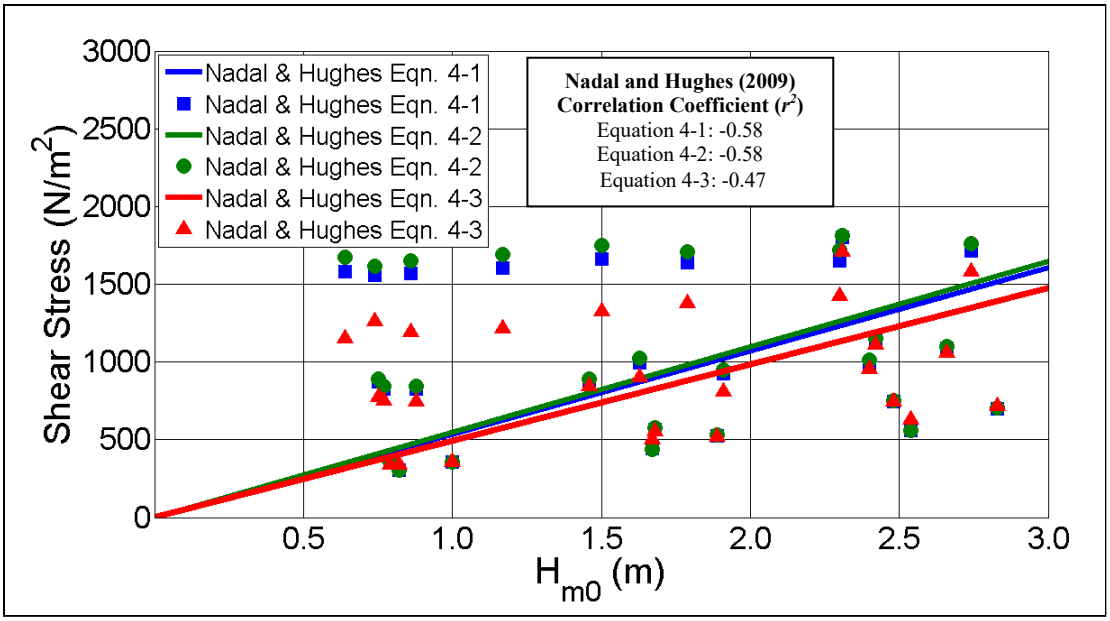

Figure 4.19 Nadal and Hughes (2009) Average Combined Overtopping Wave Height and Shear Stress

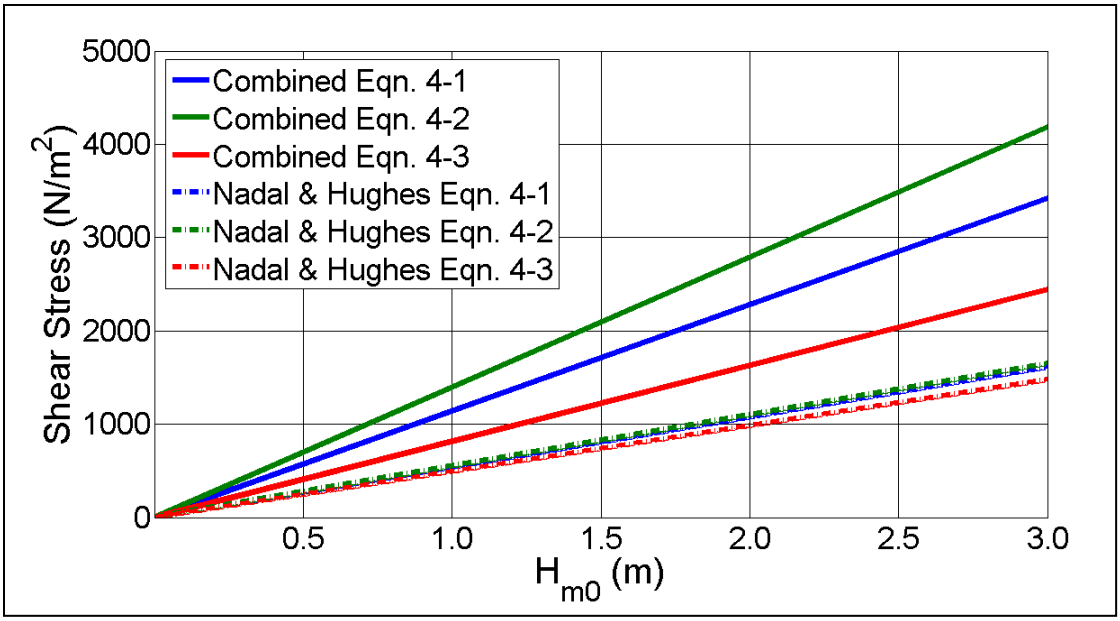

Figure 4.20 Nadal and Hughes (2009) and Current Work Average Combined Overtopping Wave Height and Shear Stress Comparison

Table 4.20 Hughes and Shaw (2011) Average Combined Overtopping Shear Stress

Run	Negative Freeboard	H_{m0}	Average Discharge	Average Combined Overtopping Shear Stress		
				Equation 4-1	Equation 4-2	Equation 4-3
	(m)	(m)	(m^3/s per m)	(N/m^2)	(N/m^2)	(N/m^2)
26	0.27	0.88	0.45	782	842	1,424
28	0.27	1.76	0.84	1,497	1,638	1,974
29	0.38	2.59	1.31	2,183	2,452	2,531
30	1.03	0.69	2.06	1,873	2,300	1,102
31	1.09	1.63	2.26	2,494	3,147	1,972
32	1.08	2.51	2.66	3,143	3,941	2,219
33	1.57	0.68	3.23	2,445	3,179	1,210
34	1.58	1.63	3.53	3,245	4,172	1,804
35	1.58	2.45	3.90	3,916	4,895	2,291

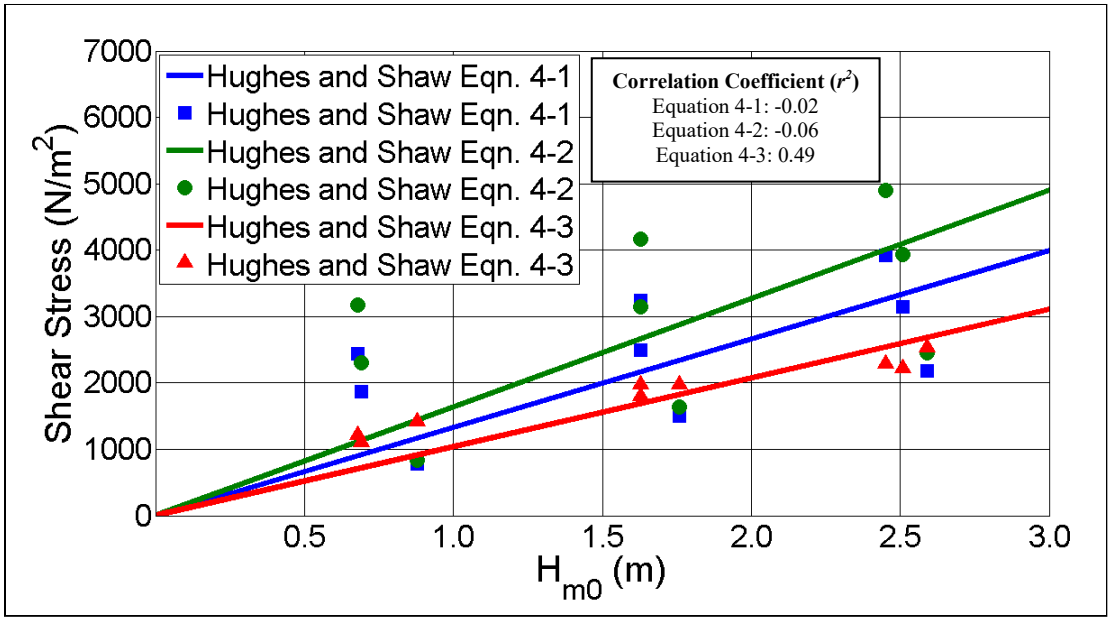

Figure 4.21 Hughes and Shaw (2011) Average Combined Overtopping Shear Stress

Combined overtopping peak shear stresses will likely be the design shear stress for levees subjected to overtopping, and Equation 4-3 appears to be a more realistic estimate of shear stress when compared to Equation 4-1 and 4-2. The following analysis examines combined overtopping peak discharge estimated by Equation 4-3. Table 4.21 lists the 1/3, 1/10, and 1/100 highest average shear stress and root-mean-square wave height during combined overtopping. As an example, the 1/3 highest average shear stress would be the average of the 30 largest shear stresses in a 90 wave test. Root-mean-square wave height was estimated using Equations 2-63 and 2-64 from Nadal and Hughes (2009). Figures 4.22 and 4.23 display combined overtopping highest average shear stress as a function of significant wave height and root-mean-square wave height, respectively.

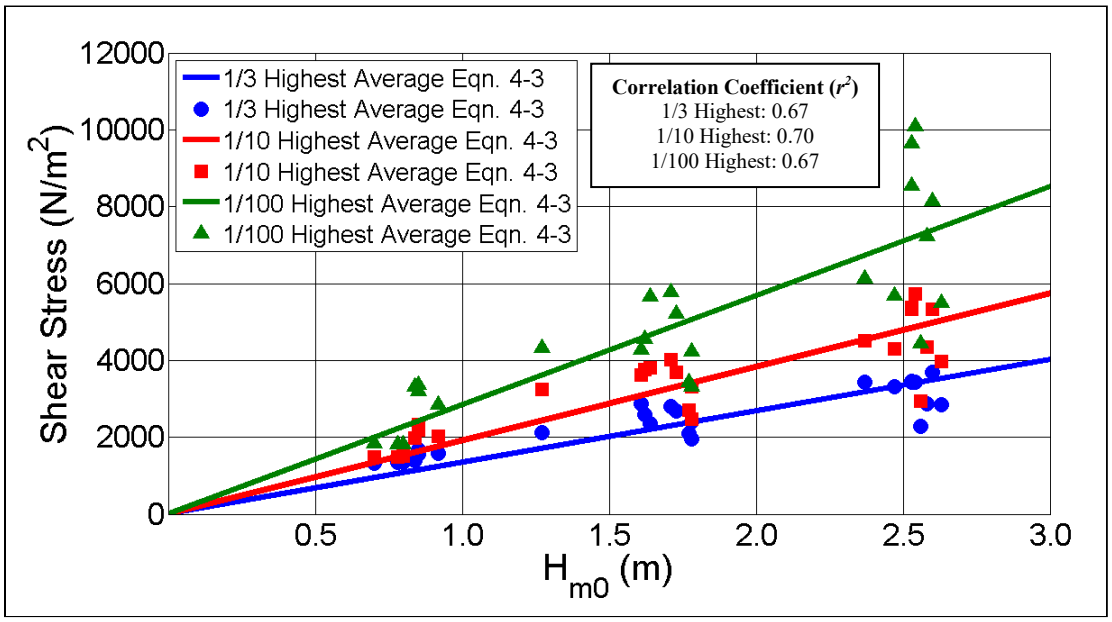

Figure 4.22 Combined Overtopping Highest Average Shear Stress Estimated by Significant Wave Height

Table 4.21 Combined Overtopping Highest Average Shear Stress Estimated by Equation 4-3

Run	Negative Freeboard	H_{rms}	Average Discharge	Highest Average Combined Overtopping Shear Stress Estimated by Equation 4-3		
				1/3	1/10	1/100
	(*m*)	(*m*)	(m^3/s *per m*)	(N/m^2)	(N/m^2)	(N/m^2)
26	—	—	0.86	1,573	2,029	2,859
28	—	—	1.11	1,965	2,477	3,305
29	—	—	1.25	2,109	2,701	3,435
30	—	—	1.39	2,393	3,313	4,237
31	—	—	1.28	2,283	2,948	4,451
32	—	—	1.65	2,836	3,962	5,489
33	—	—	1.76	2,877	4,352	7,236
34	1.09	0.40	1.92	1,679	2,333	3,360
35	1.08	0.41	1.90	1,554	2,197	3,193
36	1.09	0.39	1.91	1,402	1,992	3,311
37	1.09	0.83	2.26	2,862	3,629	4,281
38	1.11	0.87	2.34	2,675	3,703	5,218
39	1.09	0.88	2.33	2,806	4,020	5,782
40	1.10	1.10	2.47	3,315	4,309	5,675
41	1.12	1.21	2.78	3,686	5,326	8,139
42	1.15	1.21	2.90	3,439	5,322	8,547
43	1.60	0.22	3.45	1,331	1,493	1,851
44	1.59	0.28	3.43	1,346	1,479	1,816
45	1.58	0.30	3.42	1,345	1,522	1,810
46	1.59	0.61	3.45	2,115	3,238	4,333
47	1.60	0.80	3.46	2,589	3,751	4,548
48	1.60	0.81	3.46	2,348	3,817	5,662
49	1.61	1.10	3.49	3,435	4,520	6,133
50	1.61	1.27	4.08	3,449	5,372	9,656
51	1.66	1.27	4.21	3,425	5,727	10,088

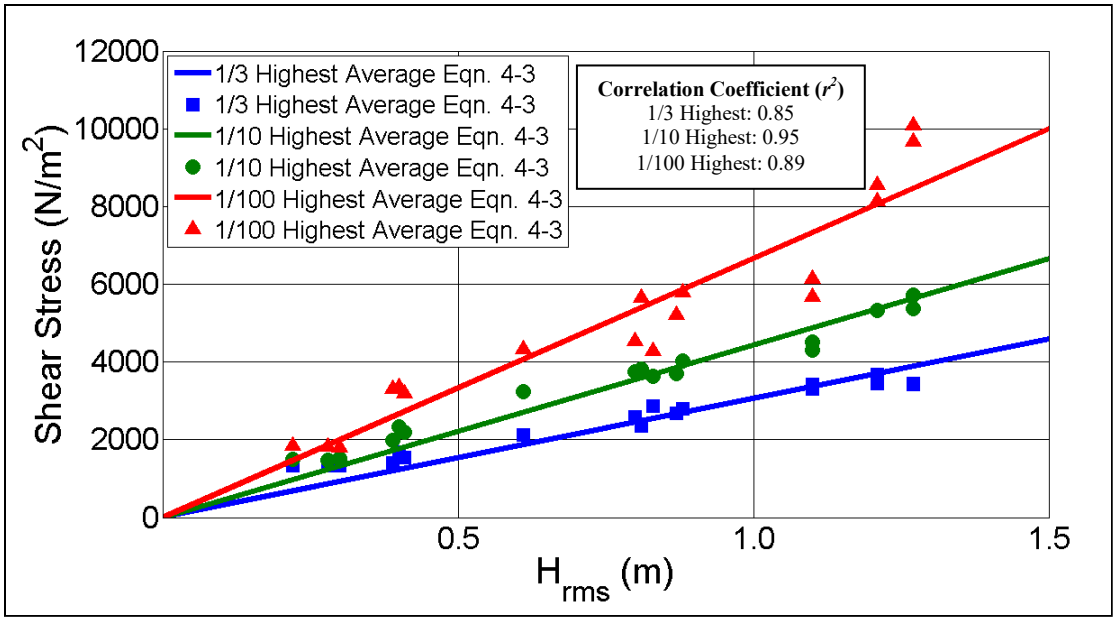

Figure 4.23 Combined Overtopping Highest Average Shear Stress Estimated by Root-mean-square Wave Height

Nadal and Hughes (2009) developed Equations 2-60 through 2-64 to estimate highest average combined overtopping shear stress between PG4 and PG7. These equations relate root-mean-square wave height (H_{rms}) to shear stress using specific weight to create non-dimensional relationships. Equations 2-60 through 2-62 had correlation coefficients of 0.94 or above using Nadal and Hughes (2009) data. This method of combined overtopping shear stress estimation tends to create well correlated relationships. The Nadal and Hughes (2009) study is compared to this thesis in Figure 4.24.

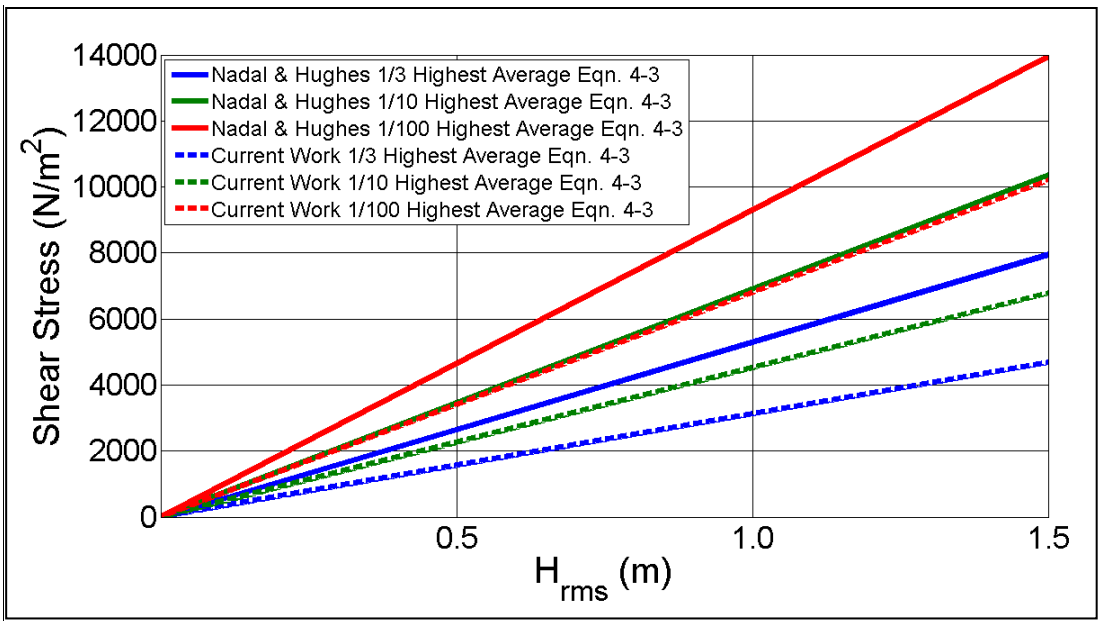

Figure 4.24 Nadal and Hughes (2009) Highest Average Combined Overtopping Shear Stress Comparison with Current Work

Data from Nadal and Hughes (2009) was used to estimate shear stress and predicted slightly larger combined peak overtopping shear stresses compared to this thesis. The difference in shear stress estimation is likely a function of preprocessing methods, and Nadal and Hughes (2009) estimation of veloicty measurements along the landward slope from recorded measurements on the levee crest.

Hughes and Shaw (2011) estimate peak combined overtopping shear stresses shown in Table 4.22 between PG2 and PG6. Equation 4-3 predicts larger 1/3, 1/10, and 1/100 highest average shear stress than Equations 4-1 and 4-2 for the majority of runs 13 through 21. This trend does not agree with this thesis or Nadal and Hughes (2009). These data may still have noise that was not removed by filtering methods. Figure 4.24 displays values from Table 4.22 with a correclation coefficeint of 0.90 for the 1/3 highest average, 0.94 for the 1/10 highest average, and 0.76 for the 1/100 highest average.

Table 4.22 Hughes and Shaw (In Press) Combined Overtopping Highest Average Shear Stress Estimated by Equation 4-3

Run	Negative Freeboard	H_{rms}	Average Discharge	Highest Average Combined Overtopping Shear Stress Estimated by Equation 4-3		
				1/3	1/10	1/100
	(*m*)	(*m*)	(m^3/s *per m*)	(N/m^2)	(N/m^2)	(N/m^2)
13	0.27	0.41	0.45	1,891	2,258	2,927
14	0.27	0.72	0.84	2,825	3,625	5,745
15	0.38	0.97	1.31	4,095	5,918	10,892
16	1.03	0.34	2.06	1,408	1,767	2,338
17	1.09	0.83	2.26	3,543	4,815	6,191
18	1.08	1.18	2.66	4,114	5,671	7,424
19	1.57	0.21	3.23	1,392	1,542	1,784
20	1.58	0.83	3.53	3,021	4,763	6,210
21	1.58	1.23	3.90	4,332	6,045	7,867

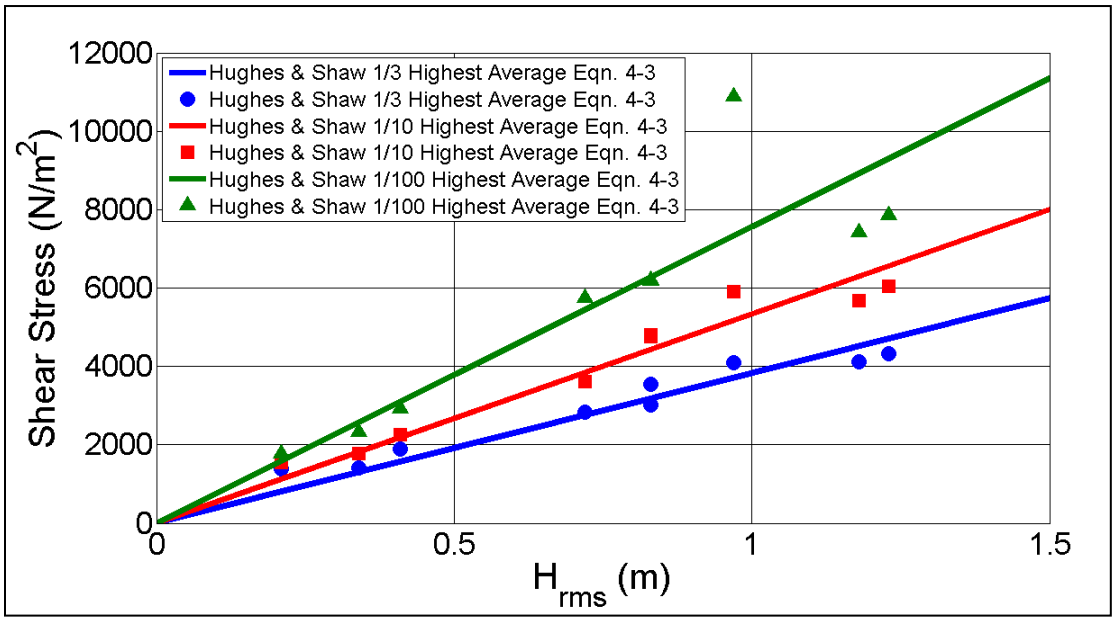

Figure 4.25 Hughes and Shaw (2011) Highest Average Combined Overtopping Shear Stress

The landward slope is divided into two zones as shown in Figure 4.9. Shear stress along Zone 1 is estimated using physical model data from Hughes and Shaw (2011) and shear stress along Zone 2 is estimated using data measured from the same physical model. Nadal and Hughes (2009) describe combined overtopping shear stress as a function of significant wave height. This method is sound and can be nondimensionalized by including specfic weight. Equations 4-6 and 4-7 estimate combined overtopping 1/100 highest average shear stress as a function of wave height and specific weight for Zone 1 and Zone 2 respectively. The coefficeint of correlation for Equation 4-6 is 0.91 and 0.89 for Equation 4-7.

$$\tau_{WS,Zone1} = 0.77\gamma H_{rms} \tag{4-6}$$

$$\tau_{WS,Zone2} = 0.68\gamma H_{rms} \tag{4-7}$$

4.4 Example of Shear Stress Estimates on an Earthen Levee

The previous sections describe analyses used to estimate surge and combined overtopping shear stress for earthen levees with 1H:3V landward slope and a 3.0 m crest width. These shear stress estimates are valid for overtopping flows with negative freeboards between 0.3 and 1.5 m, wave heights between 0.9 and 2.5 m, and peak wave periods of 6 to 14 s.

As an example, a levee with the dimensions tested was designed and built decades ago but faces surge overtopping due to a tropical storm. Figure 4.25 shows prototype dimensions. Rapidly deployable protective measures are being sought that can withstand the projected 1 m surge overtopping. Example parameters are listed in Table 4.23

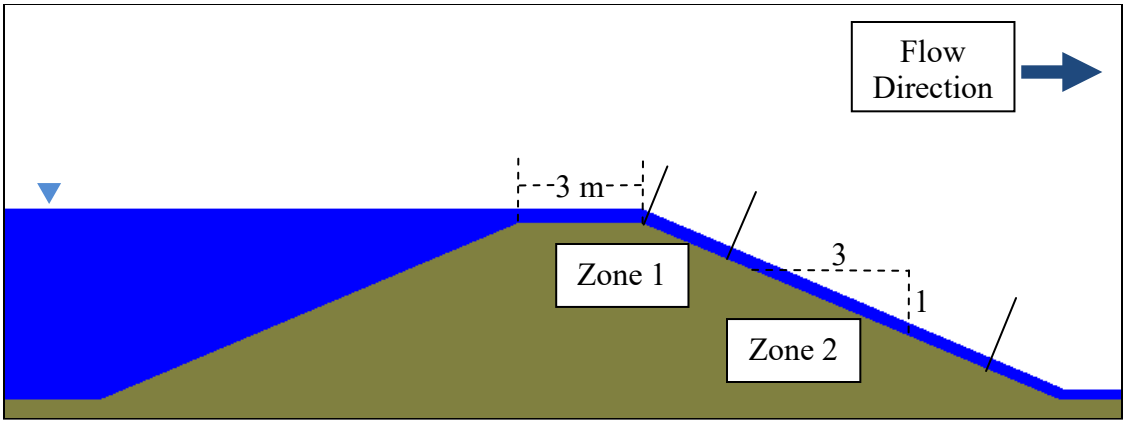

Figure 4.26 Surge Overtopping Example

Table 4.23 Example Parameters

Negative Freeboard, R_c	**Significant Wave Height, H_{m0}**	**Crest Width**	**Landward Slope, $sin\theta$**	**Gravity, g**	**Specific Weight, γ**
(m)	(m)	(m)		(m/s^2)	(N/m^3)
1.0	1.5	3.0	1H:3V = 0.316	9.8	9,800

Equation 2-1 is used to estimate discharge during surge overtopping and Equations 4-4 and 4-5 are used to estimate surge overtopping shear stress. As shown in the calculations below, the protective measure must withstand a surge overtopping shear stress of 670 N/m^2 in Zone 1 and 570 N/m^2 in Zone 2. Table 4.24 lists shear stress values for several negative freeboards.

Table 4.24 Surge Overtopping Shear Stress Values

Negative Freeboard	Surge Overtopping Discharge	Surge Overtopping Shear Stress	
R_c	q_s	$\tau_{s,Zone1}$	$\tau_{s,Zone2}$
(m)	$(m^3/s\ per\ m)$	(N/m^2)	(N/m^2)
0	0.00	0	0
0.5	0.60	238	202
1	1.70	673	571
1.5	3.13	1,237	1,049

$$q = {}^2/_3\, R_c\sqrt{{}^2/_3\, gR_c} = {}^2/_3\,(1)\sqrt{{}^2/_3\,(9.81)(1)} = 1.70\ \frac{m^3}{s} per\ m \qquad \text{(Eqn. 2-1)}$$

$$\tau_{S,Zone1} = 395C_sq_s = 395(1)(1.7) = 670\ N/m^2 \qquad \text{(Eqn. 4-4)}$$

$$\tau_{S,Zone2} = 335C_sq_s = 335(1)(1.7) = 570\ N/m^2 \qquad \text{(Eqn. 4-5)}$$

Let's say the same levee and freeboard conditions also included a 1.5 m significant wave height (H_{m0}). Equations 4-6 and 4-7 are used to estimate the combined overtopping 1/100 highest average peak shear stress. Equations 2-38, 2-63, and 2-64 are used to convert H_{m0} to H_{rms}. First, Equation 2-38 is used to estimate combined overtopping discharge, then Equations 2-63 and 2-64 estimate H_{rms}. Finally Equations 4-6 and 4-7 estimate peak combined overtopping discharge for each zone. As shown in the following calculations, Zone 1 has a combined overtopping shear stress of 8,100 N/m^2 and Zone 2 has a combined overtopping shear stress of 7,100 N/m^2.

$$q_{ws} = \left(0.34 + \left(-\frac{R_c}{H_{m0}}\right)^{1.58}\right)\sqrt{gH_{m0}} = \left(0.34 + \left(-\frac{-1.0}{1.5}\right)^{1.58}\right)\sqrt{9.8 * 1.5}$$
$$= 3.32\ \frac{m^3}{s} per\ m \qquad \text{(Eqn. 2-38)}$$

$$d_m = 0.4\left[\frac{1}{g\sin\theta}\right]^{1/3}(q_{ws})^{2/3} = 0.4\left[\frac{1}{9.8 * 0.316}\right]^{1/3}(3.32)^{2/3} = 0.61\ m \qquad \text{(Eqn. 2-63)}$$

$$H_{rms} = 3.43 * exp\left(\frac{R_c}{H_{m0}}\right) * d_m = 3.43 * exp\left(\frac{-1.0}{1.5}\right) * 0.61 = 1.07\ m \qquad \text{(Eqn. 2-64)}$$

$$\tau_{WS,Zone1} = 0.77\gamma H_{rms} = 0.77 * 9800 * 1.07 = 8{,}100\ N/m^2 \qquad \text{(Eqn. 4-6)}$$

$$\tau_{WS,Zone2} = 0.68\gamma H_{rms} = 0.68 * 9800 * 1.07 = 7{,}100\ N/m^2 \qquad \text{(Eqn. 4-7)}$$

Table 4.25 Example Combined Overtopping Shear Stress Values

Negative Freeboard	**Significant Wave Height**	**Combined Overtopping Discharge**	**Average Landward Slope Flow Thickness**	**RMS Wave Height**	**Combined Overtopping Shear Stress**	
R_c	H_{m0}	q_{ws}	d_m	H_{rms}	$\tau_{ws,Zone1}$	$\tau_{ws,Zone2}$
(m)	*(m)*	*(m^3/s per m)*	*(m)*	*(m)*	*(N/m^2)*	*(N/m^2)*
0.5	1	2.11	0.45	0.94	7,082	6,254
1	1	4.19	0.71	0.90	6,757	5,967
1.5	1	7.01	1.00	0.76	5,749	5,077
0.5	1.5	1.98	0.43	1.06	8,017	7,080
1	1.5	3.32	0.61	1.07	8,088	7,143
1.5	1.5	5.14	0.81	1.02	7,725	6,822
0.5	2	2.00	0.44	1.16	8,775	7,749
1	2	2.99	0.57	1.18	8,902	7,861
1.5	2	4.32	0.72	1.17	8,840	7,807
0.5	2.5	2.07	0.45	1.25	9,442	8,338
1	2.5	2.85	0.55	1.26	9,533	8,418
1.5	2.5	3.89	0.68	1.27	9,593	8,472

CHAPTER V

SUMMARY AND CONCLUSIONS

This thesis examined surge and combined overtopping of levees typical to the Gulf Coast. A 25:1 length, 5:1 time-scaled physical model was tested with 36 runs. Each run was a variation of three negative freeboards (0.3 to 1.5 m), three wave heights (0.9 to 2.5 m), and three wave periods (6 to 14 s). Flow thickness was recorded at seven locations along the levee crest and landward slope, and velocity was recorded at two locations on the landward slope. A pressure gauge system recorded depth, and a laser Doppler Velocimeter system recorded velocities. Surge overtopping conditions were recorded until waves reached the levee, and combined overtopping conditions were recorded after a buffer period to let waves fully develop. The LDV system did not record the initial steady surge velocity during the smallest magnitude negative freeboard condition.

Depths and velocities were preprocessed by synchronizing the starting times of each recording system, adjusting depth measurements to bottom out at zero, and converting to prototype units. Depth and velocity outliers were also removed. Combined overtopping produced prototype-scale velocity near 16 m/s at PG7 and prototype-scale flow thickness of 2.7 m at PG4 with a maximum instantaneous discharge of nearly 21 m^3/s per m. Discharge, significant wave height, and freeboard were compared to previous studies and are in good agreement.

Equations 4-1 through 4-3 were used to estimate shear stress during surge and combined overtopping along the landward slope. Similar to previous studies, an approximation of shear stress accounting for spatially changing depths and temporally and spatially changing velocities (Equation 4-3) estimated the smallest shear stress when compared to the other equations because the flow was still accelerating. Equations 4-4 and 4-5 estimate surge overtopping shear stress as a function of discharge. Several previous studies had similar results. A numerical model predicted similar flow parameters and shear stresses.

This thesis along with a previous study was used to develop a relationship for determining representative landward slope shear stress. Maximum combined overtopping shear stresses reached 10,000 N/m^2 along the landward slope. Zone 1 experienced smaller shear stresses compared to Zone 2; see Figure 4.21. Several assumptions were made to calculate Zone 1 shear stress which need further examination; see Section 4.3.1. Equations 4-4 and 4-5 were developed to predict landward slope shear stress during surge overtopping and Equations 4-6 and 4-7 for combined overtopping.

The objective of this thesis was to develop a prediction of peak shear stresses along the landward slope of a levee; see Equations 4-4 through 4-7. Multiple studies have examined surge and combined overtopping flow conditions but few studies have researched surge and combined overtopping shear stress. This thesis builds off a previous study (Nadal and Hughes 2009) by measuring depth and velocity at two levee landward slope locations allowing for shear stress estimation in unsteady, non-uniform flow. Estimates from this thesis are in good agreement with previous studies (Hughes and Nadal 2009 and Nadal and Hughes 2009).

REFERENCES

Aquaveo. 2010. *About Us*. Aquaveo Water Modeling Solutions. South Jordan, Utah. http://www.aquaveo.com/about-us

ASCE Katrina External Review Panel. 2007. *The New Orleans Hurricane Protection System: What Went Wrong and Why*. Reston, Virginia: ASCE.

Berger, C and J Tate. 2009. *Guidelines for Solving Two Dimensional Shallow Water Problems with the ADapative Hydraulics (ADH) Modeling System*. https://adh.usace.army.mil/

Briaud, J, H Chen, A Govindasamy, and R Storesund. 2008. Levee Erosion by Overtopping in New Orleans during the Hurricane Katrina. *Journal of Geotechnical and Geoenvironmental Engineering*. Volume 134, Issue 5: Pages 618 to 632, ASCE.

Budhu, Muni. 2008. *Foundations and Earth Retaining Structures*. Danvers, MA: John Wiley & Sons, Inc.

Chaudhry, H. 1993. *Open-Channel Flow*. Englewood Cliffs, NJ: Prentice Hall, Inc.

CHL. 2009. *About Us*. Engineering Research and Development Center, United States Army Corps of Engineers. http://chl.erdc.usace.army.mil/about.

Department of Homeland Security (DHS). 2008. One Team, One Mission, Securing Our Homeland. *US Department of Homeland Security Strategic Plan Fiscal Years 2008-2013*.

Drain, L. 1980. *The Laser Doppler Technique*. New York, NY: John Wiley & Sons Ltd.

FHWA. 2005. Design of Roadside Channels with Flexible Linings. *Hydraulic Engineering Circular No. 15*. Volume 3, Federal Highway Administration.

García, M. 2008. Sediment Transport and Morphodynamics. *Sedimentation Engineering Processes, Measurements, Modeling, and Practice. ASCE Manuals and Reports on Engineering Practice No. 110*. Reston, VA: Pages 21–164, ASCE.

Goda, Y and Y Suzuki. 1976. Estimation of Incident and Reflected Waves in Random Wave Experiments. *Proceedings 15th International Coastal Engineering Conference*. Volume 1: Pages 828–845, ASCE.

Henderson, F. 1966. *Open Channel Flow*. New York, NY: MacMillan Company.

Hughes, S. 1993. *Physical Models and Laboratory Techniques in Coastal Engineering*. Advanced Series on Ocean Engineering, Volume 7. Singapore: World Scientific Publishing Company, Inc.

Hughes, S. 2008. Combined Wave and Surge Overtopping of Levees: Flow Hydrodynamics and Articulated Concrete Mat Stability. *ERDC/CHL TR-08-10*. US Army Corp of Engineers Engineer Research and Development Center, Coastal and Hydraulics Laboratory.

Hughes, S and N Nadal. 2009. Laboratory Study of Combined Wave Overtopping and Storm Surge Overflow of a Levee. *Coastal Engineering*. Volume 56: Pages 244-359, Elsevier.

Hughes, S and J Shaw. 2011. Continuity of Instantaneous Overtopping Discharge with Application to Stream Power Concepts. *Journal of Waterway, Port, Coastal, and Ocean Engineering*. Volume 137, Number 1: Page Numbers Not Yet Assigned.

Hunt, A. 1959. Design of Seawalls and Breakwaters. *Journal of Waterways and Harbors Division*. Volume 85, Issue 3: Pages 123-152, ASCE.

Irish, J, D Resio, and J Ratcliff. 2003. The Influence of Storm Size on Hurricane Surge. *Journal of Physical Oceanography*. Volume 38, Issue 9: Pages 2003-2013, American Meteorological Society.

Munson, B, D Young, and T Okkishi. 2006. *Fundamentals of Fluid Mechanics, Fifth Edition*. Hoboken, NJ: John Wiley & Sons Inc.

Murphy, G. 1950. *Similitude in Engineering*. New York, NY: The Ronald Press Company.

Nadal, N and S Hughes. 2009. Shear Stress Estimates for Combined Wave and Surge Overtopping at Earthen Levees. *ERDC/CHL CHETN-III-79*. US Army Corp of Engineers Engineer Research and Development Center, Coastal and Hydraulics Laboratory.

Okayasu, A, T Suzuki, and Y Matsubayashi. 2005. Laboratory Experiment and Three-Dimensional Large Eddy Simulation of Wave Overtopping on Gentle Slope Seawalls. *Coastal Engineering Journal*. Volume 47, Issues 2 and 3: Pages 71-89, World Scientific.

Panton, R. 2005. *Incompressible Flow*. Hoboken, NJ: John Wiley & Sons Inc.

Pullen, T, N Allsop, T Bruce, A Kortenhaus, H Schüttrumpf, and J Van der Meer. 2007. *EurOtop:Wave Overtopping of Sea Defences and Related Structures: Assessment Manual*, EA, ENW, and KFKI.

Reeve, D, A Soliman, and P Lin. 2008. Numerical Study of Combined Overflow and Wave Overtopping Over a Smooth Impermeable Seawall. *Coastal Engineering*. Volume 55: Pages 155-166, Elsevier.

Schüttrumpf, H and H Oumeraci. 2005. Layer Thicknesses and Velocities of Wave Overtopping Flow at Seadikes. *Coastal Engineering*. Volume 52: Pages 473-495, Elsevier.

Schüttrumpf, H, J Moller, H Oumeraci, J Grune, and R Weissmann. 2001. Effects of Natural Sea States on Wave Overtopping of Sea Dikes. *Proceeding of International Symposium on Ocean Wave Measurements and Analysis (Waves 2001)*, San Francisco. Pages 1565–1574.

Sharp, J and W McAnally. In Review. *Numerical Levee Overtopping Grid for Storm Surge*. Advances in Water Resource Engineering.

Skoglund, V. 1967. *Similitude Theory and Application*. Scranton, PA: International Textbook Company.

SMS. 2010. *AQUAVEO Water Modeling Solutions*. http://www.ems-i.com/

Sturm, T. 2001. *Open Channel Hydraulics*. New York, NY: McGraw-Hill Companies, Inc.

US Army Engineer Research and Development Center (ERDC). 2008. *Fact Sheet*. Engineering Research and Development Center, United States Army Corps of Engineers. http://www.erdc.usace.army.mil/pls/erdcpub/WWW_WELCOME.Navigation_PAGE?tmp_Next_Page=39

van der Meer, J. 2002. *Technical Report: Wave Run-up and Wave Overtopping at Dikes*. Technical Advisory Committee of Flood Defence. Delft, The Netherlands.

Wurbs, R and W James. 2002. *Water Resource Engineering*. Upper Saddle River, NJ: Prentice Hill, Inc.

APPENDIX A

PREPROCESSED DEPTH, VELOCITY, AND DISCHARGE DATA

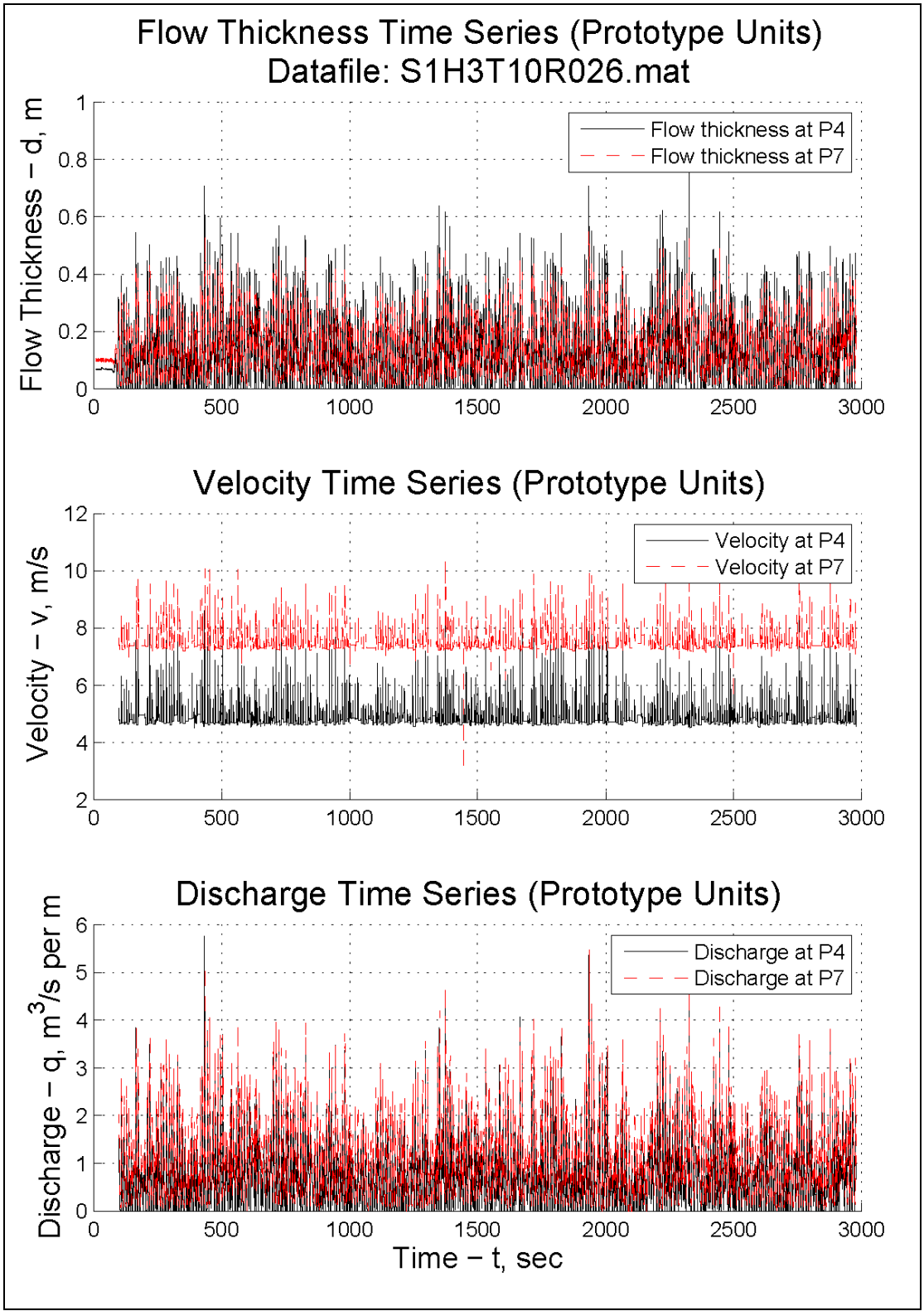

Figure A.1 Depth, Velocity, and Discharge at PG4 and PG7, Run 26

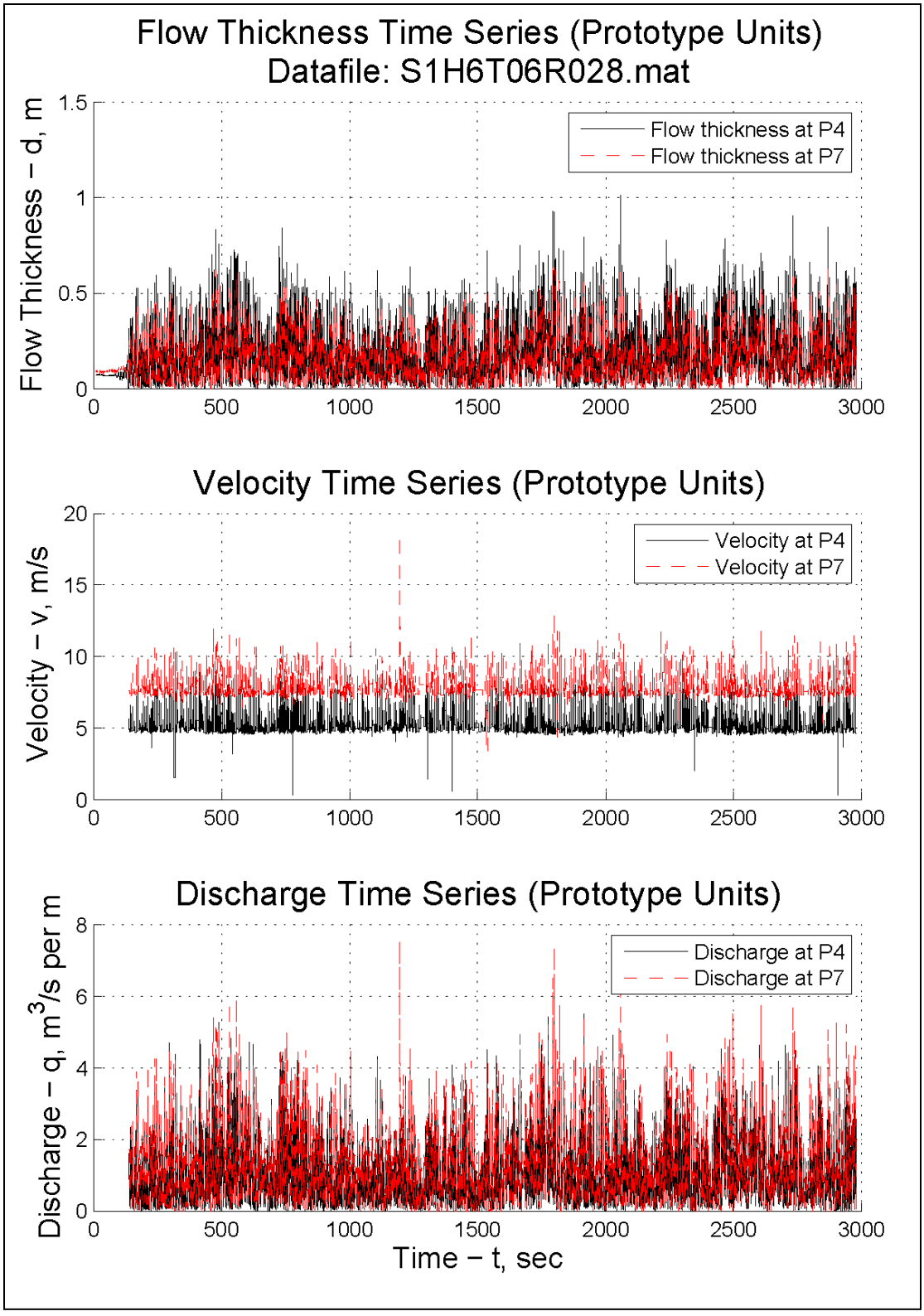

Figure A.2 Depth, Velocity, and Discharge at PG4 and PG7, Run 28

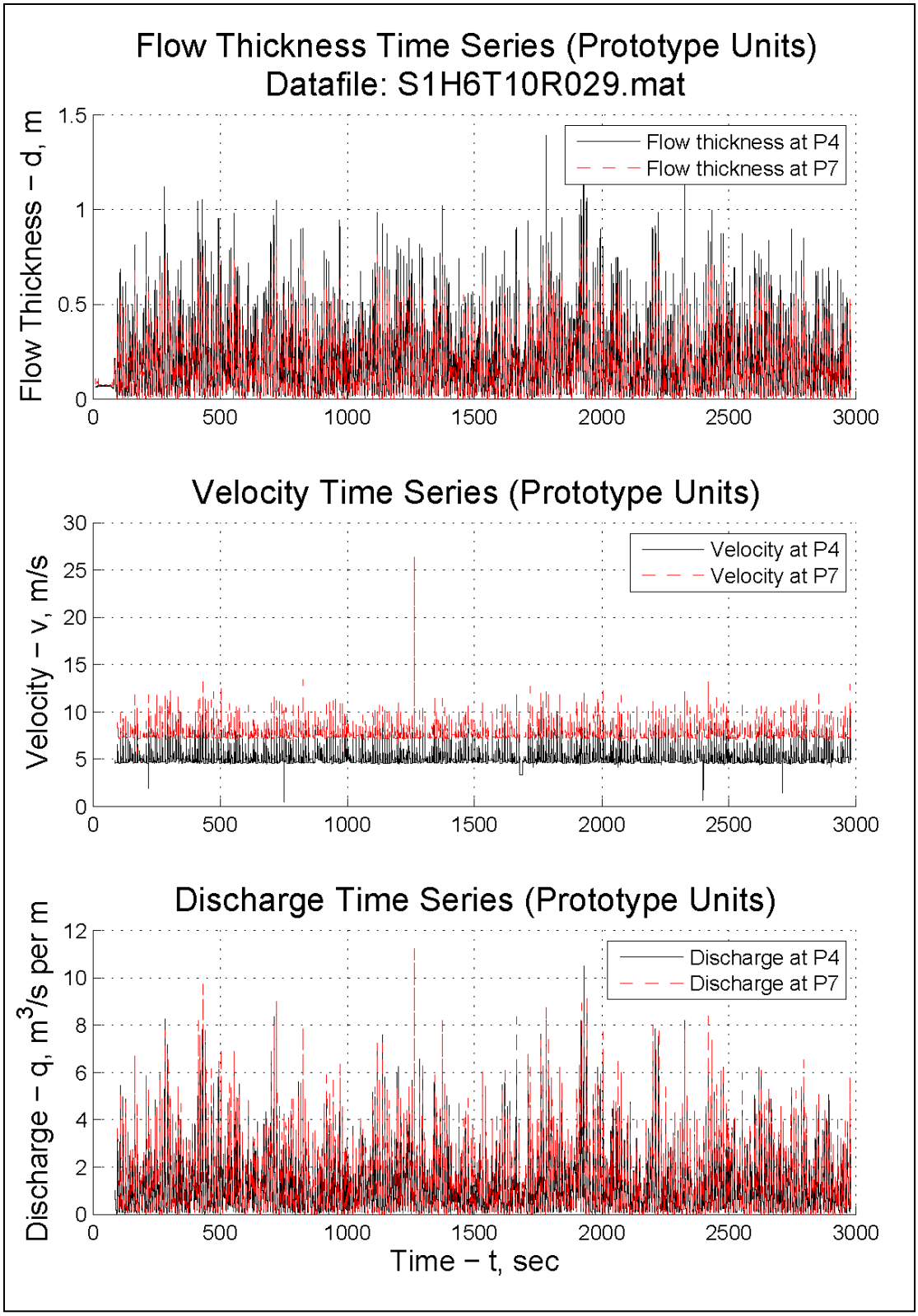

Figure A.3 Depth, Velocity, and Discharge at PG4 and PG7, Run 29

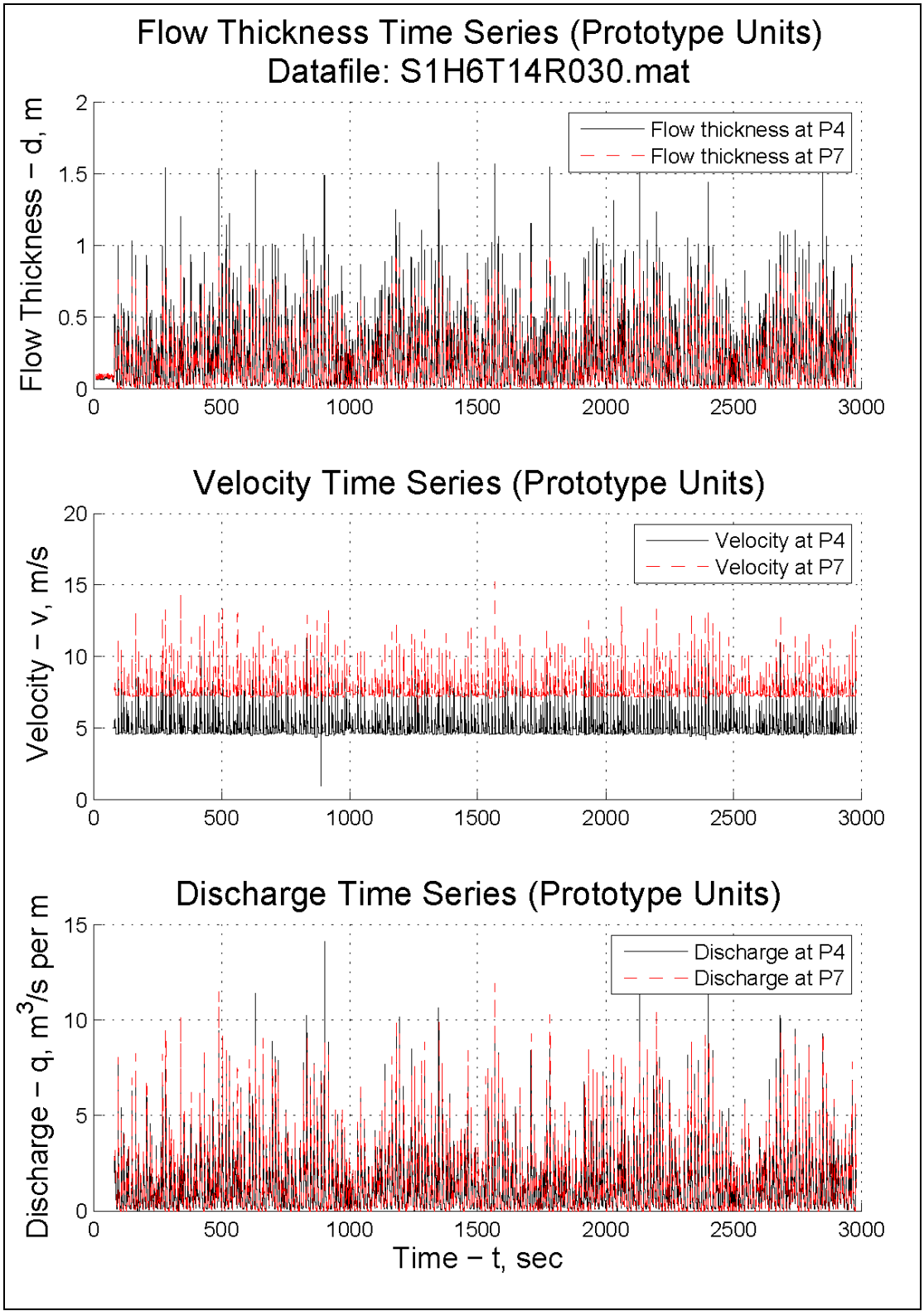

Figure A.4 Depth, Velocity, and Discharge at PG4 and PG7, Run 30

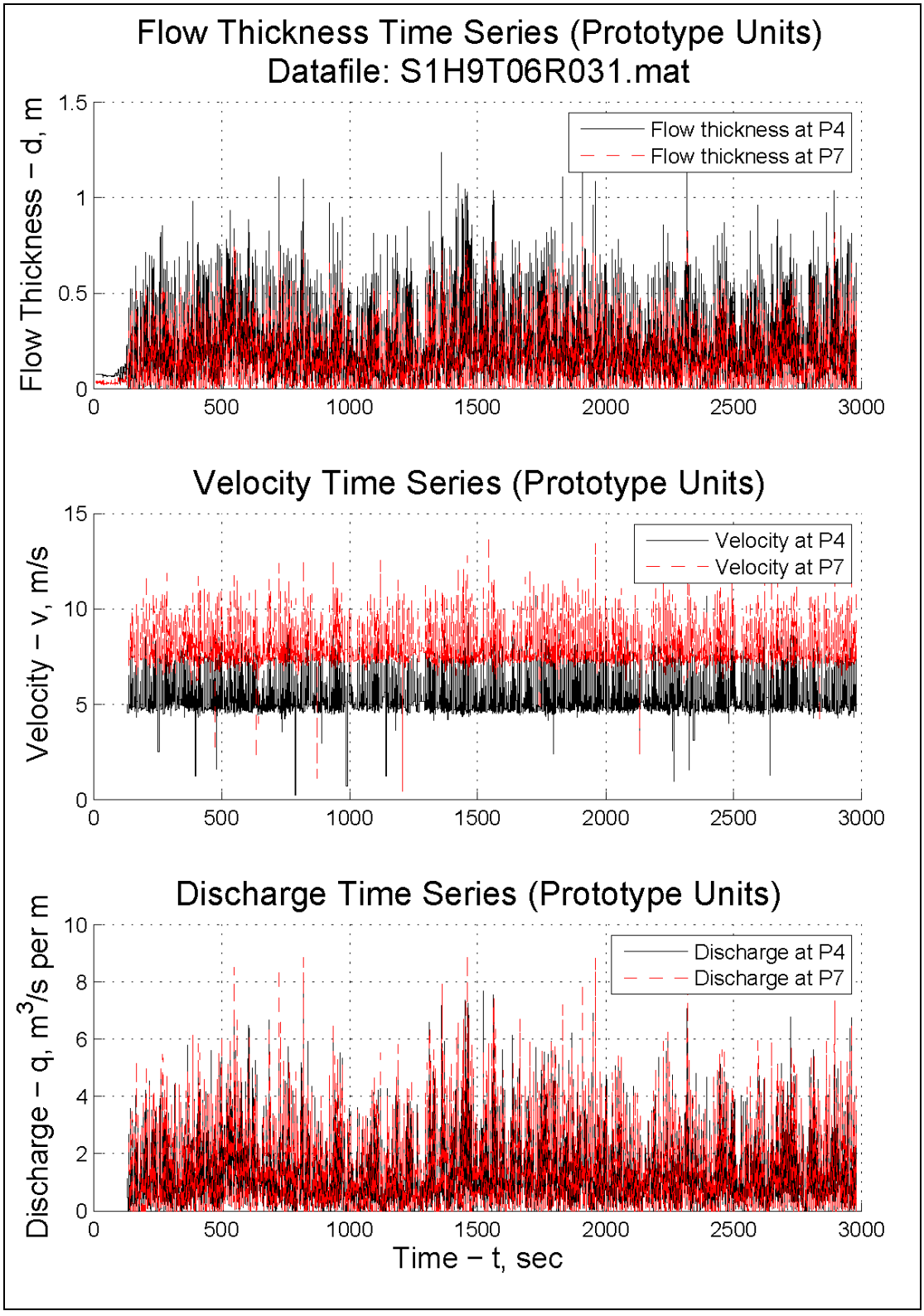

Figure A.5 Depth, Velocity, and Discharge at PG4 and PG7, Run 31

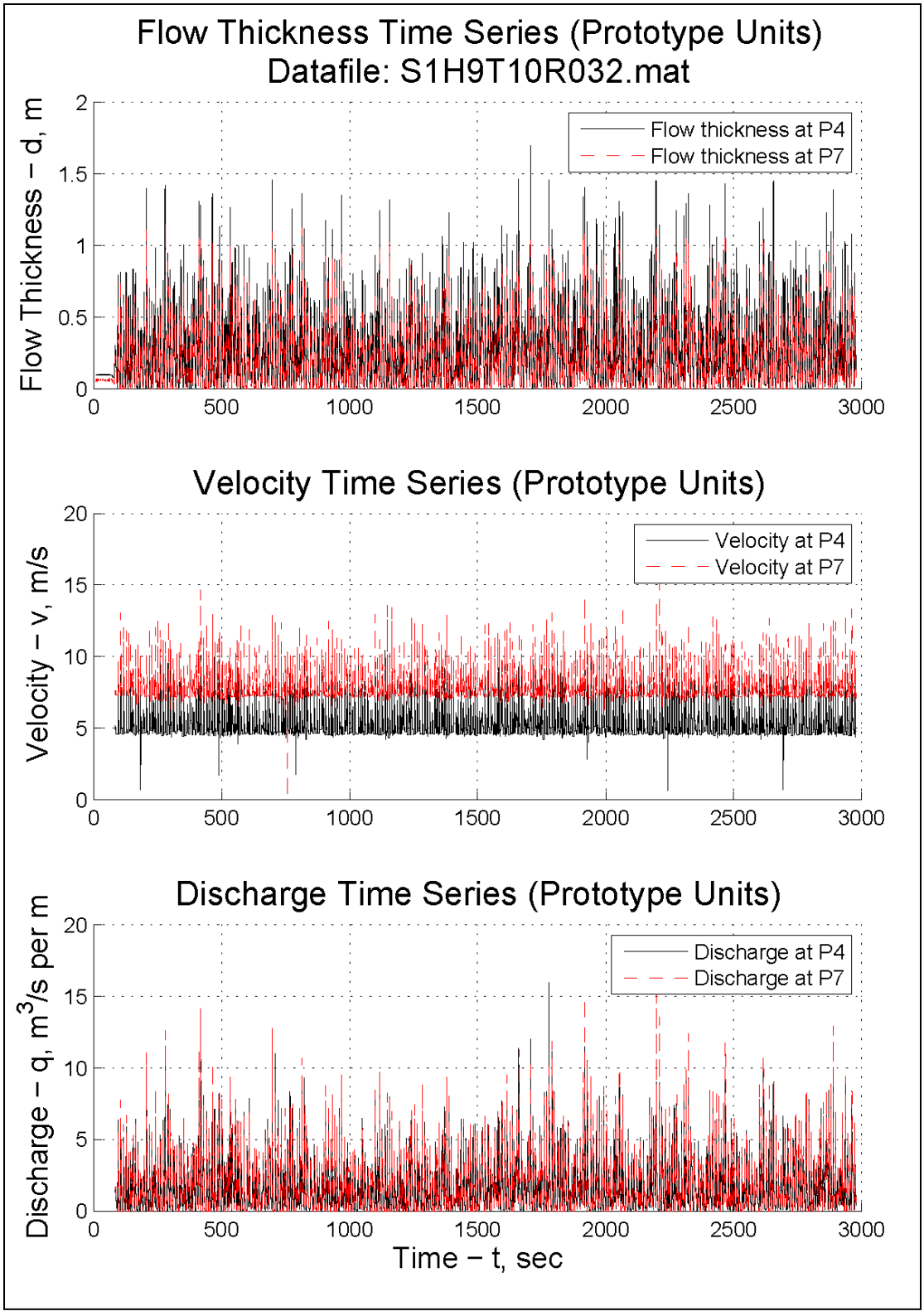

Figure A.6 Depth, Velocity, and Discharge at PG4 and PG7, Run 32

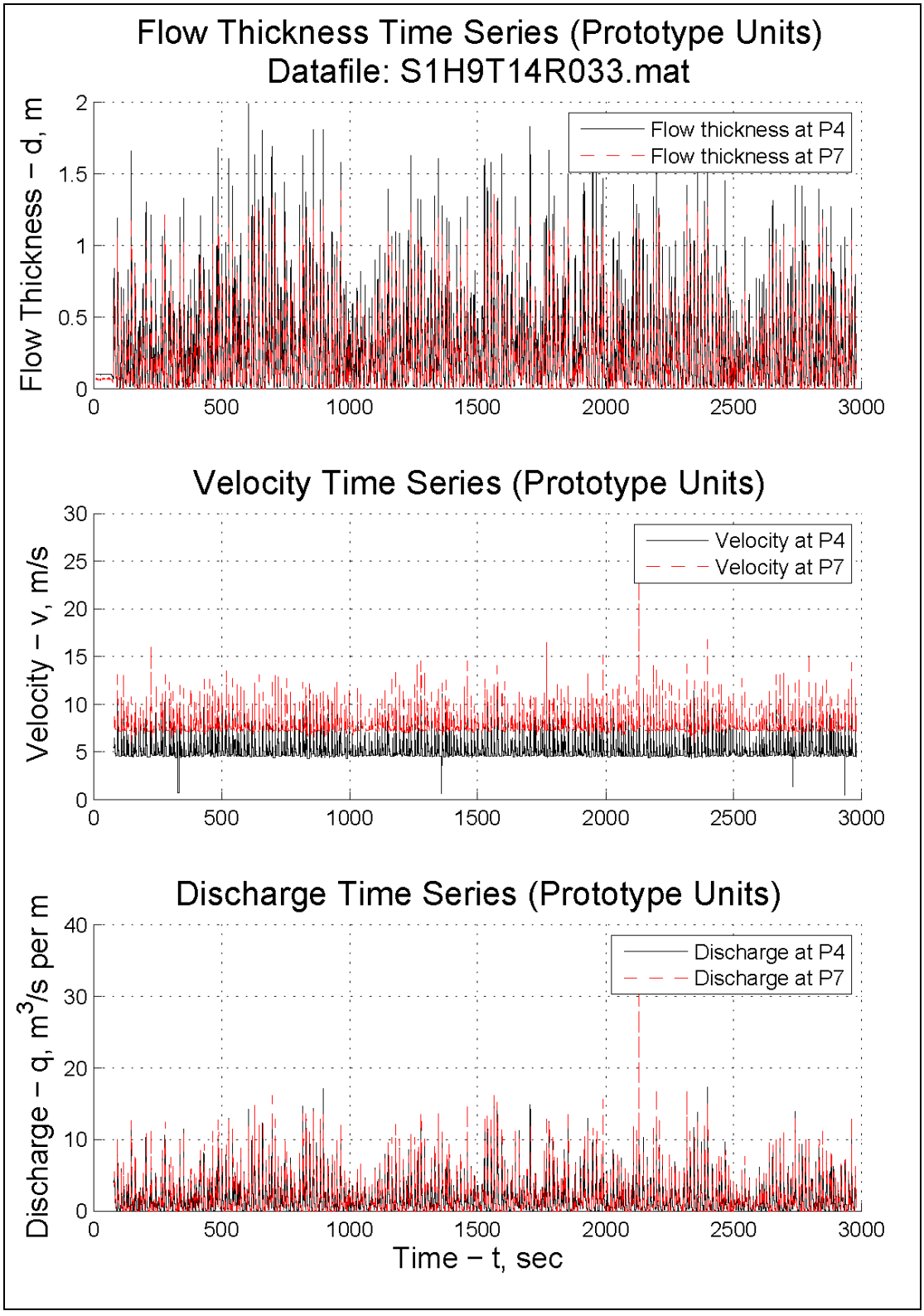

Figure A.7 Depth, Velocity, and Discharge at PG4 and PG7, Run 33

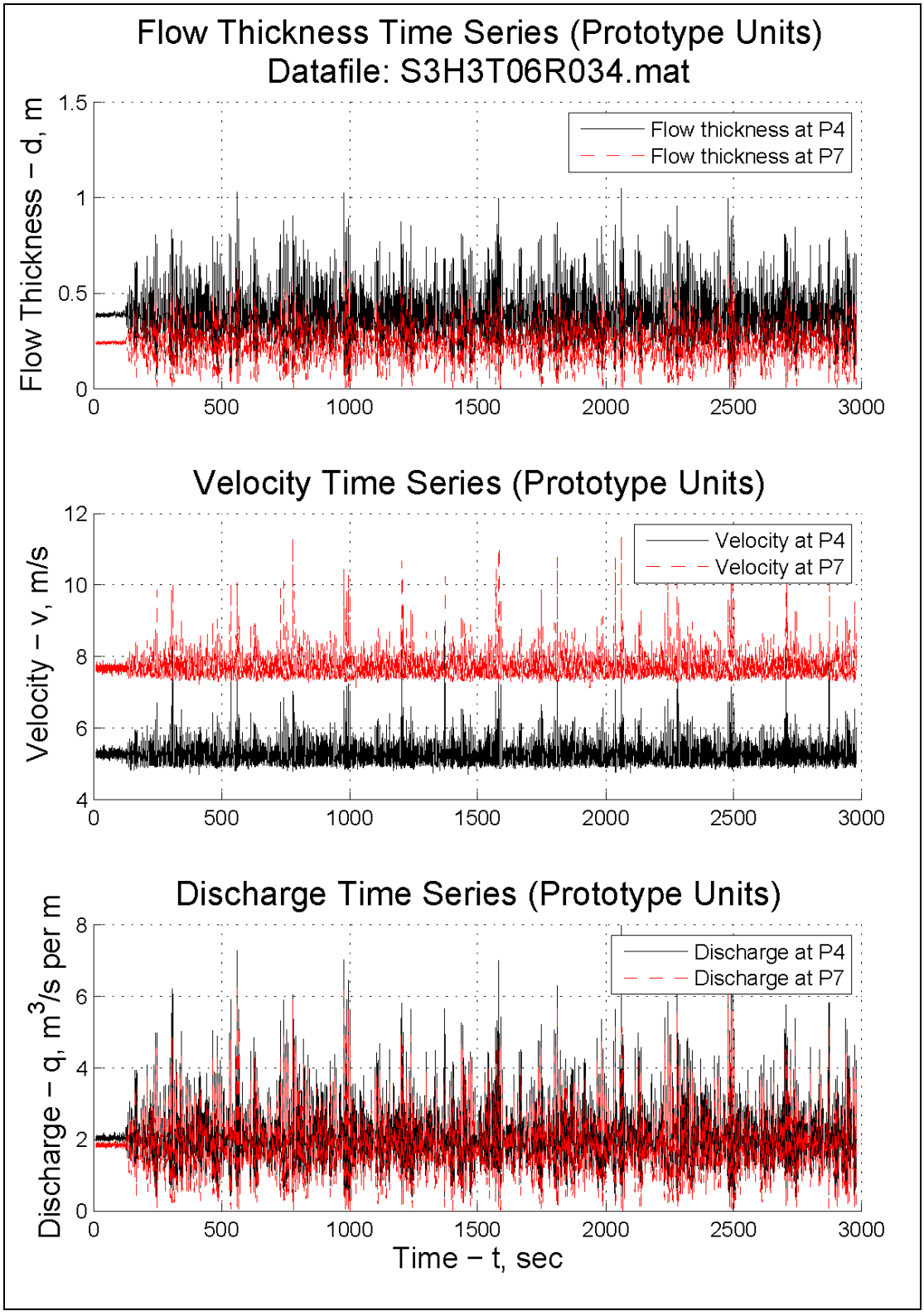

Figure A.8 Depth, Velocity, and Discharge at PG4 and PG7, Run 34

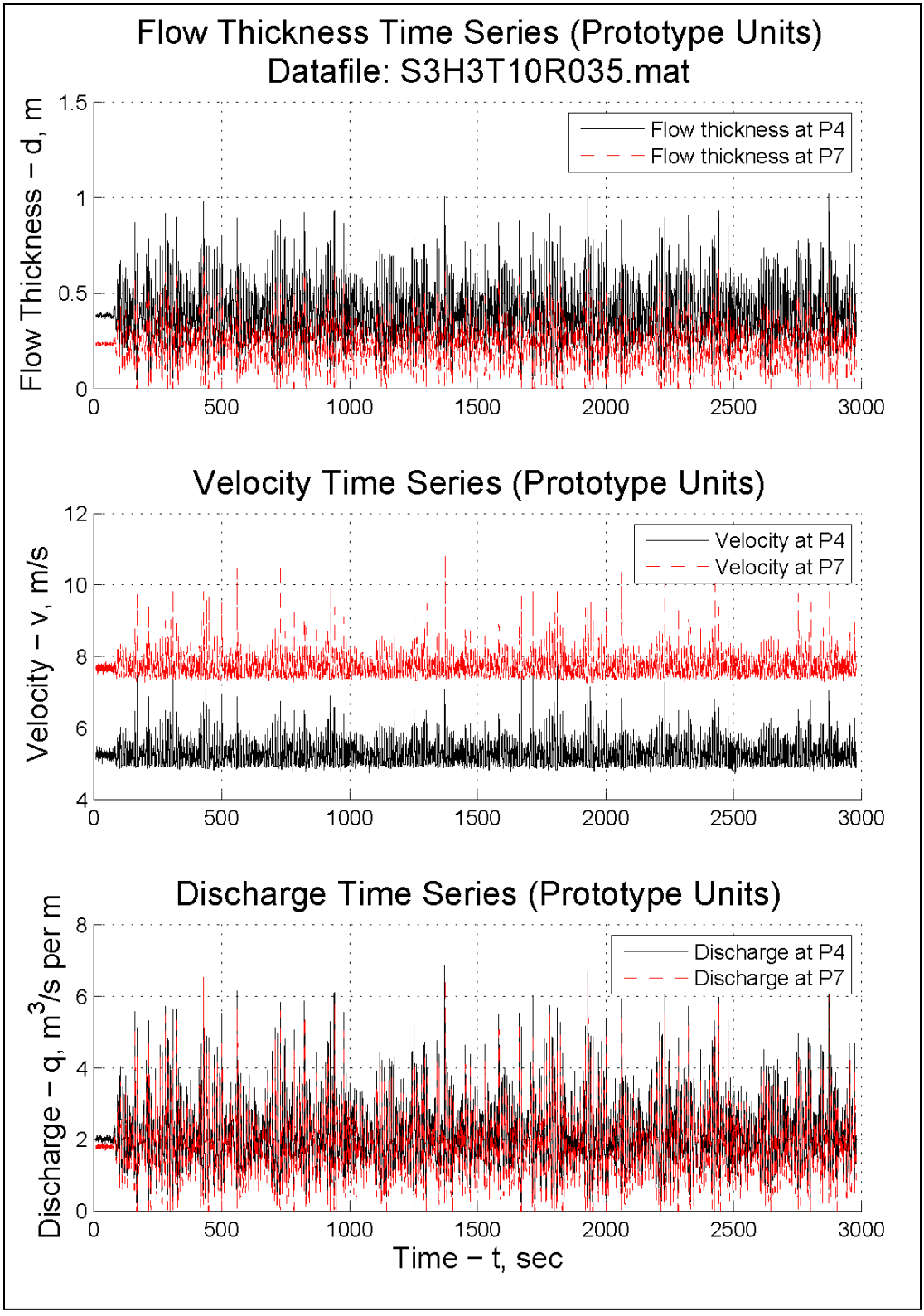

Figure A.9 Depth, Velocity, and Discharge at PG4 and PG7, Run 35

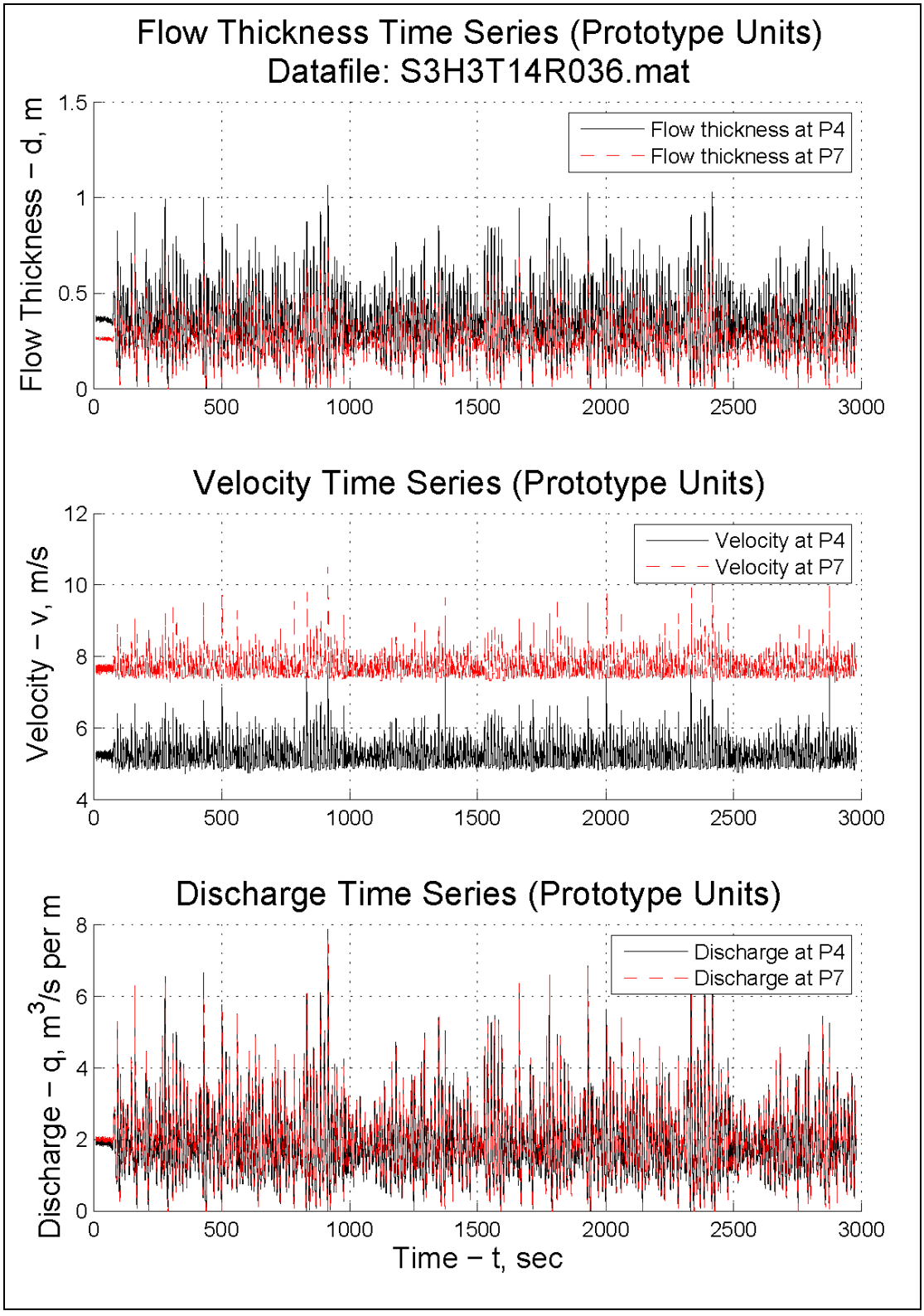

Figure A.10 Depth, Velocity, and Discharge at PG4 and PG7, Run 36

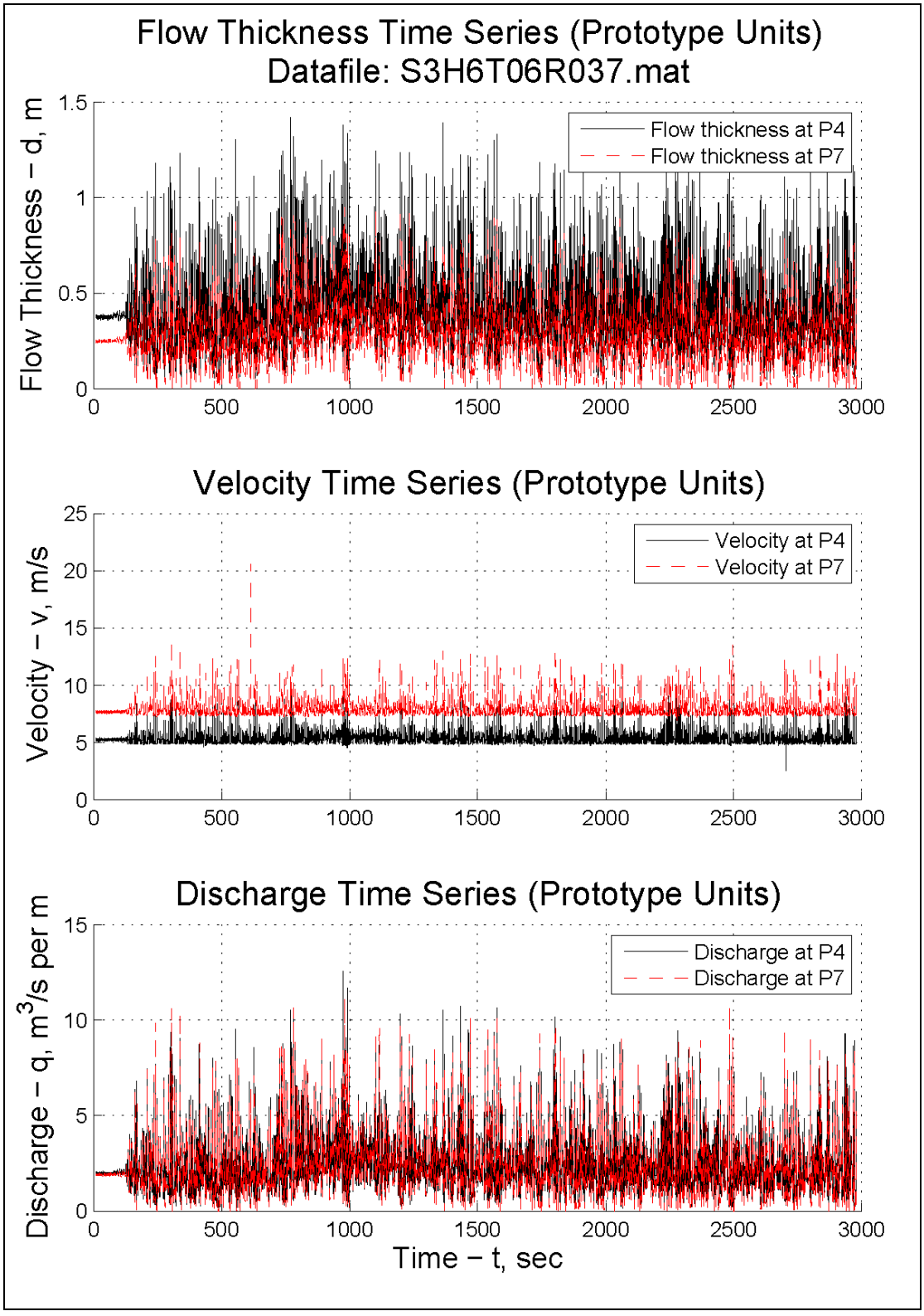

Figure A.11 Depth, Velocity, and Discharge at PG4 and PG7, Run 37

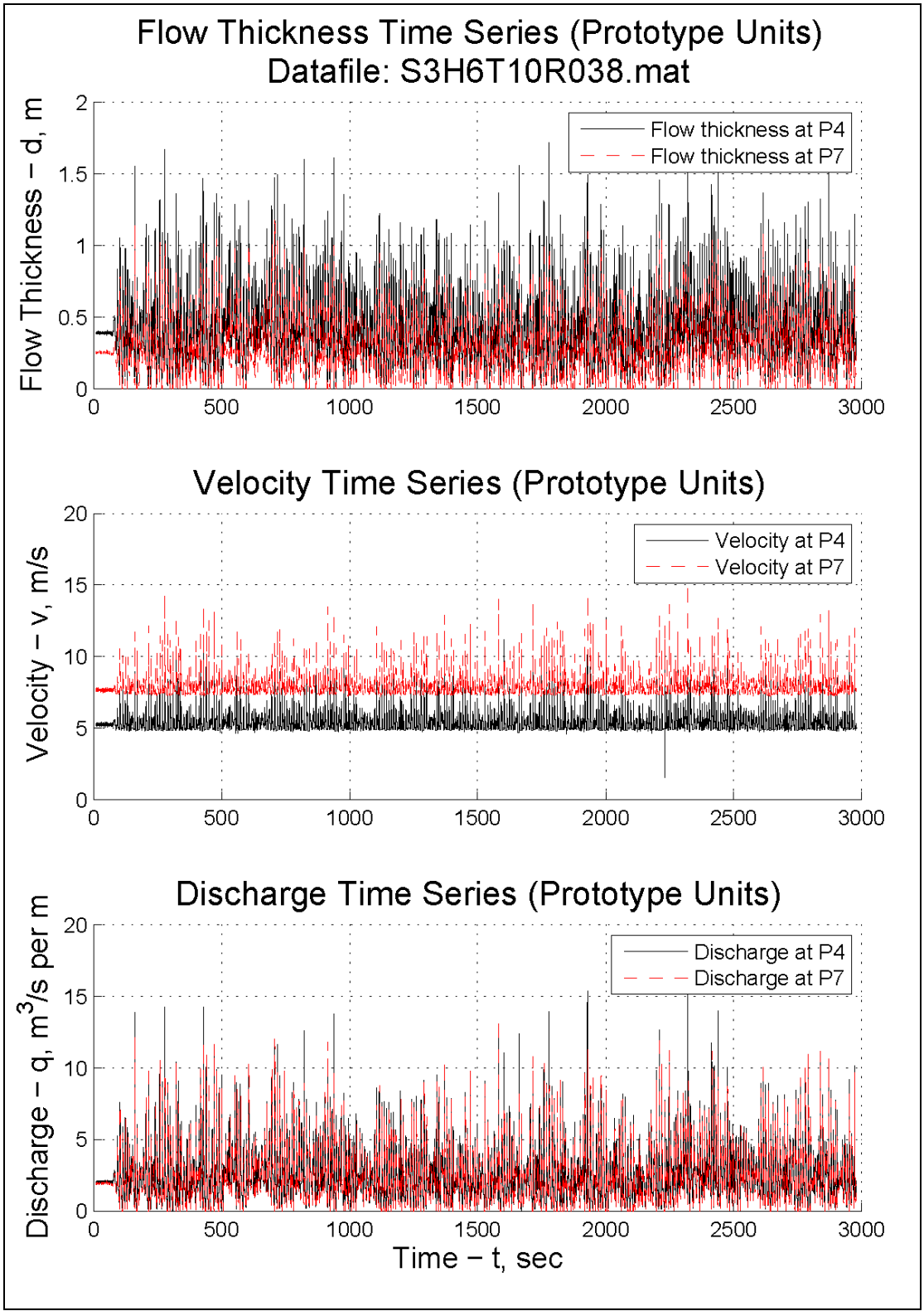

Figure A.12 Depth, Velocity, and Discharge at PG4 and PG7, Run 38

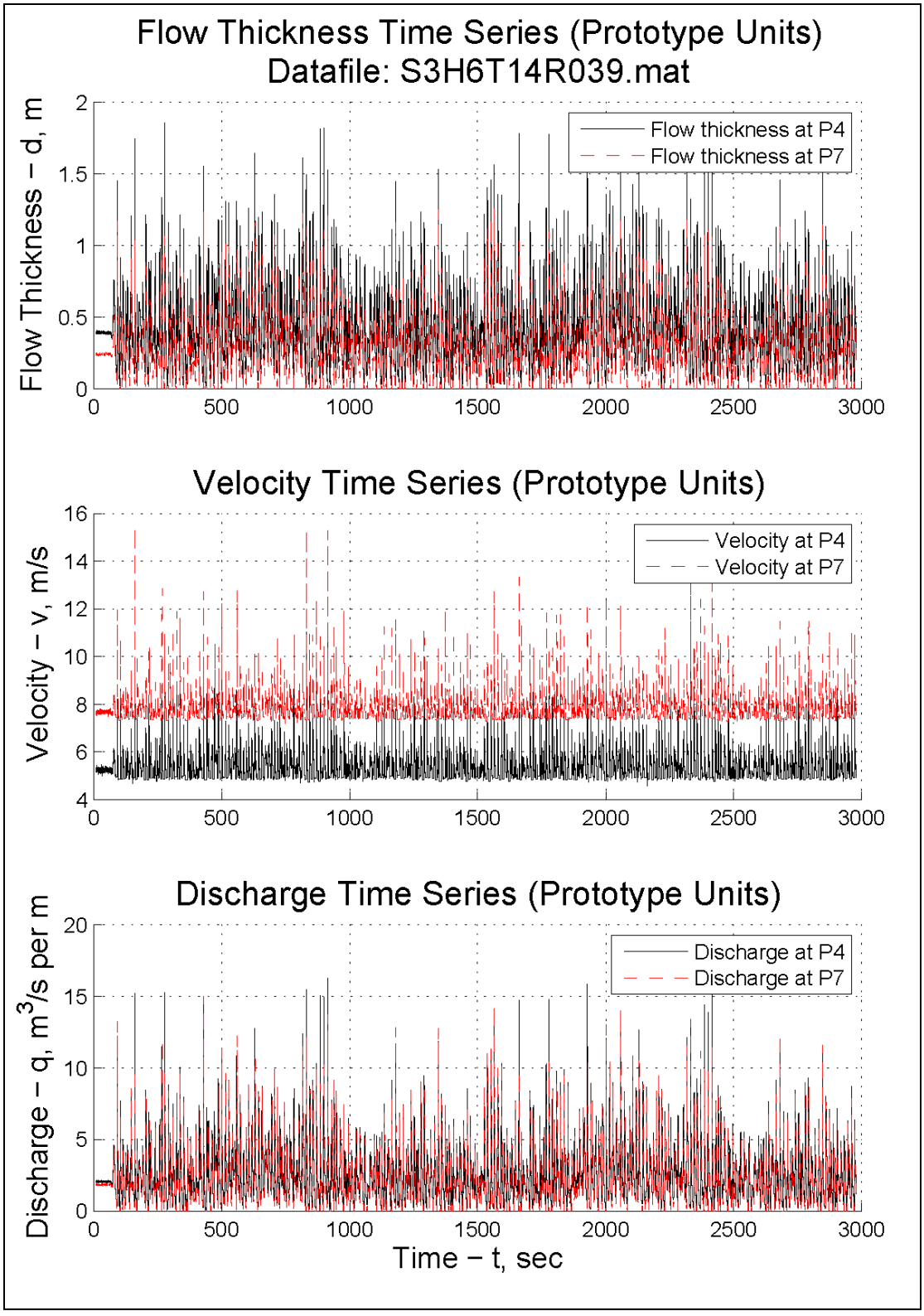

Figure A.13 Depth, Velocity, and Discharge at PG4 and PG7, Run 39

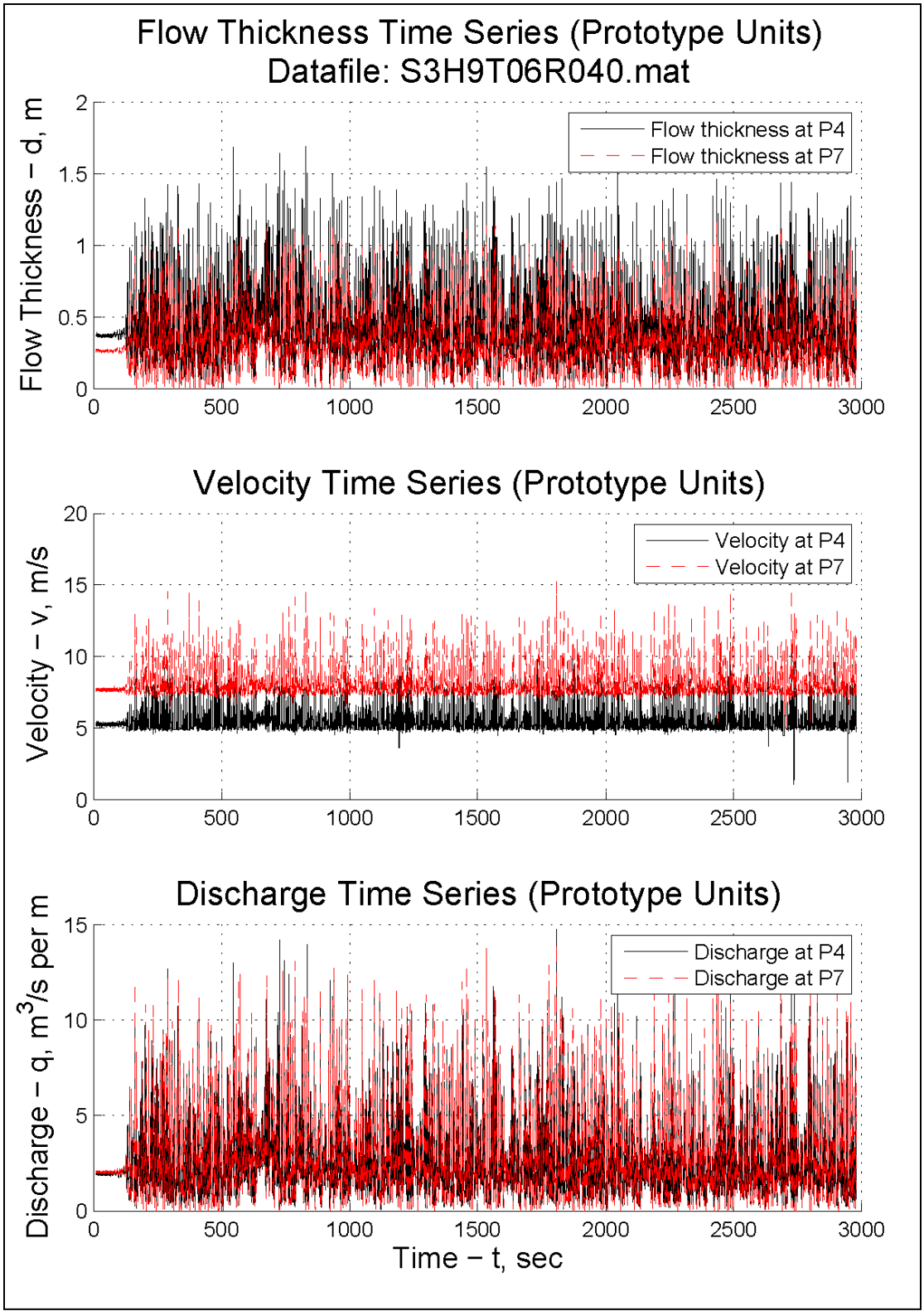

Figure A.14 Depth, Velocity, and Discharge at PG4 and PG7, Run 40

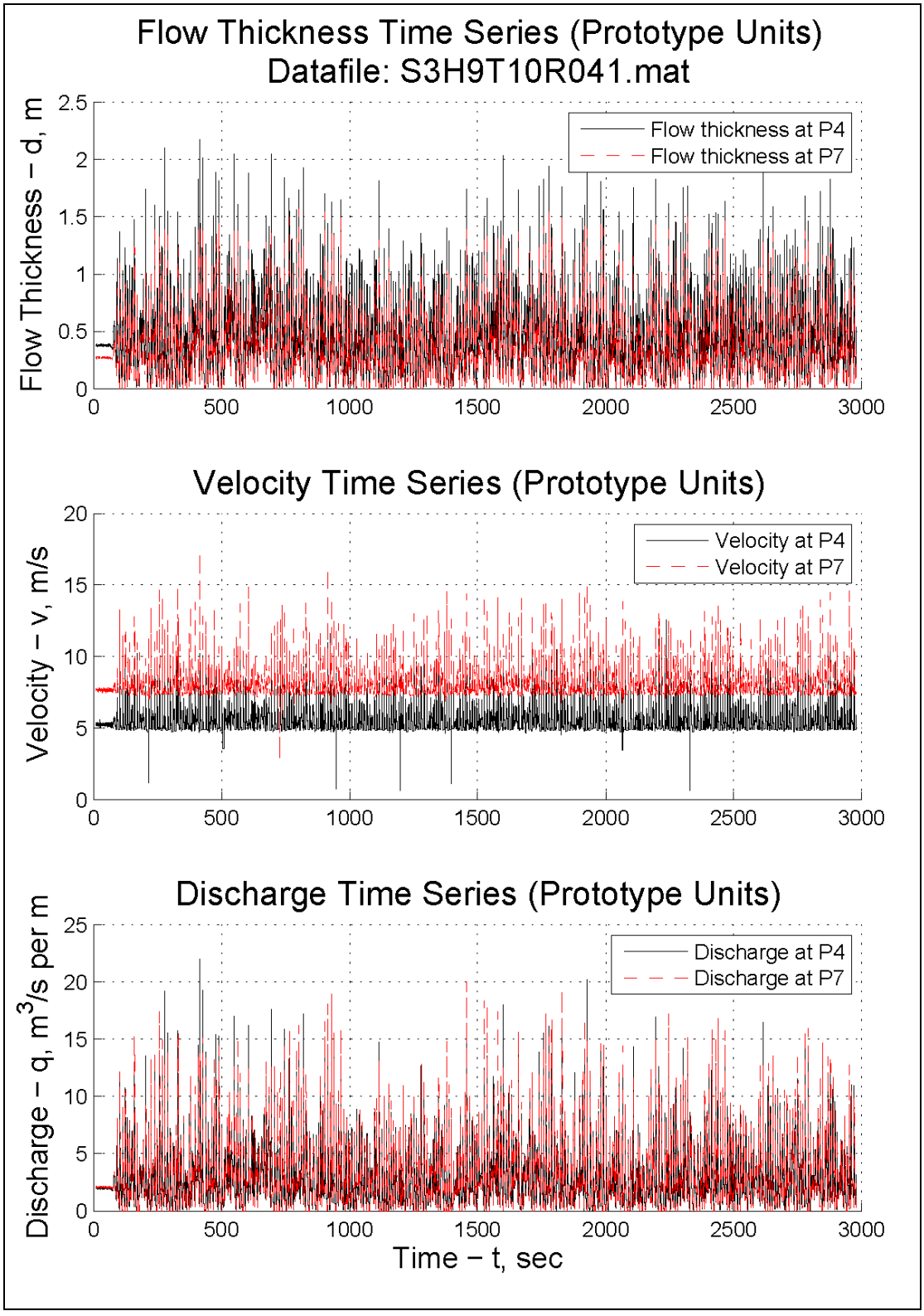

Figure A.15 Depth, Velocity, and Discharge at PG4 and PG7, Run 41

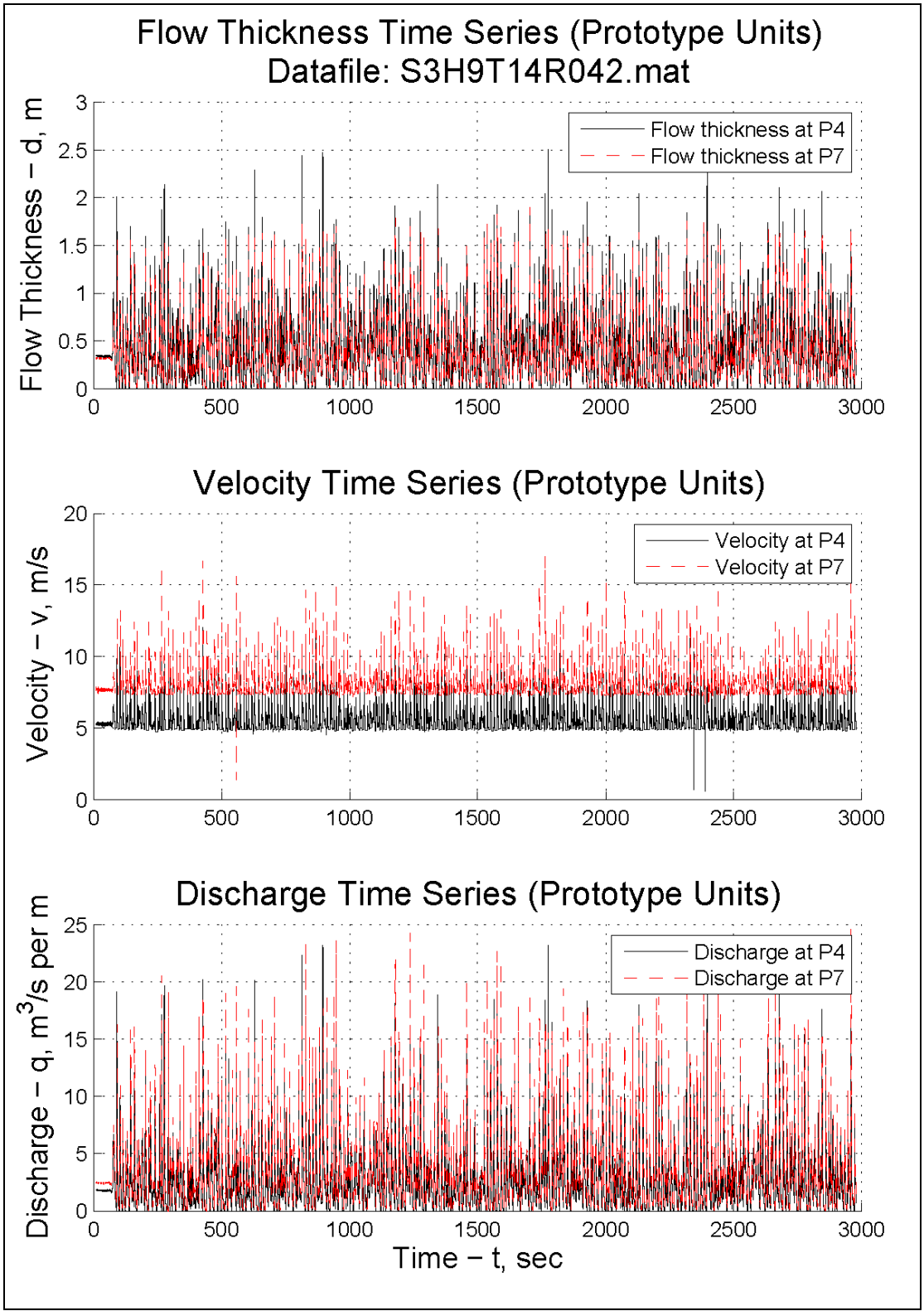

Figure A.16 Depth, Velocity, and Discharge at PG4 and PG7, Run 42

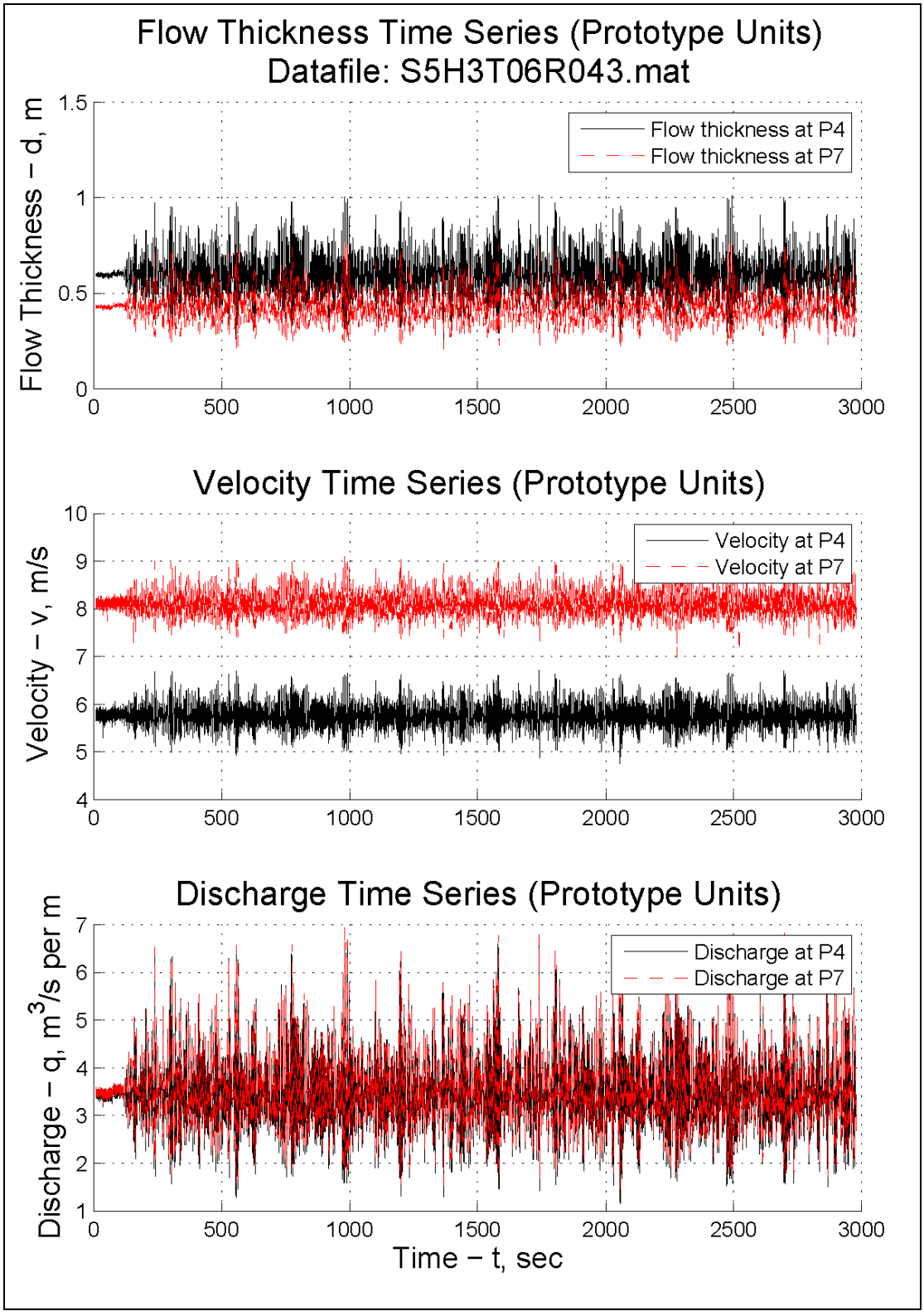

Figure A.17 Depth, Velocity, and Discharge at PG4 and PG7, Run 43

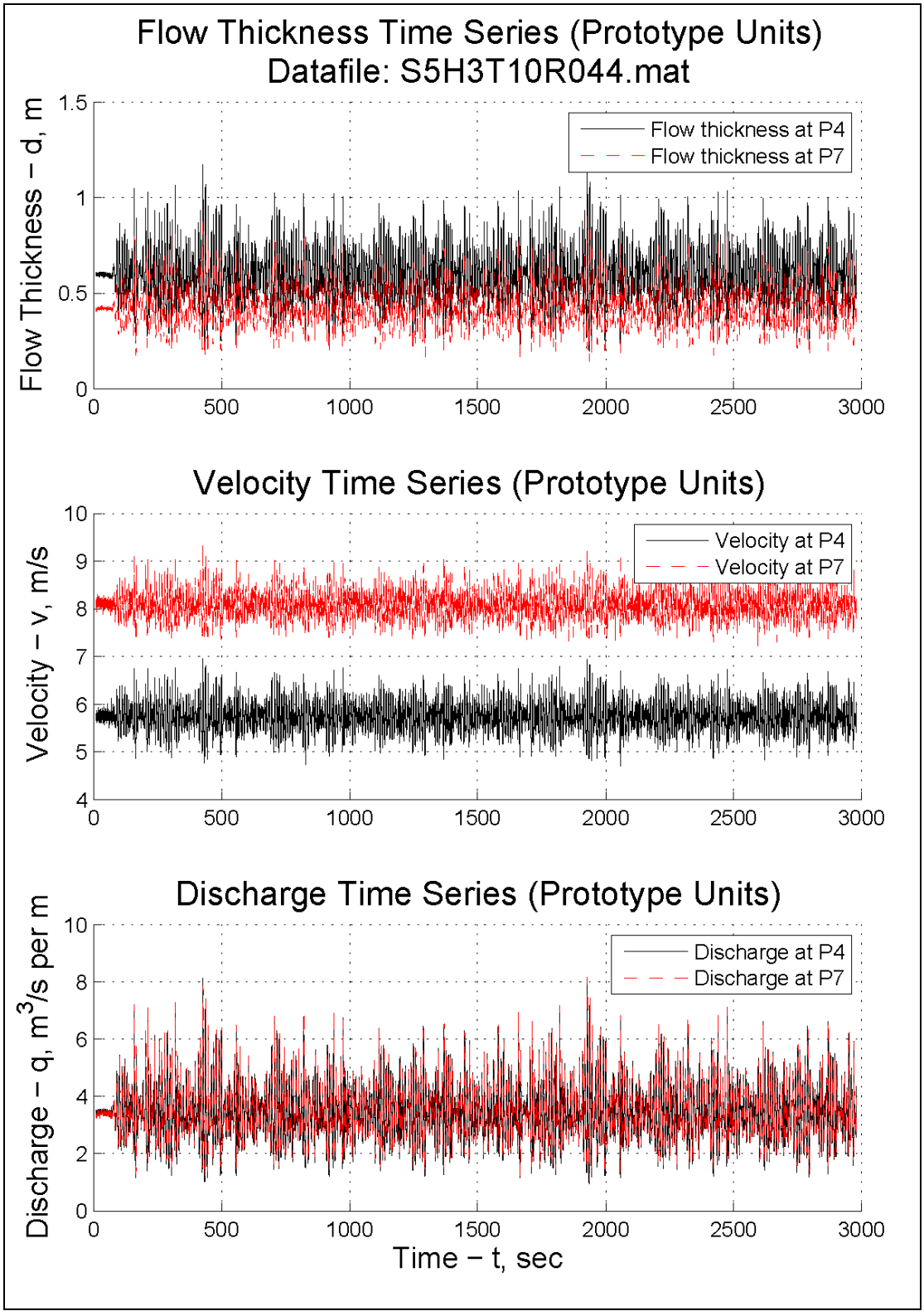

Figure A.18 Depth, Velocity, and Discharge at PG4 and PG7, Run 44

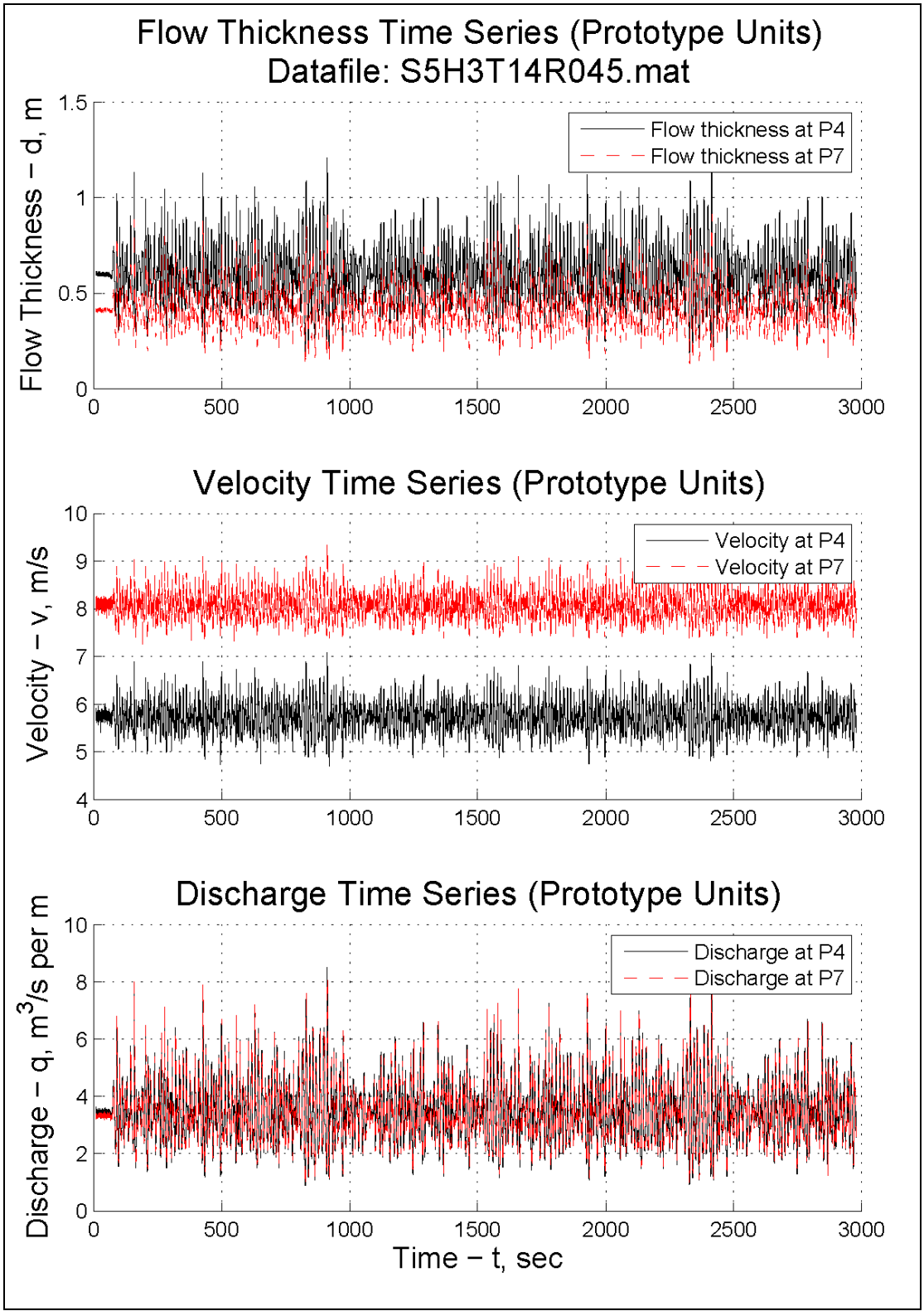

Figure A.19 Depth, Velocity, and Discharge at PG4 and PG7, Run 45

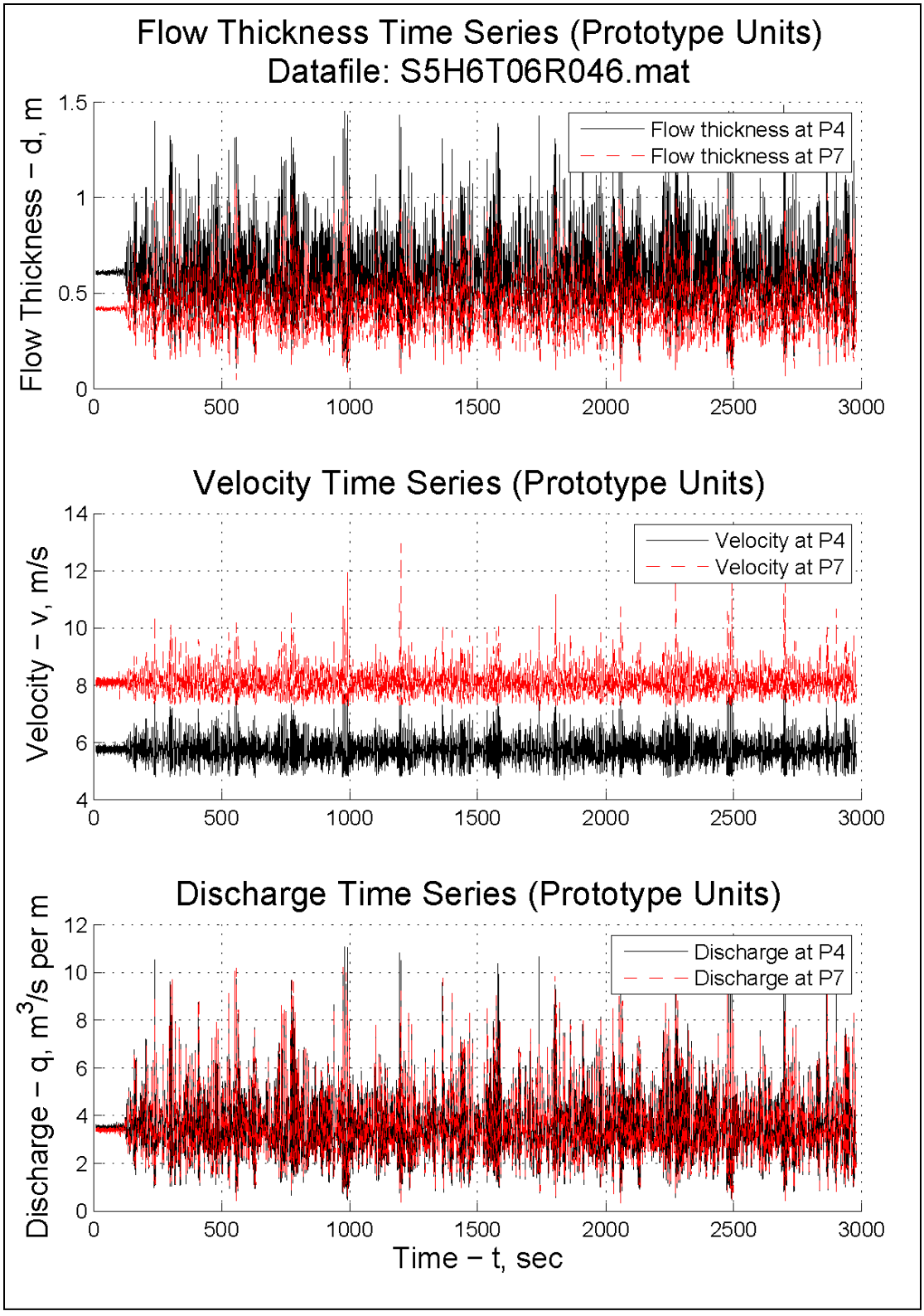

Figure A.20 Depth, Velocity, and Discharge at PG4 and PG7, Run 46

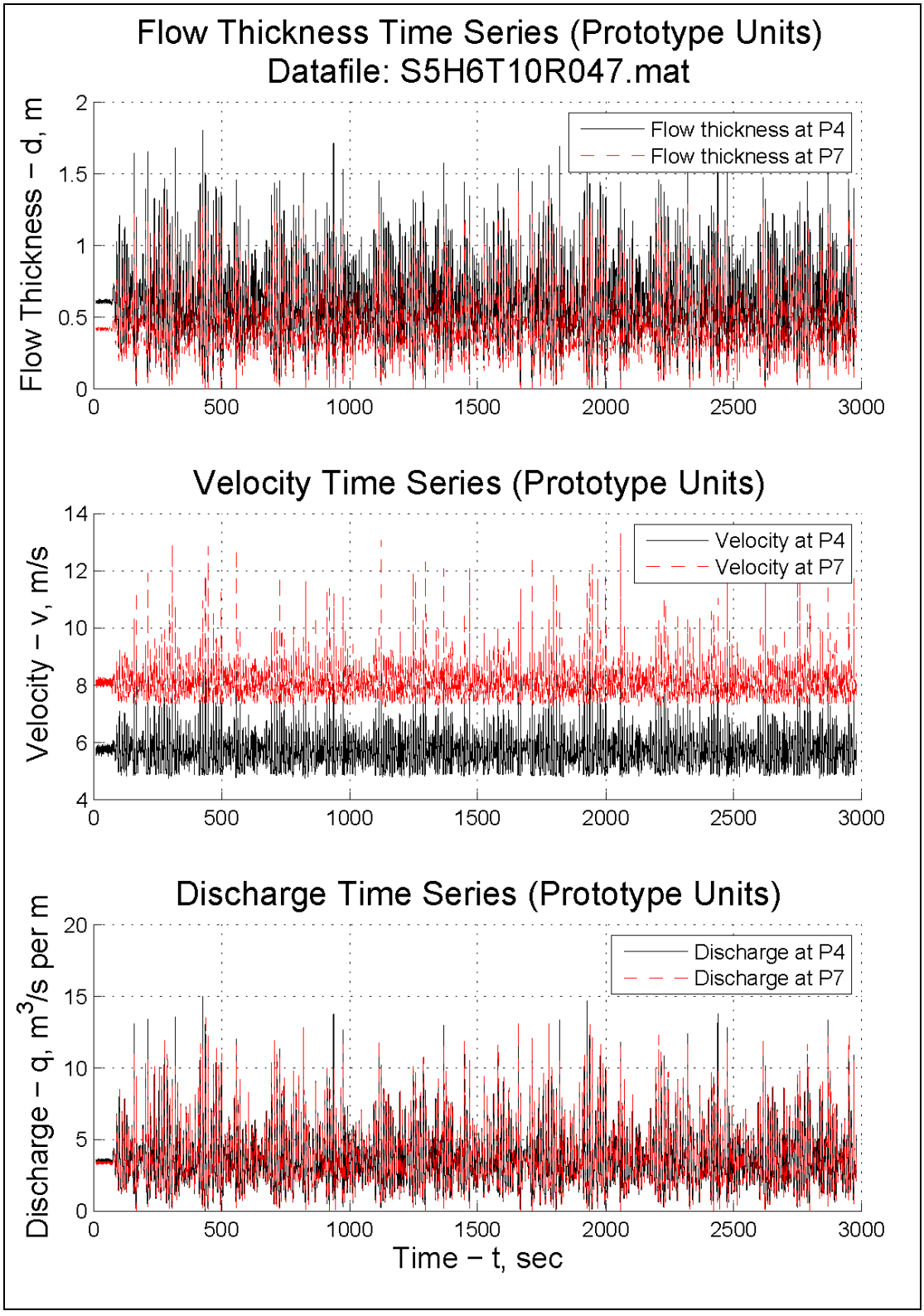

Figure A.21 Depth, Velocity, and Discharge at PG4 and PG7, Run 47

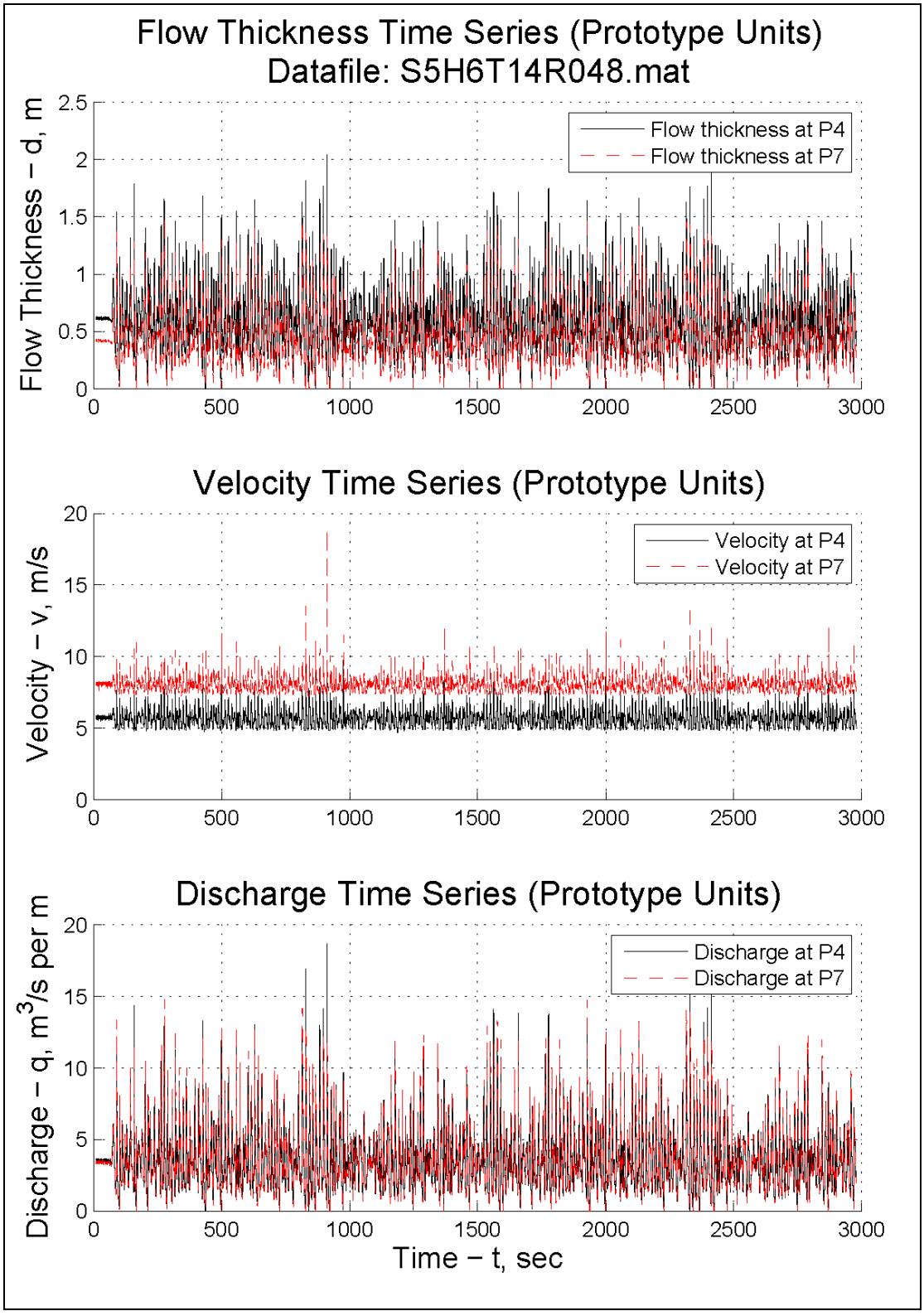

Figure A.22 Depth, Velocity, and Discharge at PG4 and PG7, Run 48

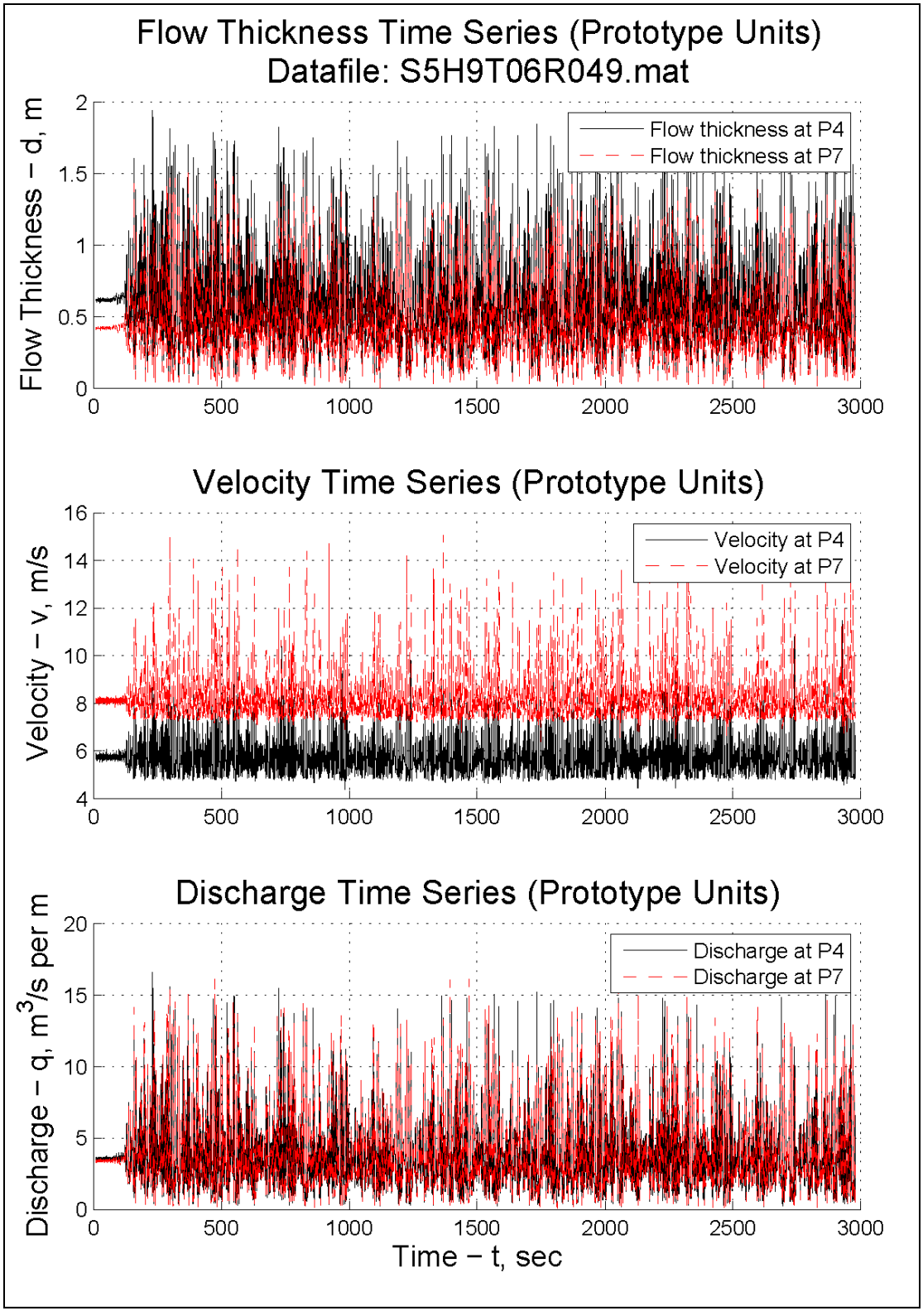

Figure A.23 Depth, Velocity, and Discharge at PG4 and PG7, Run 49

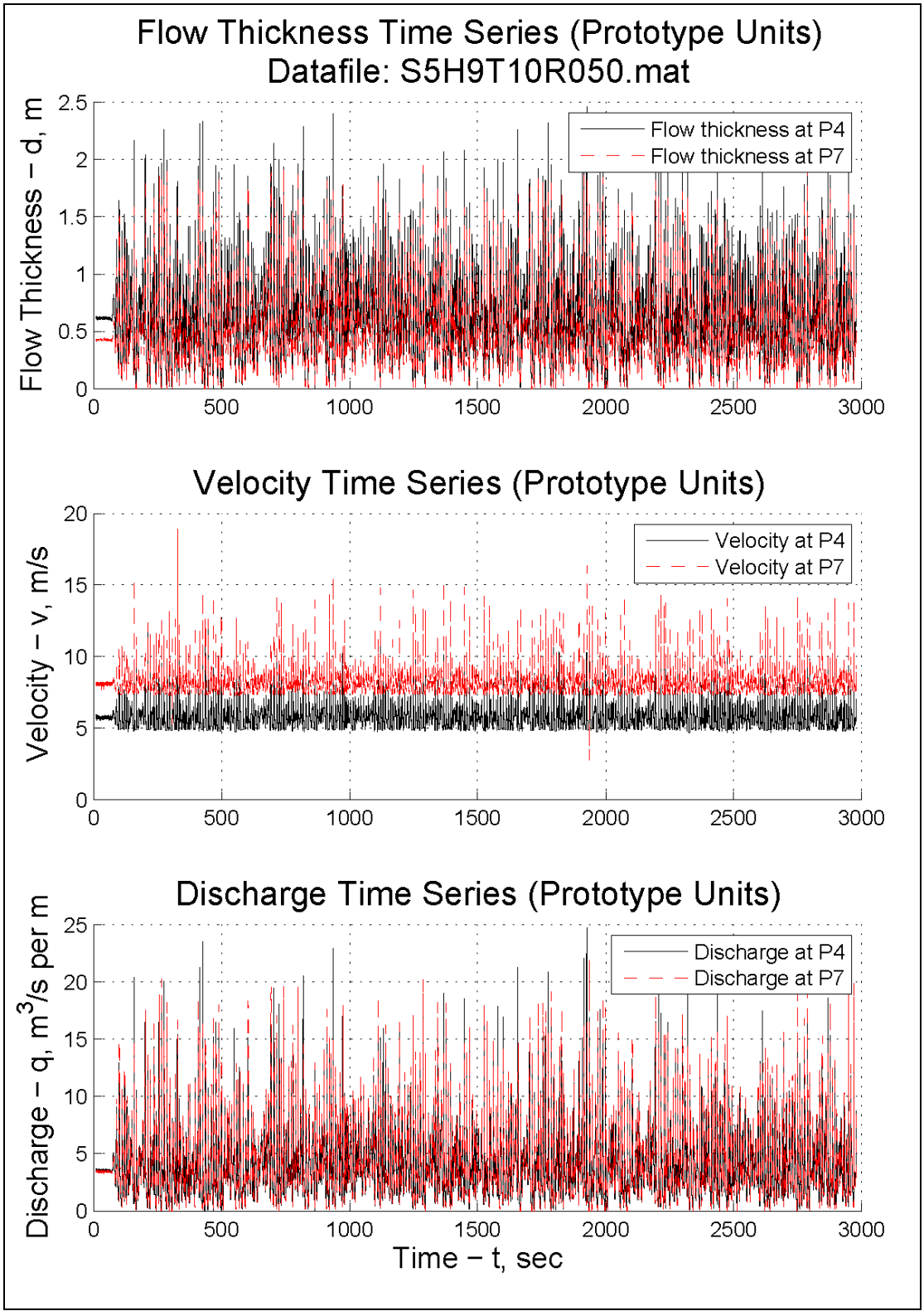

Figure A.24 Depth, Velocity, and Discharge at PG4 and PG7, Run 50

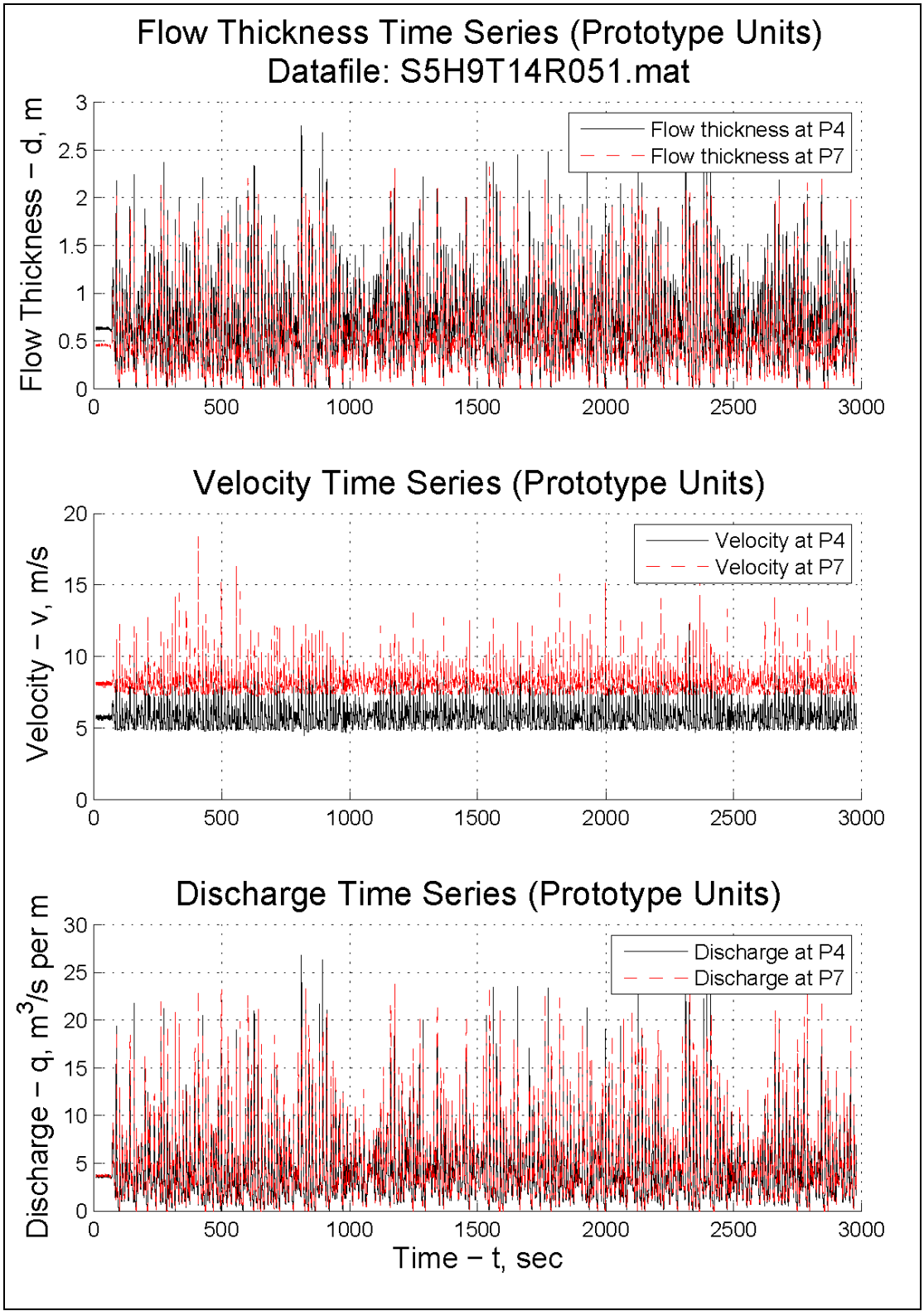

Figure A.25 Depth, Velocity, and Discharge at PG4 and PG7, Run 51

APPENDIX B

PREPROCESSED WAVE DATA

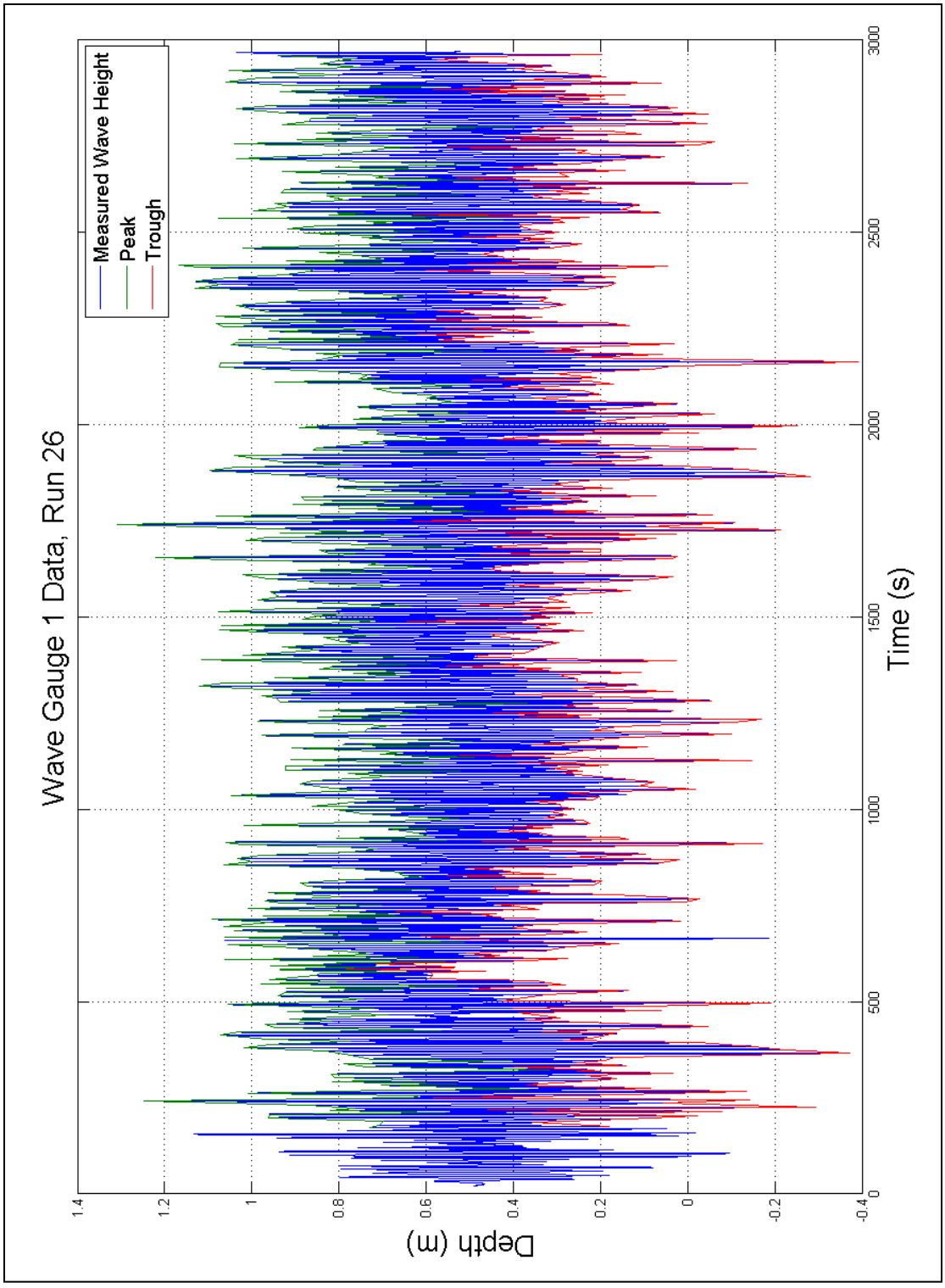

Figure B.1 Wave Gauge Data, Run 26

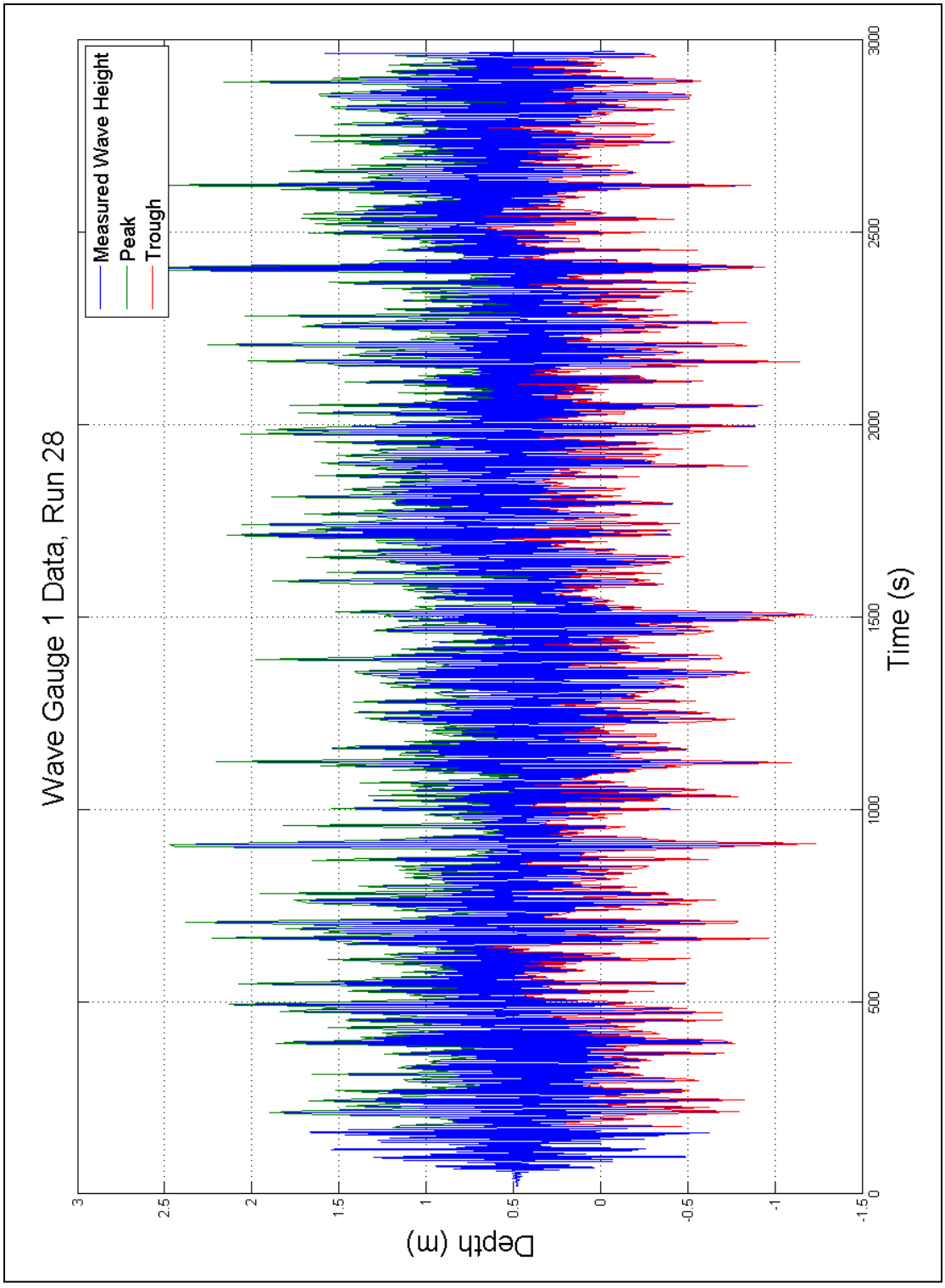

Figure B.2 Wave Gauge Data, Run 28

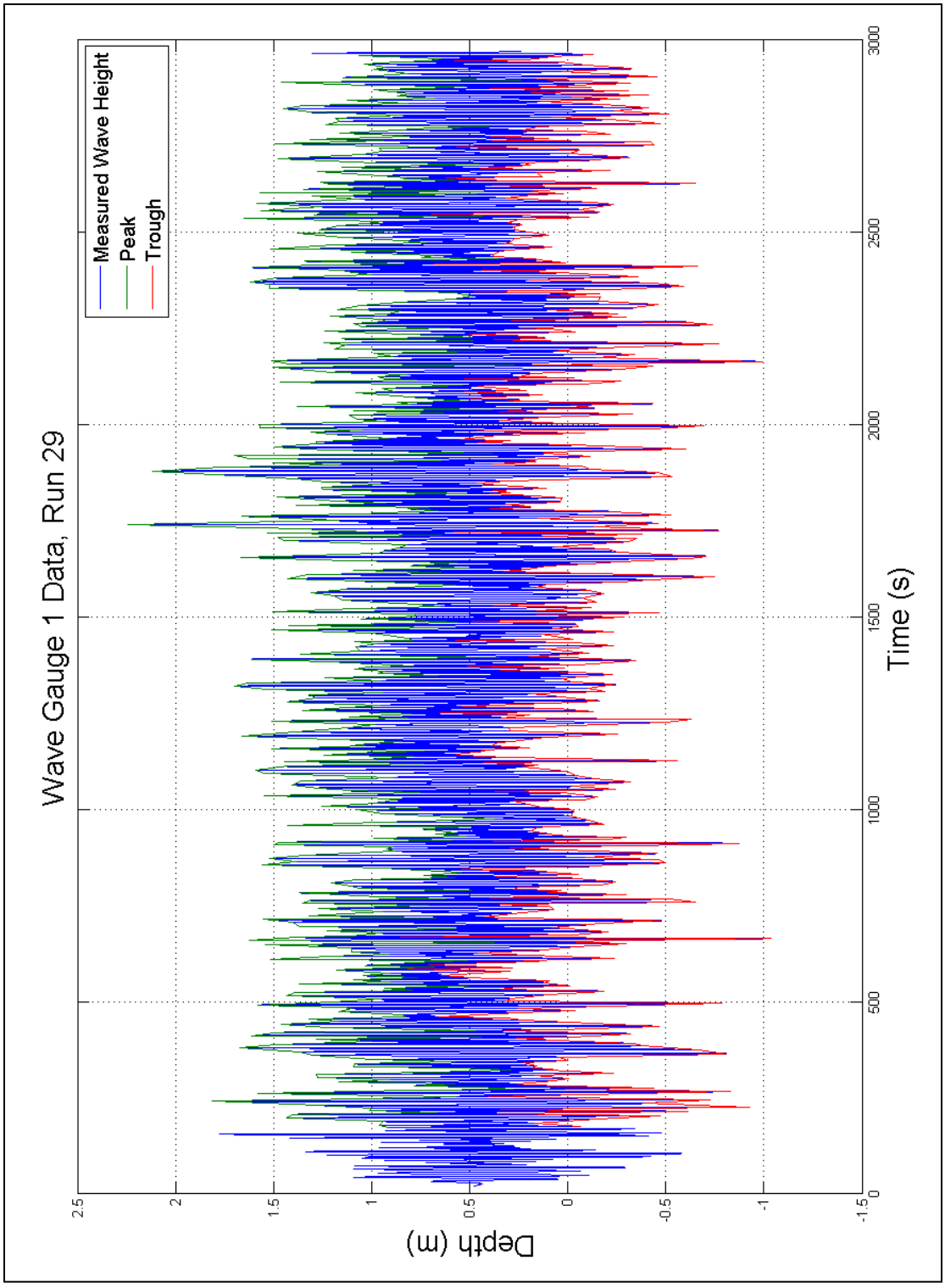

Figure B.3 Wave Gauge Data, Run 29

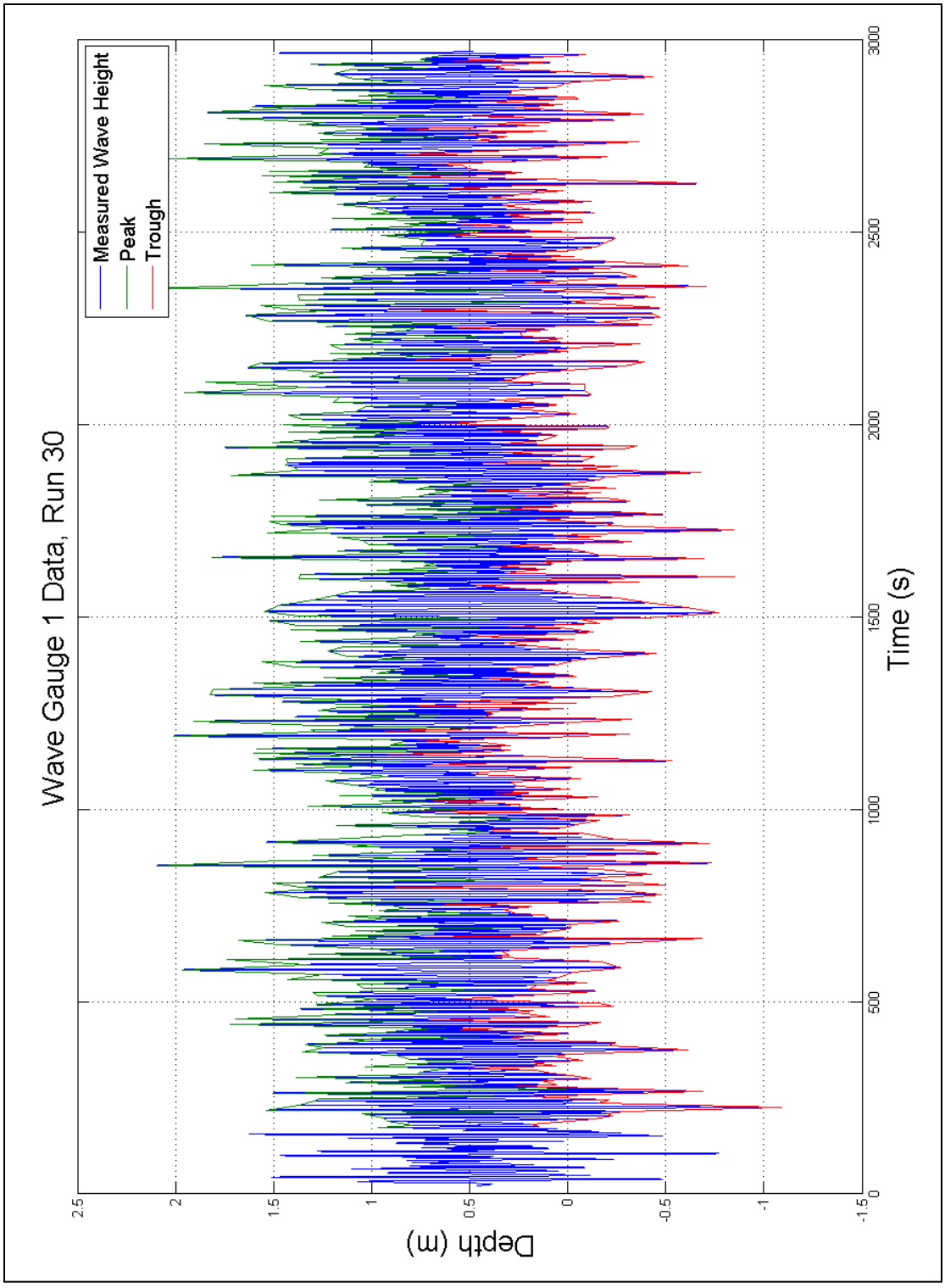

Figure B.4 Wave Gauge Data, Run 30

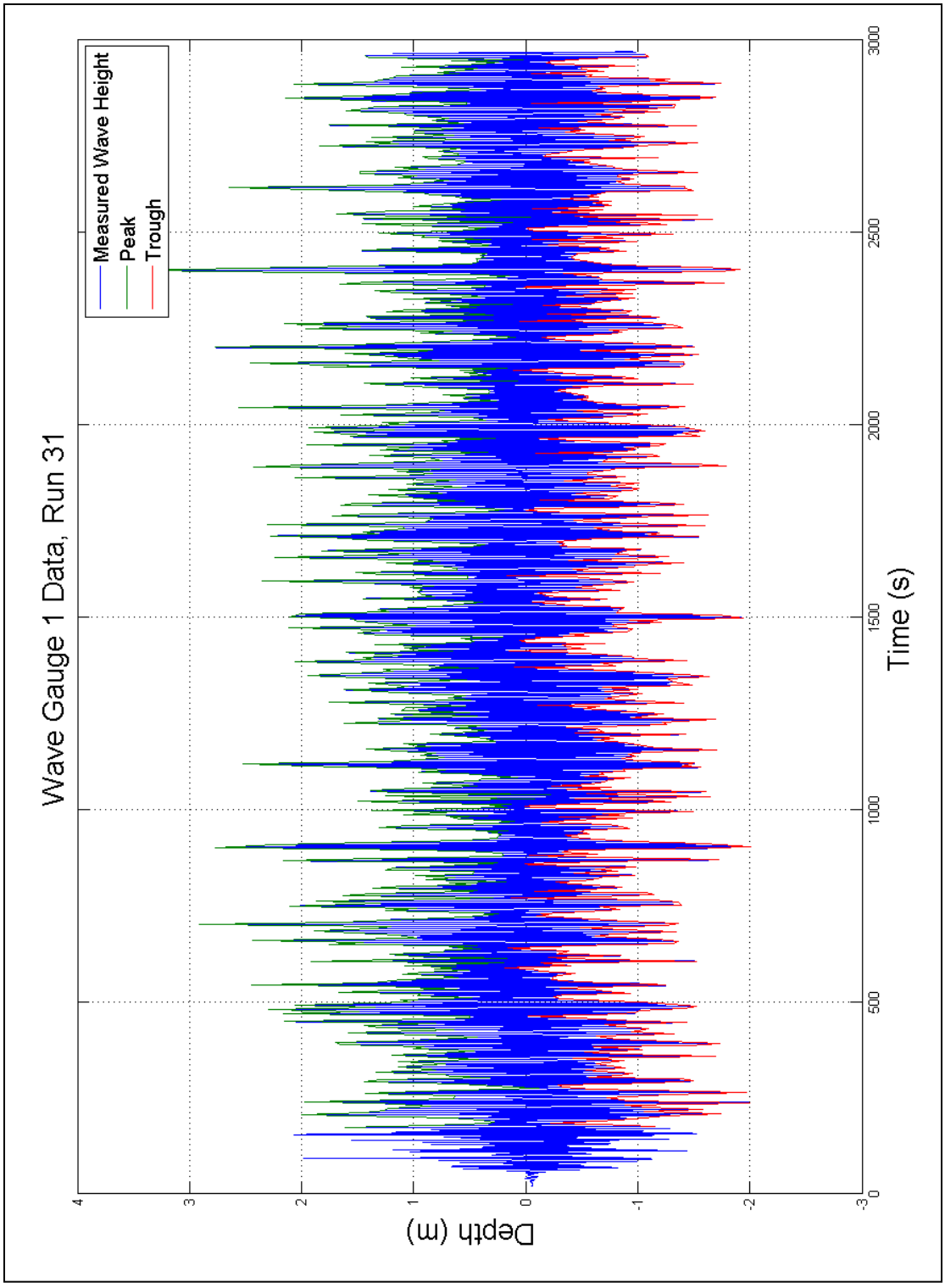

Figure B.5 Wave Gauge Data, Run 31

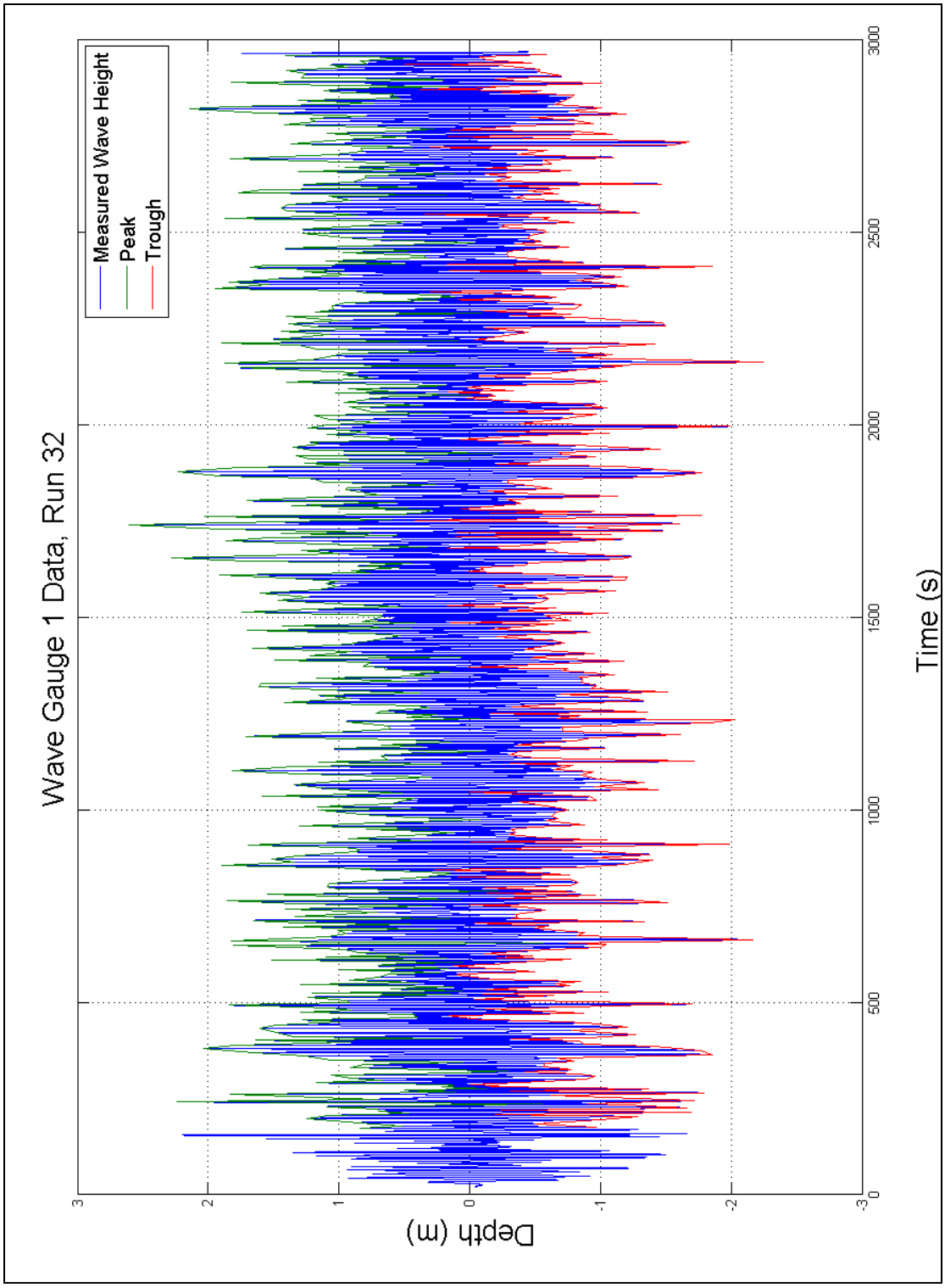

Figure B.6 Wave Gauge Data, Run 32

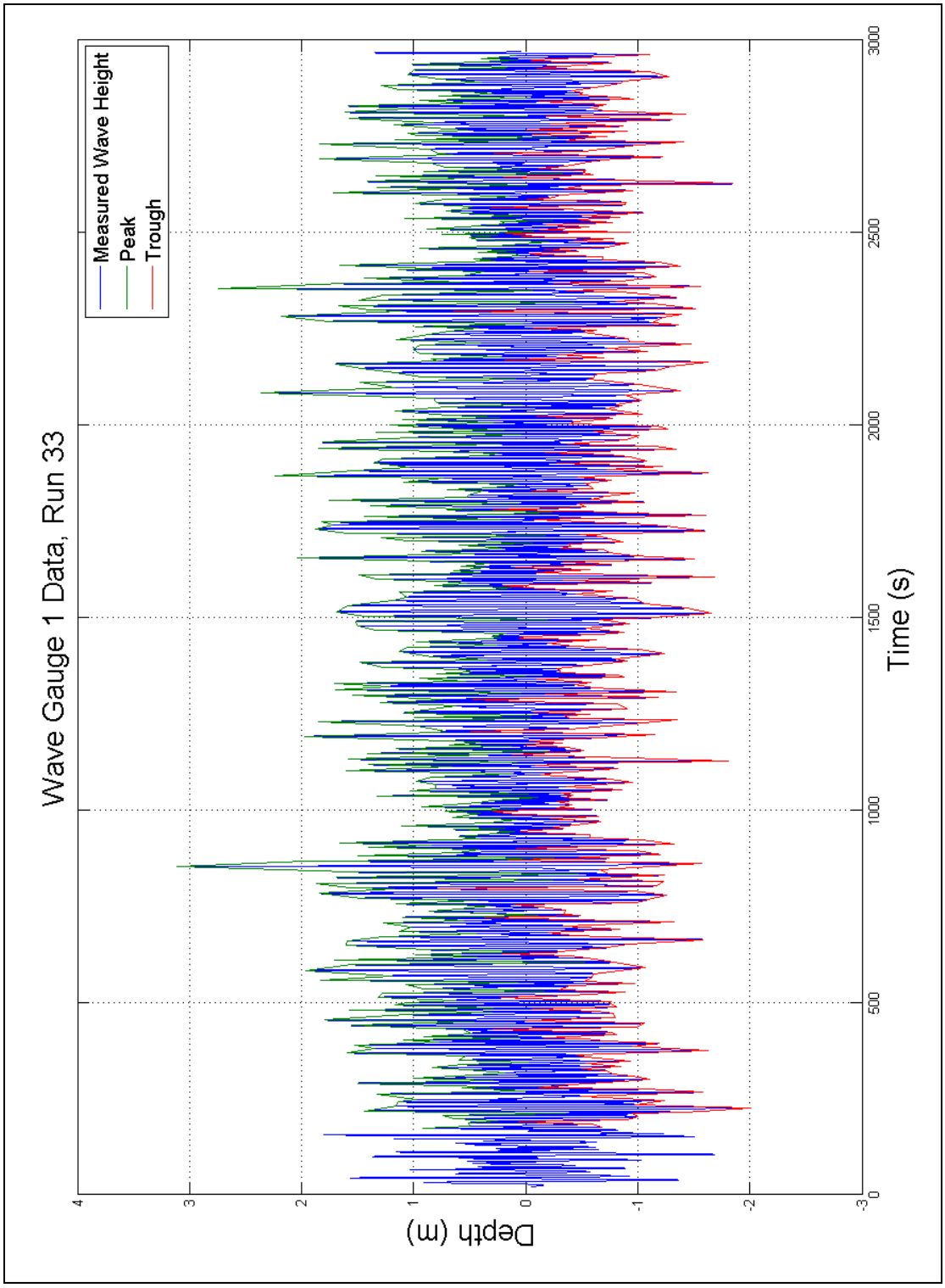

Figure B.7 Wave Gauge Data, Run 33

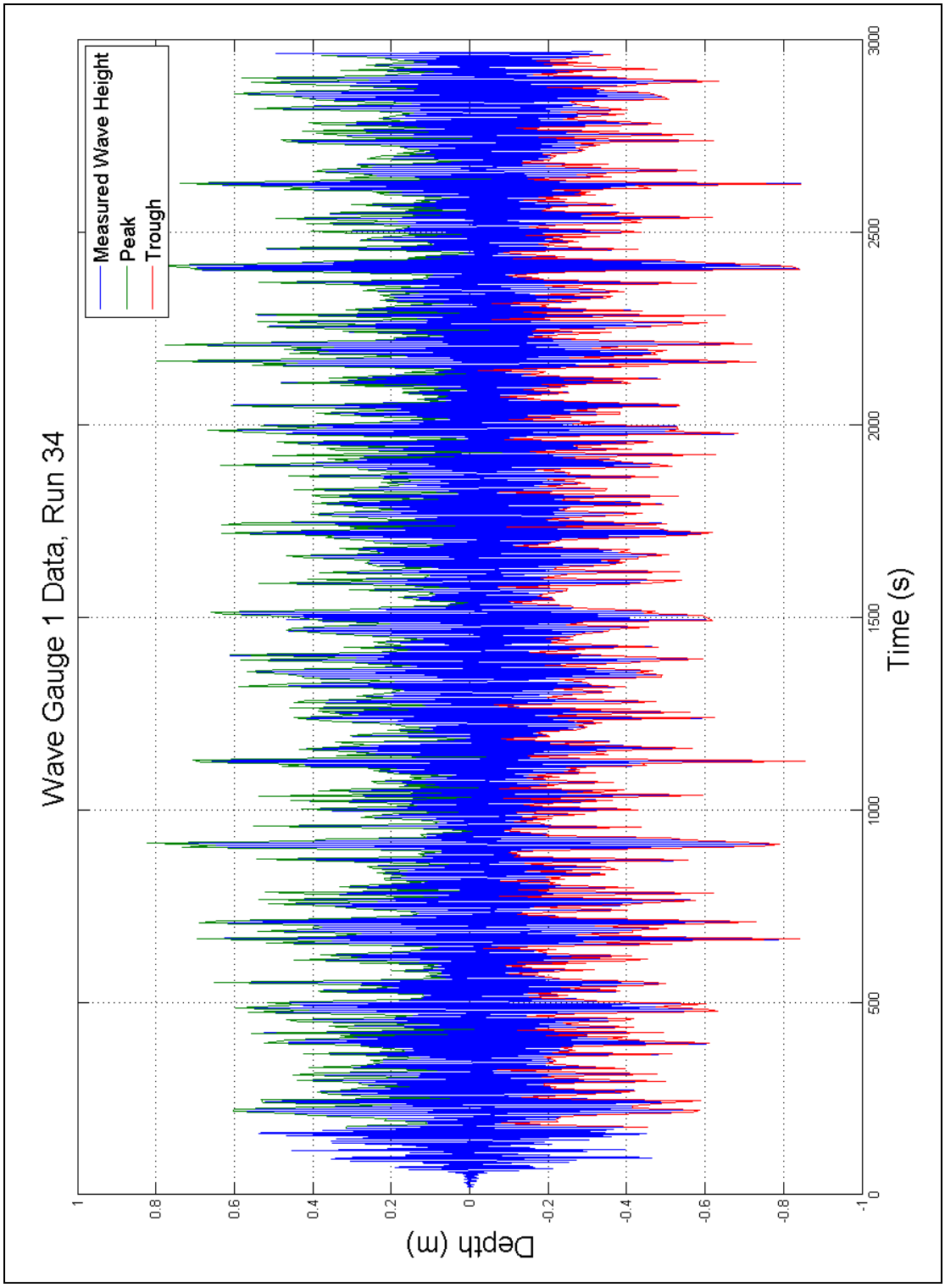

Figure B.8 Wave Gauge Data, Run 34

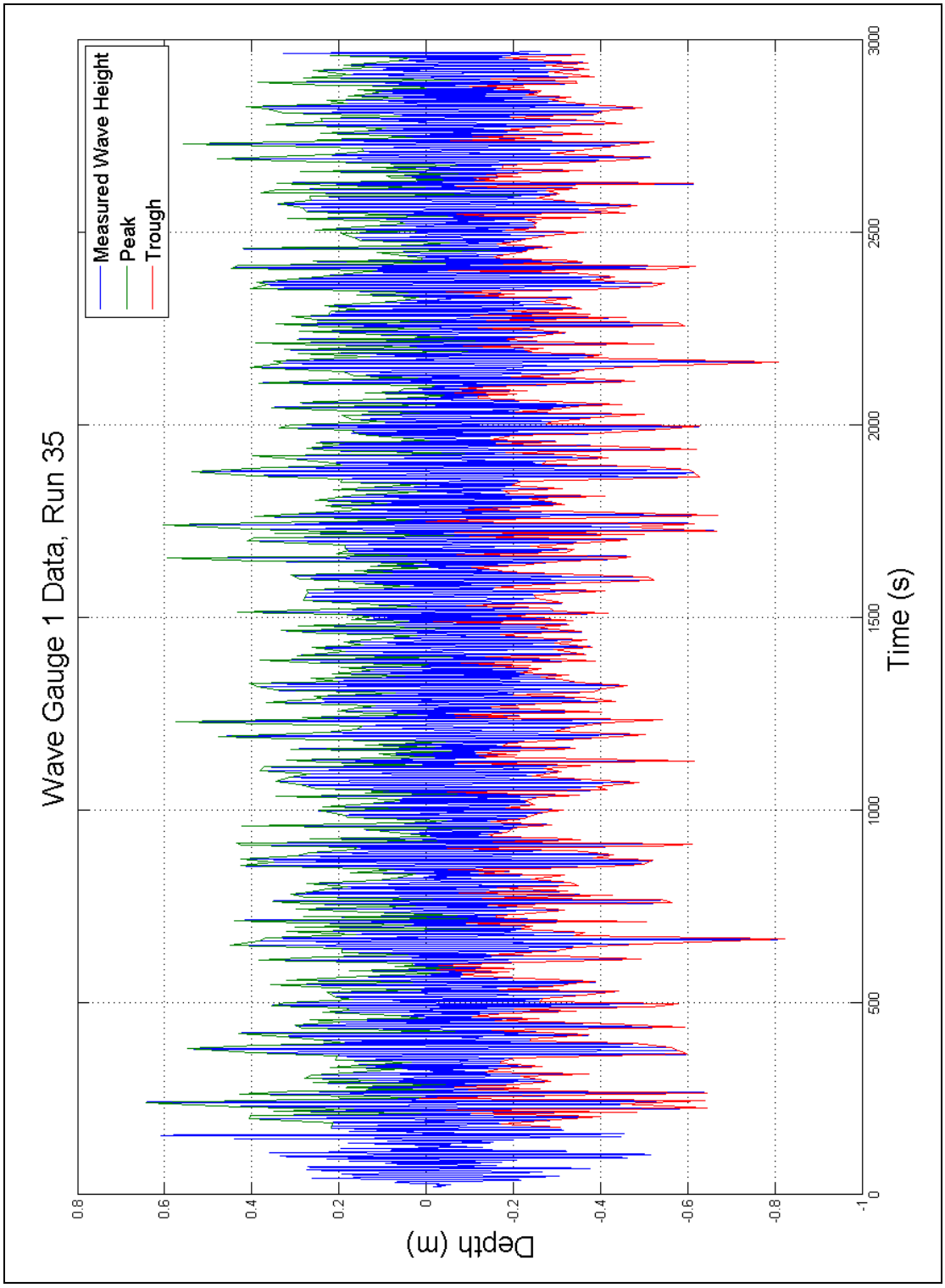

Figure B.9 Wave Gauge Data, Run 35

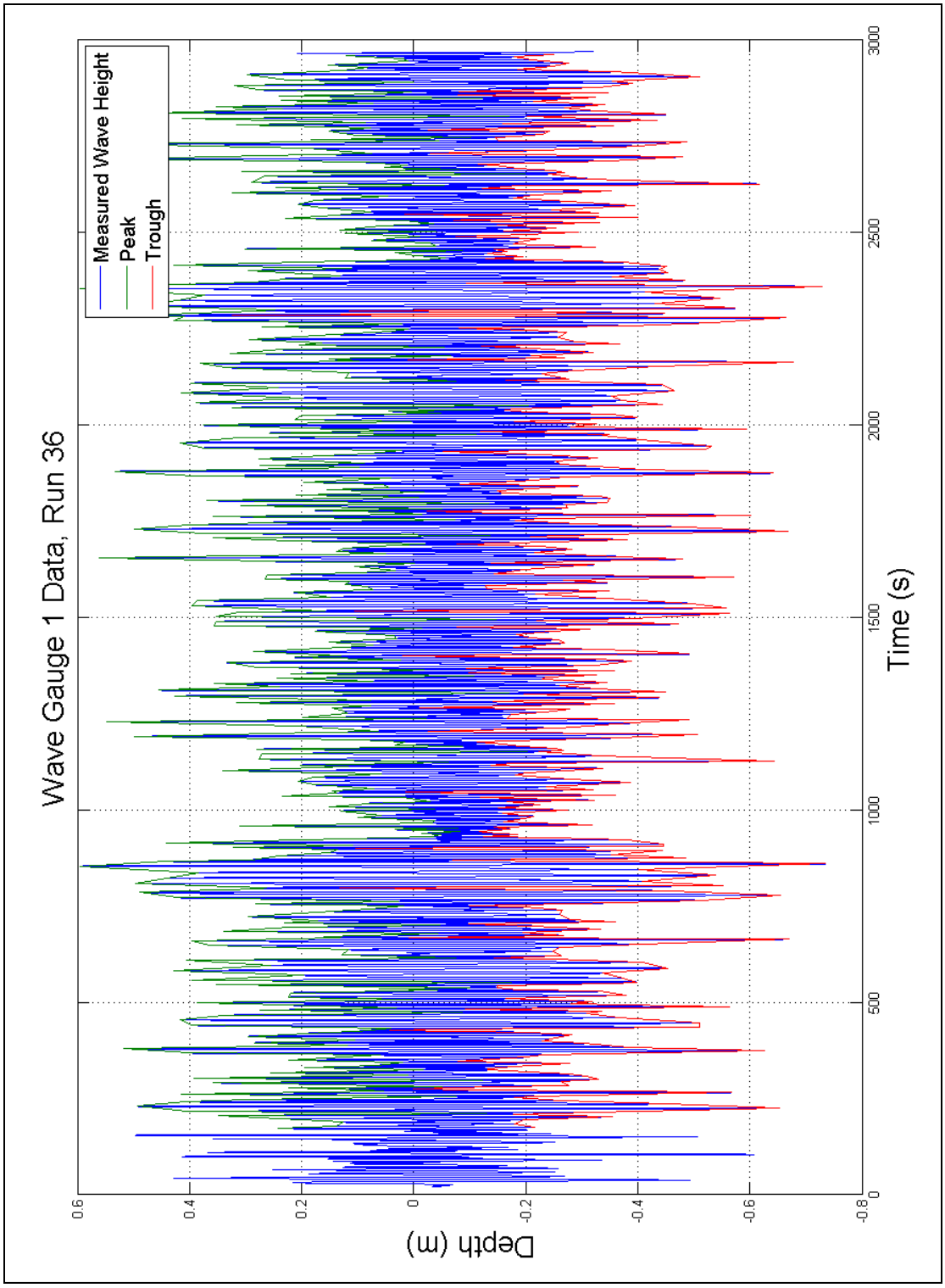

Figure B.10 Wave Gauge Data, Run 36

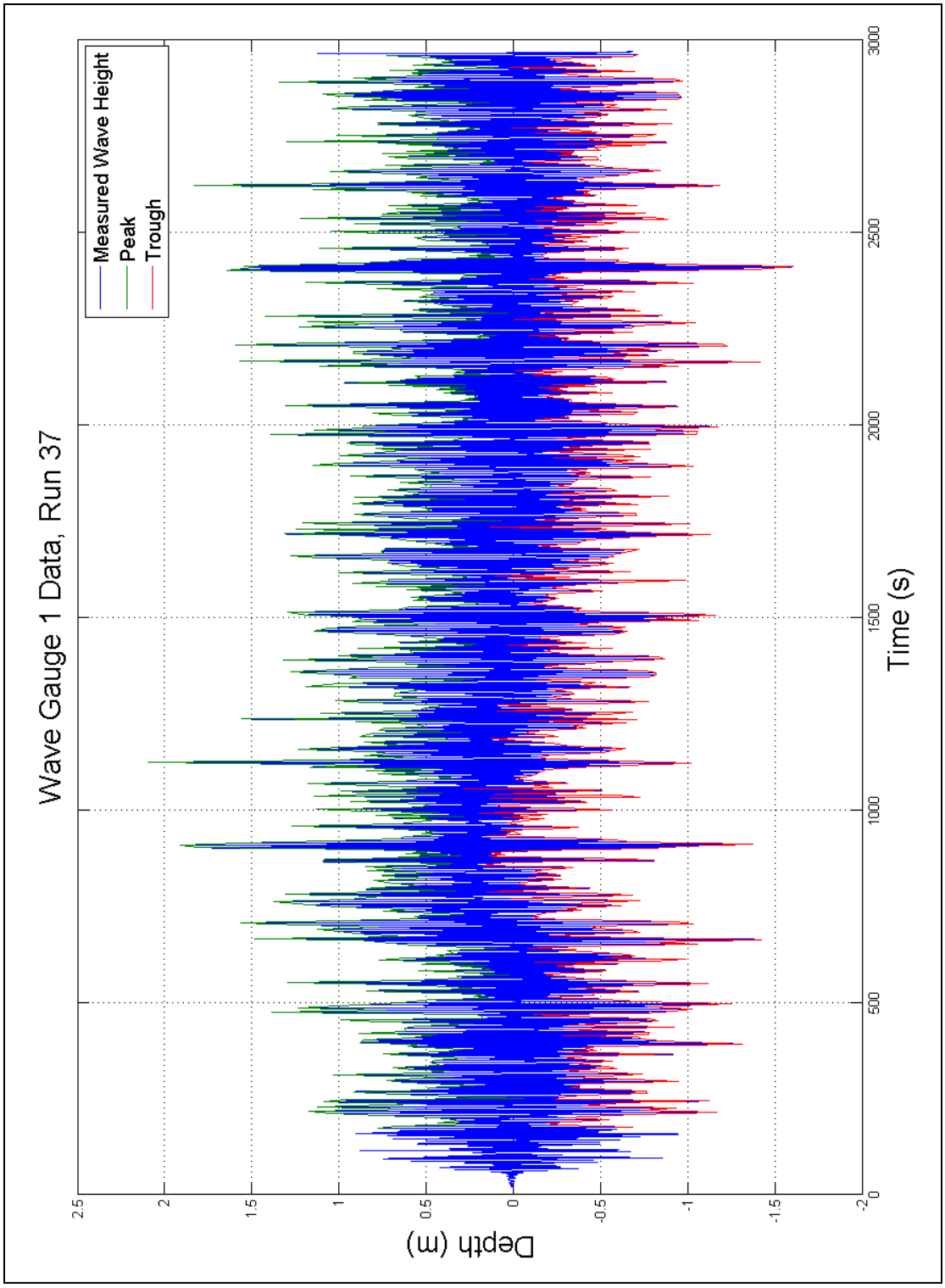

Figure B.11 Wave Gauge Data, Run 37

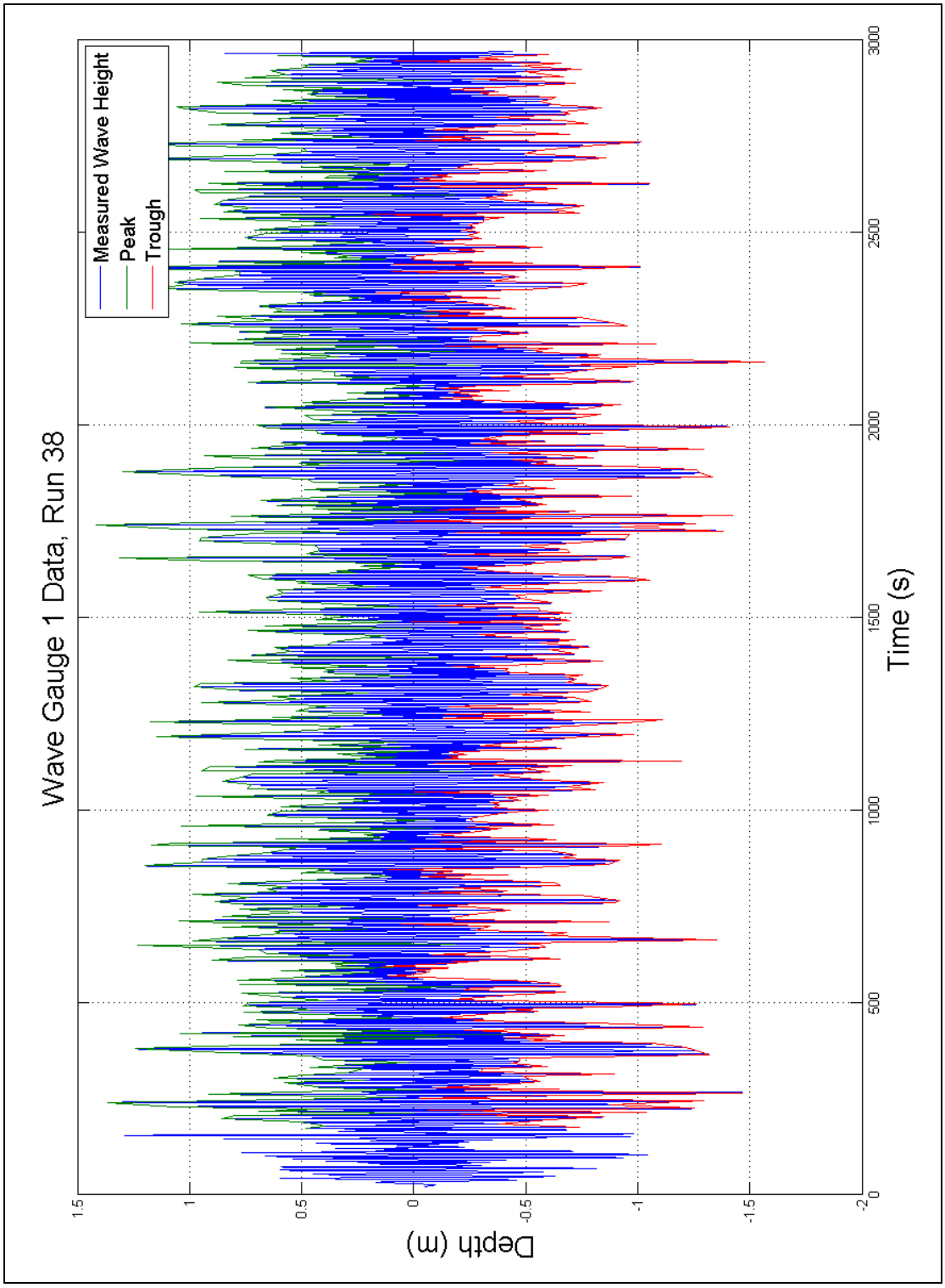

Figure B.12 Wave Gauge Data, Run 38

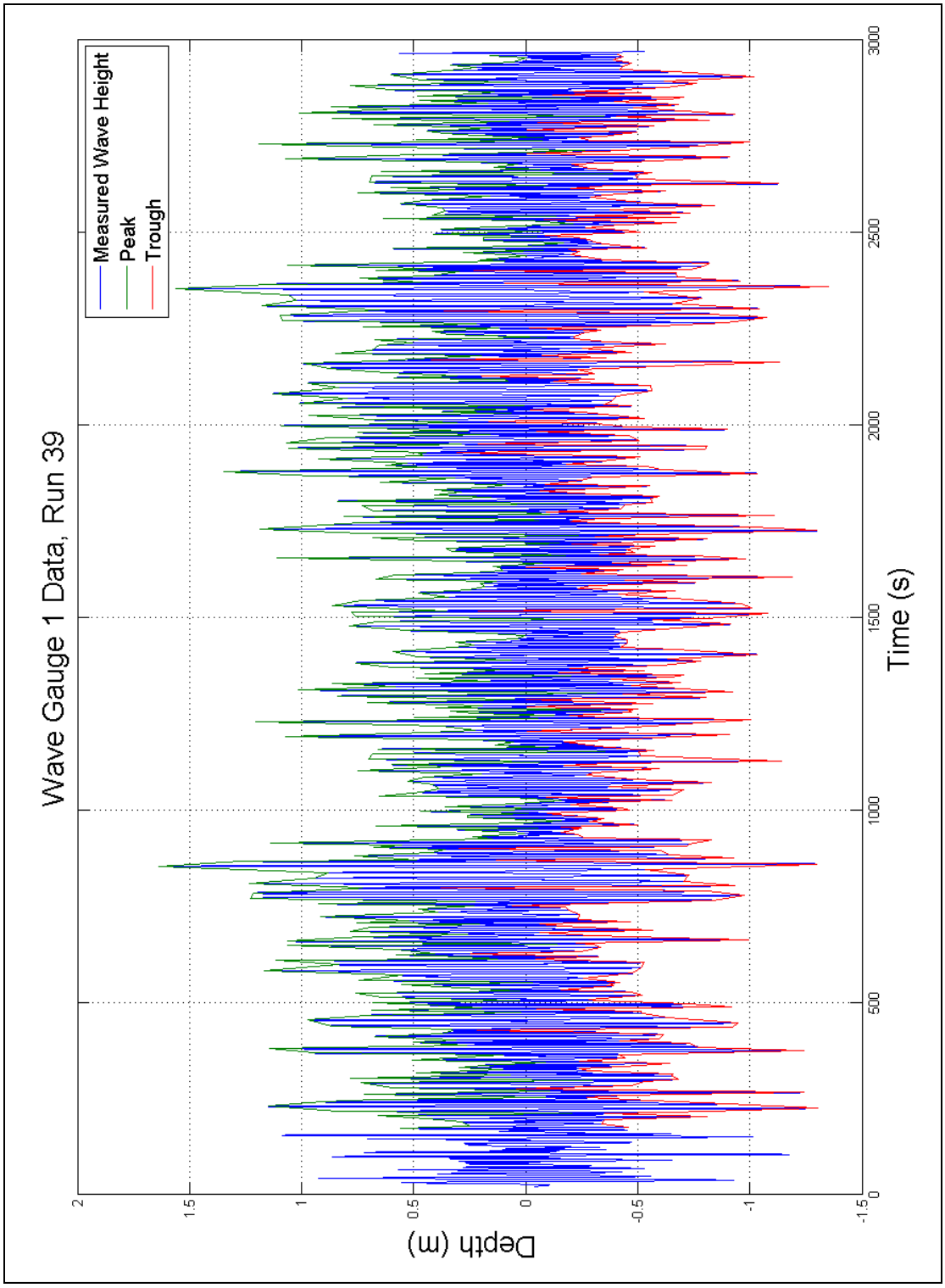

Figure B.13 Wave Gauge Data, Run 39

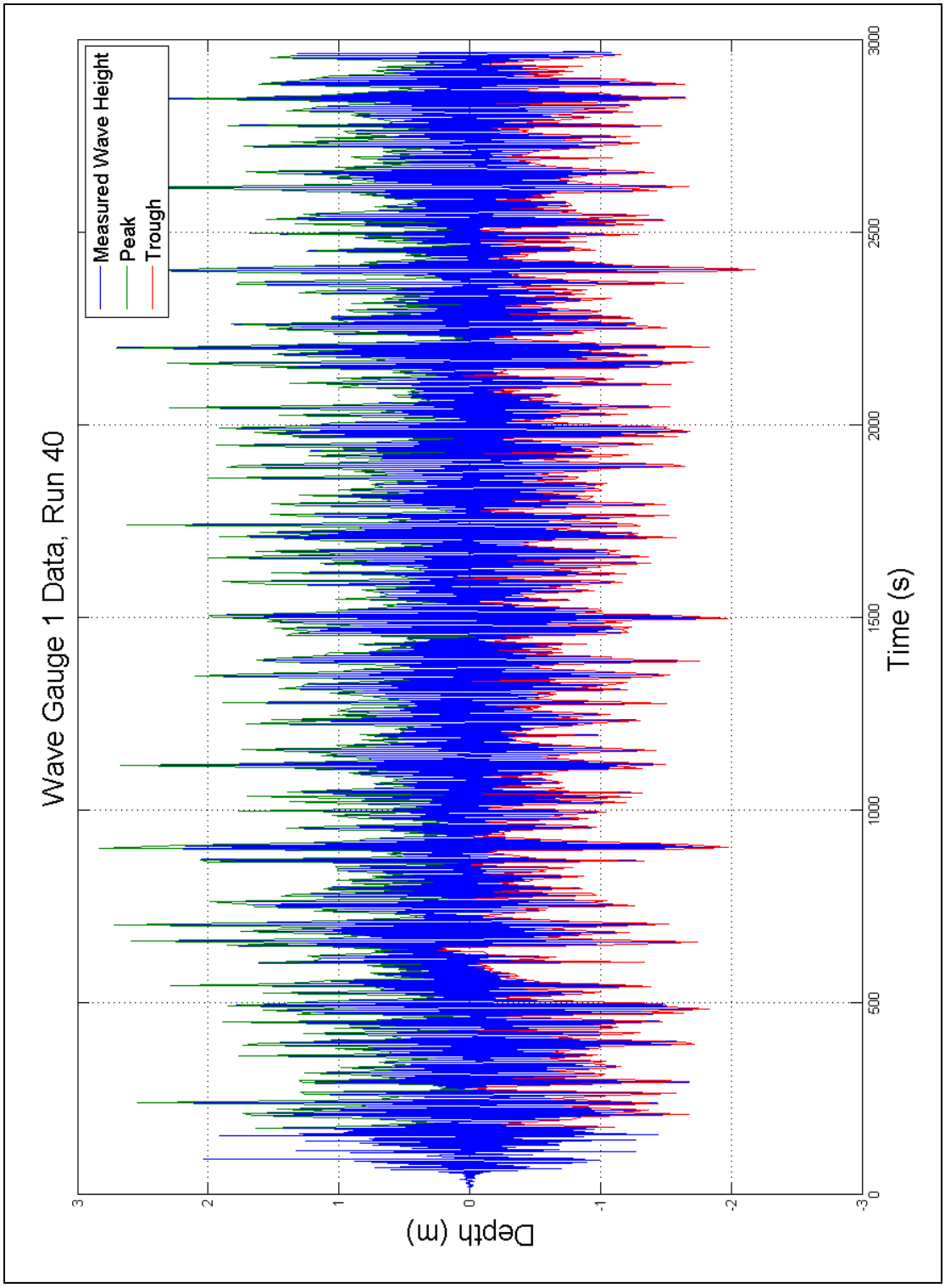

Figure B.14 Wave Gauge Data, Run 40

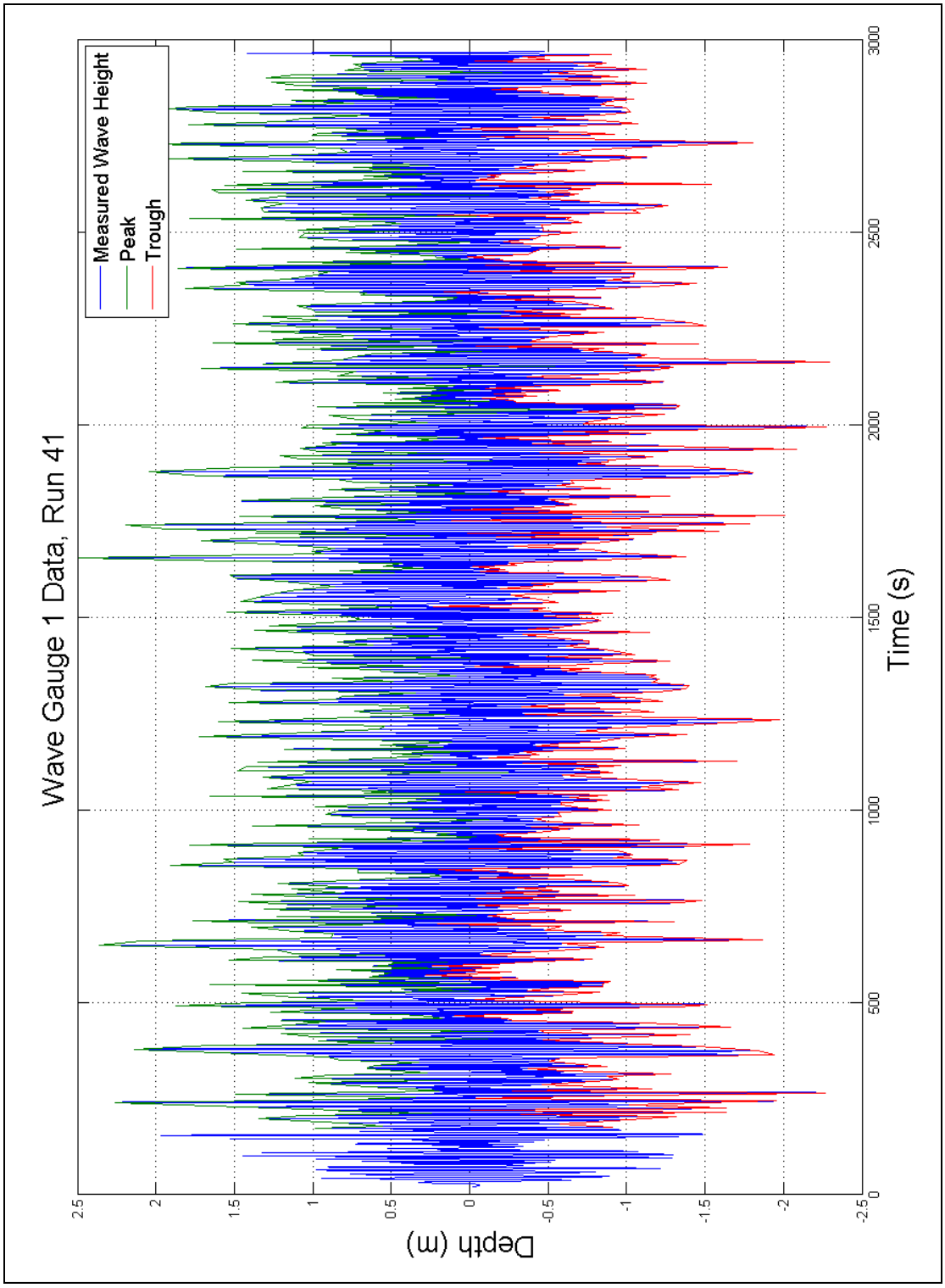

Figure B.15 Wave Gauge Data, Run 41

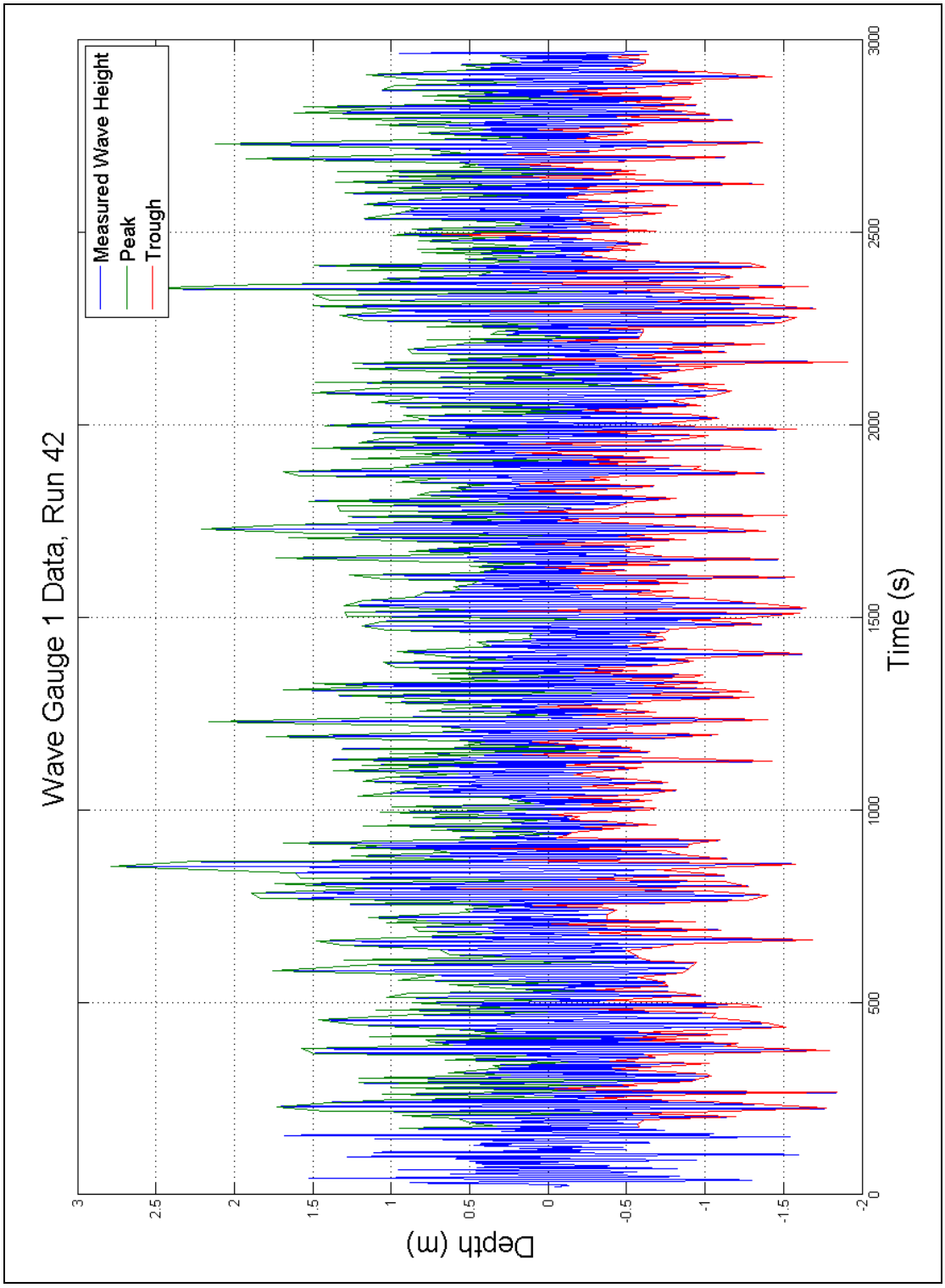

Figure B.16 Wave Gauge Data, Run 42

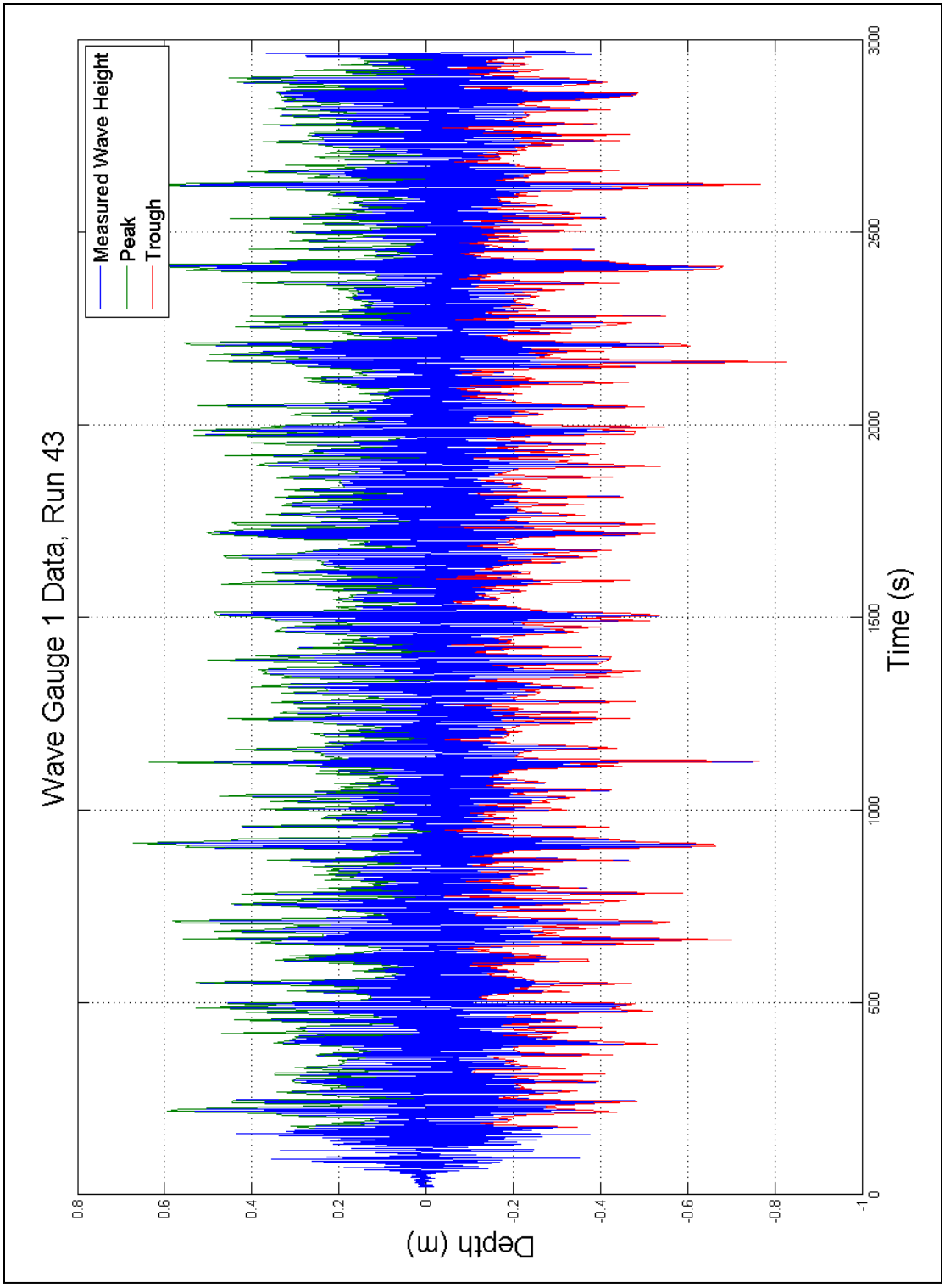

Figure B.17 Wave Gauge Data, Run 43

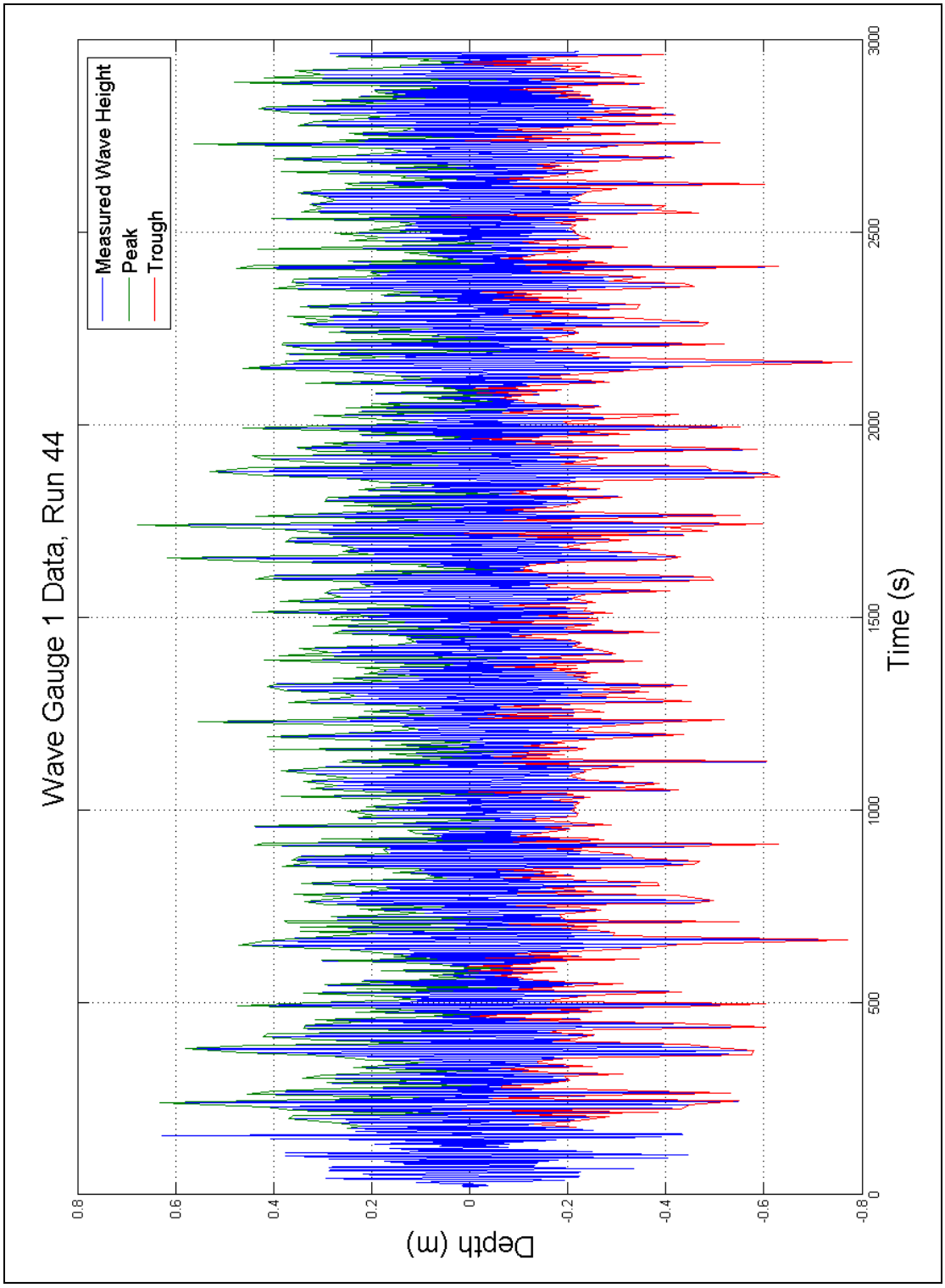

Figure B.18 Wave Gauge Data, Run 44

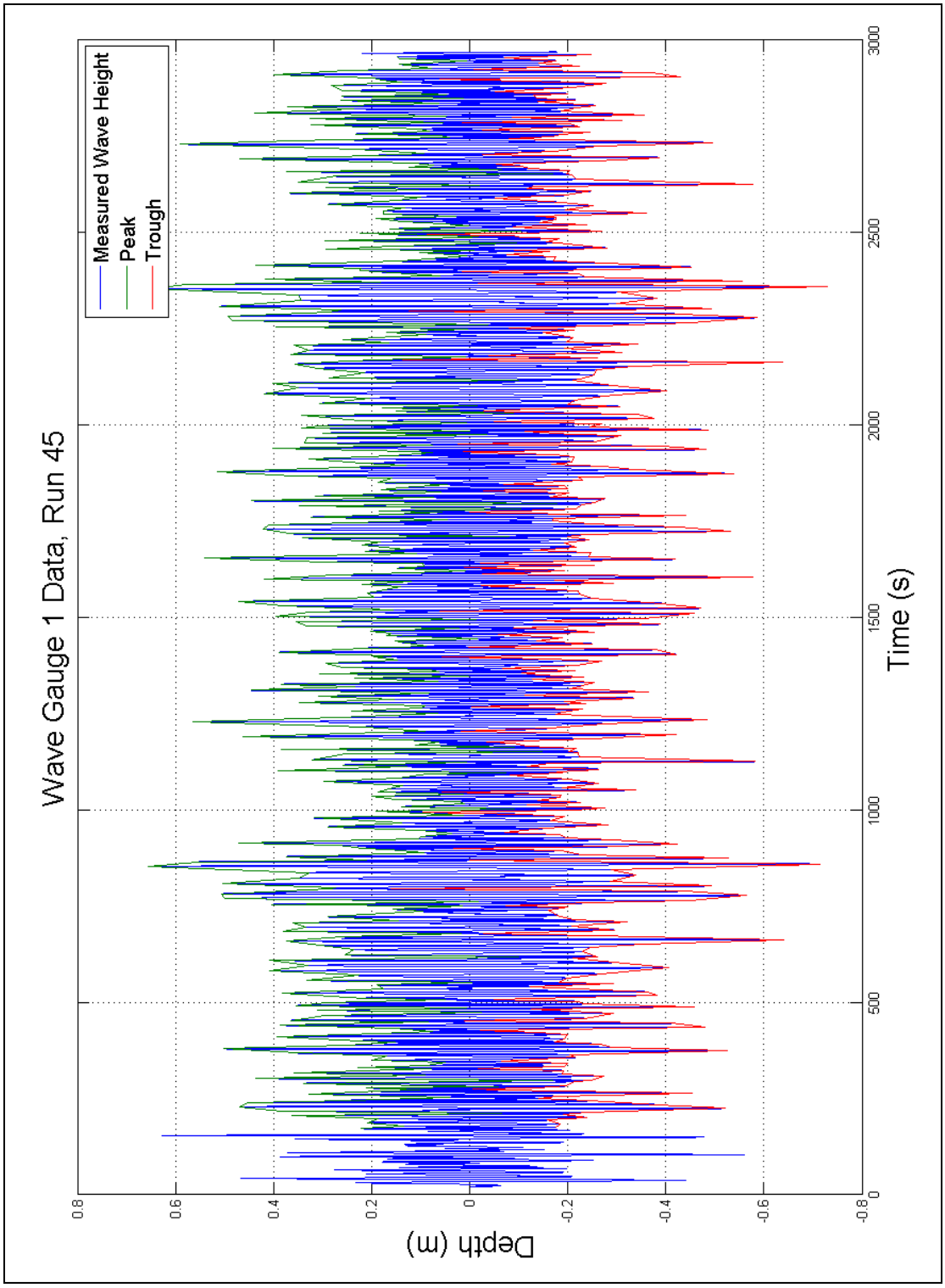

Figure B.19 Wave Gauge Data, Run 45

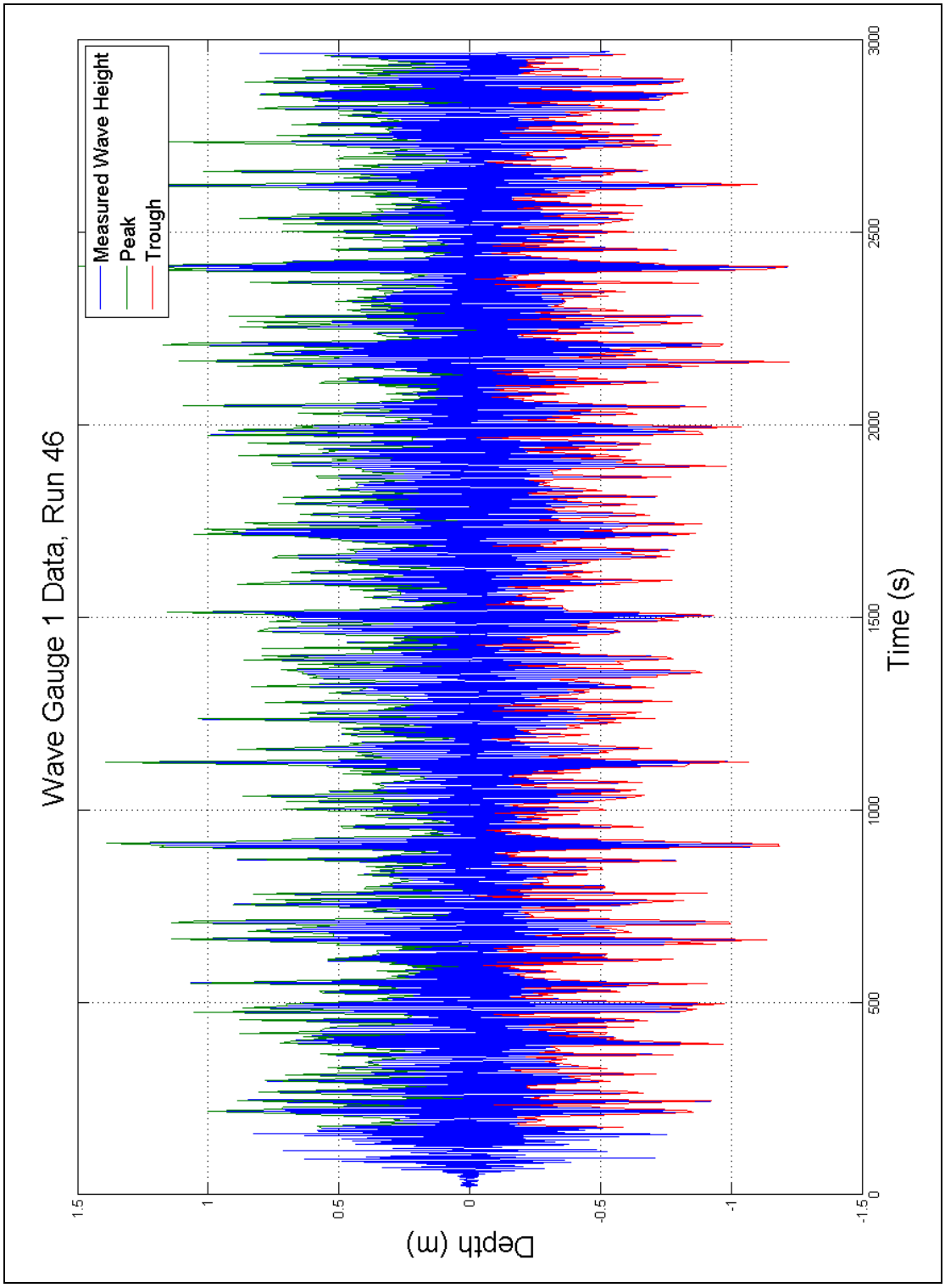

Figure B.20 Wave Gauge Data, Run 46

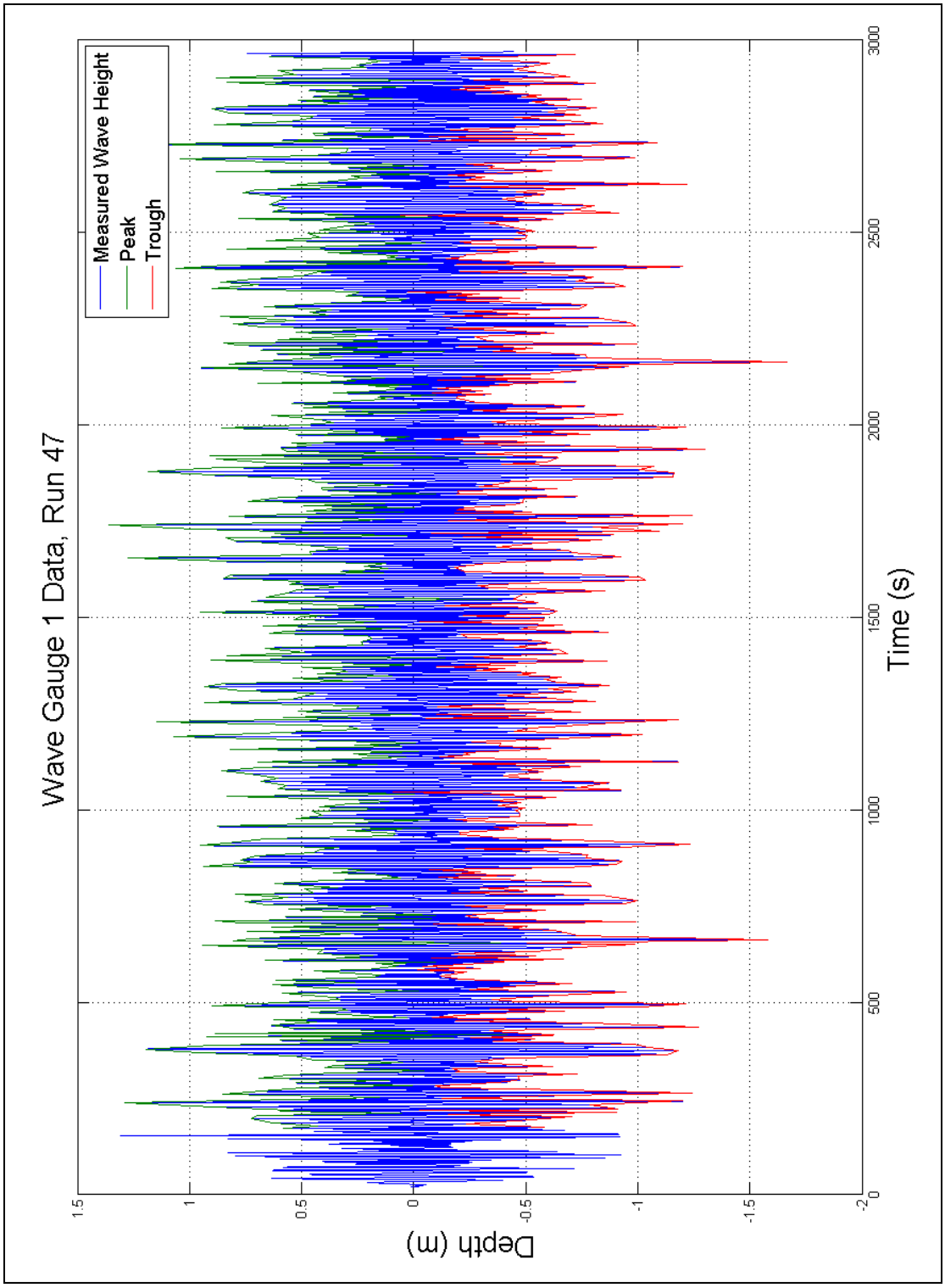

Figure B.21 Wave Gauge Data, Run 47

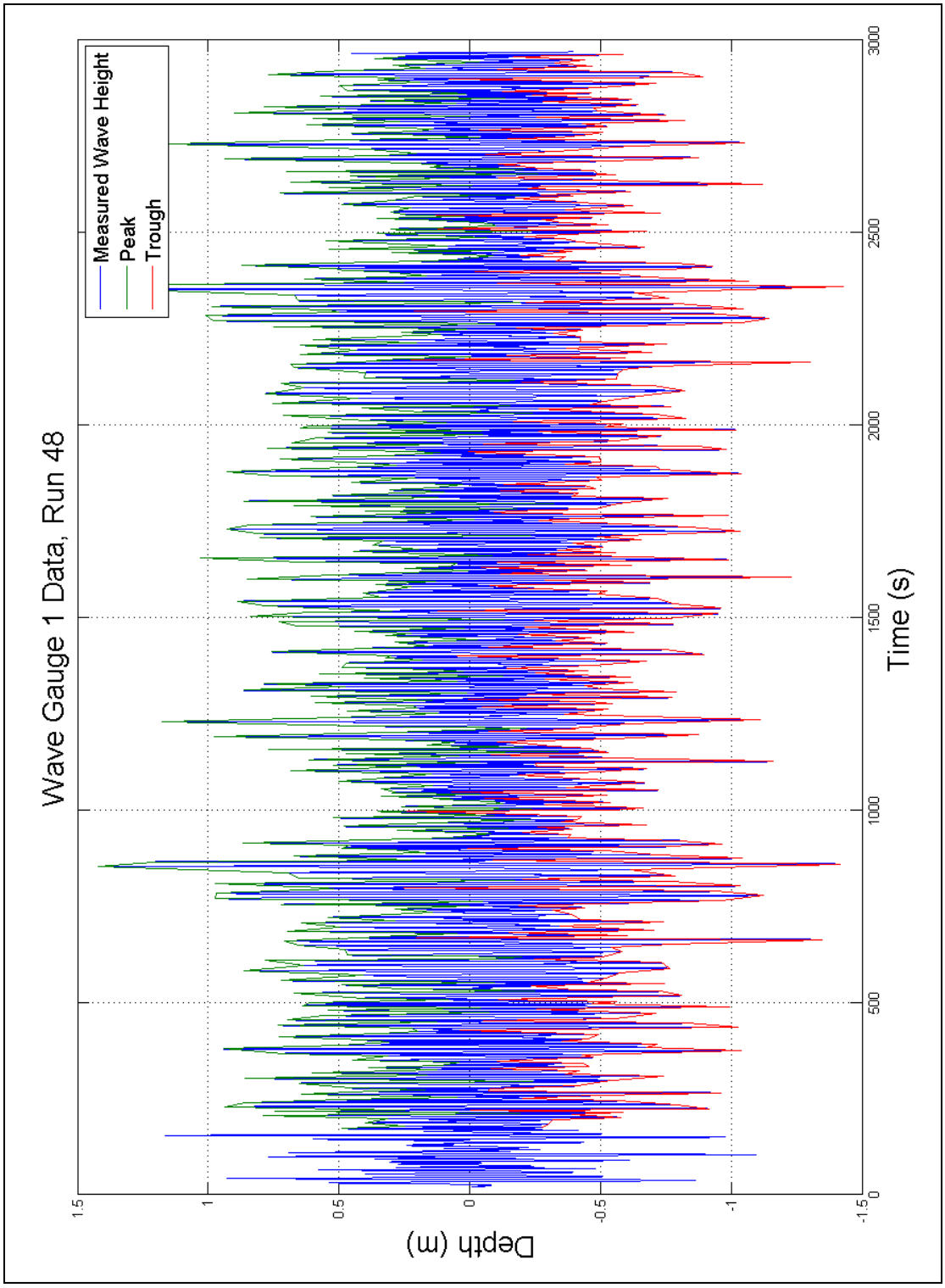

Figure B.22 Wave Gauge Data, Run 48

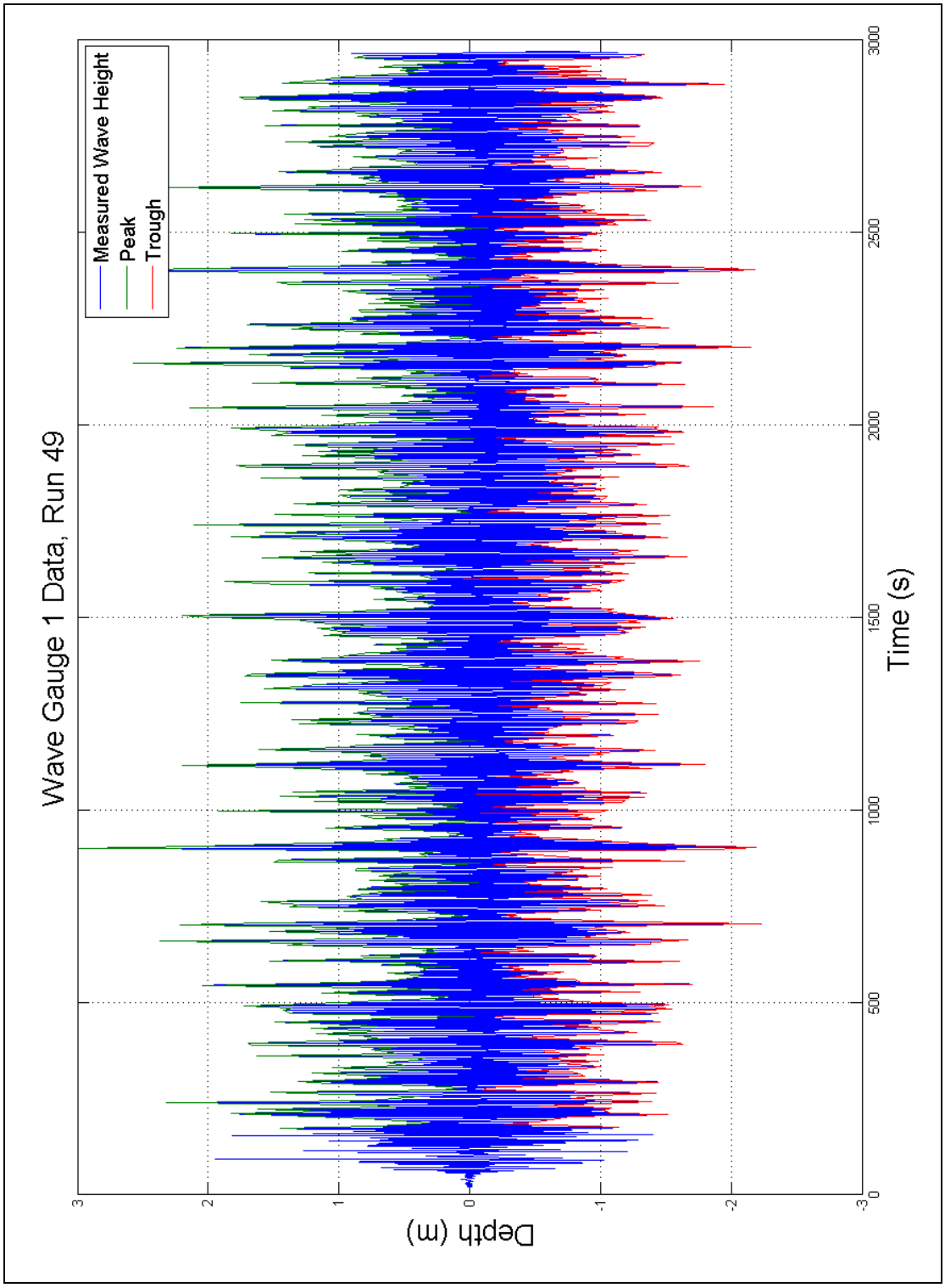

Figure B.23 Wave Gauge Data, Run 49

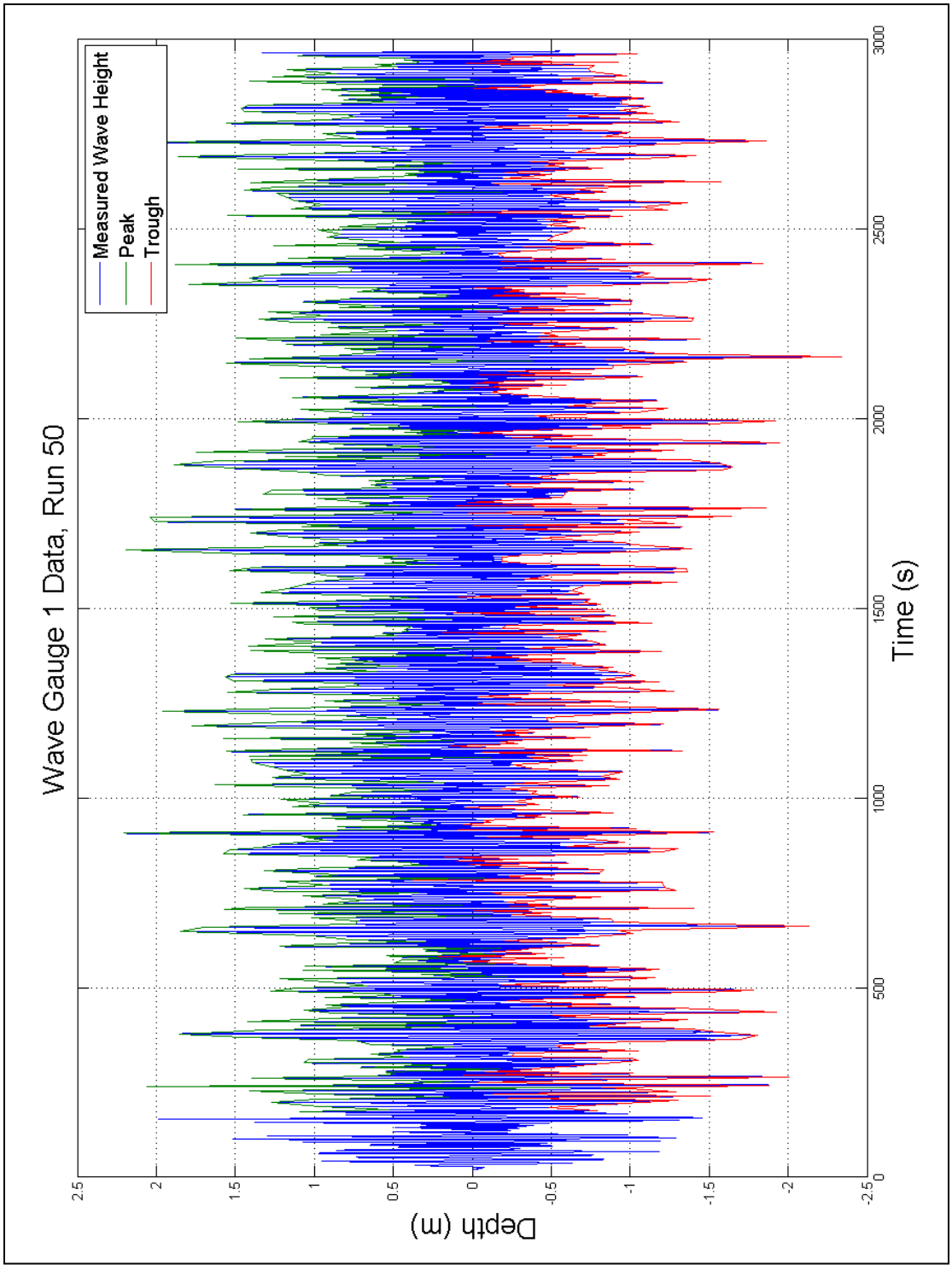

Figure B.24 Wave Gauge Data, Run 50

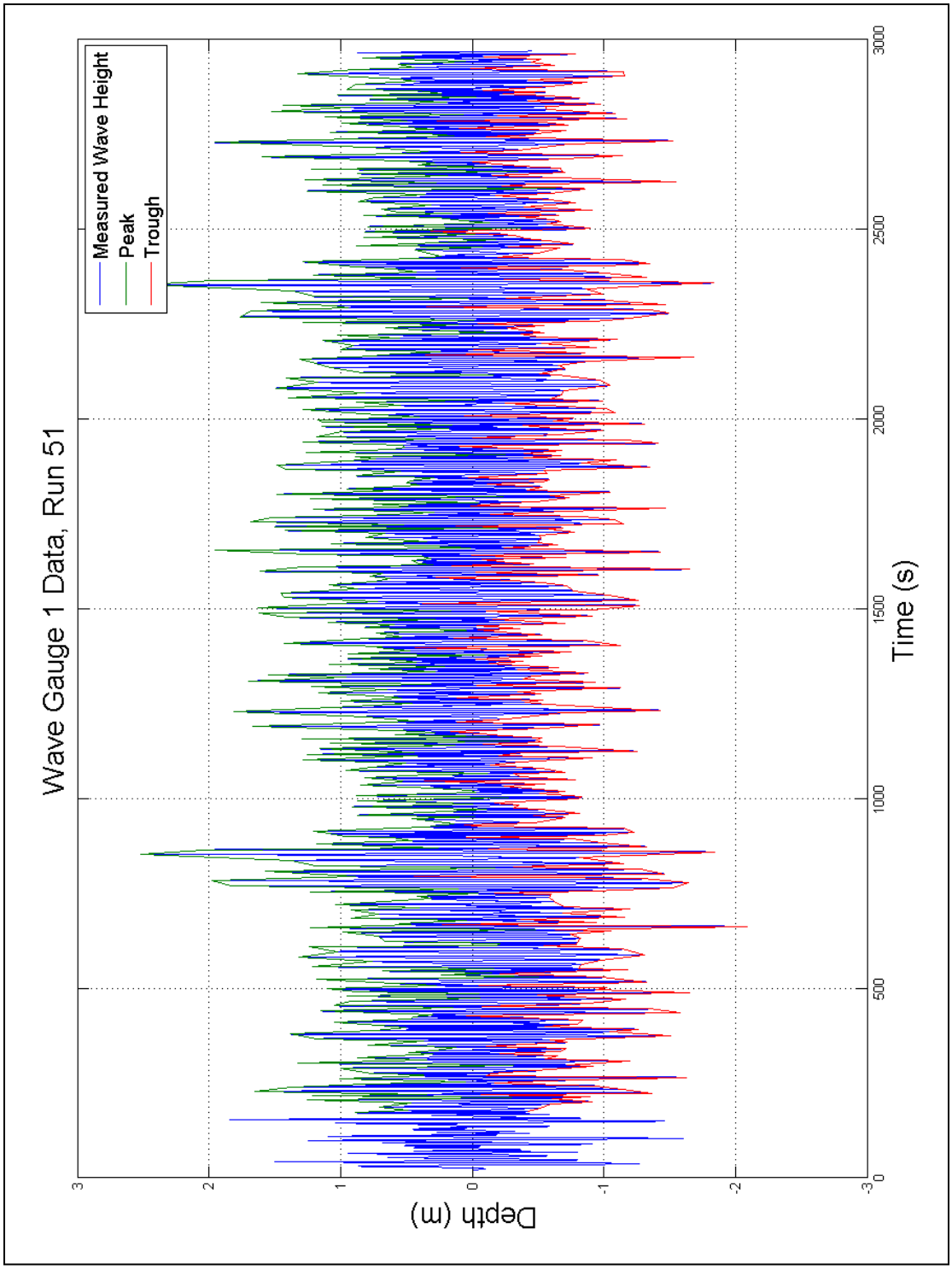

Figure B.25 Wave Gauge Data, Run 51

APPENDIX C

SHEAR STRESS DATA

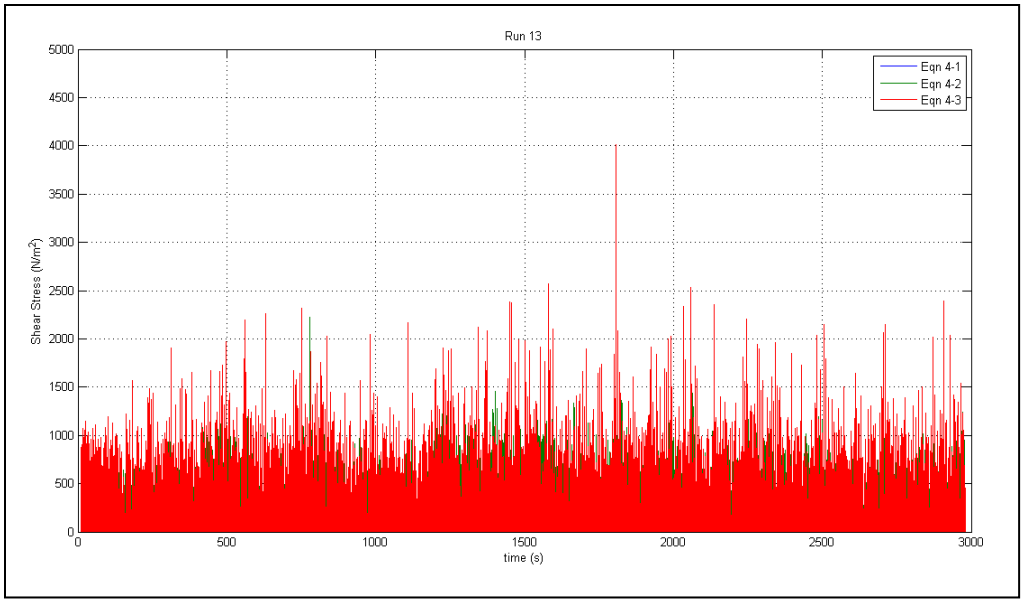

Figure C.1 Shear Stress Estimation, Run 13

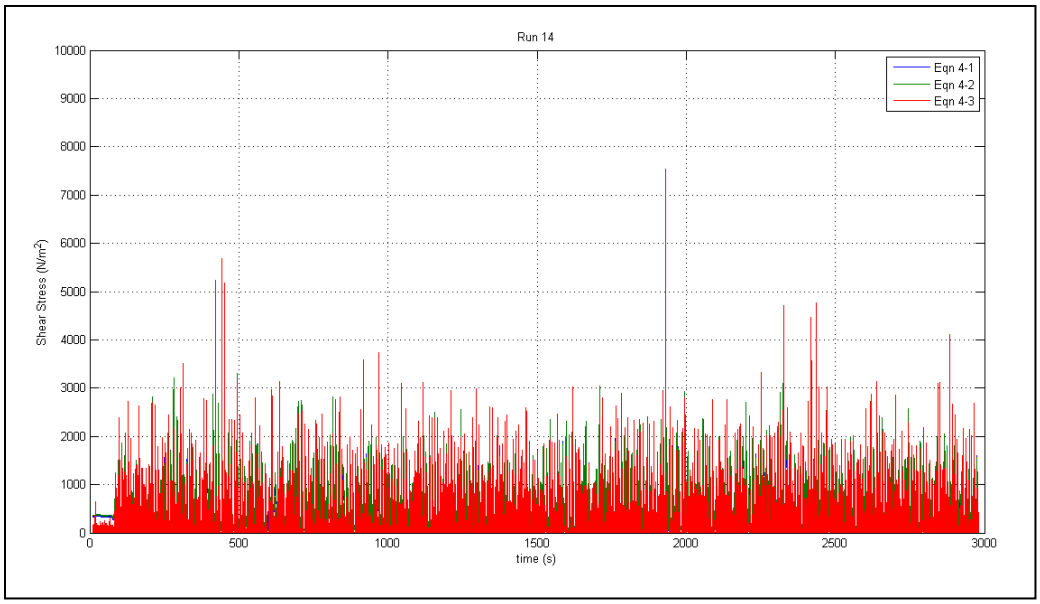

Figure C.2 Shear Stress Estimation, Run 14

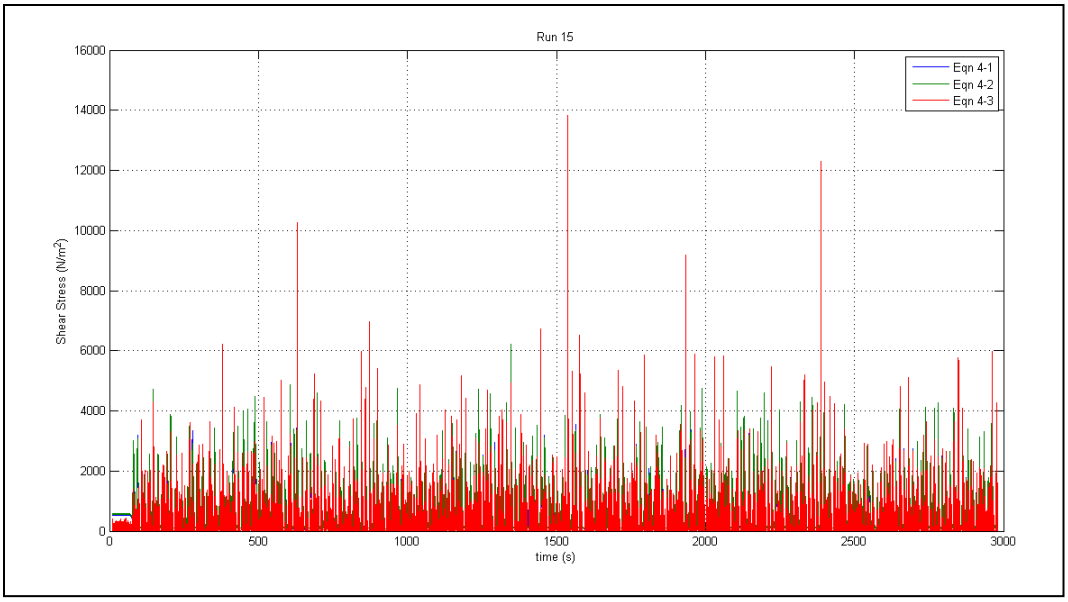

Figure C.3 Shear Stress Estimation, Run 15

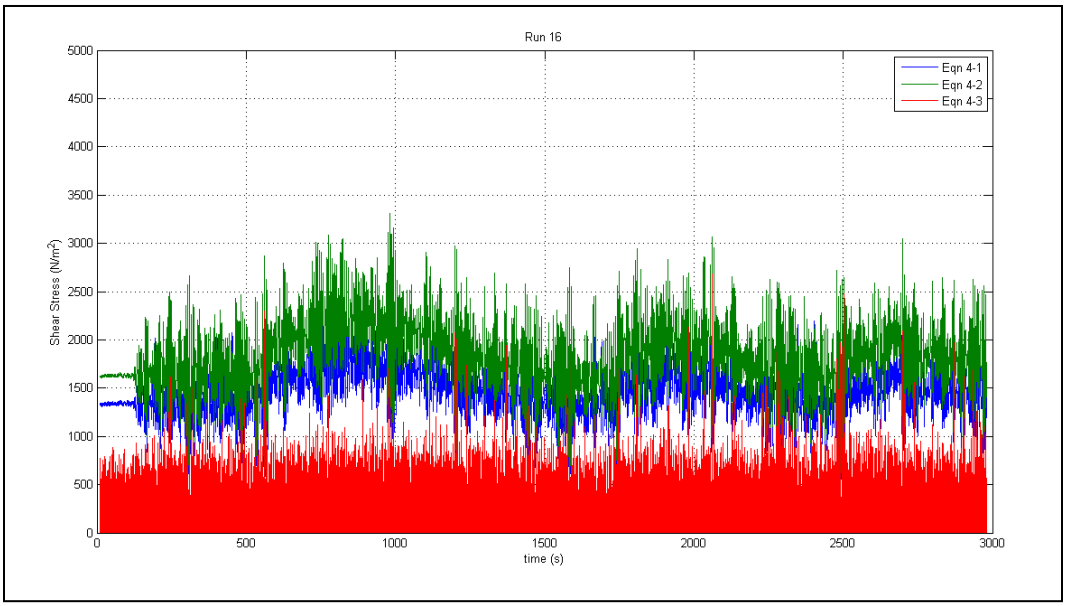

Figure C.4 Shear Stress Estimation, Run 16

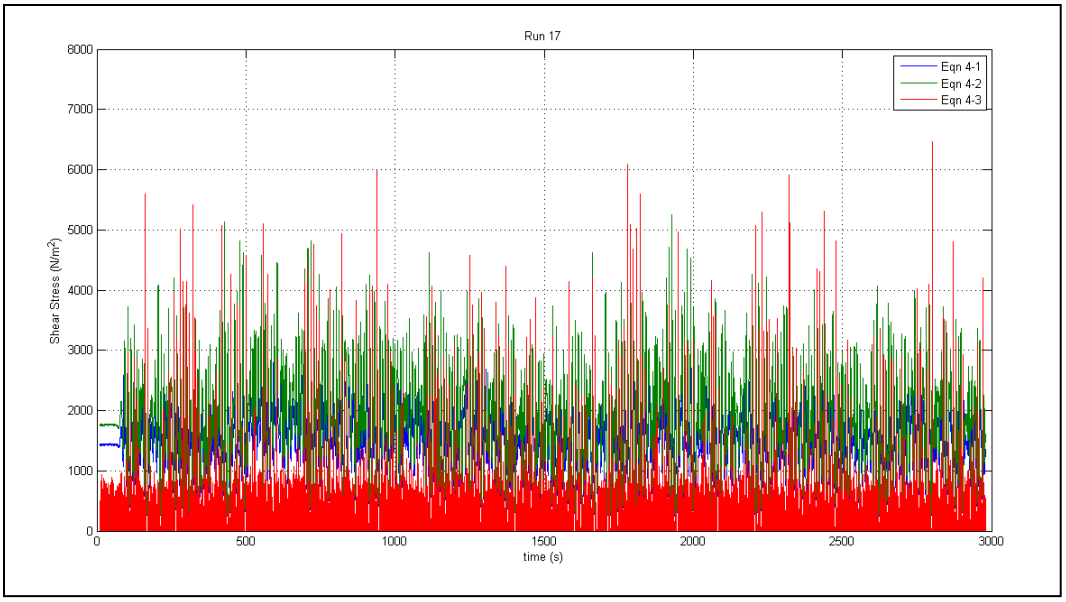

Figure C.5 Shear Stress Estimation, Run 17

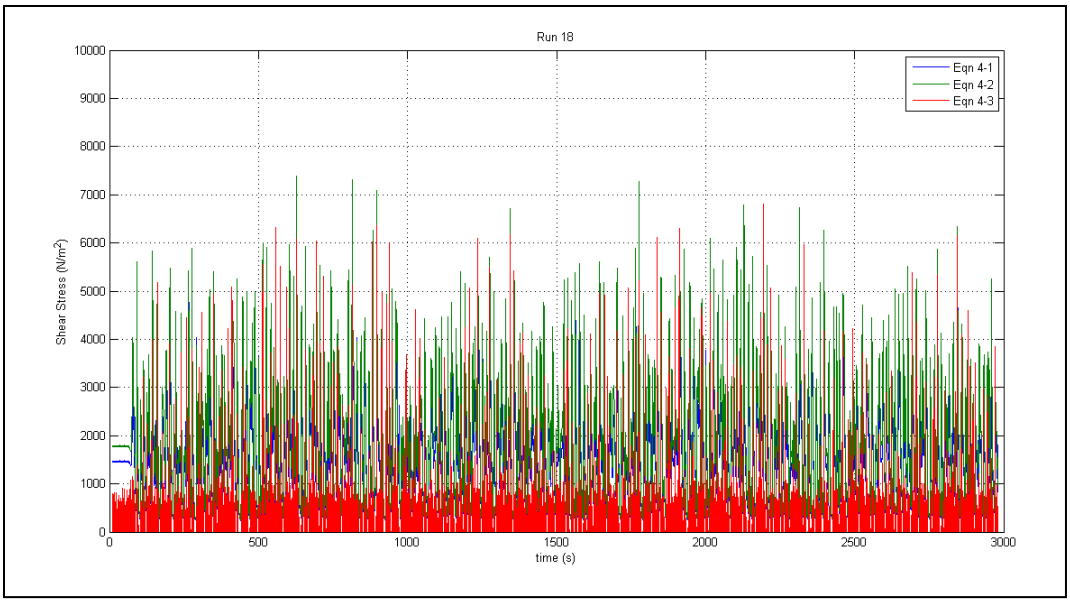

Figure C.6 Shear Stress Estimation, Run 18

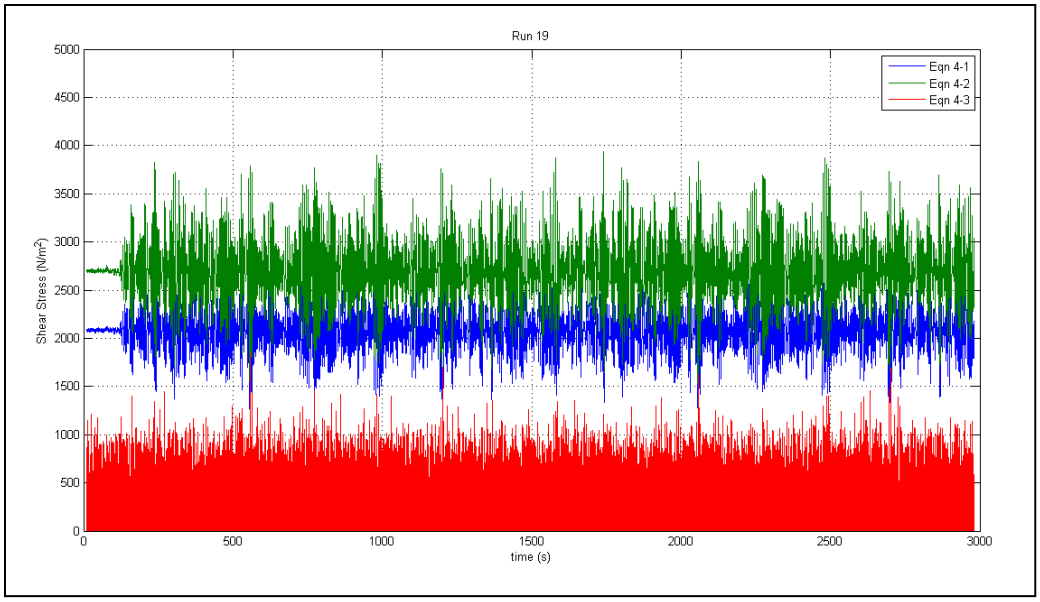

Figure C.7 Shear Stress Estimation, Run 19

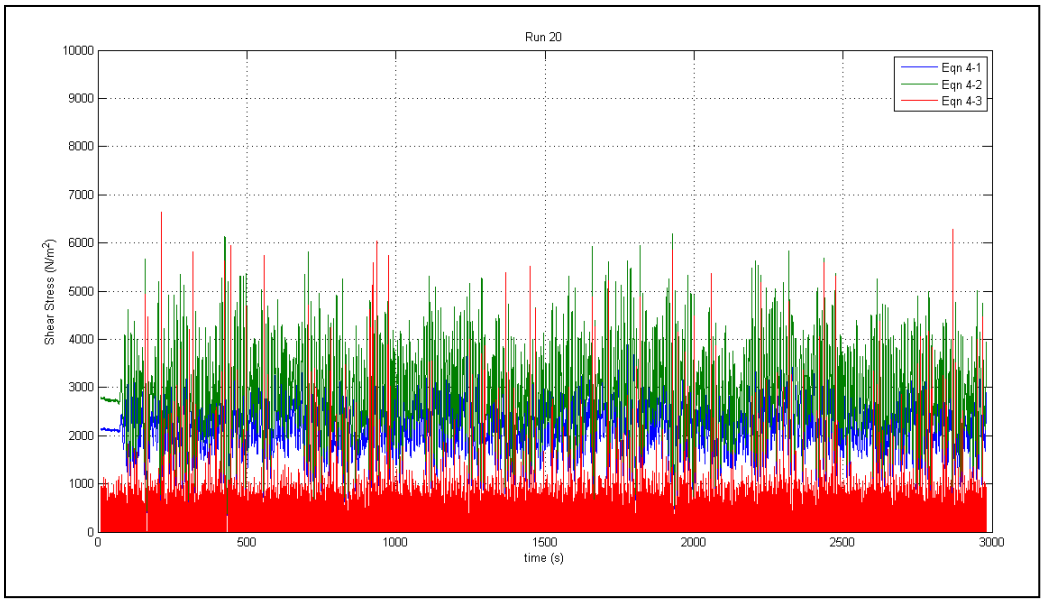

Figure C.8 Shear Stress Estimation, Run 20

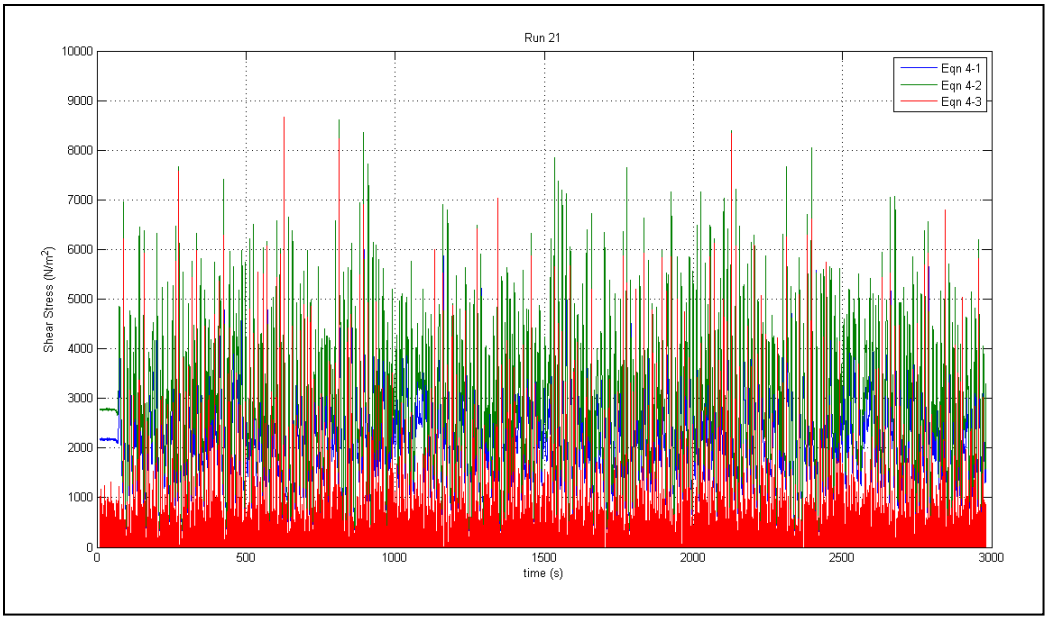

Figure C.9 Shear Stress Estimation, Run 21

Runs 22-25 are test runs that were not included in any research.

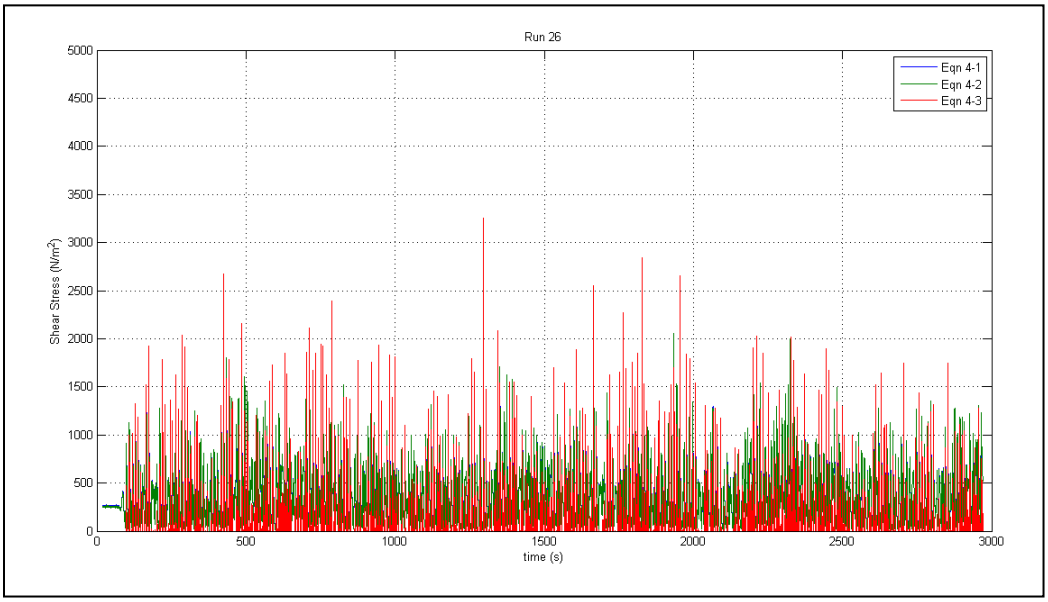

Figure C.10 Shear Stress Estimation, Run 26

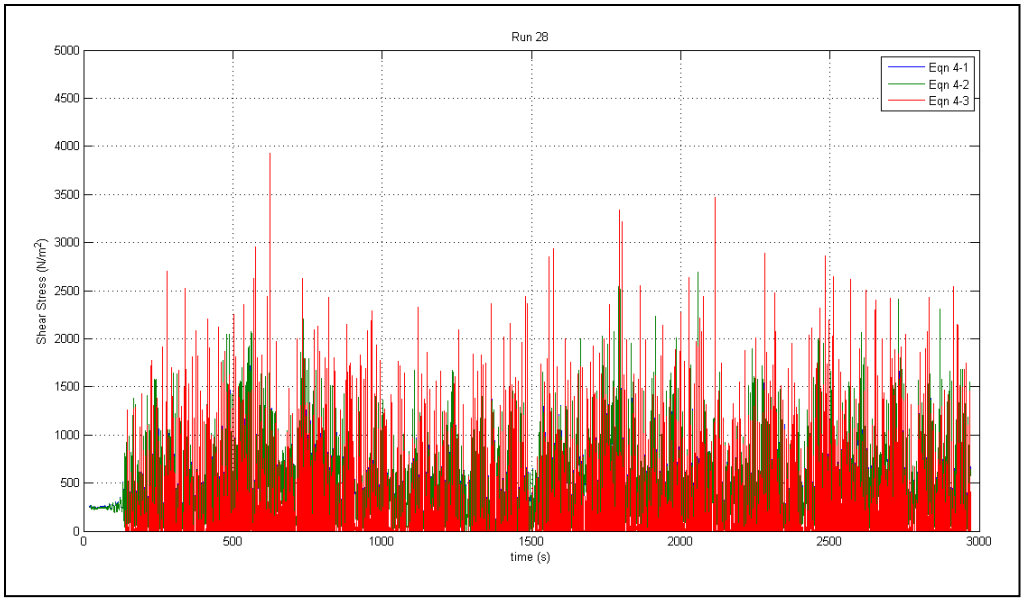

Figure C.11 Shear Stress Estimation, Run 28

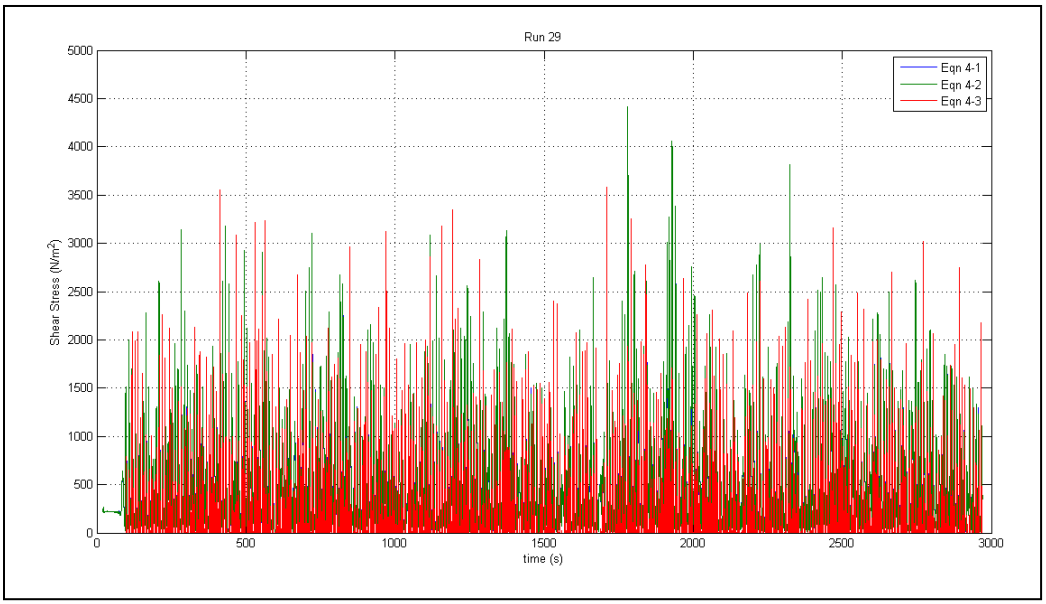

Figure C.12 Shear Stress Estimation, Run 29

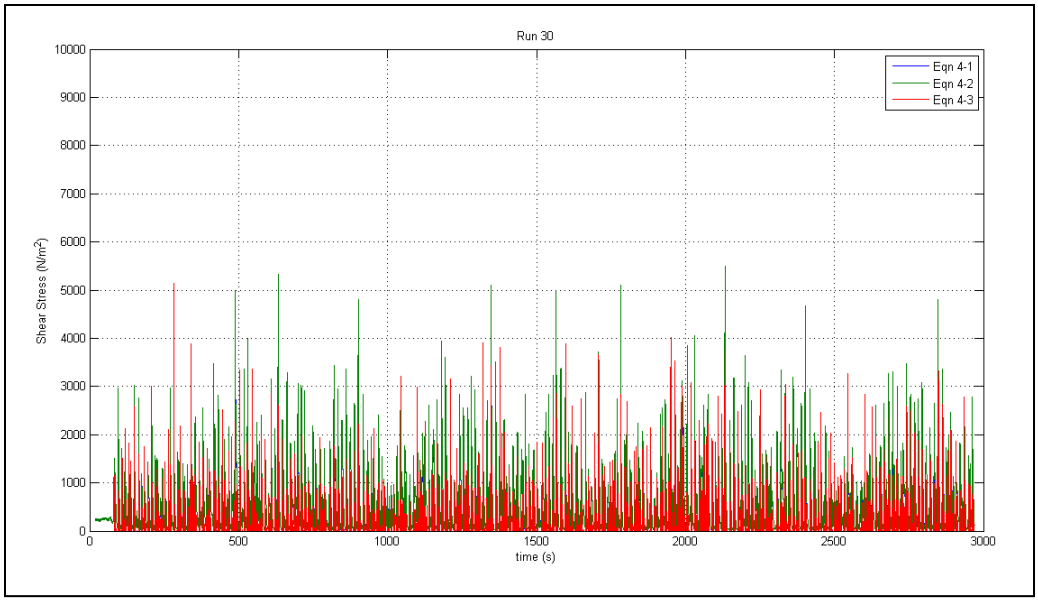

Figure C.13 Shear Stress Estimation, Run 30

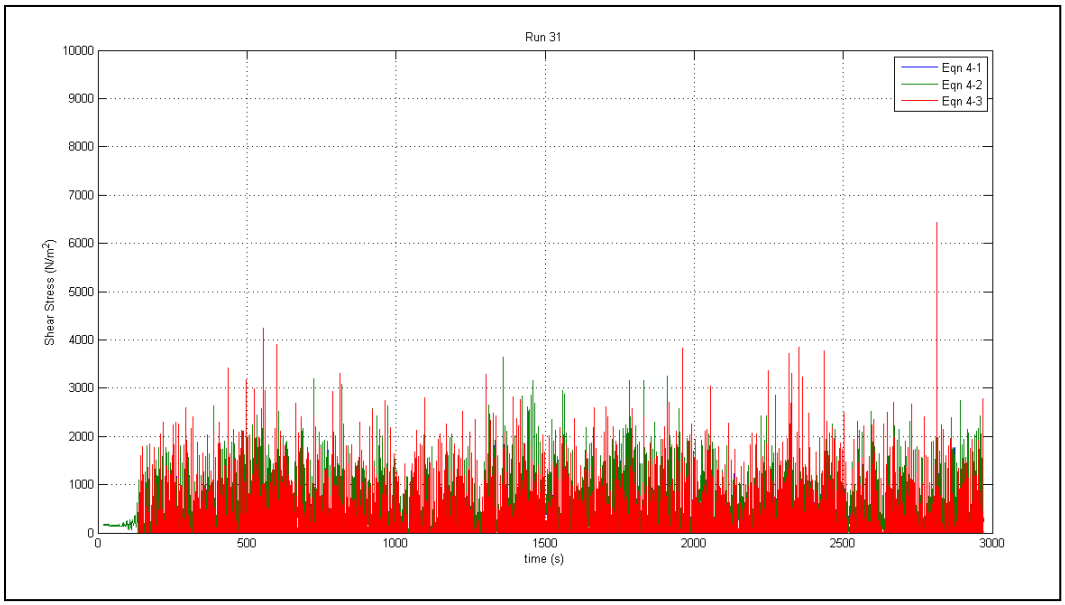

Figure C.14 Shear Stress Estimation, Run 31

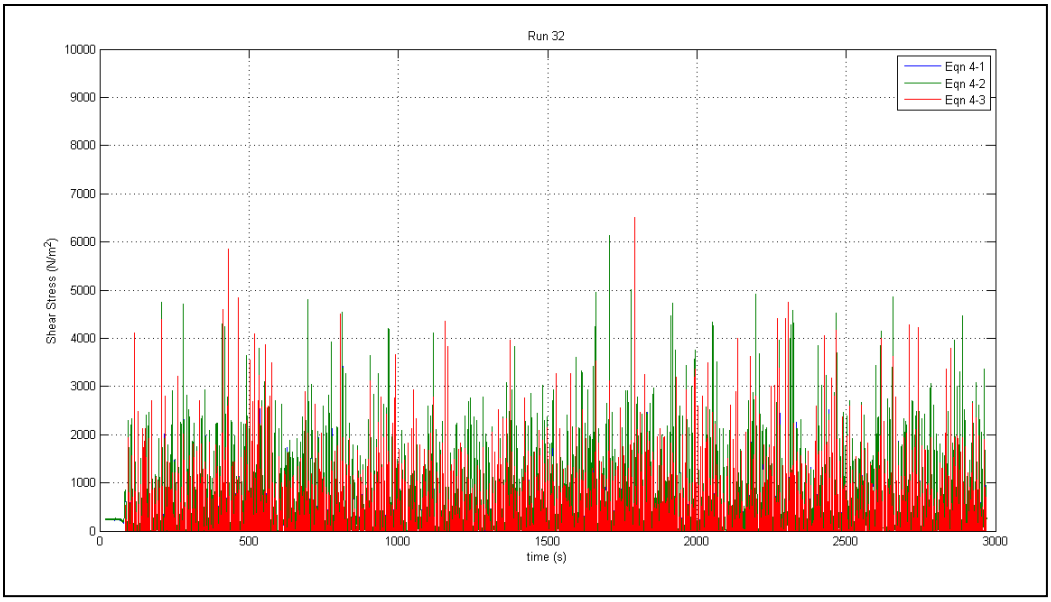

Figure C.15 Shear Stress Estimation, Run 32

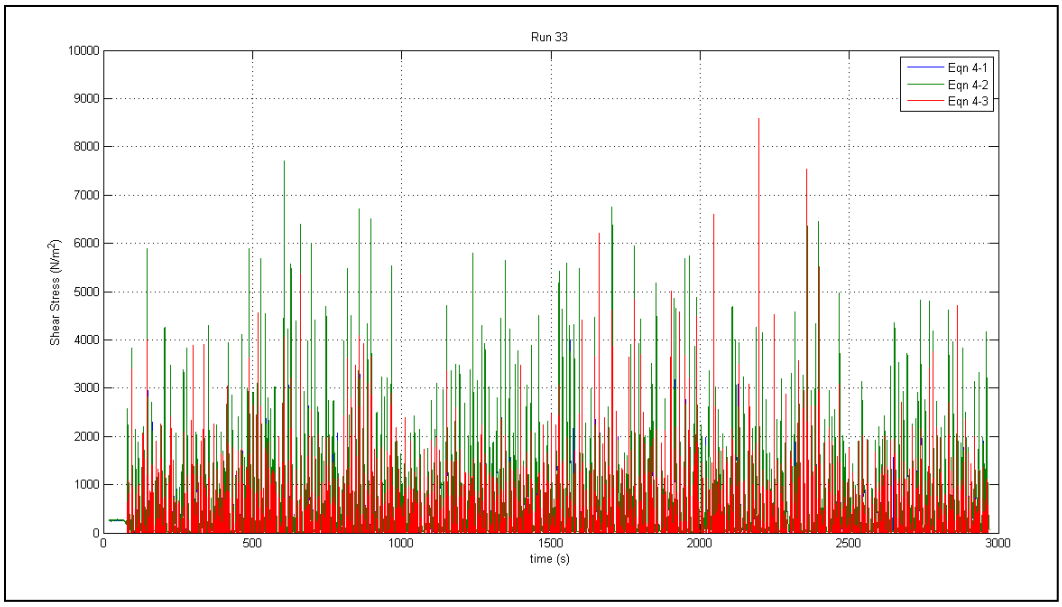

Figure C.16 Shear Stress Estimation, Run 33

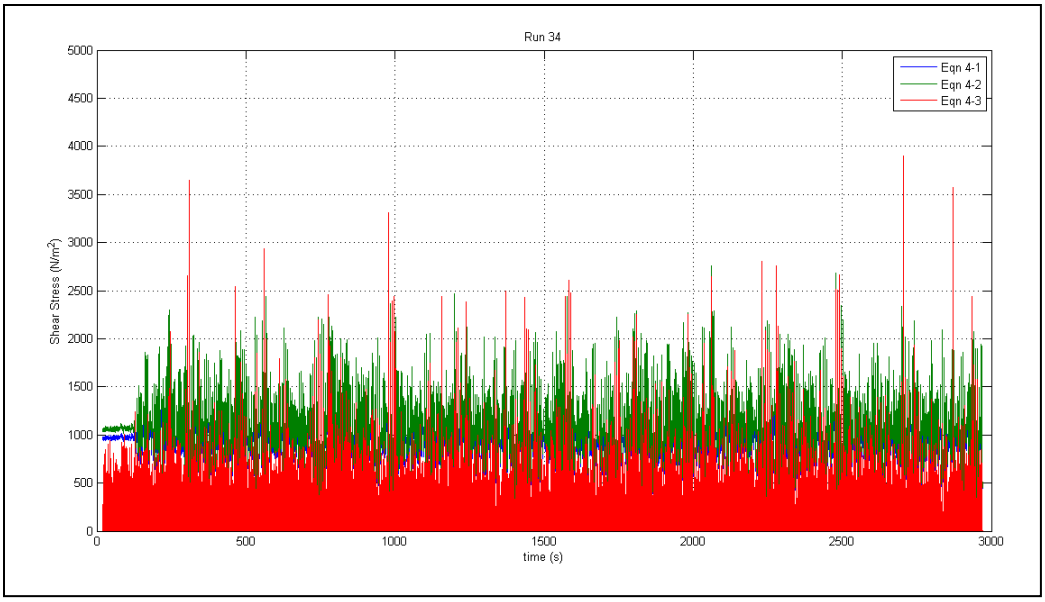

Figure C.17 Shear Stress Estimation, Run 34

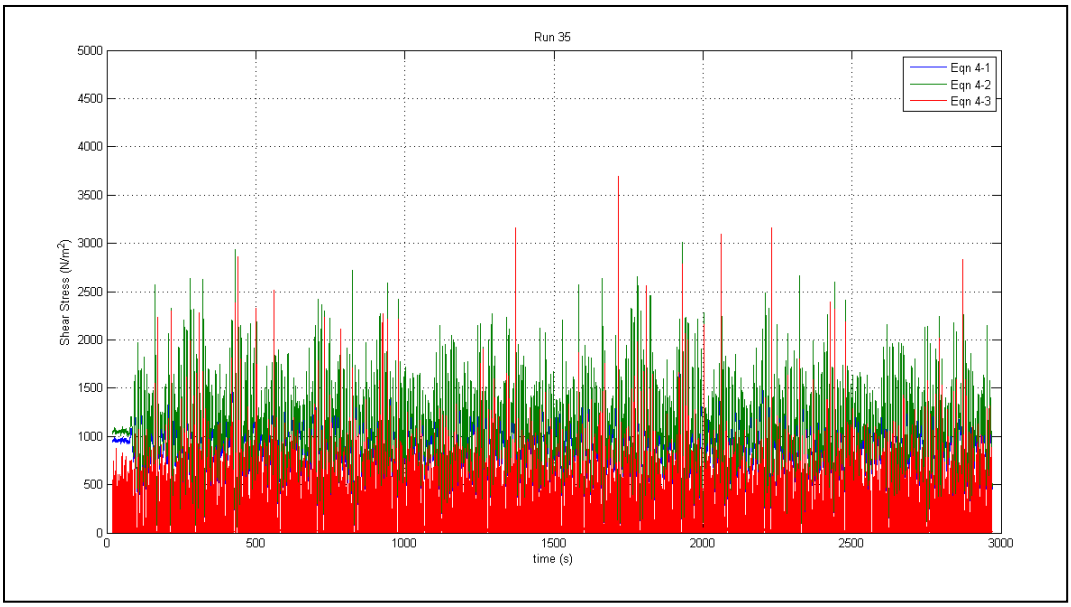

Figure C.18 Shear Stress Estimation, Run 35

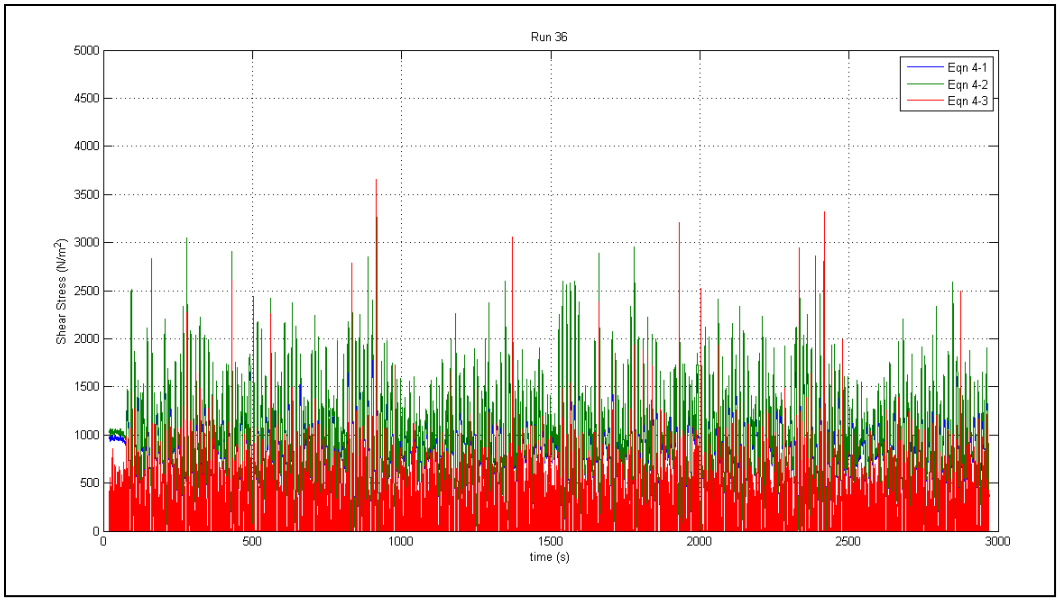

Figure C.19 Shear Stress Estimation, Run 36

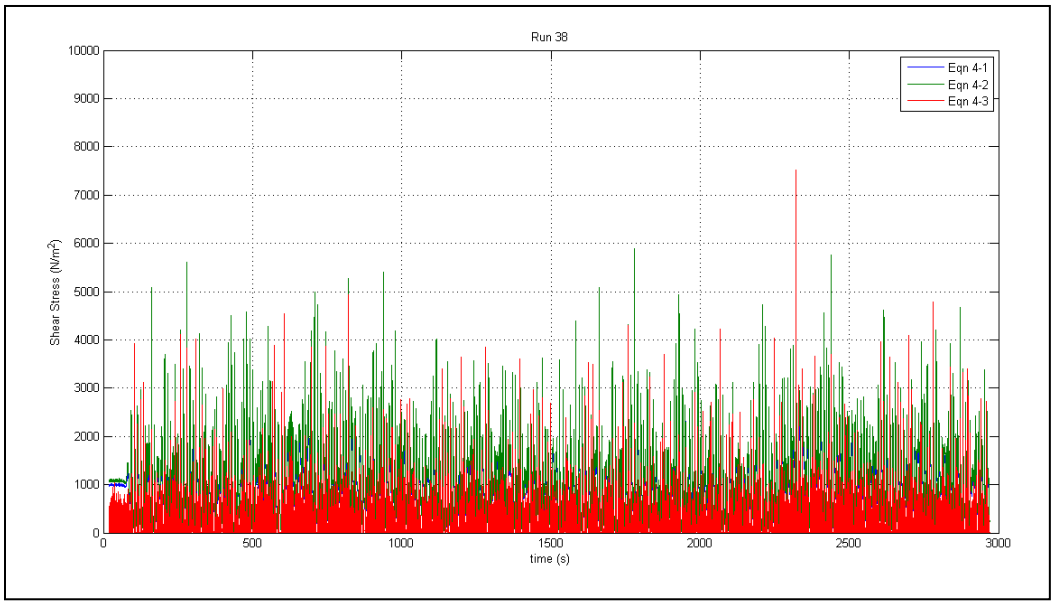

Figure C.20 Shear Stress Estimation, Run 37

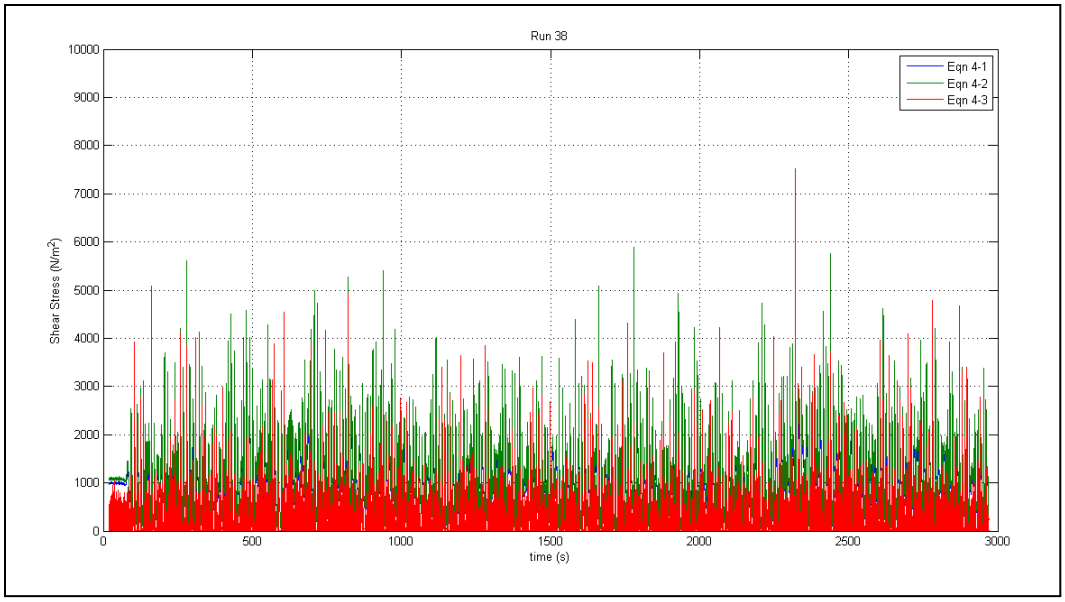

Figure C.21 Shear Stress Estimation, Run 38

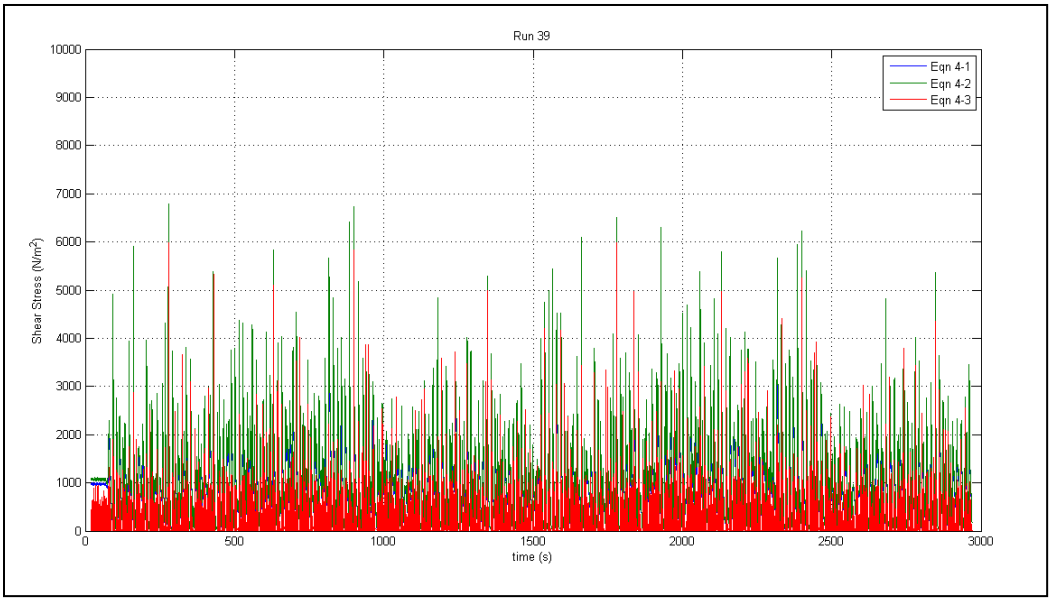

Figure C.22 Shear Stress Estimation, Run 39

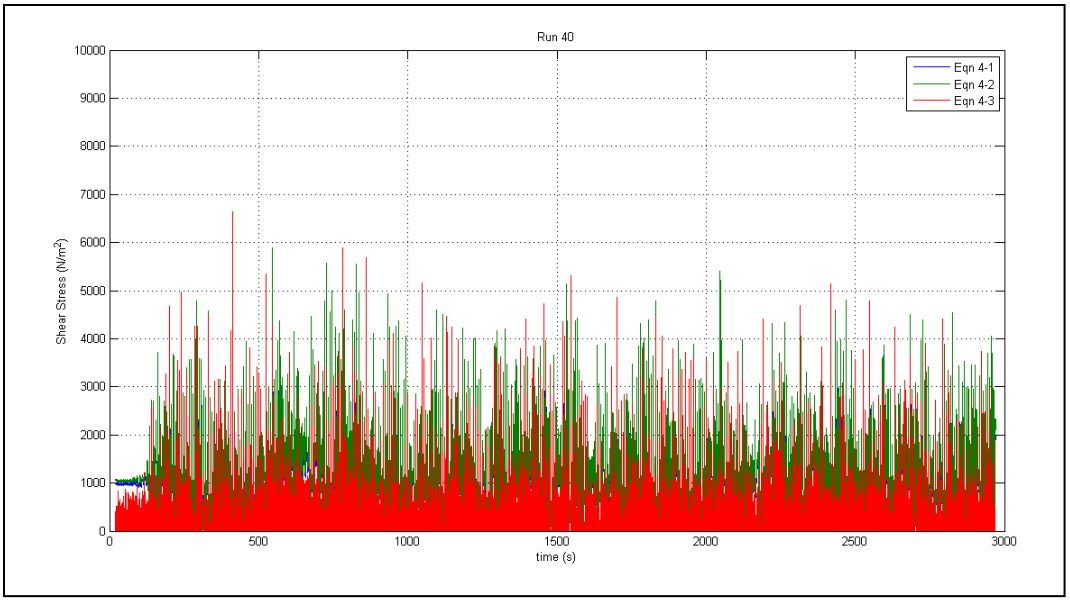

Figure C.23 Shear Stress Estimation, Run 40

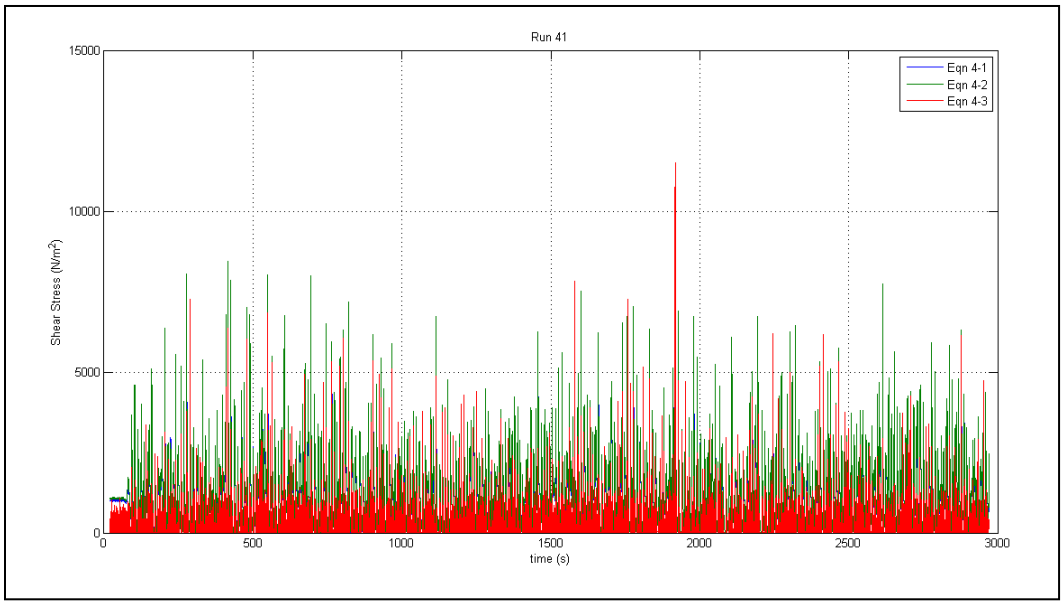

Figure C.24 Shear Stress Estimation, Run 41

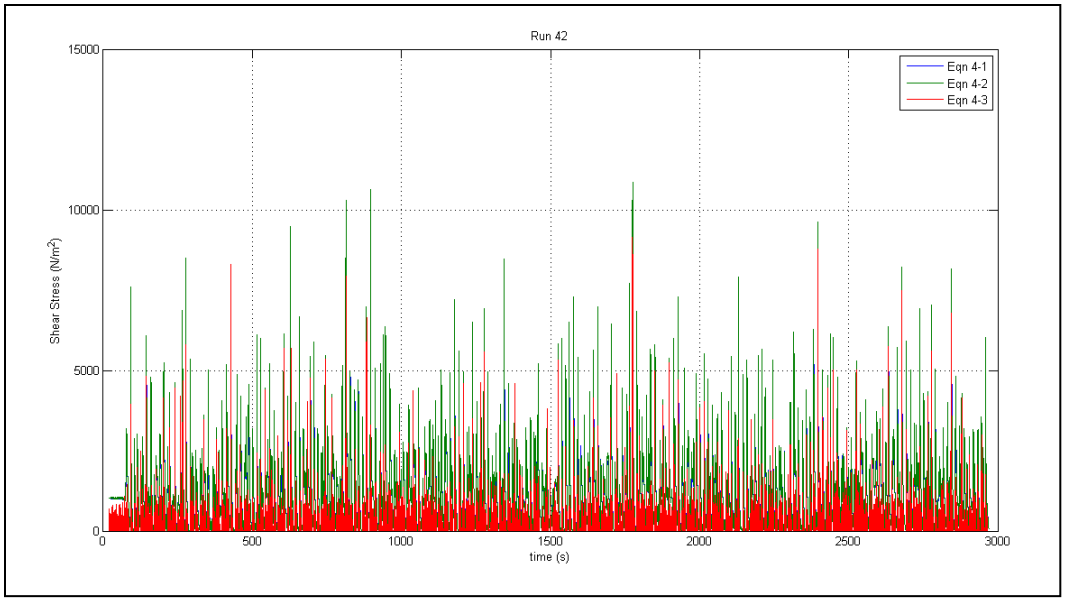

Figure C.25 Shear Stress Estimation, Run 42

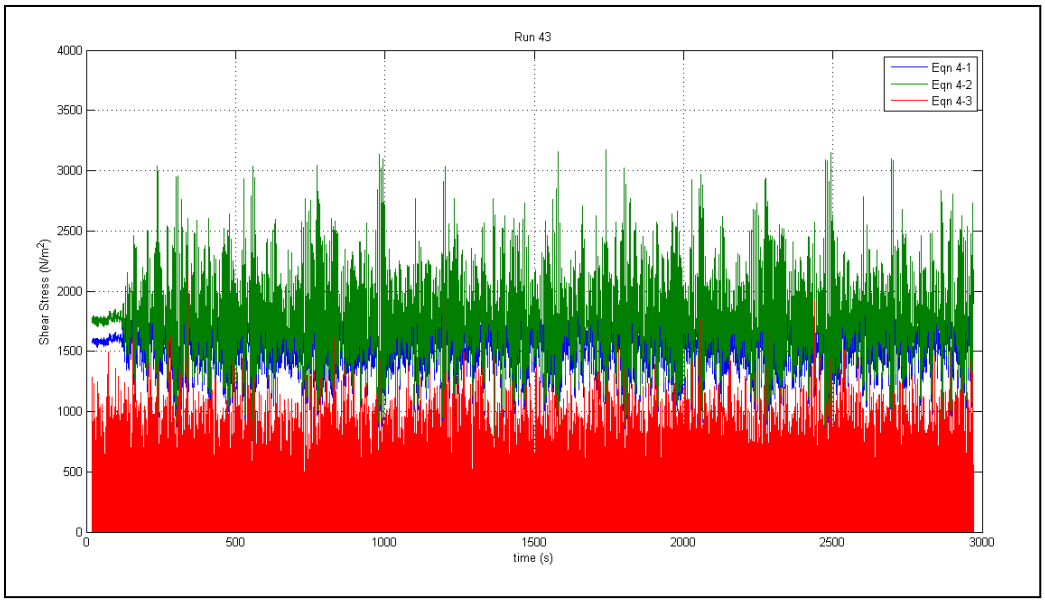

Figure C.26 Shear Stress Estimation, Run 43

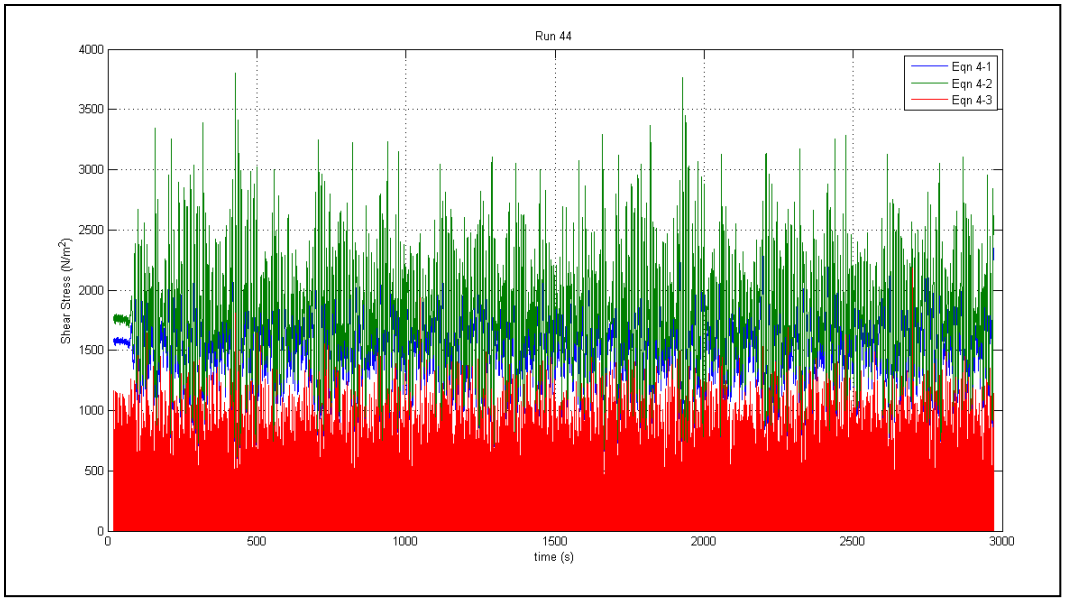

Figure C.27 Shear Stress Estimation, Run 44

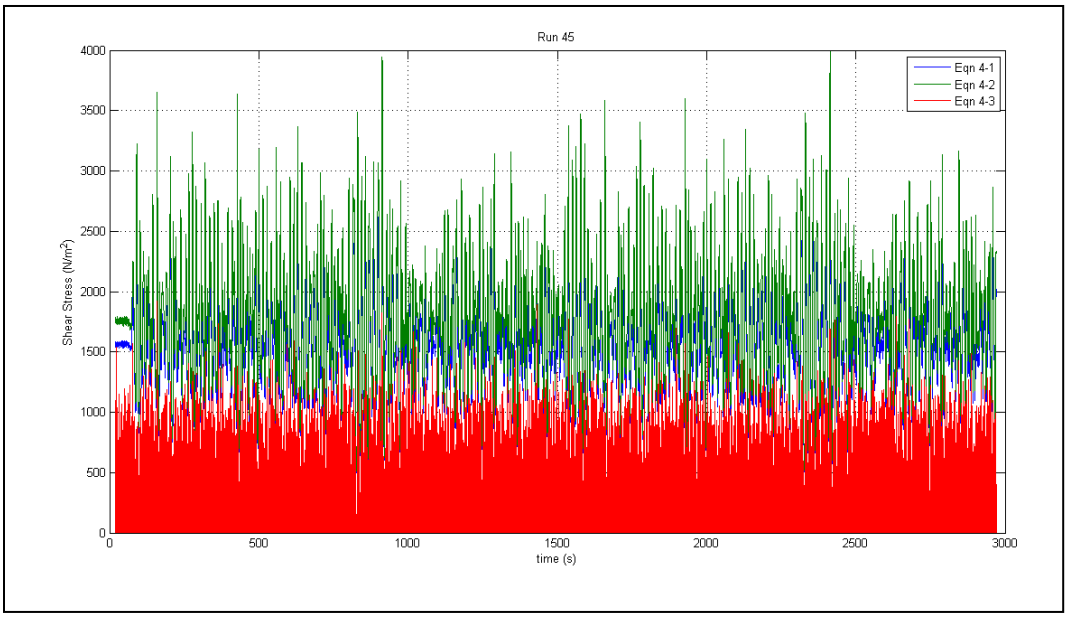

Figure C.28 Shear Stress Estimation, Run 45

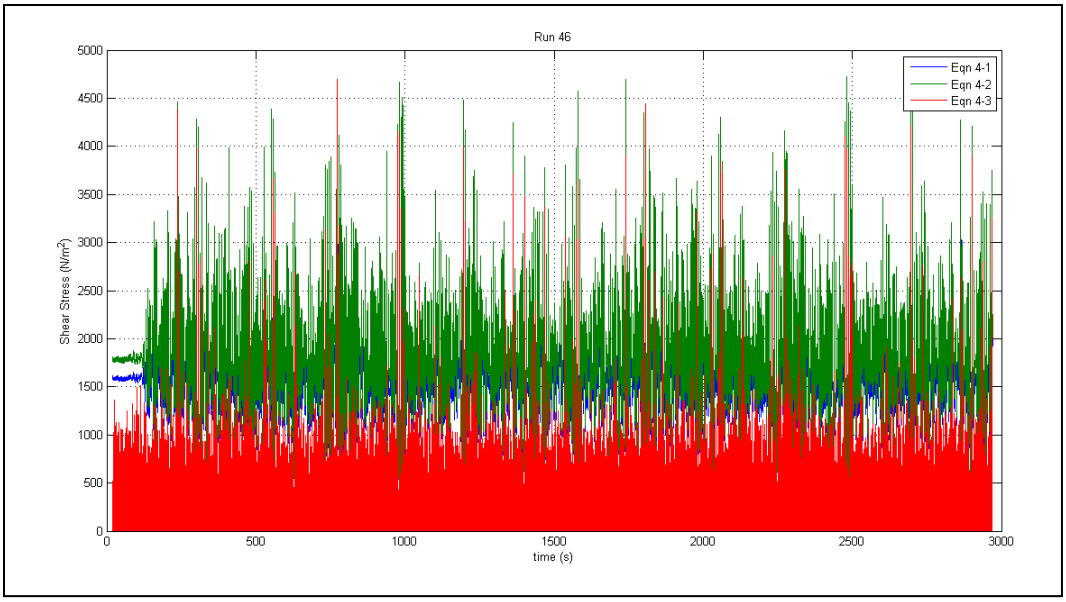

Figure C.29 Shear Stress Estimation, Run 46

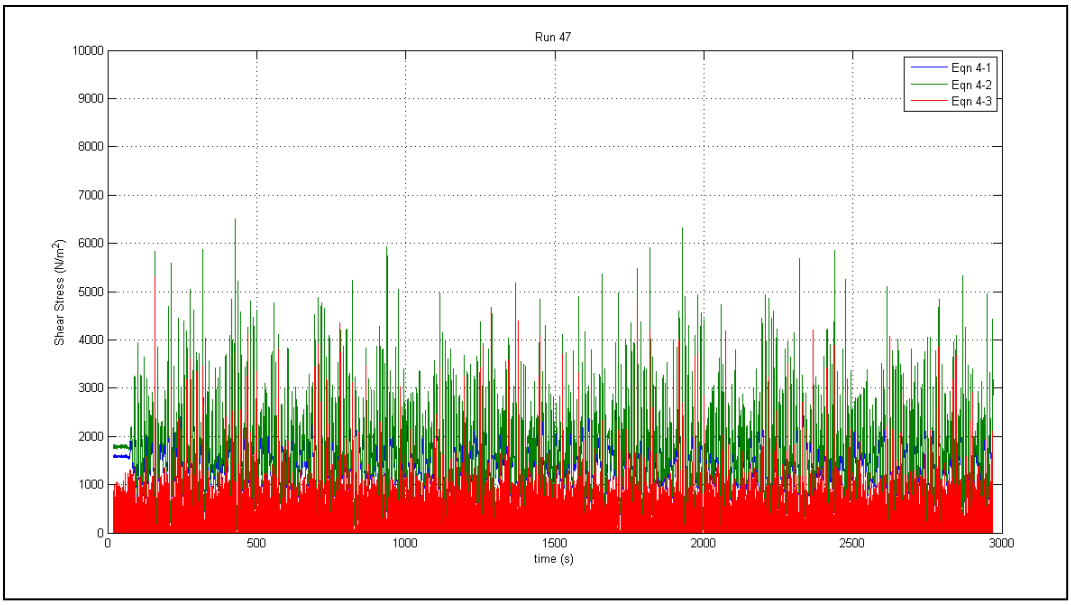

Figure C.30 Shear Stress Estimation, Run 47

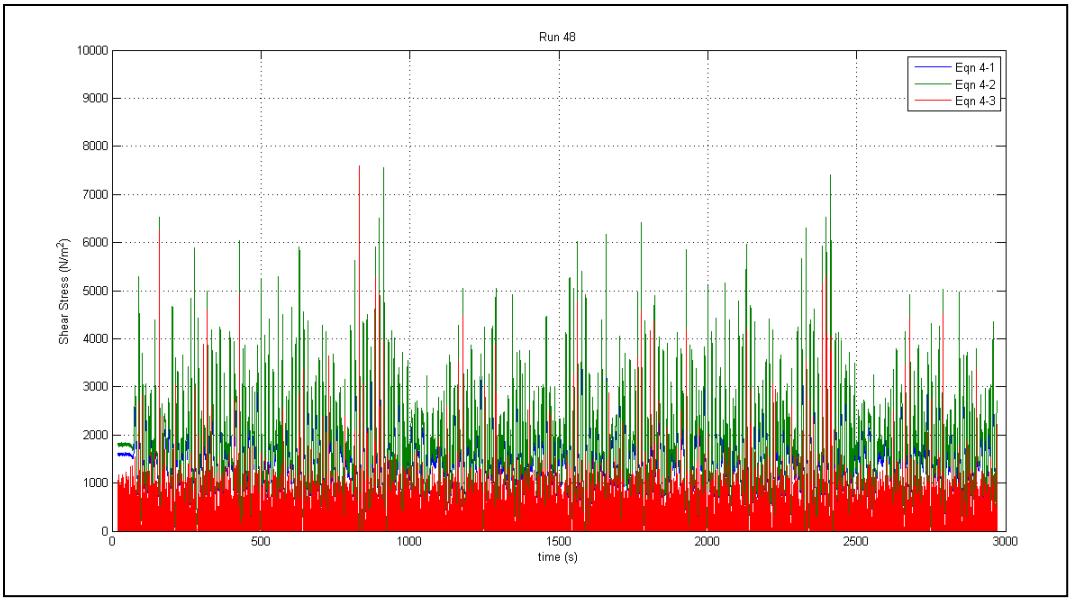

Figure C.31 Shear Stress Estimation, Run 48

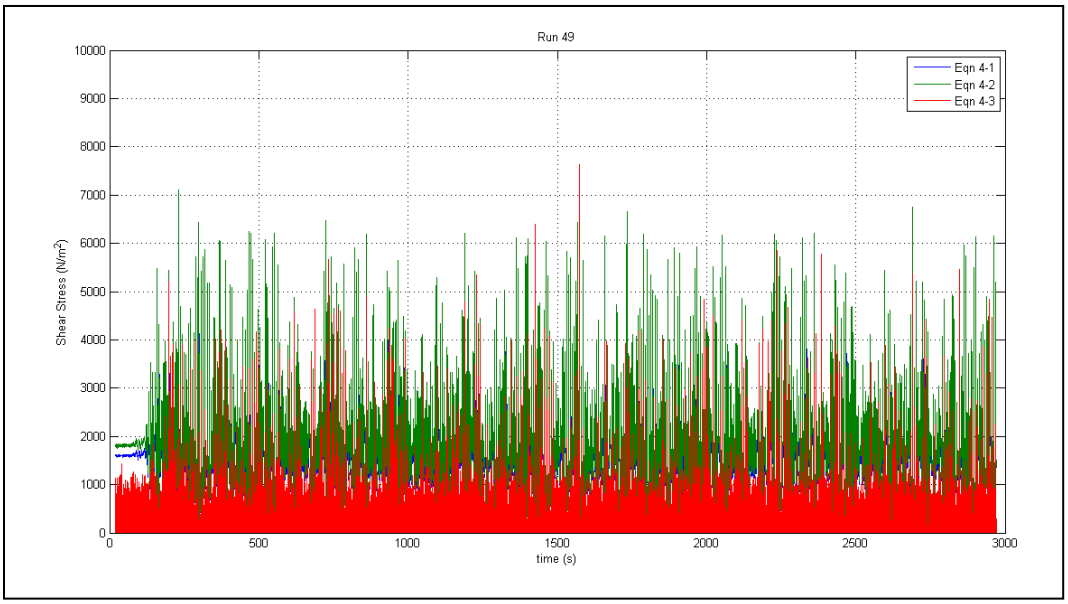

Figure C.32 Shear Stress Estimation, Run 49

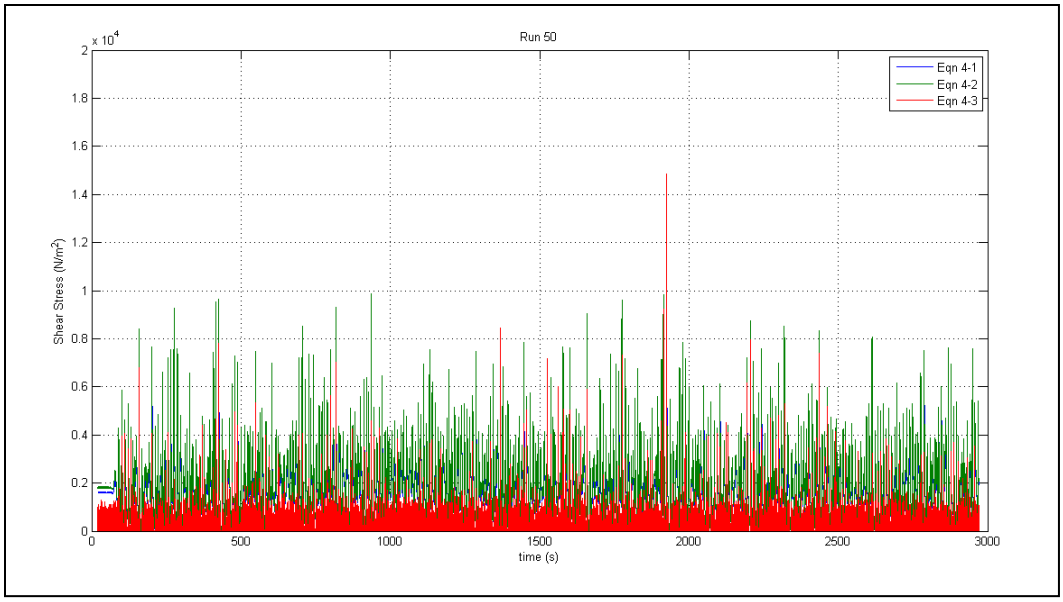

Figure C.33 Shear Stress Estimation, Run 50

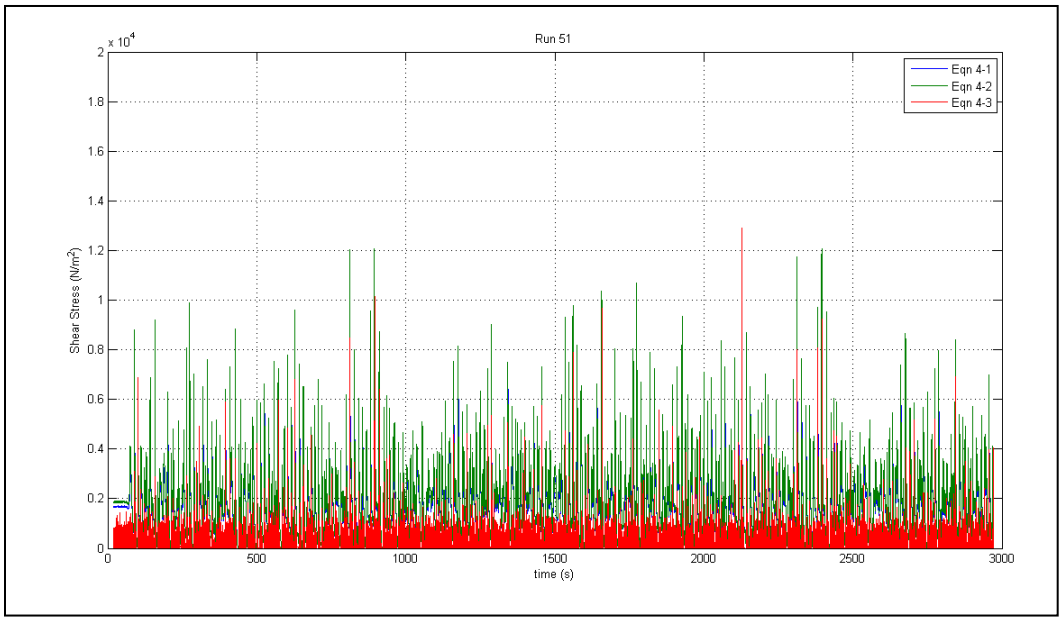

Figure C.34 Shear Stress Estimation, Run 51